Revista ALC⬢NPAT

Commemorative issue
Revista Alconpat
10 years of history
(2011 - 2021)

Revista
ALC⬢NPAT
eISSN: 2007 - 6835

Message from the Editor in Chief

JOURNAL OF THE LATIN-AMERICAN ASSOCIATION OF QUALITY CONTROL, PATHOLOGY AND RECOVERY OF CONSTRUCTION

With great satisfaction, we present the second issue of the eleventh year of the ALCONPAT Journal.

The objective of the Journal is the publication of contributions on basic or applied research directly related to solving problems about quality control, pathology and recovery of constructions, with related case studies being welcome in these areas.

This V11N2 edition begins with a work from **Brazil**, where Heber M. Paula and colleagues evaluate the incorporation of plant biomass ash, eucalyptus chips (ECA), sugarcane bagasse (SCBA) and rice husks (RHA), in mixed cement and lime mortars, considering their properties and mechanical performance. The mix by volume was 1: 1: 6, for a partial replacement of Portland cement with a content of 15 and 30%. The tests for the residues were for the characterization of the particles and pozzolanic activity, while the mortars were subjected to analysis in the fresh and hardened state. From the results obtained, the pretreatments (sieving and grinding) and the lime added to the mixture improved the reactivity of the ashes. The best performance was presented for mortars with 15% substitution, mainly for those containing RHA.

In the second work, from **Brazil**, Milton Paulino Costa Junior and S. M. M. Pinheiro verify the relationship between the action of loads that induce cracks and the durability of reinforced concrete. Prismatic test models (specimens) were produced and for two years these samples were subjected to artificial salt spray, under the action of a permanent central load, short-term central load without load (reference), with a 7-day cure. Chloride penetration tests and microstructural analyzes were performed, in addition to crack mapping. It was found that the load did not influence the chloride penetration results, however, it is observed that the micrographs and microanalysis show a formation of deterioration products and possible microorganisms, in comparison with the test tubes that did not suffer load.

The third work in this issue is from **Mexico**, where Jorge Uruchurtu-Chavarín and colleagues analyze the performance of reinforced concrete (RC) against corrosion, applying a chitosan coating to the rod. The specimens were prepared with different amounts of chitosan using solvents of apple cider vinegar, acetic acid, and sugar cane alcohol vinegar, and were subjected to electrochemical tests of polarization curves (PC), half-cell potential (HCP), electrochemical noise (EN) and linear polarization resistance (LPR). The amount of chitosan and optimal layers (thickness) were determined with an improvement in the protective properties, and low corrosion rates were obtained from concrete exposed to chlorides for 200 days. Preservation of coating on steel in concrete turns out to be interesting for future studies.

In the fourth article from **Brazil**, Fernanda Giannotti da Silva Ferreira and colleagues studied the incorporation of glass powder into conventional concrete for its influence on mechanical strength and durability. The objective of this work was to validate the durability of ultra high-performance cementitious compounds (CCUAD) with partial replacement of cement by finely ground glass, through the chloride migration test, using the NT Build 492 method. Specimens containing values of 0%, 10%, 20%, 30% and 50% of glass powder in relation to the volume of cement were evaluated 28 days of age. The results indicated that, with low values, the glass powder does not impair the properties of the composites and, at higher levels, the composites maintain adequate mechanical characteristics and durability.

The fifth article, by Giovana Costa Reus and colleagues, comes from **Brazil** and its main objective is to propose a standard procedure that enables the use of the colorimetric method to measure the depth of chloride penetration during inspections of concrete structures exposed to both chlorides and to carbonation. To avoid the occurrence of "false positive" results, solutions of calcium hydroxide ($Ca(OH)_2$) and sodium hydroxide (NaOH) were tested as pretreatment. The tests were carried out on carbonated only samples, and on carbonate and chloride contaminated samples. The results showed that the NaOH solution eliminates carbonation interference. Therefore, a suitable method was arrived at for entering chloride contamination depth readings in field inspections of concrete structures.

The sixth work of this issue is written by Gilberto Ramos-Torres and colleagues from **Mexico**. They discuss the method of the elastic invariant of stiffness that allows obtaining the mechanical response of the bridge superstructure; it is based on the impact response of known masses applied to the center of the span to obtain the maximum displacement that defines the point stiffness. This is compared with the values of the curve formed with the stiffness invariants, constructed from the design characteristics of the bridge. The method was implemented in two bridges located on federal highway No. 14 of the State of Sonora Mex., with results consistent with the damage reported. The evaluation was qualitative from a global parameter, obtained in environmental conditions in the absence of wind and at constant temperature, suitable for the diagnosis of the present structural state, having limitations in skewed bridges.

In the seventh work, from **Brazil**, G. S. Munhoz and colleagues verified the fatigue safety of a bridge designed in 1987 according to current Brazilian regulations. A structural model was built to determine and verify the most critical section considering the Brazilian standard model and the vehicle spectrum in the literature. According to the stress variation method, it was concluded that the concrete subjected to compression meets the criteria, but the steel section is not sufficient to resist the shear and bending stresses. By the Palmgren-Miner rule, the fatigue life of the reinforcement subjected to bending is 13.91 years. A more detailed analysis of the structure and the load spectrum is necessary to confirm these results.

In the eighth work, from **Brazil**, CS Silva and colleagues do a documentary investigation on the alkali / aggregate reaction (AAR) that has affected many foundations, which indicates the importance of carrying out a verification of the recovery procedures, which is carried out on fifty foundations. The objective was to build a profile of the recovery processes through a consultation with inspection

companies or recovery executors in the city of Recife and neighboring cities. For this, a questionnaire with seventeen questions was applied methodologically. These results allowed to establish the similarities of the affected foundations, the diagnosis, the processes applied in the recovery, the advances in materials, the conditions for the use of the reinforcement, the costs, and allowed to identify the foundations that left an inspection window for additional controls. The result was an evaluation of the treatments in the bases affected by the AAR chemical reaction.

The article that closes the edition is by Pedro Castro Borges from **Mexico** and the Editorial Board of the Alconpat Journal. The objective of this article is to present to the community the achievements and challenges to come of the Alconpat Journal in its first ten years of existence. A narration was made of: how the idea of having a scientific / technical journal at Alconpat International came about; when, how and where the discussions and the project took place; the implementation, the first issue, the punctuality; the requirements and challenges to meet for the first indexations (Scielo México, Scielo WoS, Redalyc, Latindex, Google); the Conacyt projects that made it possible to gradually meet the requirements for eventual applications at higher indexes (Scopus and WoS), repositories, directories (DOAJ) and super servers; electronic markings, publication in three languages (Spanish, Portuguese and English), administrative times for every specific issue, etc. In the end, an extensive thanks are extended to all those who have participated in these initial 10 years and the program of activities for the academic celebration, held on May 19, 2021 in virtual mode, was added for posterity.

We are confident that the articles in this issue will constitute an important reference for those readers involved with questions of evaluations and characterizations of materials, elements, and structures. We thank the authors participating in this issue for their willingness and effort to present quality articles and meet the established deadlines.

On behalf of the Editorial Board

Pedro Castro Borges

Editor in Chief

Revista ALC ONAT NPAT

CONTENT

Page

Characterization and feasibility of using vegetable biomass ash in mortar

C. F. Gonçalves[1] , A. F. Soares[2] , H. M. Paula[1]*

*Contact author: heberdepaula@hotmail.com

DOI: https://doi.org/10.21041/ra.v11i2.484

ABSTRACT

The present research aims to evaluate the incorporation of vegetable biomass ash, eucalyptus chips (ECA), sugarcane bagasse ash (SCBA) and rice husk ash (RHA), in mixed mortars of cement and lime, considering its properties and mechanical performance. The volume ratio was 1: 1: 6 for a partial replacement of Portland cement at a rate of 15 and 30%. The tests for the residues were a characterization of the particles and pozzolanic activity, while that of the mortars was an analyses in the fresh and hardened state. From the results, pretreatments (sieving and grinding) and lime added to the mixture improved the reactivity of the ashes and the best performance was presented for mortars with 15% substitution, mainly for those containing RHA.

Keywords: mortars; partial replacement of cement; supplementary cement materials; vegetable biomass ash.

_____

[1] Master's Degree in Civil Engineering, Faculty of Engineering, Federal University of Catalão, Catalão, Brazil.

[2] Department of Civil Engineering, Faculty of Engineering, Federal University of Goiás, Catalão, Brazil.

Contribution of each author

In this work, the author C. F. Gonçalves was responsible for the analysis, discussion of the results, writing and review of the paper. Author A. F. Soares developed the experimental methodology, carried out experiments and collected data. The author H. M. Paula contributed with the original idea, coordination of experiments, guidance and supervision of all activities.

Discussions and subsequent corrections to the publication

Any dispute, including the replies of the authors, will be published in the second issue of 2022 provided that the information is received before the closing of the first issue of 2022.

Caracterização e viabilidade de utilização de cinzas de biomassa vegetal em argamassa

RESUMO

O presente trabalho tem como objetivo avaliar a incorporação de cinzas de biomassa vegetal, cavaco de eucalipto (ECA), bagaço de cana-de-açúcar (SCBA) e casca de arroz (RHA), em argamassas mistas de cimento e cal, considerando suas propriedades e desempenho mecânico. O traço em volume foi 1:1:6, para uma substituição parcial do cimento Portland a teores de 15 e 30%. Os ensaios para os resíduos foram de caracterização das partículas e atividade pozolânica, as argamassas foram submetidas a análises no estado fresco e endurecido. Dos resultados, os pré-tratamentos (peneiramento e moagem) e a cal adicionada a mistura melhoraram a reatividade das cinzas, o melhor desempenho foi apresentado para argamassas com 15% de substituição, principalmente para aquelas contendo RHA.

Palavras-chave: argamassas; substituição parcial do cimento; materiais cimentícios suplementares; cinza de biomassa vegetal.

Caracterización y viabilidad del uso de cenizas de biomasa vegetal en mortero

RESUMEN

El presente trabajo tiene como objetivo evaluar la incorporación de cenizas de biomasa vegetal, chips de eucalipto (ECA), bagazo de caña de azúcar (SCBA) y cáscaras de arroz (RHA), en morteros mixtos de cemento y cal, considerando sus propiedades y rendimiento mecánico. La mezcla por volumen fue 1: 1: 6, para un reemplazo parcial de cemento Portland de 15 y 30%. Las pruebas para los residuos fueron de caracterización de las partículas y actividad puzolánica, mientras que los morteros fueron sometidos a análisis en estado fresco y endurecido. De los resultados obtenidos, los pretratamientos (tamizado y molienda) y la cal añadida a la mezcla mejoraron la reactividad de las cenizas y el mejor comportamiento se presentó para los morteros con 15% de sustitución, principalmente para los que contienen RHA.

Palabras clave: morteros; reemplazo parcial de cemento; materiales de cemento suplementarios; cenizas de biomasa vegetal.

Characterization and feasibility of using vegetable biomass ash in mortar
Gonçalves, C. F., Soares, A. F., Paula, H. M.

1. INTRODUCTION

Civil construction is a segment that accounts for a high demand of raw materials, while releasing significant amounts of CO_2 into the atmosphere (Noor-ul-Amin, 2014; Berenguer et al., 2018). To minimize this problem, some agricultural residues have been incorporated by the construction industry (Chatveera and Lertwattanaruk, 2014). Moreover, much of this is because ash has pozzolanic properties, which plays a significant role when incorporated into cement (Hossain et al., 2016).

This property is identified in materials called pozzolanic that have silica or alumina in the state amorphous, which when in contact with water, react with the calcium oxide found in lime or in cement that give rise to a substance with cementicious properties (ASTM C 618-19; Farinha et al., 2018). To achieve this, in addition to a non-crystalline state, pozzolans must have a refinement of their particles, that is, they present a specific elevated surface area (Roselló et al., 2017).

The physical, chemical and mineralogical composition of these agro-industrial residues is varied, depending on the type of biomass, species, growth condition, harvest techniques, transport, storage, combustion process and many other conditions that can improve - or not - its content (Zajac et al., 2018). In general, it comprises aluminosilicates in the amorphous and crystalline phase, whereby silicon dioxide has the highest percentage in RHA and SCBA samples, as well as oxide of aluminum in ashes from wood origin (Farinha et al., 2018; Fernandes et al., 2016; Kazmi et al., 2017; Ukrainczyk et al., 2016).

Oxides of other metals are also present, such as iron, magnesium, calcium, and potassium.

In addition, there are carbonates and unburned carbon found in forest ash, such as ECA. Moreover, when applied in cementitious systems, they are responsible for a greater demand for water in the mixture, due to the high loss on ignition (Arif et al., 2016; Ban and Ramli, 2010; Garcia and Sousa-Coutinho, 2013; Ribeiro et al., 2017).

Despite this, the different levels of substitution can lead to an improvement of the properties of durability, resistance of the mortar, a decrease in the material cost in the construction (Hossain et al., 2016), good compaction and low evolution of the heat during hydration (Noor-ul-Amin, 2014). These are effective in controlling expansions of deterioration caused by alkali-aggregate reactions (Esteves et al., 2012) that can reduce the use of fossil fuels, form raw materials and generate income for workers involved in transportation, infrastructure, technological development processes and the application itself (Prasara-A and Gheewala, 2017).

Therefore, using ash as a partial substitute material for cement goes beyond sustainable issues, and encompasses economic and social issues (Prasara-A and Gheewala, 2017). However, commercializing waste and its application in construction is almost non-existent, even with the growing interest in supplementary cementitious materials from biomass in scientific research (Roselló et al., 2017), or with the possibility that new materials can improve the performance of buildings and materials, promoting greater quality control and minimizing the development of pathologies, for example. Therefore, further studies regarding the feasibility of using combustion residues in mortars and concrete should be conducted (Ukrainczyk et al., 2016).

These studies were developed because, in addition to the ashes showing good results when used as partial substitutes for Portland cement, they are by-products of cheap and abundant commodities worldwide, disposed of in landfills without any environmental concerns (Moraes et al., 2014; Zajac et al., 2018; Berenguer et al., 2018). In 2012, 34 million tons of RHA were discarded. In the following year, in the United States, it is estimated that 1.25 to 5.6 tons of SCBA were produced (Martirena and Monzó, 2017; Paris et al., 2016). The increased use of biomass for energy generation is one of the most important sources of renewable production and has projected growth for the future, also accounting for a greater availability of ash (Zajac et al., 2018).

There is confirmation that countries such as Brazil may have industries that may benefit from

biomass residues for applications in construction, as discussed in the study by Moraes et al. (2014) and Regô et al. (2015), for example. The former analyzed the possible uses of by-products of the rice chain, and the latter characterized the RHA produced in the country and its application in cementitious matrices. As a result, the two authors cited found the same advantages mentioned in the article previously. They also identified that the ash produced in Brazil has a chemical composition that does not vary much, and this makes the material easier to use as a component of mortars.

Taking this into account, the aim of the present work is to verify the technical feasibility of using different types of biomass ashes - ECA, SCBA and RHA -, at different percentages of substitution, as supplementary cementitious material in mixed mortars, which contain two agglomerates in their composition, i.e., cement and lime, aiming at the partial reduction of Portland cement.

2. MATERIALS AND METHODS

2.1 Materials and characterization

The reference mortar used is of the mixed type - Portland cement, hydrated lime, natural fine aggregate and treated water, such as those specified by NBR 13529 (ABNT, 2013). The cement is the high initial strength (CP - V ARI) or type III, for NBR 5733 (ABNT, 1991) and ASTM C 150M-20, respectively. The cement was chosen because it has few or no additions in its composition, providing a better investigation of the behavior of the material according to the incorporation of waste.

The lime used is the hydrated type with carbonates, classified as CH - III, according to NBR 7175 (ABNT, 2003) and ASTM C 206-3, giving the mixture greater plasticity, better workability and greater water retention, besides being traditionally used in the region and easy to obtain. Finally, the small aggregate is the dry natural sand, with commercial denomination of "medium" and specifications according to NBR 7211 (ABNT, 2009), without any kind of treatment such as sieving or washing. The sand was extracted by dredging it in the Veríssimo and Paranaíba rivers in the city of Catalão - GO.

The three types of vegetable biomass ash used are combustion by-products, used for heat and energy generation, classified as class C by ASTM C 618 and vegetable pozzolan for concrete use. The ECA was obtained from a mining and processing plant of niobium and phosphate, the residue comes from using eucalyptus chips in furnaces for heat generation to dry the phosphate rock, where temperatures reach between 1000 and 1100 °C. The SCBA, supplied by a sugar, ethanol and energy producing plant, is removed from boilers, where the sugarcane bagasse was burned for energy generation. RHA is a by-product of the food industry, which uses the bark for heat generation to process coffee. For RHA and SCBA, no information was made available regarding the process of obtaining the residues.

The chemical composition determined by Resende (2013), de Souza et al. (2014) and Berenguer et al. (2018) comprises ashes with similar particularities to those studied here. The X-ray fluorescence spectrometry technique was used and is presented in Table 1.

Table 1. Oxide concentration (% by mass) of the analyzed ashes.

Compound	ECA (Resende, 2013)	RHA (de Souza et al., 2014)	SCBA (Berenguer et al., 2018)
SiO_2	6.38	93.25	84.86
Al_2O_3	22.60	<0.1	1.91
Fe_2O_3	10.90	0.02	3.83
CaO	27.40	0.57	2.96
MgO	6.15	0.19	2.54
TiO_2	2.41	<0.1	0.75
P_2O_5	2.75	0.51	0.38
Na_2O	0.28	-	0.47
K_2O	4.29	.18	1.38
MnO	0.41	0.25	0.19

2.2 Treatment of ashes
The biomass residues were submitted to pretreatments of sieving and milling ensuring an increase in the specific surface with particles of lesser granulometry, thus helping the occurrence of the pozzolanic activity. These procedures were suggested by Ramos et al. (2013), Matos and Sousa-Coutinho (2013), Salvo et al. (2015), Modolo (2015), Ataie and Riding (2016). Thus, the ashes were passed through the 50-mesh sieve (opening of 297 µm), eliminating coarse particles, mostly composed of inert material, such as soil and rock fragments. Then, they were ground in a ball mill for 30 min at a rotation of 30 rpm - for longer periods, the particles began to aggregate (Xu et al., 2015).

2.3 Standards and experimental trials
2.3.1 Particle characterization
The particle density test followed the methodology proposed by the Brazilian Agricultural and Research Company - EMBRAPA (2011) using the volumetric balloon method. The samples of 20 g, separated in containers of known mass, were placed in an oven to dry at 105 °C for 24 hours. Later, they were cooled in a desiRHAtor, weighed, and transferred to a 50 ml volumetric flask containing ethyl alcohol to remove the air or voids from the ashes and cement.
For the fineness index of ash, NBR 15894-3 (ABNT, 2010), 20 g of the sample were dispersed in 400 ml of 12.5 g/l sodium hexametaphosphate solution and sieved in a 45 µm mesh, nominal diameter of 200 mm, under a constant flow of 5 l/s flow water for 10 min. The retained material was transferred to a watch glass, placed in an oven to dry at 105 °C for 24 hours, thus determining its dry mass. The samples with 20% or more material retained in the 45 µm sieve can be classified as pozzolan, NBR 12653 (ABNT, 2014).
Regarding the fineness index of cement, NBR 11579 (ABNT, 1991), and adopting the manual method, the 75 µm sieve (number 200) was used. The test consists of sieving so that, initially, 50 g of the sample were weighed, and the process finished only when the passing material corresponded to a mass less than 0.05 g. This property can also be evaluated following the indications of NBR NM 76 (ABNT, 1998) or ASTM C 204-05 for the Blaine Method.
Gravimetry tests made it possible to determine the moisture content, NBR NM 24 (ABNT, 2003) and ASTM D 3173-73, where 1 g of each sample was weighed, dried in an oven at 105 ± 4 ° C for 30 min, with subsequent periods of 10 min, until the mass reached was constant. The results determined should be less than or equal to 3 (three), as indicated in NBR 12653 (ABNT, 2014).
In loss on ignition, NBR NM 18 (ABNT, 2004) by Method nº 1, the ash samples were calcined in a muffle furnace - Bravac M2 Electric Stainless -, for 50 min at 900 ºC at a heating rate of 35 ºC/min. After firing, the crucibles were left for 5 (five) hours in the muffle furnace and later placed

in a desiRHAtor for cooling and future weighing. The same procedure should be performed following the recommendations of ASTM D 7348 - 13, in a single step, at a maximum temperature of 900 ºC (Method B). To be classified as pozzolan, NBR 12653 (ABNT, 2014), the loss limits must be less than or equal to 6.

2.3.2 Proportioning, molding of specimens and curing
The influence of partial substitution of RHA, SCBA and ECA on the performance of mortar was studied by comparing the behavior of one trace taken as a reference, without residues, and another with the substitution of 15 and 30% by mass of Portland cement for each type of ash, Table 2. These substitution levels were defined, based on the best results presented in the research conducted by Paris et al. (2016), Hossain et al. (2016), Abbas et al. (2017), Izabelle et al. (2011), Resende (2013) and Ukrainczyk et al. (2016).
The volume was 1:1:6 (cement, lime and sand) and can be used as laying and coating mortar for ASTM C 270-19, mortar type N. Considering the analyses of Dubaj (2000) and Campos (2014), this proportion showed a better performance for mortar properties. The amount of water was determined through the consistency index, NBR 13276 (ABNT, 2016), fixed at 265 ± 5 mm.
The prismatic specimens with partial substitution of cement were identified with the acronym for each ash - RHA, ECA and SCBA - and with index 15, for those with 15% substitution, or 30, for those with 30% substitution. The specimens molded with the reference trace were identified with the acronym RS (reference specimen).
The mass proportioning used to prepare the mortar specimens was carried out so that the total dry material of the mixture was equal to 2.5 kg, Table 2. The mixture was prepared from the mass proportion used in the preparation of the mortar specimens was carried out so that the total dry material of the mixture was equal to 2.5 kg, Table 2. The mixture was prepared according to the method specified by NBR 16541 (ABNT, 2016), without a mechanical mixer. To reach the established consistency index, the consistency test was performed by the flow table, NBR 13276 (ABNT, 2016).

Table 2. Mass proportion (kg) of the materials used to produce mortars.

Sample	Cement	Lime	Dry sand	Ashes	Water
CPR	0.258			0.000	0.625
RHA15	0.219			0.039	0.750
RHA30	0.181			0.077	0.650
SCBA15	0.219	0.103	2.130	0.039	0.625
SCBA30	0.181			0.077	0.625
ECA15	0.219			0.039	0.670
ECA30	0.181			0.077	0.725

After the mixture was prepared, the specimens (CDP) were molded in a prismatic format, with dimensions of 4cm x 4cm x 16cm. Three specimens were produced by age for the reference mortar and for each type of ash with the two replacement strips, totaling 42 specimens (NBR 13279, 2005; BS EN 1015-11). After molding, the molds with the mixture were wrapped by film paper and subjected to dry curing in a laboratory environment, at a temperature of 23 ± 2 ºC and relative humidity of 60 ± 5%.
It is known that, with the loss of water and moisture during curing, the mechanical and water absorption properties will be compromised, hence the need for to be carried out within the standards established by ASTM C 309-19 and ASTM C 1315-19. However, the choice for a non-submerged cure reflects the character of the research in identifying the behavior of ashes in cementitious

systems, especially regarding their ability to interfere with the moisture needed to hydrate the cement.

After 48 hours, given the end of the curing period, the CDP were removed from the molds and wrapped again in film until carrying out the mechanical resistance tests.

2.3.1 Evaluation of mortars in the hardened state

The tensile tests in simple flexion and compression, NBR 13279 (ABNT, 2005) and BS EN 1015-11, were made in order to analyze the development of the mechanical strength of the mortar over the curing time at 14 and 28 days. The resistance analysis was performed only for these ages since the pozzolanic reaction occurs slowly and, therefore, according to Ataie and Riding (2016), for early ages, satisfactory results are not obtained.

The results found for compressive and tensile strength in flexion at 14 and 28 days were obtained by calculating the average strength of the six specimens tested for compression, and the three tested for flexural tensile strength, using the multiple analysis of means adopting the Tukey method at 5% (p <0.05) of confidence level. In addition, the maximum absolute deviation value of 0.5 MPa was respected for the individual results achieved in compression and 0.3 MPa for those achieved in the flexural tensile test, NBR 13279 (ABNT, 2005).

The capillarity water absorption test was performed at 28 days, as prescribed by NBR 15259 (ABNT, 2005). Initially, the mass of each specimen that was still dry was determined, and then the samples were placed on a support inside a container with water in partial immersion for a constant water slide of 5 ± 1 mm. Finally, each sample was removed from the container, dried with a damp cloth, and weighed at 10 min and at 90 min given the start of the test.

3. RESULTS AND DISCUSSION

The physical and chemical characterization analyzed in this study, important for understanding the behavior of particles and their influence on pozzolanic reactions, was made from the results obtained for the particle density (PD), the fineness (F) of each element, water content (U) and loss on ignition (LOI). From the results shown in Table 3, it can be observed that the samples containing SCBA had a lower volume in their composition, as well as in the studies by Kazmi et al. (2017) as this quantity is inversely proportional to PD (Aprianti et al., 2016). Therefore, for ECA, the lowest PD value found, the volume is ten times greater than it would be if there were no substitution, according to Gluitz and Marafão (2013), and which will influence the strength of mortars as will be seen below.

Table 3. Physical characterization of the elements used

Sample	PD (g/cm³)	F	U	LF
Cement	2.73	3.14%	-	-
ECA	0.25	52.63%	6.59%	70.20%
RHA	0.55	78.67%	1.81%	5.79%
SCBA	0.84	31.72%	0.60%	11.65%

In addition, based on the PD, the process of accommodating the particles that make up the cementitious system can be understood. There is a better mechanical performance when they are strongly interlaced and where there are few voids. Thus, the best resistance results should be seen in the SCBA and RHA, because after being previously treated - ground and sieved - the samples showed a higher DP. Without this treatment for ECA, the strength or other property of the mortar

could be negatively affected, making the substitution of cement by ashes, for example, inept (Martirena and Monzó, 2017; Farinha et al., 2018).

However, knowing that the behavior of a mortar is governed by other properties, grinding and sieving could make the ashes highly reactive as observed by Roselló et al. (2017), and with the pozzolanic activity taking place, the mechanical performance of the system can be satisfactory. Therefore, analyzing the results for the fineness index and following the specifications of ASTM C 618-19, SCBA is in fact a pozzolana, the maximum content of material retained in the 45 µm sieve is 34%, compared to 31, 72% accumulated. For NBR 12653 (ABNT, 2014) none of the ashes would be a pozzolanic material; the maximum content is 20%.

However, even though they are not pozzolans within the limits established by current regulations, the smallest particles, that is, not much material going through the 45 µm sieve, are concentrated close to the aggregate interface and cement matrix, causing a filler effect. This can contribute to resistance gain in the hardened state (Khan et al., 2017; Aprianti et al., 2016; Resende, 2013). This phenomenon is the same as that observed in cementitious systems containing hydraulic lime.

While for fresh mortar, the fineness index reveals those of lesser value, in the SCBA case, there is no change in workability for any substitution range because particles larger than 45 µm affect the plasticity of the mixture (Netto, 2006). Similarly, for the RHA, there is a greater loss of workability, especially when the increase in cement replacement is from 15 to 30%. These are assertions that are equally proven by the consistency index, which are within the limits established by NBR 13276 (ABNT, 2016), Figure 1.
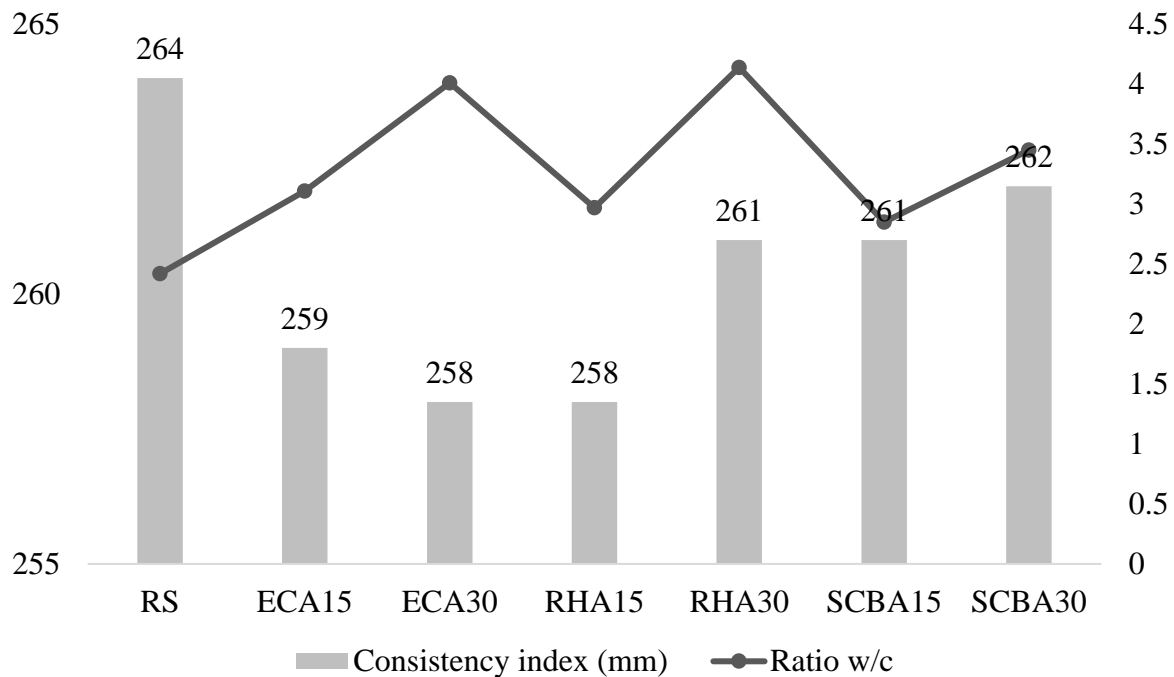
Figure 1. Chart results for consistency index and w/c ratio.

From the fineness index test, a visual analysis of the samples retained in the sieve was also performed. For the ECA, applying sodium hexametaphosphate, a dispersing chemical compound (Mauri et al., 2011), the presence of small crystals was noted. These particles account for the high-water content in the sample, Figure 1, due to the high absorption capacity (Netto, 2006). This explains not only the accentuated volume of water, which favors the maintenance of workability (Ataie, 2016), but also the humidity, which is satisfactory during the mortar curing (Rajamma et al., 2009).

Due to the hygroscopic nature of these crystalline elements, with more water released, there is a greater loss of mass of the ECA when subjected to the loss on ignition test, and for this reason there was a 70.20% loss, the largest among the analyzed ash. In addition, this occurrence is also due to the presence of unburned organic matter (Prasara-a, 2017), which during heating in a muffle, releases another portion of CO_2 and water.

Nevertheless, the presence of these crystals is not favorable to the properties of the mortar. For Aprianti et al. (2016), amorphous elements are more reactive. However, due to the fact that a large part of the retained material is crystalline and that its fineness reached a value of 52.63%, it is possible that the rest of the sample, through-pass and amorphous material, compensated for the reactivity of the ash. Thus, for ECA, the considerable gain in strength is a function of the volume of ash added to the mortar due to its low PD, as previously indicated.

Regarding the water demand in the samples, using the consistency index, Figure 1, in relation to the CPR, there is a high amount of water for mixtures containing ash in partial replacement for cement, except for SCBA. The largest amount required was for the RHA30 trace with 20% more when compared to CPR. According to Ukrainczyk et al. (2016), this occurs because of the irregular and bulky shape of the ashes. Berra et al. (2015) show the high specific surface area of ash compared to Portland cement, in addition to the porous nature of its particles, as suggested by Arif et al. (2016).

These characteristics are other factors that also account for greater water absorption. Another is the presence of a large amount of organic matter available for hydration during the mortar hardening, as identified by Rajamma et al. (2009) and previously confirmed by the loss on ignition test. It can be observed, therefore, that the workability decreased when there was the presence of ash in partial replacement to cement, corroborating the results obtained by Belviso (2018), Aprianti et al. (2016), Ukrainczyk et al. (2016) and those discussed here.

Despite this, the decrease found was 2.3% compared to the 34.4% cited in the literature. This difference was due to the size of the selected particles. Ukrainczyk et al. (2016), for example, used materials with particles up to 80 µm. In this study, we opted for those with max. 75 µm, a value considered satisfactory by Ataie and Riding (2016) to ensure reactivity, which is inversely proportional to the particle density, and therefore positively influence the mechanical properties of the mortar.

In general, considering the analyses for ECA, which are inverse to those observed in SCBA and RHA, and following the requirements of NBR 12653 (ABNT, 2014), only the last two can be classified as class N pozzolans, for content of water, moisture and loss on ignition. Both reached a moisture content of less than 3% and did not exceed 10% of the loss on ignition value. Moreover, adding the behavior of the ash before the properties of the mortar in the plastic state, workability and water absorption, a better reactivity is expected in samples containing RHA.

Therefore, regarding the results, there was no significant gain in compressive strength at 14 days for any of the samples, Figure 2, as shown in Paris et al. (2016) and Abbas et al. (2017). CPDs with a 15% cement replacement content achieved better mechanical performance, especially for ECA15. This is related to factors such as the lower rate of cement replacement (Garcia and Sousa-Coutinho, 2013; Carrasco et al., 2014; Ukrainczyk et al., 2016), the greater amount of reactive material, the better workability, when compared to CDP, and greater water absorption.
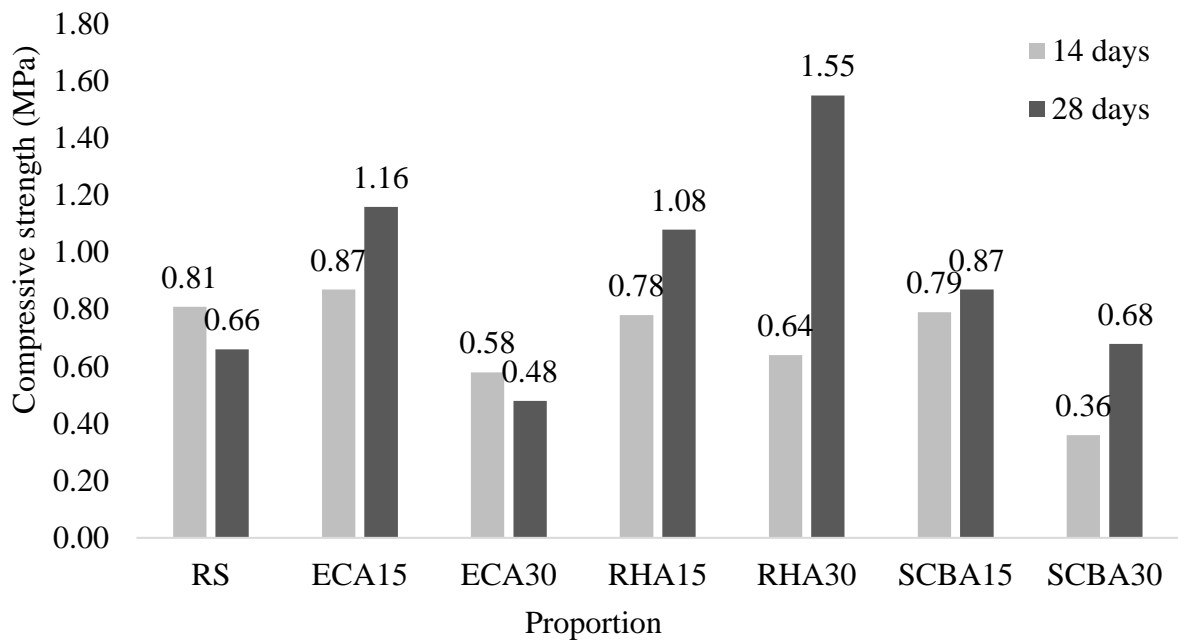
Figure 2. Bar chart showing a comparison between the average resistance achieved in the simple compression test for each trace at 14 and 28 days (Tukey method $p < 0.05$).

The cause of the poor performance of CPD is justified by the non-occurrence of the synergistic effect between cement hydration and the pozzolanic reaction, which directly influences the compression strength of the mortar (Isaia, 2003; Berra et al., 2015). On the one hand, the poor hydration action is possibly due to the use of wooden molds for molding the CDP, a material of a permeable nature, and little water retention during curing, as expected. On the other, the slow gray-cement reaction, Carrasco et al. (2014) and Rosales et al. (2017), suggest that long periods are necessary for there to be effects considered positive in resistance to compression.

At 28 days, the ECA30 did not show resistance gain as the causes are the same as those pointed out for the ECA15 at 14 days. This confirms that the ashes tend to contribute to the development of mechanical resistance due to their pozzolanicity and hydraulic activity, as in Berra et al. (2015). The best results were obtained for samples with a content of 15% and for RHA30. These were also identified by Rajamma et al. (2009) and Wang (2015). In RHA30, the sample with the greatest resistance gain is due to the high amount of silica in its composition (Fernandes et al., 2016), shown in Table 1, which can react more easily with the released CH, increasing the strength of mortars (Jamil et al., 2016).

Thus, it can be affirmed that, even without significant gain in compressive strength, the partial replacement of cement with biomass ash was considered acceptable for 15% by mass. The results identified in Figure 2 and those found by Rajamma et al. (2015), Garcia and Sousa-Coutinho (2013), Carrasco et al. (2014) and Ukrainczyk et al. (2016) point out that the resistance of samples containing ash is greater than that found in CPR for different curing times, that is, 28 days for those containing the biomass residue and 90 days for those without any additional cementitious material. Analogously, analyzing the results obtained for flexural tensile strength, Figure 3, it was observed that only the SCBA30 and RHA30 traces did not exceed the CPR resistance and that for ECA30 the same value at 14 days was reached. For the age of 28 days, the traces containing ash obtained a better performance for tensile strength in flexion than for simple compression, confirming the delayed effect of gray-cement reactions, mainly for a 15% replacement.
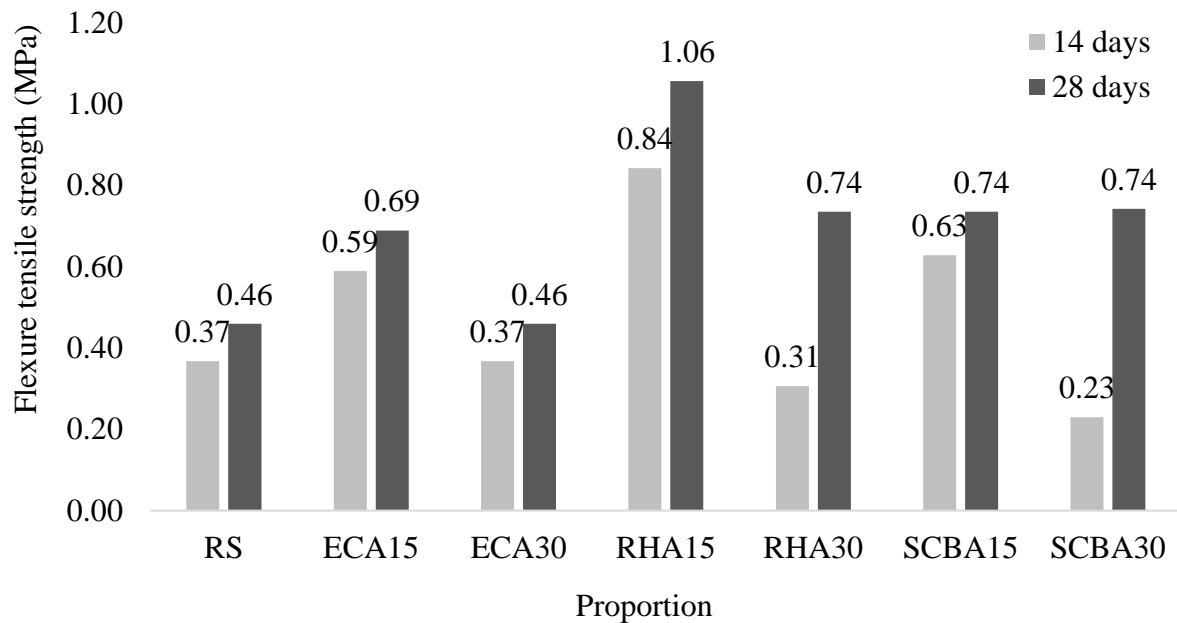
Figure 3. Comparison between the average resistance achieved in the flexural tensile test for each trace at 14 and 28 days (Tukey method p <0.05).

However, the results for flexion differ from those obtained by Rajamma et al. (2009), where there was a gradual reduction in resistance with the increase in the percentage of ash and, consequently, an increase in pozzolanic reactions, especially for replacement rates greater than 20% (Chowdhury et al., 2015). This phenomenon can be controlled by re-burning residues and grinding processes, as was done for the ashes studied here, confirming the need to submit them to these types of pretreatments, as indicated by Jamil et al. (2016).

Finally, to identify the water absorption phenomenon, the specifications presented by NBR 15259 (ABNT 2005) were followed. It states that the capillarity absorption index must be calculated as the average of the three specimens submitted to immersion in water for 10 min and 90 min, Figure 4.
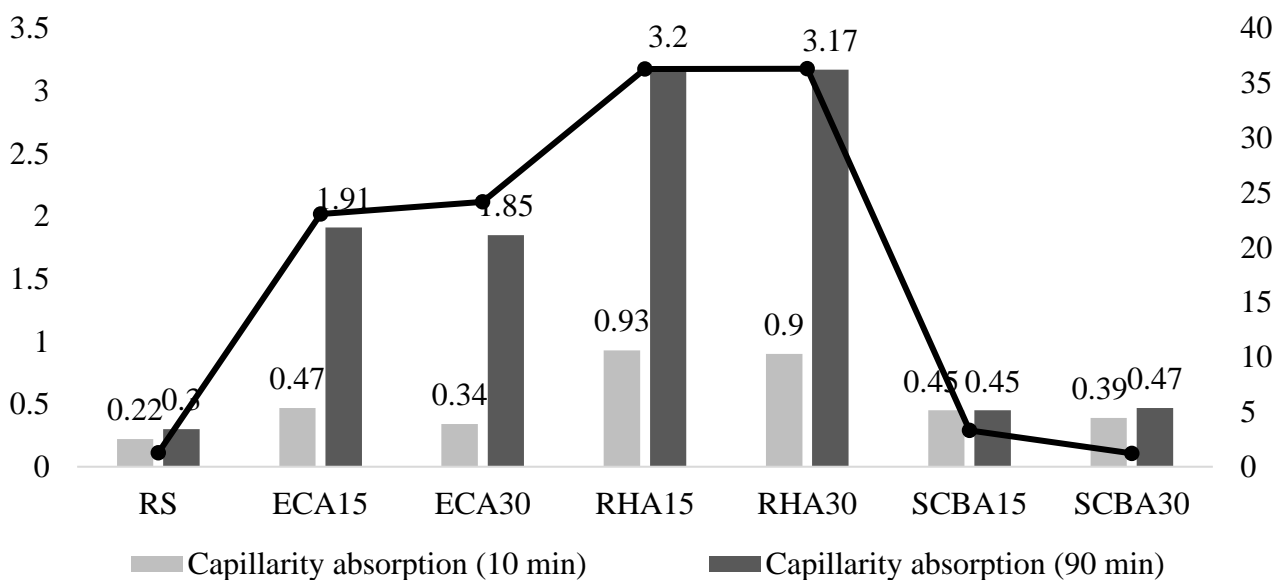
Figure 4. Absorption test at 28 days.

From the results found, the absorption rate decreases, even if expressively, as the cement replacement rate increases from 15 to 30%. Jamil et al. (2016) and Elinwa and Ejeh (2003) identified a reduction in water absorption when the mortar has 15% ash in its composition, at a rate of 0.8 to 1.25%. As a rule, it is accepted that this limit is less than or equal to 10%. However, it diverged from the studies by Chowdhury et al. (2015), in which the ash absorption and addition ratio is directly proportional.

For the highest values, ECA30 and ECA15, they occurred due to the presence of open pores in the structure, confirming the results for the granulometry and fineness index tests. In the presence of particles of different sizes, the water absorption capacity is increased. Therefore, due to the uniformity and fineness of the SCBA, the penetration of water in them has values close to those of the CPR. Thus, it is concluded that the absorption decreases as the amount of voids decreases, thus the SCBA can be used as filling material. It is also clear that, by increasing the ash percentages, the permeable voids will be filled, minimizing the absorption rate (Jamil et al., 2016; Rosales et al., 2017; Carrasco et al., 2014).

Concerning the cure, according to Aprianti et al. (2016), when incorporating fine material into cementitious systems, different procedures should be used to promote this concrete hydration. One option is to use superplasticizers (Ukrainczyk et al., 2016) to fix the w/c ratio and guarantee conditions of execution and performance (Carasek, 2010). For Ramos et al. (2013), Ataie and Riding (2016) the ideal value of the w/c ratio is equivalent to 0.4 and 0.45, respectively.

Given this, the ash with the greatest potential to improve the characteristics of mortar as a partial substitute for cement is RHA. Concerning ECA and SCBA, their potential as a filling material should be assessed, and a mortar that contains the three types together should be studied.

4. CONCLUSION

The use of ash as a component of mortar was clear. Materials that have this particularity are known as supplementary cementitious materials. All the data found in this research are also identified in the literature. The pretreatments reduced the granulometric variation of the ashes, increasing their specific surface, and the particles were better accommodated, showed greater reactivity. The content of unburned organic influenced the loss of ignition, but not enough to prevent better results in the hardened state when compared to the reference mortar.

It should be mentioned that from all the analyses made, mortars containing RHA achieved the best mechanical development. The behavior of ECA and SCBA suggests its application as a substitute for sand, for example, and may be the object of study in future research. The filling effect was identified by the resistance gain that occurred due to the behavior of the particles, like those of lime, occupying voids in the cement matrix. Using it as a substitute for cement should not be ruled out.

As for the substitution content, for the chosen bands, 15% is the ideal substitution content, however higher substitution contents may result in mortars with less mechanical resistance or more porous. The reference must therefore be the application of the mortar, whether laying or covering, whether external or internal area. Those studied here, due to their 1:1:6 trace and the results obtained, could be used for laying masonry or for ceramic tiles. However, the technical feasibility for these applications can only be proven by carrying out new studies.

Regarding water absorption, which was high for all ash contents, the mortar is highly porous. Ashes should be treated before being used (here they were ground and sieved). After doing this we suggest reburning the ash, that is, the residue needs to be ground, sieved and burnt. By doing this, the pozzolanic activity improves and voids that exist in the mortar will decrease. In addition, we suggest using an additive that will control the water-cement ratio.

12

Characterization and feasibility of using vegetable biomass ash in mortar
Gonçalves, C. F., Soares, A. F., Paula, H. M.

5. ACKNOWLEDGEMENTS

6. REFERENCES

Abbas, S., Kazmi, S. M. S., Munir, M. J. (2017), *Potential of rice husk for mitigating the alkali-silica reaction in mortar bars incorporating reactive aggregates.* Construction and Building Materials. 132:61-70. https://doi.org/10.1016/j.conbuildmat.2016.11.126

Aprianti, E., Shafigh, P., Zawawi, R., Hassa, Z. F. A. (2016), *Introducing an effective curing method for mortar containing high volume cementitious materials.* Construction and Building Materials.107:365-377. https://doi.org/10.1016/j.conbuildmat.2015.12.100

Arif, E., Clark, M. W., Lake, N. (2016), *Sugar cane bagasse ash from a high efficiency co-generation boiler: Application in cement and mortar production.* Construction and Building Materials. 128:287-197. https://doi.org/10.1016/j.conbuildmat.2016.10.091

Associação Brasileira de Normas Técnicas. (1991). *NBR 11579: Cimento Portland – Determinação da finura por meio da peneira 75 µ (nº 200).* Rio de Janeiro.

Associação Brasileira de Normas Técnicas. (1991). *NBR 5733: Cimento Portland com alta resistência inicial.* Rio de Janeiro.

Associação Brasileira de Normas Técnicas. (2003). *NBR 7175: Cal hidratada para argamassas – Requisitos.* Rio de Janeiro.

Associação Brasileira de Normas Técnicas. (2003). *NBR NM 24: Materiais pozolânicos – Determinação do teor de umidade.* Rio de Janeiro.

Associação Brasileira de Normas Técnicas. (2004). *NBR NM 18: Análise química – Determinação da perda ao fogo*. Rio de Janeiro.

Associação Brasileira de Normas Técnicas. (2005). *NBR 13279: Argamassa para assentamento e revestimento de paredes e tetos – Determinação da resistência à tração na flexão e à compressão*. Rio de Janeiro.

Associação Brasileira de Normas Técnicas. (2005). *NBR 15259: Argamassa para assentamento e revestimento de paredes e tetos – Determinação da absorção de água por capilaridade e do coeficiente de capilaridade.* Rio de Janeiro.

Associação Brasileira de Normas Técnicas. (2010). *NBR 15894-3: Agregados para concreto – Especificação.* Rio de Janeiro.

Associação Brasileira de Normas Técnicas. (2013). *NBR 13529: Revestimento de paredes e tetos de argamassas inorgânicas — Terminologia*. Rio de Janeiro.

Associação Brasileira de Normas Técnicas. (2014). *NBR 12653: Materiais pozolânicos - Requisitos.* Rio de Janeiro.

Associação Brasileira de Normas Técnicas. (2016). *NBR 13276: Argamassa para assentamento e revestimento de paredes e tetos – Determinação do índice de consistência.* Rio de Janeiro.

ASTM International. (2005). ASTM C 204-05 *Standard Test Method for Fineness of Hydraulic Cement by Air Permeability Apparatus.* https://doi.org/10.1520/10.1520/C0204-05

ASTM International. (2009). ASTM C 206-03 *Standard Specification for Finishing Hydrated Lime.* https://doi.org/10.1520/C0206-03R09

ASTM International. (2013). ASTM D 7348 – 13 *Standard Test Methods for Loss on Ignition (LOI) of Solid Combustion Residues.* https://doi.org/10.1520/D7348-13

ASTM International. (2017). ASTM D3173 / D3173M - 17a *Standard Test Method for Moisture in the Analysis Sample of Coal and Coke.* https://doi.org/10.1520/C0204-05

ASTM International. (2019). ASTM C 1315-19 *Standard Specification for Liquid Membrane-*

Forming Compounds Having Special Properties for Curing and Sealing Concrete. https://doi.org/10.1520/C1315-19

ASTM International. (2019). ASTM C 270-19ae1 *Standard Specification for Mortar for Unit Masonry.* https://doi.org/10.1520/C0270-19AE01

ASTM International. (2019). ASTM C 309-19 *Standard Specification for Liquid Membrane-Forming Compounds for Curing Concrete.* https://doi.org/10.1520/C0309-19

ASTM International. (2019). ASTM C 618-19 *Standard Specification for Coal Fly Ash and Raw or Calcined Natural Pozzolan for Use in Concrete.* https://doi.org/10.1520/C0618-19

ASTM International. (2019). ASTM C 618-19 *Standard Specification for Coal Fly Ash and Raw or Calcined Natural Pozzolan for Use in Concrete.* https://doi.org/10.1520/C0618-19

ASTM International. (2020). ASTM C 150M-20 *Standard Specification for Portland Cement.* https://doi.org/10.1520/C0150_C0150M-20

Ataie, F. F., Riding, K. A. (2016). *Influence of agricultural residue ash on early cement hydration and chemical admixtures adsorption.* Construction and Building Materials. 106:274-281. https://doi.org/10.1016/j.conbuildmat.2015.12.091

Belviso, C. (2018), *State-of-the-art applications of fly ash from coal and biomass: A focus on zeolite synthesis processes and issues.* Progress in Energy and Combustion Science. 65:109-135. https://doi.org/10.1016/j.pecs.2017.10.004

Berenguer, R. A., Silva, F. A. N., Torres, S. M., Monteiro, E. C. B., Helene, P., Neto, A. A. de M. (2018), A influência das cinzas de bagaço de cana-de-açúcar como substituição parcial do cimento na resistência à compressão de argamassa. Revista ALCONPAT. 8(1):30-37. https://doi.org/10.21041/ra.v8i1.187

Berra, M., Mangialardi, T., Paolini, A. E. (2015). *Reuse of woody biomass fly ash in cement-based materials*. Construction and Building Materials, 76:286-296. https://doi.org/10.1016/j.conbuildmat.2014.11.052

British Standard (2002). BS EN 1015-18 *Methods of test for mortar for masonry. Determination of water absorption coefficient due to capillary action of hardened mortar.*

British Standard (2019). BS EN 1015-11 *Methods of test for mortar for masonry. Determination of flexural and compressive strength of hardened mortar.*

Campos, M. O. (2014), "*Estudo da resistência de aderência à tração e ao cisalhamento de revestimentos de argamassa em substratos de concreto*". Dissertação Mestrado em Engenharia Civil, Universidade Federal de Goiás, p. 321.

Carasek, H. (2010), Argamassas. In: ISAIA, G. C. (Ed.). *"Materiais de Construção Civil e Princípios de Ciência e Engenharia de Materiais"*. IBRACON, São Paulo, p.1-37.

Carrasco, B., Cruz, N., Terrados, J., Corpas, F. A., Pérez, L. (2014), *An evaluation of bottom ash from plant biomass as a replacement for cement in building blocks.* Fuel Processing Technology. 118:272-280. https://doi.org/10.1016/j.fuel.2013.10.077

Chatveera, B., Lertwattanaruk, P. (2014), *Evaluation of nitric and acetic acid resistance of cement mortars containing high-volume black rice husk ash.* Journal of Environmental Management. 133:365-373. https://doi.org/10.1016/j.jenvman.2013.12.010

Chowdhury, S., Mishra, M., Suganya, O. (2015), *The incorporation of wood waste ash as a partial cement replacement material for making structural grade concrete: An overview.* Ain Shams Engineering Journal. 6 (2):429-437. https://doi.org/10.1016/j.asej.2014.11.005

de Souza, L. M. S., Fairbairn, E. M. R., Filho, R. D. T., Cordeiro, G. C. (2014), *Influence of initial CaO/SiO$_2$ ratio on the hydration of rice husk ash-Ca(OH)$_2$ and sugar cane bagasse ash-Ca(OH)$_2$ pastes.* Química Nova. 37 (10):1600-16605. http://dx.doi.org/10.5935/0100-4042.20140258

Dubaj, E. (2000), *"Estudo comparativo entre traços de argamassa de revestimento utilizadas em Porto Alegre"*. Dissertação Mestrado em Engenharia Civil, Universidade Federal do Rio Grande do Sul, p. 115.

Gonçalves, C. F., Soares, A. F., Paula, H. M.

Elinwa, A. U., Ejeh, S. P. (2003), *Effects of incorporation of sawdust incineration fly ash in cement pastes and mortars.* Asian Architecture Build Eng. 3:1-7. http://dx.doi.org/10.3130/jaabe.3.1

Esteves, T. C., Rajamma, R., Soares D., Silva, A. S., Ferreira, V. M., Labrincha, J. A. (2012), *Use of biomass fly ash for mitigation of alkali-silica reaction of cement mortars.* Construction and Building Materials. 26:687-693. https://doi.org/10.1016/j.conbuildmat.2011.06.075

Fernandes, I. J., Calheiro, D., Kieling, A. G., Moraes, C. A. M., Rocha, T. L. A. C., Brehm, F. A., Modolo, R. C. E. (2016), *Characterization of rice husk ash produced using different biomass combustion techniques for energy.* Fuel Processing Technology. 165:351-359. https://doi.org/10.1016/j.fuel.2015.10.086

Garcia, M. L., Sousa-Coutinho, J. (2013), *Strength and durability of cement with forest waste bottom ash.* Construction and Building Materials. 41:897–910. https://doi.org/10.1016/j.conbuildmat.2012.11.081

Gluitz, A. C., Marafão, D. (2013), "*Utilização da cinza da madeira de eucalipto na substituição parcial do cimento Portland em argamassa".* Trabalho de Conclusão de Curso, Universidade Tecnológica Federal do Paraná, p. 53.

Hossain, M. M., Karim, M. R., Hasan, M. K., Zain, M. F. M. (2016), *Durability of mortar and concrete made up of pozzolans as a partial replacement of cement: A review.* Construction and Building Materials. 116:128-140. https://doi.org/10.1016/j.conbuildmat.2016.04.147

Isaia, G. C., Gastaldini, A. L. G., Moraes, R. (2003), *Physical and pozzolanic action of mineral additions on the mechanical strength of high-performance concrete.* Cement and Concrete Composites. 25:69-76. https://doi.org/10.1016/S0958-9465(01)00057-9

Jamil, M., Khan, M. N. N., Karim, M. R., Kaish, A. B. M. A., Zain, M. F. M. (2016), *Physical and chemical contributions of Rice Husk Ash on the properties of mortar.* Construction and Building Materials. 128:185-198. https://doi.org/10.1016/j.conbuildmat.2016.10.029

Kazmi, S. M. S., Munir, M. J., Patnaikuni, I., Wu, F. (2017), *Pozzolanic reaction of sugarcane bagasse ash and tis role in controlling alkali silica reaction.* Construction and Building Materials. 148:231-240. https://doi.org/10.1016/j.conbuildmat.2017.05.025

Khan, M. N. N., Jamil, M., Karim, M. R., Zain, M. F. M., Kaish, A. B. M. A. (2017), *Filler Effect of Pozzolanic Materials on the Strength and Microstructure Development of Mortar.* Journal of Civil Engineering. 21:274-284. https://doi.org/10.1007/s12205-016-0737-5

Martirena, F., Monzó, J. (2017), *Vegetable ashes as Supplementary Cementitious Materials.* Cement and Concrete Research. https://doi.org/10.1016/j.cemconres.2017.08.015

Mauri, J., Ruiz, H. A., Raphael, B. A. F., Ker, J. C., Rezende, L. R. M. (2011), *Dispersantes químicos na análise granulométrica de latossolos.* Revista Brasileira de Ciência do Solo. 34:1277-1284. https://doi.org/10.1590/S0100-06832011000400021

Modolo, R. C. E., Silva, T., Senff, L., Tarelho, L. A. C., Labrincha, J. A., Ferreira, V. M., Silva, L. (2015), *Bottom ash from biomass combustion in BFB and its use in adhesive-mortars.* Fuel Processing Technology. 129:192-202. https://doi.org/10.1016/j.fuproc.2014.09.015

Netto, R. M. (2006), "*Materiais pozolânicos".* Dissertação Mestrado em Construção Civil, Universidade Federal de Minas Gerais, p.149.

Noor-Ul-Amin, S. (2014), *A multi-directional utilization of different ashes.* Royal Society of Chemistry Advances. 4(107):62769–62788. https://doi.org/10.1039/C4RA06568A

Prasara-a, J., Gheewala, S. H. (2017), *Sustainable utilization of rice husk ash from power plants: A review.* Journal of Cleaner Production. 167:1020-1028. https://doi.org/10.1016/j.jclepro.2016.11.042

Rajamma, R., Ball, R. J., Tarelho, L. A. C., Allen, G. C., Labrincha, J. A., Ferreira, V. M. (2009), *Characterization and use of biomass fly ash in cement-based materials.* Journal of Hazardous Materials. 172(2-3):1049-1060. https://doi.org/10.1016/j.jhazmat.2009.07.109

Rajamma, R., Senff, L., Ribeiro, J. A., Ball, R. J., Aleen, G. C., Ferreira, V. M. (2015), *Biomass*

fly ash effect on fresh and hardened state properties of cement-based materials". Composites Part B: Engineering. 77:1-9. https://doi.org/10.1016/j.compositesb.2015.03.019

Ramos, T., Matos, A. M., Sousa-Coutinho, J. (2013), *Mortar with wood waste ash: Mechanical strength carbonation resistance and ASR expansion.* Construction and Building Materials. 49:343–351. https://doi.org/10.1016/j.conbuildmat.2013.08.026

Resende, D. S. (2013), "*Estudo do efeito da incorporação de cinzas de cavaco de eucalipto como material cimentício suplementar".* Tese Doutorado em Engenharia de Materiais, Universidade Federal de Ouro Preto, p. 168.

Rosales, J., Cabrera, M., Beltrán, M. G., López, M., Agrela, F. (2017), *Effects of treatments on biomass bottom ash applied to the manufacture of cement mortars*. Journal of Cleaner Production. 154:424-435. https://doi.org/10.1016/j.jclepro.2017.04.024

Roselló, J., Soriano, L., Santamarina, M. P., Akasaki, J.L., Monzó, J., Payá, J. (2017), *Rice straw ash: A potential pozzolanic supplementary material for cementing systems.* Industrial Crops and Products. 103:39-50. https://doi.org/10.1016/j.indcrop.2017.03.030

Salvo, M., Rizzo, M. C., Novajra, G., Canonico, F., Bianchi, M., Ferraris, M. (2015), *Biomass ash as supplementary cementitious material (SCM).* Advances in Applied Ceramics. 114:S3-S10. https://doi.org/10.1179/1743676115Y.0000000043

Ukrainczyk, N., Vrbos, N., Koenders, E. A. B. (2016), *Reuse of Woody Biomass Ash Waste in Cementitious Materials.* Chemical and Biochemical Engineering Quarterly. 30(2):137-148. http://dx.doi.org/10.15255/CABEQ.2015.2231

Wang, S. (2015), *Cofired biomass fly ashes in mortar: Reduction of Alkali Silica Reaction (ASR) expansion, pore solution chemistry and the effects on compressive strength.* Construction and Building Materials. 82:123-132. https://doi.org/10.1016/j.conbuildmat.2015.02.021

Xu, W., Lo, Y. T., Ouyang, D., Memon, A., Xing, F., Wang, W., Yuan, X. (2015), *Effect of rice husk ash fineness on porosity and hydration reaction of blended cement paste.* Construction and Building Materials. 89:90-101. https://doi.org/10.1016/j.conbuildmat.2015.04.030

Zajac, G., Szyszlak-Bargłowicz, J., Gołebiowski, W., Szczepanik, M. (2018), *Chemical Characteristics of Biomass Ashes.* Energies. 11(11):2-15. https://doi.org/10.3390/en11112885

Durability analysis of reinforced concrete with loading induced cracks

S. M. M. Pinheiro[1] (iD), M. P. Costa Junior[1]* (iD)

*Contact author: milton.paulino@gmail.com

DOI: https://doi.org/10.21041/ra.v11i2.510

ABSTRACT

The objective of this study is to verify the relationship between the action of loads inducing cracks and the durability of reinforced concrete. Prismatic specimens were produced and for two years these samples were subjected to artificial salt spray, under the action of different types of loading and unloaded (reference), with moist curing for 7 days. Chloride penetration tests and microstructural analysis were carried out. It was observed that loading did not influence the results of chloride penetration. However, it was observed that in the micrographs and microanalysis of the cracked samples the clearer formation of deterioration products and possible microorganisms, compared to the samples that did not suffer loading.

Keywords: durability; loading; cracking; chlorides; microscopy.

---

[1] Departamento de Engenharia Civil, Universidade Federal do Espírito Santo, Vitória, Brasil.

Contribution of each author

In this work, the author M. P. Costa Junior contributed with the activities of conceptualization, development, results and discussion, writing and preparation of the original text; S. M. M. Pinheiro contributed to the activities of conceptualization, development, results and discussion.

Discussions and subsequent corrections to the publication

Any dispute, including the replies of the authors, will be published in the second issue of 2022 provided that the information is received before the closing of the first issue of 2022.

Análise da durabilidade de concreto armado com fissuras induzidas por carregamento

RESUMO

O objetivo desse trabalho é verificar a relação entre a ação de carregamentos induzindo fissuras e a durabilidade do concreto armado. Foram produzidos corpos-de-prova prismáticos e durante o período de dois anos estas amostras foram submetidas à névoa salina artificial, estando sob a ação de carregamento central permanente, carregamento central de curta duração e sem carregamento (referência), sendo realizados ensaios de penetração de cloretos e análise microestrutural, além do mapeamento das fissuras. Verificou-se que o carregamento não influenciou nos resultados de penetração de cloretos, porém, nas micrografias e microanálises das amostras fissuradas observou-se a formação de produtos de deterioração e possíveis microorganismos, em comparação aos corpos-de-prova que não sofreram carregamento.
Palavras-chave: durabilidade; carregamento; fissura; cloretos; microscopia.

Análisis de durabilidad del hormigón armado con fisuras inducidas por la carga

RESUMEN

El objetivo de este trabajo es verificar la relación entre la acción de cargas que inducen fisuras y la durabilidad del hormigón armado. Fueron producidos modelos de prueba (especímenes) prismáticos y durante dos años estas muestras fueron sometidas a niebla salina artificial, bajo la acción de una carga central permanente, carga central a corto plazo sin carga (referencia), con un curado de 7 días. Se realizaron pruebas de penetración de cloruros y análisis microestructurales, además del mapeo de fisuras. Se encontró que la carga no influyó en los resultados de penetración de cloruros, sin embargo, se observa que las micrografías y microanálisis muestran una formación de productos de deterioro y posibles microorganismos, en comparación con las probetas que no sufrieron carga.
Palabras clave: durabilidad; carga; craqueo; cloruros; microscopía.

1. INTRODUCTION

The causes of the deterioration process of reinforced concrete are directly related to the action of aggressive agents. Among the various existing agents (carbon dioxide, chloride ions and sulphate attack), there is the deleterious action of chlorides and carbon dioxide (CO2), which have been extensively studied in recent years and which are still a great challenge for the good performance of reinforced concrete structures. Thus, the structures that are exposed to the marine and urban environment demand a minimum quality of the material to ensure its design life and durability (Andrade, 2005; Cascudo, 2005; Silvestro et al., 2021).

In addition to chemical causes, the causes of the mechanical deterioration process are highlighted, such as overload and cyclical loads; whose main symptom is concrete cracking. These cracks must be controlled for three main reasons: durability due to the risk of corrosion of the reinforcement, aesthetic appearance, and functional requirements such as hygiene (proliferation of fungi, microorganisms, etc.) and permeability to gases and water (Ghali and Favre, 1994; Hearn and Figg, 2001).

Under natural exposure conditions, the durability of concrete is controlled by its ability to prevent the transport of ions and fluids. Concrete is often subject to several types of stress (thermal, mechanical, etc.) that generate tensile stresses that exceed the material's resistance, generating cracks, which can affect the transport of aggressive agents to the mixture (Lim et al., 2000; Hearn and Figg, 2001; Mehta and Monteiro, 2014).

Cracks manifested due to the action of external loads can act as an important factor for the entry of aggressive agents such as chloride ions and CO_2 (carbonation). However, studies show that cracks are not the biggest factor for deterioration of the structure by corrosion (entry of aggressive agents) if they do not exceed the openings stipulated by international standards and NBR 6118 (ABNT, 2014). In this case, the quality of the covering concrete and the nominal covering itself are more relevant to its durability (Konin et al., 1998; Helene and Diniz, 2001; Alexander et al., 2001; Cascudo, 2005).

Regardless of loading, the characteristics of cracks (connectivity, opening, width, length) play a fundamental role in the durability of concrete structures. In this sense, NBR 6118 (ABNT, 2014) establishes the maximum characteristic opening for cracking (identified in the standard as Wk) and protection of reinforcement in terms of durability. This standard defines the maximum crack opening of 0.4mm for reinforced concrete, which varies depending on the class of environmental aggressiveness, the type of concrete structure and the combinations of service actions.

The penetration and diffusion of chloride ions can occur through the crack as shown in Figure 1.
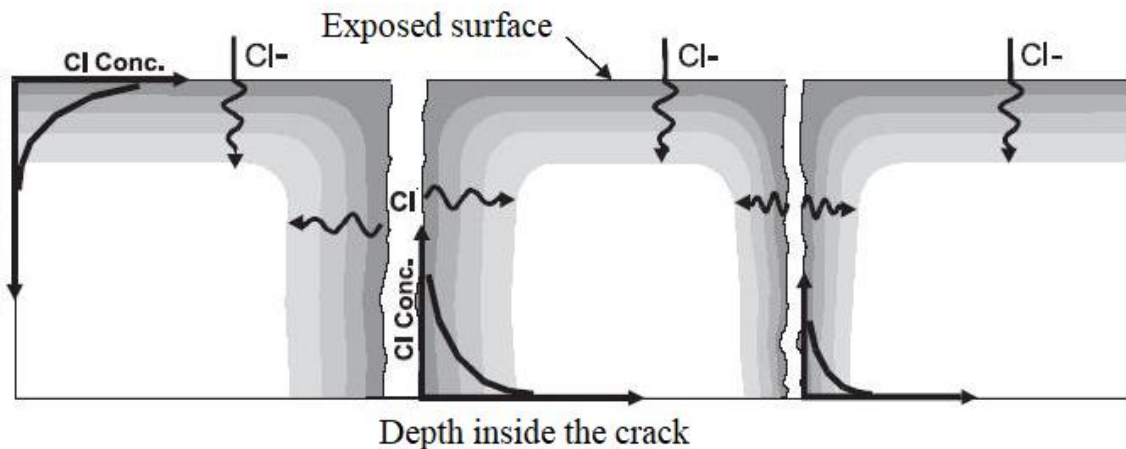

Figure 1. Penetration of chlorides on the surface and between cracks (Ismail et al., 2006).

Cracks act as a gateway for aggressive agents, which have a significant effect on the diffusion of chlorides, as they facilitate the movement of these agents through concrete, the intensity of which is directly dependent on crack opening (Wang et al., 2016).

When the chloride ions are inside the crack, they can penetrate at different depths, starting from the surface inside, becoming dissolved in the aqueous phase of the pores, forming the free chlorides, which can trigger the process of material deterioration. It is also observed that the concentration of chlorides is high on the exposed surface of the concrete. However, when it penetrates the crack opening, it decreases with the increase in depth from the surface of the material (Ismail et al., 2006; Figueredo, 2005; Win et al., 2004).

In addition to free chlorides in concrete pore solutions, you can also find them: chemically combined with CSH, or as chloroaluminates, physically adsorbed to pore walls or free in concrete pore solutions (Romano, 2009; Crauss, 2010).

Of the chloride ions that penetrate the concrete, part binds to tricalcium aluminate (C_3A) forming mainly calcium chloroaluminate, also known as Friedel's salt - $C_3A.CaCl_2.10H_2O$, which is incorporated into the hydrated cement phases. Another part is absorbed on the surface of the pores and the rest is dissolved in the aqueous phase of the pores, which form the free chlorides that are dangerous and cause damage to the structure (Helmuth and Stark, 1992; Figueredo, 2005; Crauss, 2010).

In general, there will always be a state of balance between the three forms of occurrence of these ions, so that there will always be a certain content of free Cl$^-$ in the liquid phase of the concrete (Helmut and Stark, 1992; Fortes and Andrade, 1995; Cascudo, 1997). Cements with low levels of C_3A have less ability to immobilize chloride ions by the formation of hydrated calcium chloroaluminate. With the formation of this compound, there is a decrease in the concentration of free chloride ions in the aqueous solution of the concrete pores.

The penetration of chlorides in the form of free chlorides depends on factors such as the type of positive ions (cations) associated with the chlorides, the moment of access to the concrete before or after it hardens, the presence of another negative ion (anion) such as sulfate, the type of cement used in the production of concrete, the quality of concrete production and curing, the ambient humidity, the water/cement ratio, the carbonation state and the consumption of cement per m^3 of concrete. Analyzing the resistance to the penetration of chloride ions, Leng et al. (2000) and Oh et al. (2002) found that the diffusion of chloride ions increases with the increase in the water/cement ratio, and cements with fly ash and blast furnace slag have high resistance to diffusion (Helene, 1997; Song et al., 2008; Lawrence, 2006).

In this context, this article presents an analysis of the durability in reinforced concrete under different loading conditions, during a period of 24 months. Depth of penetration of chloride ions was analyzed, in addition to the microstructural analysis.

2. PROCEDURE

The experimental program was carried out following these steps: characterization of the material and dosage of the specimens. After dosing, two types of specimens were molded (prismatic and cylindrical).

After molding and deformation, the prismatic specimens underwent wet curing for 7 days, then different types of loads were applied and they were subjected to salt spray, in a natural environment until the test dates (ages 6, 12, 18 and 24 months). At these ages, chloride depths were evaluated, and Microstructural Analysis (SEM and EDS) was performed.

As for the cylindrical specimens, after molding, they were deformed and cured (wet curing) for 28 days. At the end of this period, tests of axial compression strength were performed.

The study ended with the analysis of the results and final considerations. All these steps will be

more detailed below.

As for the materials, the Portland cement used in this study was CP III 40-RS (Portland Blast Furnace cement), whose granular slag content of blast furnace in the cement can reach 75%. The following materials were used for the composition of the mixture: river sand (medium), available and used in the region of Campinas - SP, crushed stone 9.5 / 25 (B1 - basalt) with a maximum characteristic dimension of 19mm and polyfunctional base additive of lignosulfonate, with a specific mass of 1.18 g / cm³. In the production of the prismatic concrete specimens, a CA50 steel bar with a nominal diameter of 10 mm was used.

The experimental mixtures were chosen according to the dosage of the concrete used in this research, whose proportion of agglomerate;aggregates adopted was 1:5. In this sense, meeting this requirement, the adopted mix was 1: 2: 3 (cement: sand: gravel) (in mass), with a water / cement ratio of 0.42.

The choice of cement: sand: gravel ratio of 1: 2: 3 was due to its good mortar content. The water / cement ratio of 0.42 was adopted to obtain more resistant concrete when exposed to aggressive media, according to NBR 6118 (ABNT, 2014). The class adopted for the cast concrete in this study was C50. The mix and the water/cement ratio adopted in this study have been used and evaluated since 2000 within the research project on durability of the covering layer, at Unicamp's building materials laboratory.

The amount of additive used was necessary to maintain an adequate workability for the molding of the specimens on a vibrating table, due to the low water/cement ratio used. The consistency index, determined by the slump test (4 ± 1 cm), was found by means of a cone trunk (according to NBR 16889, 2020). This abatement value, although not widely used in current studies, was adopted for concrete, since it was desired to obtain a minimum workability in which the concrete was molded to produce prismatic specimens with mechanical vibration.

The consumption of materials used for the molding of the prismatic and cylindrical specimens can be seen in table 1.

Table 1. Specification of the materials used in the experimental study.

	Cement (Kg/m³)	Additive (Kg/m³)	Sand (Kg/m³)	Gravel (Kg/m³)	Water (Kg/m³)
1 : 2 : 3 : 0,42	398	2,4	796	1194	167

Cylindrical specimens were used to characterize the concrete, evaluating its mechanical property (resistance to axial compression) (Table 2).

Table 2. Series of cylindrical specimens.

Series	Type or curing	Date of test
M6um	Immersed until the test date	28 days
M12um		
M18um		
M24um		

The mixture used was mechanical, using a concrete mixer with an inclined axis. For each series, 4 cylindrical specimens with 10 cm in diameter and 20 cm in height were molded and tested at the age of 28 days, according to NBR 5739 (ABNT, 2018). The specimens were molded in two layers, on a vibrating table, in the time necessary to allow adequate compaction of the concrete in the mold, according to NBR 5738 (ABNT, 2015).

After molding, the specimens were covered with plastic canvas until the moment of deformation, which occurred 48 hours after the moment of molding. This release period was adopted due to the deformation of the prismatic specimens. Then, the specimens were subjected to immersed curing for 28 days.

Six prismatic specimens were molded for each age (6, 12, 18 and 24 months), 2 specimens of the sample without loading, 2 specimens of the sample under central loading of short duration and 2 specimens of the sample under permanent central loading, in the dimensions of 1.39x0.1x0.1m. The molds were defined in these dimensions because they are the same used in other research studies carried out at Unicamp's Building Materials Laboratory.

The mixing of the concrete to produce prismatic specimens was mechanical in a concrete mixer with an inclined axis. A CA50 steel bar with a nominal diameter of 10 mm (Ø 10), with a nominal coverage of 30 mm was used, although steel corrosion is not the scope of this work. The coverage adopted (30 mm) was defined according to the study carried out by Martins (2001), in addition to the study by Midness and Young (1981), Illston (1994), Alexander et al. (2001) and Figueiredo and Nepomuceno (2004).

The prismatic specimens were molded two by two. To maintain coverage, 3 spacers of 30 mm were placed along the steel bar. Figure 2 shows the dimensions of the prismatic specimen and the position of the steel bar.
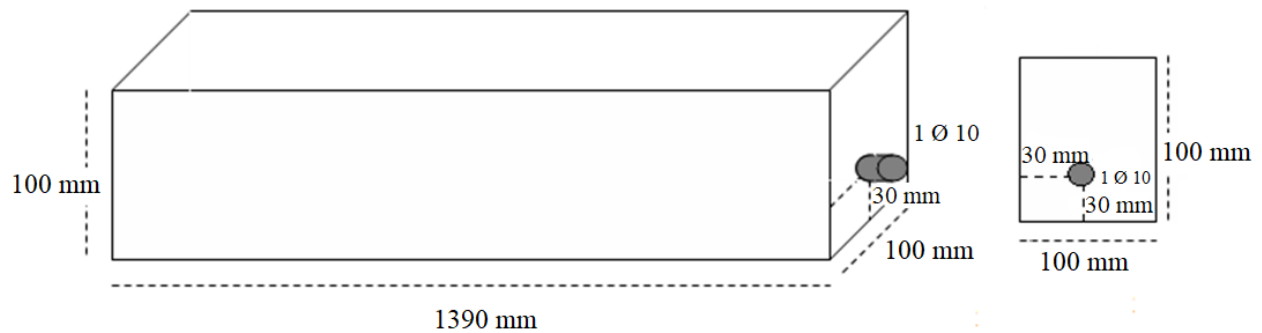
Figure 2. Scheme of dimensions of the prismatic specimens.

After molding, the prismatic specimens remained in the molds for 48 hours, covered with plastic canvas. This time was adopted because it was not possible to deform and mainly to transport these specimens before 48 hours, as they cracked during handling.

After this period, they underwent wet curing, when they were immersed in lime-saturated water until the age of 7 days. This period was defined based on the recommendations of Thomaz (2005), Castro (2003), Braun (2003) and ACI 308 (2016), which determined at least 7 days of curing, regardless of the type of cement adopted. In addition to the references, the age of 7 days of curing was adopted because this is the term used in Brazilian studies for curing structural pieces.

The way of loading the prismatic specimens was defined, which would be according to the following situations:

- Without loading (SC). It was adopted to serve as a reference in the comparison between the two other types of loading.
- Short-term central charging (CCCD). Application of a concentrated force P to the prismatic specimen until the first crack appears, and then removed. We opted for the choice of this load to check the performance of the concrete in a situation of cracks that may arise over the life of the structure due to the action of point loads, that is, cases in which there is a short-term overload on the structure, with the appearance of cracks. In this case, as the loading is of short duration, the crack may disappear when loading is removed, but stresses and internal micro-cracks in the material have already occurred.

- Permanent central loading (CCP). The prismatic specimens were loaded until the date of durability tests. This type of loading was chosen so that the prismatic specimen had superficial cracks and remained open throughout the exposure period, until the test dates. Thus, on the test dates, the influence of the crack on the depth of chloride penetration and on the microstructure of the concrete can be observed.

For the maximum crack opening, the limit established by the NBR 6118 standard (ABNT, 2014) for durability, related to cracking and protection of the reinforcement, according to the class of environmental aggressiveness, was adopted as a parameter. Thus, the maximum crack opening in the prismatic specimens, which were under constant loading, was between 0.3 mm and 0.4 mm (Figure 3). The openings of cracks were mapped over time, up to the test date of the specimens.

Figure 3. Measurement of the crack opening in the center of the prismatic specimen with a crack meter.

The prismatic specimens were under constant loading until the test dates. The diagram shown in Figure 4 shows the prismatic specimens supported by cylindrical concrete specimens (10 x 20 cm) with a central porch composed of two steel plates and two threaded bars (9.5 mm, 3 nuts, 3 washers and two steel plates of 8 x 300 x 100 mm) applying the load of 250 kgf, causing holes in the center of the beams, with openings of up to 0.3 mm (within the limits of the NBR 6118 standard). The loading was carried out by applying a torque of 0.5 Kgfm, with a torque wrench, to the threaded bars and, consequently, the concentrated force was applied to the prismatic specimen causing the crack.
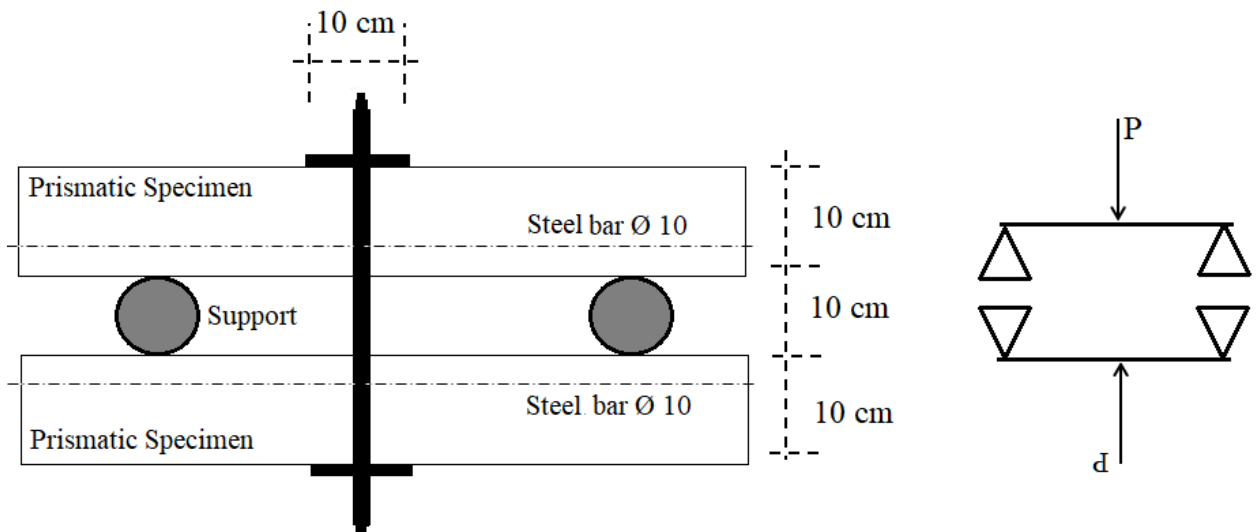
Figure 4. Permanent central loading (CCP) in the prisms.

Table 3 shows the sequence adopted for the samples of each molding series, under different loading conditions and durability test dates.

Table 3. Samples of each molding series, under loading conditions.

Sample	Sample Without loading	Sample under Loading Short Term Center	Sample under Permanent Central Loading	Date of trial
M6um	M6umSC	M6umCCCD	M6umCCP	06 months
M12um	M12umSC	M12umCCCD	M12umCCP	12 months
M18um	M18umSC	M18umCCCD	M18umCCP	18 months
M24um	M24umSC	M24umCCCD	M24umCCP	24 months

After a seven-day wet curing, the specimens passed through saline mist until the test age. The purpose of the mist was to simulate a saline environment. In that sense, a solution of NaCl was manually sprayed on the prismatic specimens until their moistening, with a periodicity of 3 times a week and three times a day.

The salt concentration in sea water is 35 grams of NaCl for each liter of water. In this sense, this amount of 35 g/l of NaCl was used for the solution simulating the salt spray.

The spraying of the chloride solution occurred until the testing dates for the prismatic specimens. The choice of this methodology was based on the study by Arya and Darko (1996), who carried out corrosion tests on concrete beams using the same procedure.

To determine the depth of penetration of chlorides, the cross section of the samples was broken, whose evaluation is carried out by spraying silver nitrate (0.1N solution) on the concrete surface, causing a photochemical reaction, where the free chlorides present in the concrete react with the silver ions of the silver nitrate solution to form a white precipitate. In areas where there are no combined chloride or chloride ions, there is the appearance of a brown color, the silver oxide, due to the reaction between the silver ions and the hydroxyls present in the pores of the cementitious material (Jucá et al., 2002; Real et al., 2015). Through this method, the objective is to evaluate whether the chloride front has reached the reinforcement. The steps of the test can be seen in Figure 5.

The cut in these prismatic specimens was carried out in the middle thirds, where you can see the compressed and stretched areas of the prismatic specimens.

24

Durability analysis of reinforced concrete with loading induced cracks
Pinheiro, S. M. M., Costa Junior, M. P.

Figure 5. Chloride penetration tests with silver nitrate spray.

For the microstructural analysis, samples were taken from the prismatic specimens immediately after they were cut or ruptured and before the durability tests were performed, so that the samples were not contaminated with silver nitrate solutions (Figure 6). In this study, only the results of microstructural analysis were presented at 6 months and 24 months, which were the first and last ages of trials, respectively.

The samples were taken from the covering areas, with a maximum depth of 1.5 cm. Samples were taken from cracked specimens, in the cracked area (the sample was taken exactly at the crack opening or the closest to it), always in the ruptured region of the prismatic specimen, to be observed by SEM. Since concrete is not a conductive material, the samples had to be metallized with gold. These samples were taken with a steel chisel and hammer. The observations were made at the National Laboratory of Luz Sincontron (LNLS), in Campinas, State of São Paulo.

The energy measure (EDS) was adopted in this study. In this case, there is the advantage of quick identification of the chemical elements present (Dedavid et al., 2007).

Area where the sample was removed for microstructure tests.
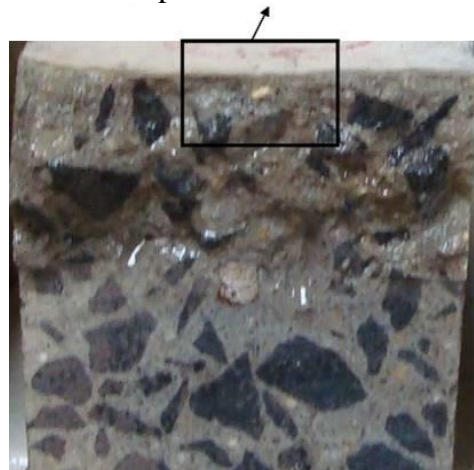
Figure 6. Place where the sample was taken for microstructure tests.

The results obtained were analyzed using descriptive statistics techniques (calculation of the mean, standard deviation) to characterize the variables (concrete properties and behavior regarding chlorides).

To determine statistically significant differences (the level of significance adopted was 5%)

between the averages of the results, parametric hypothesis tests -ANOVA and DUCAN (Montgomery, 1991) were used.

The stat graphics program was used to perform the statistical tests. The program built several tests to compare the chloride penetration averages between all samples. The F test of the ANOVA table verified if there are significant differences between the averages of the results, in relation to the types of cure and loading.

3. RESULTS

The results of resistance to axial compression at 28 days of age of the concrete, referring to the moldings made on the cylindrical specimens are shown in Table 4.

Table 4. Results of resistance to axial compression.

Concrete (cylindrical specimens)	Curing of cylindrical specimens	Age of rupture	Resistance to axial compression (MPa)	Standard deviation	Coefficient of variation
M6um	Immersed up to 28 days	28 days	66.2	4.3	6.6
M12um			50.2	2.6	5.3
M18um			59.7	4.1	7.0
M24um			56.8	2.6	4.6

As it can be seen in Table 4, the averages of the results of resistance to axial compression were in the range of 44 MPa to 66 MPa and the results decrease in this order: M6um, M18um, M24um, M12um. This difference in results may have been caused by several reasons, such as temperature and humidity at the time of molding, as well as the transportation, mixing, casting, densification and curing of the concrete used.

As for the variation coefficient, when using the parameter of the ACI 214R (2002) standard to verify how the variation attributed to sampling, sample preparation, curing and laboratory testing was, it is observed that, in the classification presented by this standard, the coefficient of variation of the M12um and M24um samples are considered good (<5.5), with the exception of the M18um and M6um samples, which despite high resistance values, are considered weak (> 5.5).

As verified in the literature, the compressive strength of concretes with the use of cements with high levels of slag tends to increase with time and the resistance gain can occur in longer periods. Studies, such as the one by Khatib and Hibbert (2005), point to an even greater growth after 28 days of age. In this sense, one can expect an even greater improvement in the resistance results of this study.

Throughout the period that the prismatic specimens submitted to permanent central loading were exposed in the environment, mapping of the cracks was performed, as shown in Figure 7 (6 months old) and Figure 8 (24 months old).

26

Durability analysis of reinforced concrete with loading induced cracks
Pinheiro, S. M. M., Costa Junior, M. P.
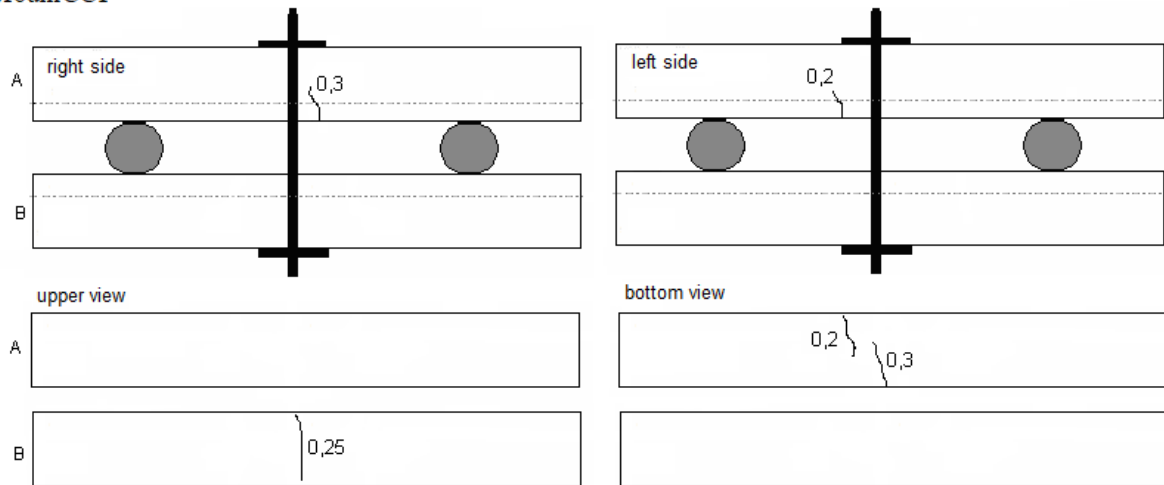
M6umCCP

Figure 7. Mapping of cracks in concretes that have been under permanent central loading for 6 months (M6umCCP).

The M6umCCP concretes in Figure 7 had crack openings of 0.2 mm and 0.3 mm. Over the exposure period there was an increase of 0.3 mm to 0.4 mm and 0.25 mm to 0.35 mm.

M24umCCP
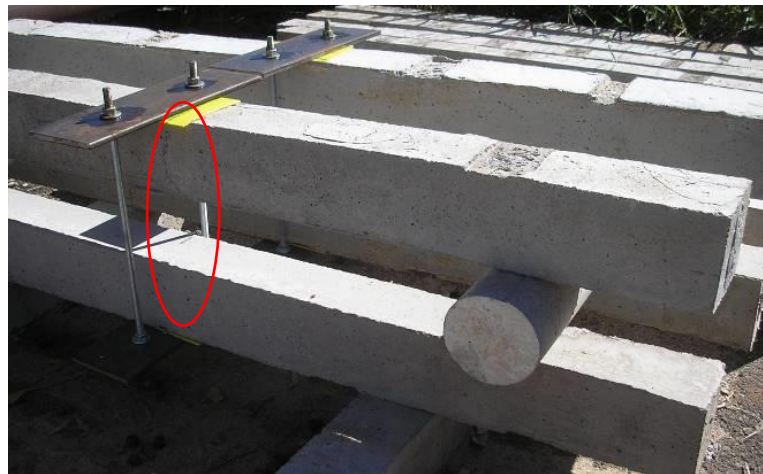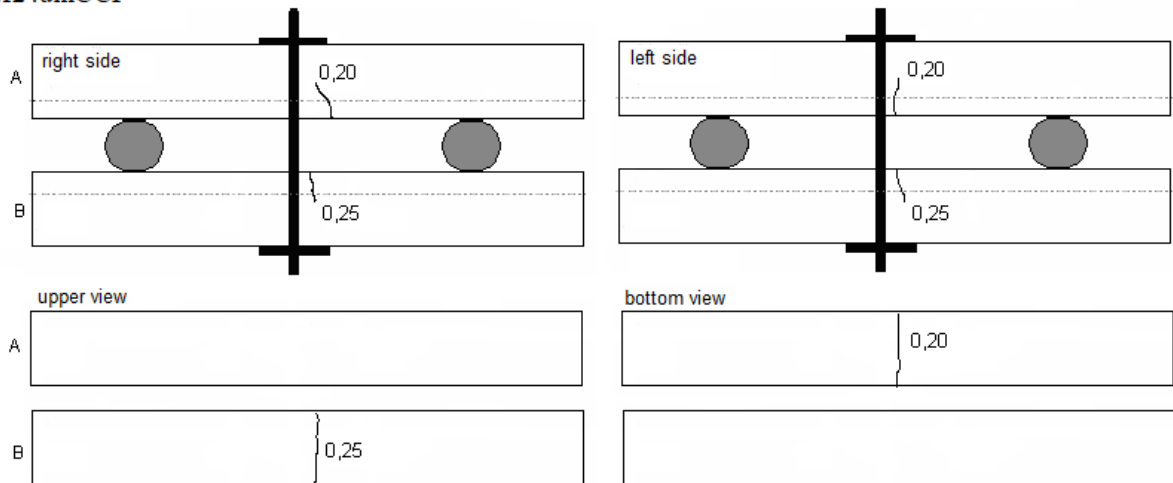
Figure 8. Mapping of cracks in concretes that have been under permanent central loading for 24 months (M24umCCP).

It was observed in the first six months of age that the gantry used for the application of the loading, as well as the monitoring of the crack opening was effective, since the crack opening was in the range of 0.3 mm and 0.4 mm, as outlined in the experimental program.

The cracks in the M24umCCP prismatic specimens (subjected to wet curing) had openings ranging from 0.20 mm to 0.25 m. At 24 months, the behavior of the fissures was like that of other ages. The initial openings were from 0.2 mm to 0.25 mm, reaching 0.4mm at the test ages.

Some factors may have caused the increase of crack openings in the specimens over time, among which we can highlight the load permanently applied to these concretes and the time they were subjected to this load. It was expected that the crack opening would not remain constant due to the material's own properties (such as creep), even with the support of the steel bar. The torque applied to the specimens may also have influenced the crack openings, because although the torque value has been defined experimentally, each concrete (at the ages of testing and curing) may present different responses, as observed in the mapping, in which some samples had larger crack openings. In studies carried out by Vidal et al. (2004; 2007) and François et al. (2006), which mapped crack openings resulting from loading, under saline environment for 14 and 17 years, respectively, two types of cracks can be observed: the transversal, induced by the loading action (bending); and the longitudinal ones in the beam that refer to the corrosion of the reinforcement, that is, cracks that coincide with the reinforcement.

3.1 Depth of chloride penetration

Table 5 shows the results of depth of penetration of chlorides in concretes without loading, under short-term central loading and under permanent central loading.

Table 5. Depth of penetration of chlorides under different loading conditions and without load application.

Sample	Average (mm)	Standard deviation
M6umSC	0.1	0.1
M12umSC	2.2	0.6
M18umSC	2.3	1.3
M24umSC	2.6	0.7
M6umCCCD	0.2	0.0
M12umCCCD	2.2	0.7
M18umCCCD	1.9	1.1
M24umCCCD	2.5	0.6
M6umCCP	3.3	1.8
M12umCCP	1.7	0.8
M18umCCP	0.3	0.0
M24umCCP	3.0	1.0

Table 6 shows the statistical comparisons between the three types of loading used in this study: one-off permanent loading - CCP, short-term loading - CCCD, without loading - SC, at the different test ages, for the results of chloride penetration.

28

Durability analysis of reinforced concrete with loading induced cracks
Pinheiro, S. M. M., Costa Junior, M. P.

Table 6. Comparison among the results of chloride penetration.

Concrete (concrete bodies) prismatic test)	Test Age	Difference between results of chloride penetration
M6umCCP – M6umCCCD	6 months	No (chloride penetration CCP > chloride penetration CCCD)
M6umCCP – M6umSC		No (chloride penetration CCP > chloride penetration SC)
M6umCCCD - M6umSC		No (chloride penetration CCCD > chloride penetration SC)
M12umCCP – M12umCCCD	12 months	No (chloride penetration CCP < chloride penetration CCCD)
M12umCCP – M12umSC		No (chloride penetration CCP < chloride penetration SC)
M12umCCCD – M12umSC		No (chloride penetration CCCD = chloride penetration SC)
M18umCCP – M18umCCCD	18 months	No (chloride penetration CCP < chloride penetration CCCD)
M18umCCP – M18umSC		No (chloride penetration CCP < chloride penetration SC)
M18umCCCD – M18umSC		No (chloride penetration CCCD < chloride penetration SC)
M24umCCP – M24umCCCD	24 months	No (chloride penetration CCP > chloride penetration CCCD)
M24umCCP – M24umSC		No (chloride penetration CCP > chloride penetration SC)
M24umCCCD – M24umSC		No (chloride penetration CCCD < chloride penetration SC)

At 6 months and 24 months, chloride penetration was higher in concretes subjected to permanent central loading compared to concretes under short-term central loading and without loading; however, in these cases there was no significant difference between the results. At 12 months of age, concretes with permanent central loading had lower chloride penetration values than concretes subjected to short-term loading and without loading, in which case there were also no significant differences between the results.

Over 24 months of age, the loading action, whether short-term or permanent, did not significantly influence the results of chloride penetration in almost all studied ages.

When comparing these results with those obtained in research by Vidal et al. (2004), Vidal et al. (2007) and François et al. (2006), it is observed that the time factor and the saline environment are fundamental for the loading and, consequently, the opening of cracks, influences the results of penetration of chlorides. Research such as that by Vidal et al. (2007), which left the samples exposed in environments under salt spray for longer than 10 years, obtained significant results only after 5 years of exposure. In this sense, longer periods should be considered in future research.

By analyzing the behavior of samples with different percentages of blast furnace slag, subjected to continuous loading, An Cheng et al. (2005) found that crack opening affects the time of onset of reinforcement corrosion. The specimens with the greatest crack opening were the ones that started the corrosive process. However, the amount of slag added to the mixture did not influence the results, that is, with the increase in the blast furnace slag content there was no decrease in the speed and propagation of reinforcement corrosion.

According to Ayra and Darko (1996), the frequency of the appearance of cracks has an influence on the intensity of corrosion that the structure is subjected to. The greater the number of cracks, the greater the intensity of corrosion in reinforced concrete. A fact to be highlighted, in this case, is the importance of the concrete cover to reduce this process. Likewise, this thickness can be as important a factor in this context as the incidence of cracks in the structure itself. Thus, attention is paid to the importance of studies on covering concrete, which makes it possible to obtain relevant information that contributes to the production of durable concrete.

As for the curing period adopted, Thomaz (2005) found that the wet curing time of 7 days is sufficient for the concrete to acquire the desired properties. However, this period depends on the type of cement and the water/cement ratio used. However, when using cements with mineral additions, longer curing time is necessary, as it is the case with cement with blast furnace slag,

whose hydration process is slower than that of ordinary cement (Çakir; Akoz, 2006; Furnas, 1997; Thomaz, 2005).

It is also observed in studies such as that by Castro (2003) and Braun (2003) that cements with a higher content of addition, such as CP III 32, require a longer curing period, compared to other types of cements.

3.2 Evaluation of the microstructure

At six months of age, only two types of samples were selected for microstructure tests. These samples were taken from the traction region of the prismatic specimens without loading (SC) and subjected to Permanent Central Loading (CCP). Both were in wet cure for 7 days before undergoing shipments. Figure 9 shows a sample without loading.
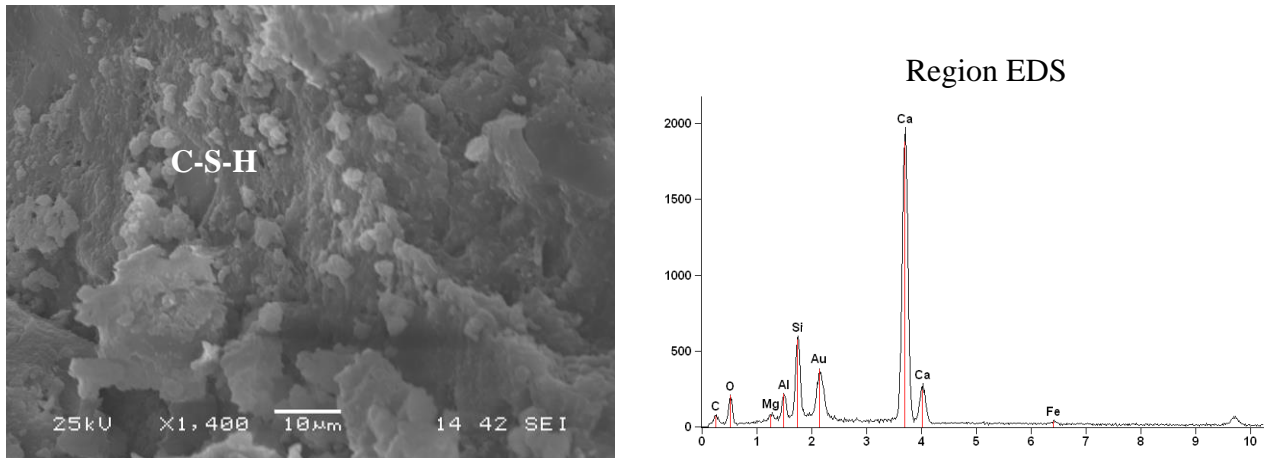
Figure 9. Concrete subjected to wet curing, without loading, at six months of age.

Figure 9 shows an area with dense and amorphous morphology (C-S-H Type III or IV), which is more common in this case because it is a sample at older ages. Cheng et al. (2005) observed in the concrete micrographs with different levels of blast furnace slag in high percentages, a denser structure, with few etringite needles and with capillary pores smaller than 50 nm, which may have been filled by products like CSH. The Au peak appeared in the EDS in the region of Figure 9 may be due to metallization with gold.

The C-S-H phase occupies a volume between 50% and 60% of cement paste solids, being the main responsible for the properties of the paste, such as the axial compression resistance. Its structure depends on the temperature and the free space in the mixture for its hydration (Baroghel-Bouny, 1994; Irassar, 2004).

This phase can be found in the following morphologies: Type I - fibrous, usually in the form of "hedgehog", when hydration is developing (early ages) out of the C_3S grain with sufficient available space; Type II - alveolar or reticulate, also called "honeycomb", which occurs in conjunction with C-S-H Type I; Type III and IV - prominent at older ages, constitutes a dense and amorphous morphology, difficult to define and can constitute a good portion of the total hydrated products. The characteristic products in more advanced stages of hydration are C-S-H type III and IV and more Ca (OH)$_2$ (Taylor, 1997; Ghosh, 2002).

According to Kurdowski (2014), there are 4 morphological forms of the C-S-H phase: fibrous, mesh, isometric and spherical conglomerate particles, belonging to the internal C-S-H and identified as a firm gel under an electron microscope.

Figure 10 shows the microstructure of the concrete subjected to permanent central loading in wet curing for 7 days, at six months of age; and Figure 11 shows the microanalysis in three points of this same concrete.
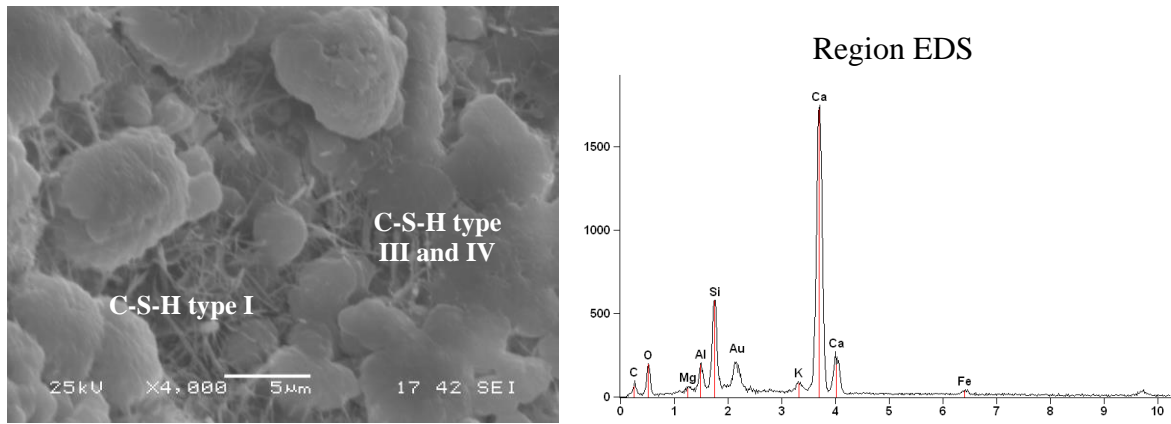
Figure 10. Concrete subjected to wet curing for 7 days and permanent central loading, at six months of age.

In the image of Figure 10 some needles are observed, but in the EDS the element sulfur (S) is not present to configure an ettringite. In this case, they can be C-S-H needles, with fibrous morphology (Type I) (Taylor, 1997; Ghosh, 2002). Phases C-S-H type III and type IV are also observed.

In blends using blast furnace cement, the C-S-H fibrillar morphology of Portland cement without additions (Portland clinker) is gradually replaced by a different morphology, which Richardson (1999) calls "sheet" or "sheet type". This author reports that this change in morphology is responsible for the better performance and greater durability of mixtures with this addition. Morphologies not yet observed at the age of 6 months of testing.

Figure 11 shows three selected points of the concrete subjected to wet curing for 7 days and permanent central loading. In the elementary composition by the EDS of the three points, the same elements Ca, Si, Al and Mg are found.
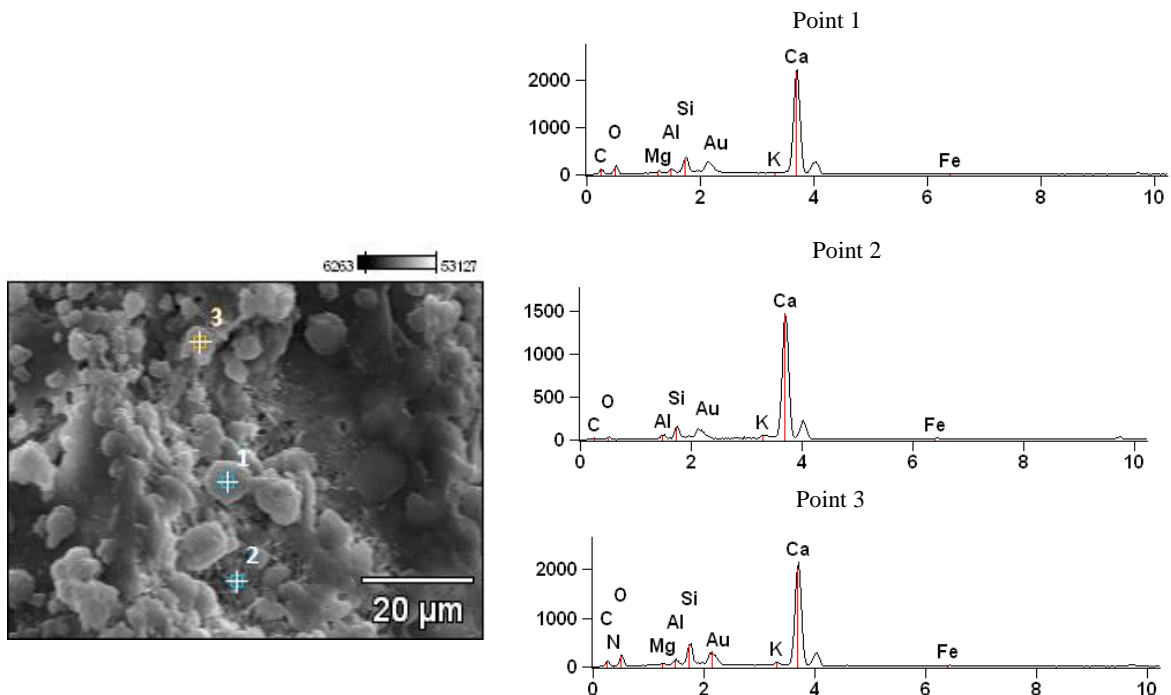
Figure 11. EDS microanalysis at three points of the concrete under permanent central loading (CCP).

In the microanalysis, we detected the presence of the elements Ca, K, Si, Al, Mg, O and C, which are typical of cement hydration products.

The C-S-H resulting from the hydration of Portland cement and blast furnace slag has similar morphologies; however, the slag grain has high percentages of Mg and Al (Richardson, 1999).

In Figure 12, a micrograph of a sample of unloaded concrete is presented, submitted to moist curing for 7 days, at 24 months of age.
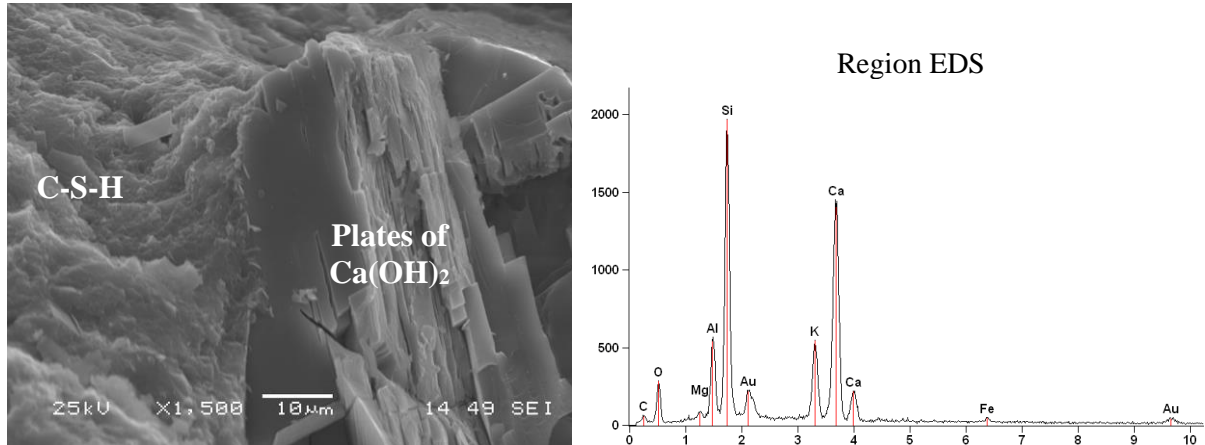
Figure 12. Micrograph and microanalysis of the unloaded concrete sample, at 24 months of age.

Figure 12 shows the presence of possible $Ca(OH)_2$ and C-S-H plaques. As verified by Baroghel-Bouny (1994) Mehta and Monteiro (2008), the phase corresponding to $Ca(OH)_2$ maintains the high alkalinity of the system, preserving the stability of the C-S-H and the concrete cover.

$Ca(OH)_2$ occupies a solids volume of 20% to 25% in the hydrated cement paste. Because of its composition with defined stoichiometry, they are formed in large crystals with hexagonal prismatic morphology. This morphology can also vary depending on the hydration temperature and the impurities present. Due to these factors, piles of large plaques can be formed.

This phase maintains the high alkalinity of the system, preserving the stability of the C-S-H and the reinforcement covering layer (Baroghuel-Bouny, 1994; Castro, 2003).

Figure 13 shows the micrographs and EDS of the concrete subjected to short-term central loading, at 24 months of age.
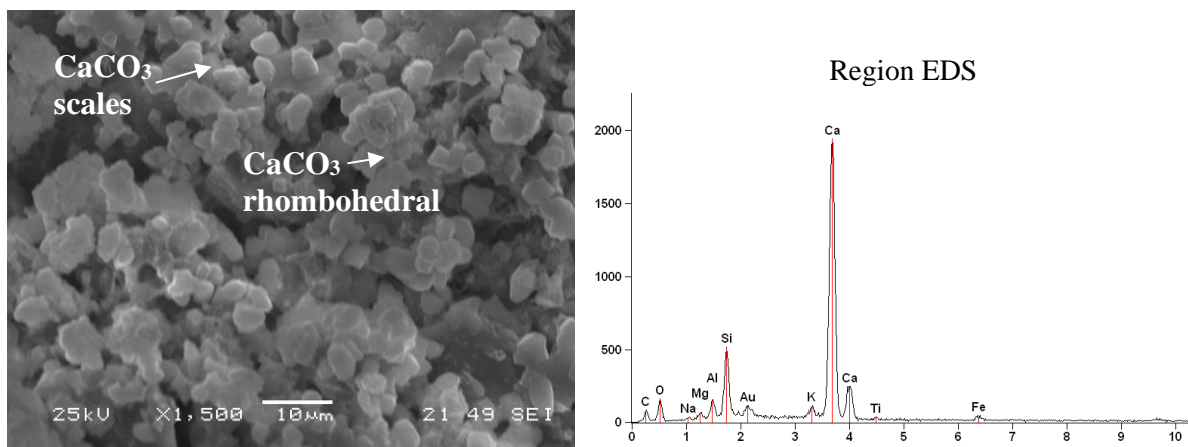
Figure 13. Micrograph and microanalysis of the concrete sample submitted to short-term central loading, at 24 months of age.

In Figure 13, it is possible to observe the formation of calcium carbonate in the form of rhombohedral crystals and in the form of scales, on a porous and possibly carbonated C-S-H. It is observed in the hydrated compounds formed, the presence of calcium carbonate ($CaCO_3$), with different morphologies on C-S-H, which may also be in the process of being modified by the action of time, and due to its porosity. The porous C-S-H phase and the formation of $CaCO_3$ indicated in Figure 13 was also observed by Sakar et al. (2001) in their study, with $CaCO_3$ in the form of scales, however, in large quantities.

The salts dissolved in sea water are mainly chlorides and sulphates. In the case of chloride ions (Cl^-), when in contact with alumina, the monochloroaluminate crystallizes in the form of unstable hexagonal plates. Chloride enters the crystalline network of hydrated silicates (C-S-H) and transforms the fibers into reticulated networks, making this phase more porous. Regourd et al. (1980) also observed the presence of $CaCO_3$ in micrographs of concrete samples (hydrated Portland cement compounds) exposed to salt spray.

Figure 14 shows the micrograph and microanalysis of the concrete subjected to permanent central loading (CCP), at 24 months of age.
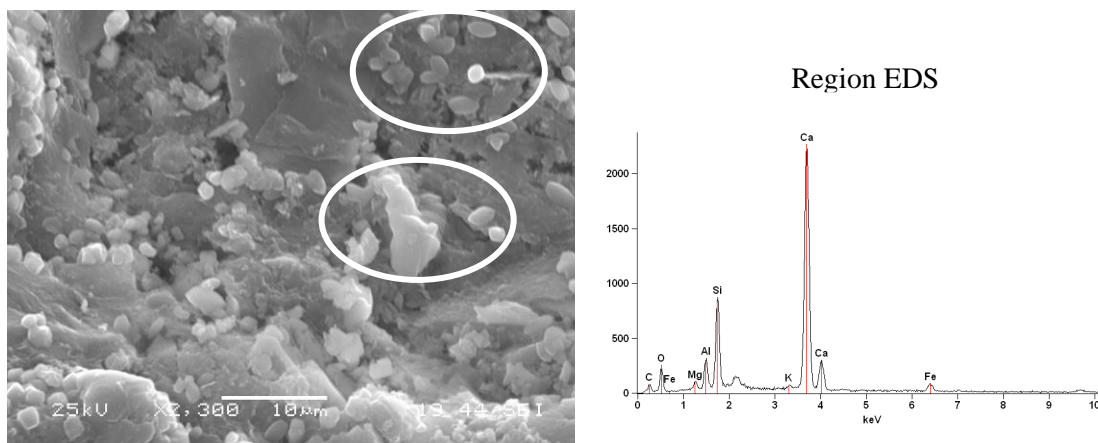
Figure 14. Micrographs and microanalyses of concretes with permanent central loading.

The sample in Figure 14 shows an area with a denser microstructure, with different $Ca(CO)_3$ morphologies. Some products that attracted attention, and that are highlighted in this micrograph, due to their morphology, can configure organic matter, probably microorganisms (Ribas Silva, 1996). However, to confirm this hypothesis, a microbiological analysis would be necessary, which was not performed because it was not the object of this study. In this case, the loading-induced cleft could have led to the entry of these microorganisms, since they were not observed in the SC and CCCD concretes.

When comparing the micrographs, as for the CCCD and CCP loads and without loading (SC), it is observed that the sample with greater compactness and less pore quantity is the reference (SC). As for the compounds formed, the carbonated C-S-H phase can be seen in the CCCD concrete micrographs. When subjected to permanent central loading, the C-S-H phase is dense with the formation of microorganisms, and the porosity in this case is not high, probably due to the wet cure at 7 days. And in the reference concrete (SC), there is the formation of $Ca(OH)_2$, as well as the dense and homogeneous C-S-H phase. Thus, the influence of cracks on the durability of the material is observed, since in the concrete with the $Ca(OH)_2$ plates there is higher alkalinity of the system and the preservation of the CSH phase, consequently, of the covering layer (Baroghel - Bouny, 1994; Mehta, Monteiro; 2008).

4. CONCLUSIONS

From the results obtained from the penetration of chlorides, it was observed that the crack opening did not influence the entry of chloride ions into the structure, with no significant differences between the types of loading and the reference concrete (without loading).

Studies carried out in Europe on this subject use longer periods of exposure to the external environment to obtain more expressive results regarding the behavior of the crack in the penetration of chloride ions in concrete. In this sense, it is seen that for the studied concretes, a longer period would be necessary to find more significant results between the types of loading and without loading. Some factors may also have contributed to this result, highlighting in this case the use of cement with the addition of blast furnace slag, which is more resistant to attack by chlorides, compared to CO2. The salt spray used also does not seem to have contributed sufficiently so that there could be differences between the types of loading and without loading.

When comparing the crack opening tolerances of the Brazilian standard with international standards, it appears that the openings allowed for the Brazilian standard are larger. The climatic conditions in Europe, with temperature variations ranging from -5 ^{o}C to 30 ^{o}C as is the case in France for example, are quite different from those in Brazil, where there are variations that range from 20°C to 35°C. However, the technological control of the quality of materials and execution in Brazil tends to be less strict. Thus, the crack openings can be an aggravating factor in this context. On the other hand, it is observed in this study that in Brazilian climatic situations, up to the age of two years, there were no significant differences between the results of samples under the loading condition determined in this study, the reference one, that is, without loading.

Up to the age of 12 months, the formation of cement hydration products was observed in micrographs and microanalyses, mainly found in the C-S-H phases, in addition to $Ca(OH)_2$ crystals, ettringite and CSH needles and slag grains with different dimensions. The deterioration products ($CaCO_3$ and carbonated C-S-H) were found after 18 months of age, in loading and curing situations. However, only at 24 months it is more evident that, in concretes subjected to the types of loading (CCP and CCCD), the presence of $CaCO_3$ and carbonated C-S-H was observed and in the sample without loading, only phases of C-S-H and $Ca(OH)_2$ were found. However, in the concrete with crack opening (CCP) possible microorganisms were found, which may have entered through the crack.

From the microstructural point of view, it was observed that at 24 months the loading influenced the results of the studied samples, since in the concretes with crack opening, the presence of microorganisms in samples subjected to permanent loading was visualized under microscopy. These compounds were only found in concretes with crack opening (in permanent central loading). In this sense, it is seen that the fissure may have been a way for these microorganisms to enter, which may have consequences on durability, as verified in the literature.

Thus, it is observed that the crack (when constantly open) can influence the microstructure of the concrete over time, depending on the preferred path for the entry of aggressive agents and microorganisms. This fact was not observed in concretes with short loading and without loading.

5. REFERENCES

ACI – American Concrete Institute (2016). *Standard practice for curing concrete. ACI 308-2016*. ACI Committee 308, 2016.

Alexander, M. G., Mackechnie, J. R., Ballim, Y. (2001), *Use of durability indexes do achieve durable cover concrete in reinforced concrete structures.* Materials science of concrete VI. Ed. By Sidney Mindess, Jan Skalny. Published by American Ceramic Society.

Andrade, T. (2005), *Tópicos de durabilidade do concreto. Concreto: Ensino, Pesquisa e Realizações.* Ed. G.C. Isaia. São Paulo: IBRACON, 2 v.Volume 2. p. 753-792.

Arya, C., Ofori-Darko, F. K. (1996). *Influence of crack frequency on reinforcement corrosion in concrete.* Cement and Concrete Research, v.26, No. 3, p. 345-353, https://doi.org/10.1016/S0008-8846(96)85022-8

Associação Brasileira De Normas Técnicas. (2014). *NBR 6118: Projeto de estruturas de concreto – Procedimento.* Rio de Janeiro.

Associação Brasileira De Normas Técnicas. (2020). *NBR 16889: Concreto - Determinação da consistência pelo abatimento do tronco de cone.* Rio de Janeiro.

Associação Brasileira de Normas Técnicas. (2015). *NBR 5738: Concreto - Procedimento para moldagem e cura de corpos de prova.* Rio de Janeiro.

Associação Brasileira de Normas Técnicas. (2018). *NBR 5739: Cimento Portland - Determinação da resistência à compressão – Método de ensaio.* Rio de Janeiro.

Baroghel-Bouny, V. (1994), *Caractérisation dês patês de ciment et des bétons – Méthodes, analyses, interpretations.* Laboratoire Central dês Ponts et Chaussés, IST – Section des publications.

Braun, V. (2003), "*Influência das condições de moldagem e cura nas características do cobrimento de diversos concretos*". Dissertação de mestrado, Universidade Federal de Goiás – UFG.

Çakir, Ö., Aköz, F. (2006), *Effect of curing conditions on the mortars with and without GGBFS.* Construction and Building Materials. https://doi.org/10.1016/j.conbuildmat.2006.08.013

Cascudo, O. (2005), "*Inspeção e diagnóstico de estrutura de concreto com problemas de corrosão da armadura*". In: Concreto: Ensino, Pesquisa e Realizações. Ed. G.C. Isaia. São Paulo: IBRACON, 2 v. Volume 2. p. 985-1016.

Cascudo, O. (1997), *O controle da corrosão de armaduras em concreto: inspeção e técnicas eletroquímicas.* São Paulo: Pini; Goiânia, GO: Editora UFG.

Castro, A. (2003), *Influência das adições minerais na durabilidade do concreto sujeito a carbonatação.* Dissertação de mestrado, Universidade de Goiás.

Cheng, A., Huang, R., Wu, J., Chen, C. (2005), Influence of GGBS on durability and corrosion behavior of reinforced concrete. Materials Chemistry and Physics, v. 93, p. 404–411. https://doi.org/10.1016/j.matchemphys.2005.03.043

Crauss, C. (2010), *Penetração de cloretos em concretos com diferentes tipos de cimento submetidos a tratamento superficial.* Dissertação de mestrado, Universidade Federal de Santa Maria-RS.

Dedavid, B. A., Gomes, C. I., Machado, G. (2007), Microscopia eletrônica de varredura: aplicações e preparação de amostras - materiais poliméricos, metálicos e semicondutores. Porto Alegre: EDIPUCRS, 60 p.

Figueiredo, C. R., Nepomuceno, A. A. (2004), *Influência da absorção na carbonatação de estruturas de concreto in loco.* 46º Congresso Brasileiro do Concreto, Florianópolis. Anais... São Paulo: IBRACON, v. 1.

Figueredo, E. P. (2005), "*Efeitos da carbonatação e de cloretos no concreto. Concreto: Ensino, Pesquisa e Realizações*". Ed. G.C. Isaia. São Paulo: IBRACON, Volume 2. p. 829-856.

Fortes, L. C., Andrade, J. C. (1995), *Corrosão na Armadura do Concreto Armado: Influência dos Agentes Cloretos e da Carbonatação.* ASTEF - Associação Técnico-Científica Engenheiro Paulo de Frontin. URL: http://www.electus.com.br/usuarios/lyttelto/InfluAgClorCarb/Influ_index.htm

François, R., Castel, A., Vidal, T., Vu, N. A. (2006), *Long term corrosion behavior of reinforced concrete structures in chloride environment.* J. Phys. IV France 136, 285–293. https://doi.org/10.1051/jp4:2006136029

Furnas, E. L. C. (1997), *Concreto massa estrutural projetado e compactado com rolo: ensaios e propriedades.* São Paulo: Pini.

Ghali, A., Favre, R. (1994), "*Concrete Structures: Stresses and Deformations*". E&FN Spon, an imprint of Chapman & Hall, 2-6 Boundary Row, London SE1 8HN, UK, second edition.

Ghosh, S. N. (2002), "*Advances in cement technology: Chemistry, Manufacture and Testing*". Second Edition, published by Tech Books International, New Delhi, India.

Hearn, N., Figg, J. (2001), *Transport mechanisms and damage: Current issues in permeation characteristics of concrete.* Materials science of concrete. Ed. By Jan Skalny, American Ceramic Society. v. VI, p.327-376.

Helene, P. R. L. (1997), *Vida útil das estruturas de concreto armado.* In: IV Congresso Íberoamericano de Patologia das Construções. VI Congresso de Controle de Qualidade – COMPAT 97. Anais... Porto Alegre: Departamento de Engenharia Civil – UFRS, p. 1-30.

Helene, P., Diniz, J. Z. (2001), *Durabilidade e vida útil das estruturas de concreto*. 43º Congresso Brasileiro de Concreto. Curso de durabilidade. 18 a 23 de agosto de 2001, Foz do Iguaçu – PR.

Helmuth, R., Stark, D. (1992), *Alkali-silica reactivity mechanisms.* Materials Science of Concrete III. Ed. By Jan Skalny. American Ceramic Society, USA.

Illston, J. M. (1994), *Construction Materials – Their nature and behaviour*. 2ª ed. London – UK: E & FN SPON, 518p.

Irassar, E. (2004), *Hormigón: Naturaleza y Propiedades. Hormigones Especiales – XV*. Reunión Técnica Ing. Marcelo Wainsztein, Asociación Argentina de Tecnología del hormigón. Santa Fe, 21 al 24 de octubre de 2004.

Ismail, M., Gagné, R., François, R., Toumi, A. (2006), *Measurement and modeling of gas transfer in cracked mortars.* Materials and Structures, v. 39, p. 43–52, https://doi.org/10.1617/s11527-005-9025-4

Jucá, T. R. P. (2002), "*Avaliação de cloretos livres em concretos e argamassas de cimento Portland pelo método de aspersão de solução de nitrato de prata*". Dissertação mestrado, Universidade Federal de Goiás. Goiânia, Brasil.

Khatib, J. M., Hibbert, J. J. (2005), *Selected engineering properties of concrete incorporating slag and metakaolin.* Construction and Building Materials, v. 19 460–472, https://doi.org/10.1016/j.conbuildmat.2004.07.017

Kim, M. Y., Yang, E. I., Yi, S. T. (2013), *Application of the colorimetric method to chloride diffusion evaluation in concrete structures.* Construction and Building Materials, v. 41, p. 239-245, https://doi.org/10.1016/j.conbuildmat.2012.11.084

Konin, A., Franfois, R., Arliguie, G. (1998), *Analysis of progressive damage to reinforced ordinary and high performance concrete in relation to loading.* Materials and Structures/Matériaux et Constructions, v. 31, p. 27-35, https://doi.org/10.1007/BF02486411

Lawrence, C. D. (2006), *Physiochemical and Mechanical Properties of Portland Cements. Lea's Chemistry of Cement and Concrete.* Ed. By Peter C Hewlett. Elsevier Butterworth Heinemann, USA.

Martins, A. R. (2001), *Efeito da cura térmica e de cimento com escória granulada de alto-forno na durabilidade do concreto de cobrimento.* Dissertação mestrado, Universidade Estadual de Campinas-SP.

Mehta, P. K., Monteiro, P. J. M. (2008), "*Concreto: microestrutura, propriedades e materiais*". 3ª Edição, São Paulo: IBRACON.

Mehta, P. K., Monteiro, P. J. M. (2014), *Concreto. Microestrutura, propriedades e materiais.* 2 ed. São Paulo: IBRACON, 751 p.

Midness, S., Young, J. F. (1981), *Concrete*. Prentice-Hall, INC. Englewood Cliffs, New Jersey – USA.

Montgomery, D. C. (1991), *Design and Analysis of Experiments*. New York: John Wiley & Sons.

Real, L. V., Oliveira, D. R. B., Soares, T., Medeiros, M. H. F. (2015), *Método colorimétrico por aspersión de nitrato de plata para la evaluación de la penetración de cloruros en concreto: estado del arte.* Revista ALCONPAT, 5(2), 149 - 159. https://doi.org/10.21041/ra.v5i2.84

Ribas Silva, M. (1996), *Climates and biodeterioration of concrete. Durability of building materials & components 7. Volume one – Prediction, degradation & materials.* Edited by Christer Sjostrom. Published by E & FN Spon. Chapman & Hall, London, UK.

Richardson, I. G. (1999). *The nature of C-S-H in hardened cements.* Cement and Concrete Research, v. 29, p. 1131–1147, https://doi.org/10.1016/S0008-8846(99)00168-4

Sarkar, S. L., Aimin, X., Jana, D. (2001), *Scanning Electron Microscopy, X-Ray microanalysis of concrete. Handbook of analytical techniques in concrete science and technology: Principles, techniques and applications.* Construction and Building Materials, USA, Ed. By V. S. RAMACHANDRAN, J. J BEAUDOIN.

Taylor, H. F. W. (1997), "*Cement Chemistry*". 2nd Edition. Published by Thomas Telford.

Vidal, T., Castel, A., Francois, R. (2004), *Analyzing crack width to predict corrosion in reinforced concrete.* Cement and Concrete Research, v. 34, p. 165–174.

Vidal, T., Castel, A., François, R. (2007), *Corrosion process and structural performance of a 17 year old reinforced concrete beam stored in chloride environment.* Cement and Concrete Research, 37 (11), p. 1551–1561. https://doi.org/10.1016/j.cemconres.2007.08.004

Regourd, M. (1980), *Structure and behavior of slag Portland cement hidrates.* In: International Congress on the Chemistry of Cement, 7Th. Proceedings. Paris.

Richardson, I. G. (1999). *The nature of C-S-H in hardened cements.* Cement and Concrete Research, v. 29, p. 1131–1147, https://doi.org/10.1016/S0008-8846(99)00168-4

Romano, F. S. (2009), *Estudo do ingresso de cloretos em concretos localizados no litoral norte do Rio Grande do Sul.* Dissertação Mestrado. Universidade Federal do Rio Grande do Sul-RS.

Silvestro, L., Romano, F. S., Dal Molin, D. C. C. (2021), Penetração de cloretos em concretos expostos em zona de atmosfera marinha por um período de 9 anos. Ambiente Construído, Porto Alegre, v. 21, n. 1, p. 101-118, https://doi.org/10.1590/s1678-86212021000100496

Song, H., Lee, C., Ann, K. Y. (2008), *Factors influencing chloride transport in concrete structures exposed to marine environments.* Cement & Concrete Composites. v. 30, p. 113–121, https://doi.org/10.1016/j.cemconcomp.2007.09.005

Taylor, H. F. W. (1997), *Cement Chemistry.* 2nd Edition. Published by Thomas Telford.

Thomaz, E. (2005), *Execução, controle e desempenho das estruturas de concreto. Concreto: Ensino, Pesquisa e Realizações.* Ed. G.C. Isaia. São Paulo: IBRACON, 2 v, volume 1. p. 527-582.

Vidal, T., Castel, A., Francois, R. (2004), *Analyzing crack width to predict corrosion in reinforced concrete.* Cement and Concrete Research, v. 34, p. 165–174, https://doi.org/10.1016/S0008-8846(03)00246-1

Vidal, T., Castel, A. François, R. (2007), *Corrosion process and structural performance of a 17 year old reinforced concrete beam stored in chloride environment.* Cement and Concrete Research, v. 37, p. 1551–1561, https://doi.org/10.1016/j.cemconres.2007.08.004

Kurdowski, W. (2014), *Cement and Concrete Chemistry.* Springer, Dordrecht, http://dx.doi.org/10.1007/978-94-007-7945-7

Hai-Long, W., Jian-Guo, D., Xiao-Yan, S., Xiao-Long Z. (2016), *Characteristics of concrete cracks and their influence on chloride penetration.* Construction and Building Materials, v. 107, p. 216-225. https://doi.org/10.1016/j.conbuildmat.2016.01.002

Use of chitosan as an organic coating to prevent / inhibit the corrosion of reinforced concrete

I. Rivera-Ortiz[1] , Y. Díaz-Blanco[1]* , C. Menchaca-Campos[1] , J. Uruchurtu-Chavarín[1]

*Contact author: yohandry.diaz@alumnos.uaem.mx

DOI: https://doi.org/10.21041/ra.v11i2.519

ABSTRACT

This work analyzes the performance of reinforced concrete (RC) against corrosion by applying a chitosan coating to the rebar. Specimens with different amounts of chitosan using solvents of apple vinegar, acetic acid and sugarcane alcohol vinegar were prepared and subjected to electrochemical polarization curves (PC), half-cell potential (HCP), electrochemical noise (EN) and linear polarization resistance (LPR) tests. The amount of chitosan and optimal layers (thickness) with an improvement in the protective properties was determined and low corrosion rates were obtained in the concrete exposed to chlorides for 200 days. The preservation of the coating on the steel in concrete turns out to be interesting for future studies.

Keywords: corrosion; inhibitor; apple vinegar; concrete; chitosan.

_____

[1] Centro de Investigación en Ingeniería y Ciencias Aplicadas (CIICAp), Instituto de Investigación en Ciencias Básicas y Aplicadas (IICBA), Universidad Autónoma del Estado de Morelos (UAEM), Cuernavaca, México.

Contribution of each author

In this work, the original idea of the research was by I. Rivera Ortiz (20%), C. Menchaca-Campos (40%) and J. Uruchurtu-Chavarín (40%). The administration of the project oversaw C. Menchaca-Campos (60%) and J. Uruchurtu-Chavarín (40%). The methodology and experimentation oversaw I. Rivera Ortiz (40%), Y. Díaz-Blanco (40%), C. Menchaca-Campos (10%) and J. Uruchurtu-Chavarín (10%). The data processing was carried out by I. Rivera Ortiz (60%) and Y. Díaz-Blanco (40%). The writing, revision and edition oversaw Y. Díaz-Blanco (80%) and J. Uruchurtu-Chavarín (20%). The analysis and discussion of results oversaw I. Rivera Ortiz (60%), C. Menchaca-Campos (20%) and J. Uruchurtu-Chavarín (20%).

Discussions and subsequent corrections to the publication

Any dispute, including the replies of the authors, will be published in the second issue of 2022 provided that the information is received before the closing of the first issue of 2022.

Utilización del quitosano como recubrimiento orgánico para prevenir/inhibir la corrosión del concreto reforzado

RESUMEN

Este trabajo analiza el desempeño del concreto reforzado (RC) frente a la corrosión, aplicando un recubrimiento de quitosano a la varilla. Los especímenes se prepararon con diferentes cantidades de quitosano usando disolventes de vinagre de manzana, ácido acético, y vinagre de alcohol de caña de azúcar, y se sometieron a pruebas electroquímicas de curvas de polarización (PC), potencial de media celda (HCP), ruido electroquímico (EN) y resistencia a la polarización lineal (LPR). Se determinó la cantidad de quitosano y capas (espesor) óptimas con una mejora en las propiedades protectoras y se obtuvieron velocidades de corrosión bajas del concreto expuesto a cloruros durante 200 días. La conservación del recubrimiento sobre el acero en el concreto resulta ser interesante para estudios futuros.
Palabras clave: corrosión; inhibidor; vinagre de manzana; concreto; quitosano.

Uso de quitosana como revestimento orgânico para prevenir/inibir a corrosão de armadura do concreto armado

RESUMO

Este trabalho analisa o desempenho do concreto armado (RC) frente à corrosão, aplicando um revestimento de quitosana na armadura. Os corpos de prova foram preparados com diferentes quantidades de quitosana utilizando solventes de vinagre de maçã, ácido acético e vinagre de álcool de cana-de-açúcar, e submetidos a ensaios eletroquímicos de curvas de polarização (PC), potencial de meia-célula (HCP), ruído eletroquímico (EN) e resistência a polarização linear (LPR). A quantidade de quitosana e camadas ideais (espessura) foram determinadas visando uma melhoria nas propriedades de proteção. Baixas taxas de corrosão foram obtidas em concretos expostos a cloretos por 200 dias. A preservação do revestimento sobre o aço no concreto destes corpos de prova torna-se interessante para estudos futuros.
Palavras-chave: corrosão; inibidor; vinagre de maçã; concreto; quitosana.

1. INTRODUCTION

Corrosion of reinforced concrete structures (RCS) is reflected in the compressive strength loss of the material, as well as in the internal stress generated by steel corrosion products formation, which is unable to be supported by a limited concrete plastic deformation and leads to cracking (Taylor, 1990). Nowadays, concrete made with Portland cement is the manufactured material most extensively used by humans, and according to international tendencies, its future is increasingly more important and significant (O Reilly, 2007).

Regarding rebar concrete corrosion, it must be emphasized the materials quality, the aggregate proportions, the constructive practice, coating thickness, water/cement (w/c) ratio, that can improve or diminish the concrete protection degree against external agents. It has to be clarified that concrete mix manufactured with Portland cement provides an adequate corrosion protection to embedded metallic materials (Hostalet Alba, 1994). This is due to the high resistivity barrier effect protecting the rebar structure from aggressive external agents and the development of a passive film over the steel surface from concrete alkalinity, maintaining protection for an infinite time, in principle. Nevertheless, steel corrosion is the main damage cause and then early failure of rebar concrete.

In marine environments, the main cause of corrosion in concrete reinforcing steel (CRS) has been identified as the chloride ions attack, which induce depassivation of the steel. These ions, when combined with water and oxygen, induce localized attack that can reduce the cross-section of the working steel. At this point, not only the economic losses caused by corrosion must be taken into account, but also losses of human lives due to structure collapse and accidents caused by failures, when strain and stresses are no longer supported by them (Pech-Canul and Castro, 2002). Similarly, modifications in concrete and metallic elements through the use of polymeric materials and coatings have been investigated for the last four decades with mixed results (Dodson, 1990).

On the other hand, the exploitation of waste and refuse to obtain high value aggregate products constitute the road to a sustainable economy. At present in the area of bio-materials science, scientists are focused on the study of chitin and chitosan among others due to their high potential applications (Anandhavelu et. al., 2017; Pakdel and Peighambardoust, 2018). Chitin is a bio-polymer present in the exoskeletons of arthropods such as: lobsters, crabs, shrimps; insects and in cellular walls of diatoms and other algae and mushrooms acting as cell reinforcements. By itself, this material is not toxic and relatively easy to degrade, so its application is environmentally acceptable (Dima and Zaritzky, 2019). It is the second most important bio-polymer in our planet (only after cellulose) and is a polysaccharide containing acetamide functional groups. Commercial chitin is obtained mainly from crustaceous exoskeletons (Gacén and Gacén, 1996).

When these groups are eliminated from chitin by the process known as deacetylation, chitosan is obtained being also a bio-polymer with a regular distribution of amine groups (Hernández Cocoletzi et. al., 2009). Chitosan presents excellent properties such as: antifungal, antiviral, antimicrobial, bio-compatibility, bio-degradability, non-toxic, emulsifier, grease and metal contamination absorbent among others, and make it considered of great application in different fields (Dima and Zaritzky, 2019). From its interesting physico-chemical, structural and functional properties, it becomes an adequate candidate for the anti-corrosion coatings development in particular due to its character as the film, bonding capacity on metallic surfaces and the possibility to form chemical complexes (Anandhavelu et. al., 2017).

Chitosan, being a partially deacetylated product of chitin, is a linear copolymer of β-(1-4)-2-amido-2-deoxy-D-glucan (glucosamine) and β-(1-4)-2-acetamido-deoxy-D-glucan (N-acetylglucosamine) (Carneiro et. al., 2013; Carneiro et. al., 2015; Bezerra, 2016), presenting a three-dimensional helical configuration stabilized through hydrogen couples amongst formed monomers (Sousa Andrade et. al., 2003). Due to its functional characteristics (Knorr, 1991;

Ashassi-Sorkhabi and Kazempour, 2020), chitin and chitosan are excellent candidates as aggregates in concrete mixtures and as a coating for reinforcing steel (RS) to avoid or diminish the corrosion and resulting products in the RC (Dodson and Hayden, 1989). Shrimp waste, which is generally responsible for an environmental problem, could become a solution for corrosion problems in structures (Martínez-Barrera et. al., 2005; Pacheco, 2010; Castelló et. al., 2019).

It has been searched the development of a method by which, improving the mechanical properties of concrete, it is possible to control and reduce the corrosion of RC, in comparison with conventional hydraulic concrete (Martínez-Barrera et. al., 2005).

In this work, the effectiveness and behavior of shrimp exoskeleton aggregate, chitin and chitosan as aggregates within the matrix were studied to evaluate the compressive strength of 5 cm x 5 cm x 5 cm mortar cubes. Chitosan coatings on encapsulated electrodes were evaluated to determine the optimal amount and the number of layers with the best performance in a solution with calcium hydroxide and calcium chloride. The best coating was applied on the steel rods embedded in concrete samples of 10 cm x 7 cm x 10 cm. The above, to analyze the electrochemical behavior of RC over time, exposed to a 3% sodium chloride solution.

2. EXPERIMENTAL PROCEDURE

2.1. Materials.
The concrete quality is highly dependent on the paste quality in a properly crafted concrete. For this research work the used materials for the elaboration of mixtures comply with the standard (ASTM C33, 2003). Ordinary Portland cement CPO 20R (Cemex), crushed stone sand (passes mesh # 4) and gravel from the region with a maximum size of 3/4" were used. The water/cement ratio was 0.5 both the mortar samples and the concrete samples. The steel formed by corrugated rods presented a diameter of 3/8 ", grade 42 with resistance of 4,200 kg/cm^2.

In the case of aggregates, exoskeletons were collected from shrimp industry waste, which represents millions tons of garbage worldwide (Hernández Cocoletzi et. al., 2009). Chitin and chitosan were acquired at the Universidad Autónoma Metropolitana, and also from dried shrimp waste.

The meshes used in the materials classification are from GRUPO FIICSA. For the study, the entire shrimp exoskeleton retained in the mesh # 4, the ground exoskeleton retained in the mesh # 30, the fiber exoskeleton retained in the mesh # 8, the chitin retained in the mesh # 8, the reagent grade chitin retained on mesh # 100 and chitosan retained on mesh # 30 were used.

2.2. Processing and synthesis of the different aggregates.
2.2.1. Shrimp exoskeleton as a solid aggregate.
Once the shrimp exoskeleton was obtained to be used as an aggregate, it was previously washed with distilled water and dehydrated in an electric oven at 200° C for 30 min. The ground exoskeleton with the desired particle sizes was obtained in a mill from the dry aggregate. Likewise, the aggregate was cut in fibers form to analyze whether the geometry had any effect on the mechanical properties of the composite material. In this way, three different geometries were processed, entire, ground and fibers exoskeleton. Chitin, reagent grade chitin and chitosan were used in the same presentation in which they were purchased.

2.2.2. Synthesis of aggregates for coating.
Several procedures were carried out for the different coating's extraction from the aggregate base material (shrimp exoskeleton, chitin and chitosan). The shrimp exoskeleton was tried to dissolve using acids, ketones and other products without any success, for which the use of the exoskeleton was discarded as an inhibitor or coating.

For the chitin and chitosan, the proposal reported in the literature was taken as a reference (Shrinivas Rao et. al., 2007). The percentage of soluble chitin was calculated by dissolving 0.1 g of chitin in 25 ml of a solution of N, N-dimethylacetamide (DMAc) with 5 % lithium chloride for 72 h, with constant stirring at room temperature and applying heat sporadically with a hot air gun (Shrinivas Rao et. al., 2007). In the case of chitin, the use of lithium chloride makes this coating unsuitable to be used, since a fundamental part of this work has been to generate products that are environmentally friendly, so the idea was discarded.

The soluble chitosan percentage was calculated by dissolving 0.1 g in 25 ml of a solution of glacial acetic acid AE2E3 (0.1M Sigma-Aldrich) for 72 h, with constant stirring at room temperature, then it was filtered with cellulose filter paper (0.45 microns) and the amount of soluble chitosan was determined by weight difference (Shrinivas Rao et. al., 2007). For chitosan, a more environmentally friendly solvent alternative was found. In this sense, the reagent grade acetic acid was replaced by apple vinegar, this to use a less aggressive solvent. Finally, it was decided to use chitosan dissolved in acetic acid and apple vinegar, varying the amount of chitosan from 0.1 g to 1g to demonstrate whether the amount of aggregate and solvent type contributed to a greater corrosion resistance.

2.3. Design and specimens fabricated procedure.
2.3.1. *Specimens for mechanical tests.*
The mortar specimens were fabricated according to the standards (ASTM C109, 2016; ASTM C192, 2014) with measurements of 5 cm x 5 cm x 5 cm. Table 1 shows the dosage and weight of all the materials for each cube of designed mortar.

Table 1. Materials dosage for each mortar sample.

Materials	Quantity of materials per sample							Materials for 1 m³
	Control sample 1	Samples with aggregates						
		2	3	4	5	6	7	
Cement CPO 20R (kg)	0.036	0.036	0.036	0.036	0.036	0.036	0.036	288
Sand (kg)	0.228	0.228	0.228	0.228	0.228	0.228	0.228	1824
Water (l)	0.018	0.018	0.018	0.018	0.018	0.018	0.018	144
Fiber exoskeleton (kg)	-	0.001	-	-	-	-	-	8
Entire exoskeleton (kg)	-	-	0.001	-	-	-	-	8
Ground exoskeleton (kg)	-	-	-	0.001	-	-	-	8
Chitin (kg)	-	-	-	-	0.001	-	-	8
Chitosan (kg)	-	-	-	-	-	0.001	-	8
Reagent grade chitin (kg)	-	-	-	-	-	-	0.001	8

Some considerations were considered for the fabrication of the specimens. The formwork was made of wood greased inside to guarantee adequate demolding of the cubes and to avoid breaking or fracture of the hardened mortar during this process. The cement-sand mixture was prepared, first mixing the solid materials and adding 1 g of each aggregates of entire exoskeleton, ground exoskeleton, fiber exoskeleton, chitin, reagent grade chitin and chitosan separately; finally, the water was added to the mixture. The paste was stirred for a few minutes until a homogeneous mixture was guaranteed and the mortar was poured into each mold. The entire process from preparation to pouring mortar mixture should not exceed 15 minutes. Specimens were identified and the surface of each mold was protected. The cubes were removed from the mold after 24 h and then cured for 28 days.

2.3.2. Metallic specimens for electrochemical tests.
Cylindrical specimens were fabricated to perform the electrochemical tests in calcium hydroxide solution (pH 13) with 3% calcium chloride. This to simulate the conditions and the behavior of chitosan coating on embedded steel in concrete, exposed to chloride ions. For the fabricated specimens, the 3/8" reinforcing rods were cut, to which a copper cable was soldered at one end to guarantee the electrical continuity of the steel and to be able to take potential and current readings. Subsequently, they were encapsulated with resin and a surface treatment was carried out on the surface of the steel with 600 sandpaper to improve the adhesion of coating. Then, the surface of the electrode was washed with distilled water, then with acetone and finally air dried. (Gholamhosseinzadeh et. al., 2019). These metallic specimens were evaluated electrochemically (with and without coating) exposed to the simulated solution.

From the coatings obtained of chitosan in the acetic acid solvents of reagent grade, apple vinegar and white vinegar of sugarcane alcohol, the specimens were immersed (dip coating) in the previously synthesized solutions with chitosan. Once the coating is formed, the samples are dried for 15 min. This process was repeated two to four more times until the surface of exposed rod was covered with several layers. With this process, coatings between 2 and 3 μm thick were achieved. The surface of encapsulated coated steel is shown in Figure 1.

Figure 1. Tone observed on the specimen surface with coating.

2.3.3. Concrete specimens for electrochemical tests.
The concrete specimens were fabricated according to the standards (ASTM C31, 2012; ASTM C192, 2014) considering a design resistance of 200 kg/cm^2 and a water/cement ratio of 0.5. Table 2 shows the dosage and weight of materials for each concrete sample. The dimensions of concrete samples were 10 cm x 7 cm x 10 cm, as represented in Figure 2.

Table 2. Materials dosage for each reinforced concrete sample.

Materials	Quantity of materials per sample			Materials for 1 m³
	Control sample 1	Samples with coating applied to reinforcing rods		
		2 (0.5gVM)	3 (0.5gAA)	
Cement CPO 20R (kg)	0.196	0.196	0.196	280
Sand (kg)	0.577	0.577	0.577	824
Gravel (kg)	0.662	0.662	0.662	946
Water (l)	0.098	0.098	0.098	140
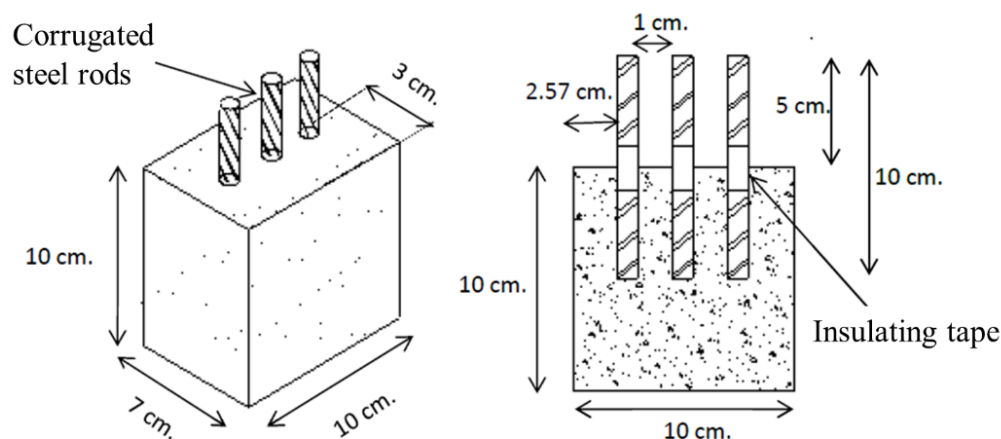
Figure 2. Geometry of the electrochemical tests specimens.

The fabrication of the concrete specimens was very similar to the procedure described of mortar cubes for the mechanical tests. In this case, the difference in the procedure consisted in the placement of the three corrugated bars of RS. This process was carried out during the pouring process of the concrete into the wooden molds.

The rods were cleaned to avoid major oxidation, grease, dust, or scale on the surface. They were visually revised looking for no fractures, deformations or imperfections that would affect the strength or adhesion to concrete. The steel rods of 10 cm were wrapped in the middle with insulating tape, approximately 2 cm, to prevent surrounding solution ingress by capillary action. The area of the steel in contact with the concrete was 13.35 cm² and two specimens were made for each coating used, as well as for the control sample.

2.4. Compressive strength test.

The compressive strength measurements of the mortars were performed to the seven cube-shaped working specimens of 5 x 5 x 5 cm, at the age of 28 days after their fabrication and curing. The specimens were placed in a hydraulic press ensuring vertical and horizontal alignment with respect to the axes of the equipment. Three specimens were tested for each aggregate incorporated into the mortar, as well as for the control sample. At the time of the sample failure due to the pressure of the press, the equipment stopped and gave a value represented as the maximum force of rupture. This value is divided by the cross-sectional area of the cube, in this way the compressive strength (f´c) was obtained. The f´c values of the samples with aggregates were compared with the design f´c of the control sample, according to the standard (ASTM C109, 2016). The compression and measurement equipment is a model 300DX, brand SATEC.

2.5. Electrochemical techniques measurement.
2.5.1. Polarization curves (PC).
The acquisition and analysis of the electrochemical data obtained from the PC technique were carried out, as represented in Figure 3.
1. Application of the PC technique to obtain potential and current density data, according to the operating parameters established in the study.
2. Graphic representation with Origin Pro software of the data obtained for each PC.
3. Determination of the electrochemical parameters of each PC such as: corrosion potential (E_{corr}), passivation current density, range of passivation potential and pitting potential.
4. Comparison of all the electrochemical parameters to determine the effect of the organic coating, according to the variables measured in the study.

> (1) Acquisition of potential and current data.
>
> ↓
>
> (2) Graphic representation of each PC data.
>
> ↓
>
> (3) Determination of E_{corr} values, current density and passivation potential range.
>
> ↓
>
> (4) Comparison of electrochemical parameters.
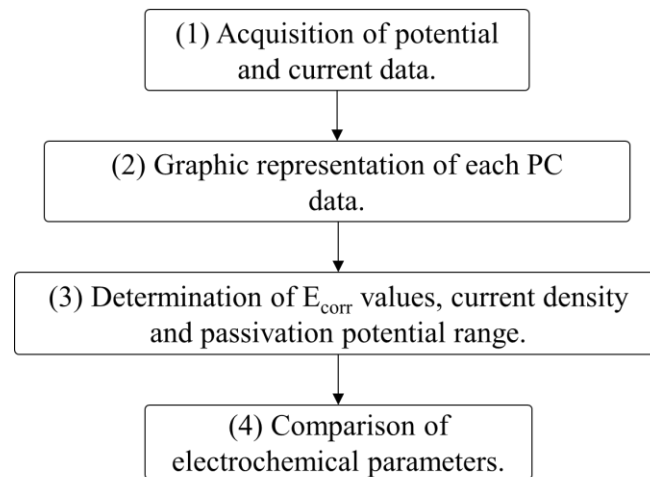
Figure 3. Block diagram for the data analysis obtained by the PC technique.

For the PC measurements, a three-electrode arrangement was used, employing a Saturated Calomel Electrode (SCE) as a reference, a working electrode (encapsulated samples) and a graphite bar as a counter electrode. Operating parameters were the following: a potential sweep of -200 mV below E_{corr} and up to +1000 mV, and a sweep rate of 100 mV/min. A 250 ml beaker was used as a container for the electrodes and the mock solution. The SCE and the graphite electrode were placed side by side and as close to the working electrode as possible within the simulated solution. Once all the electrodes were placed in the solution, a resting time of 30 min was allowed before starting the test so that the E_{corr} value would stabilize (Gholamhosseinzadeh et. al., 2019). The experiments were carried out in triplicate for each amount of chitosan, type of solvent, number of layers, storage time, as well as for the control sample, as observed in Table 3.

Table 3. Number of samples for each variable measured by the PC technique.

Number of samples of the specimens encapsulated for the measured variables of PC technique										
Coating concentration	Solvents			Storage time			Number of layers			
	Apple vinegar	Acetic acid	White vinegar	Dec. 2015	May. 2016	Mar. 2017	1	2	3	4
0 (Control)	3						3			
0.1	3	3		3	3	3				
0.2	3	3								
0.3	3	3								
0.4	3	3								
0.5	3	3	3				3	3	3	3
0.6	3	3								
0.8	3	3								
1	3	3								

First, the coatings obtained in the solvents of acetic acid and apple vinegar were evaluated for the amount of chitosan from 0.1 g and up to 1 g. Then, the behavior for the coating concentration of 0.5 g obtained in apple vinegar was compared with the PC for the same coating concentration, obtained in white vinegar of sugarcane alcohol. In addition, chitosan coating of 0.1 g dissolved in apple vinegar and stored for one and two years was evaluated to analyze its performance as a function of time. Finally, the behavior of the coating concentration of 0.5 g was analyzed as a function of the number of layers applied to the metal surface.

2.5.2. *Half-cell potential.*
The HCP measurement was performed against a SCE and with a multimeter. A reading was taken from the three steel bars embedded in the concrete and the final value from the three measurements was the averaged of them. The first reading was made at the beginning of the curing process of the samples. It was considered in each measurement that the SCE was very close to the working electrode and within the aggressive solution, without touching the bottom of the container. According to the probability corrosion criteria for the E_{corr} values in the standard (ASTM C876, 2015), the following intervals shown in Table 4 are described (Pérez-Quiroz et. al., 2008; Taji et. al., 2018; Díaz-Blanco et. al., 2019).

Table 4. Criteria of potential, according to ASTM C876.

E_{corr} values by the HCP technique (mV) vs SCE	Corrosion probability criteria
> -125	10 % of corrosion probability
-126 to -275	Intermediate corrosion risk
< -276	90 % of corrosion probability

2.5.3. Linear Polarization Resistance (LPR).

The LPR technique has been used in recent decades as a powerful tool for the analysis of CRS corrosion (Feliu et. al., 1989; Papavinasam, 2008; Zhou et. al., 2018). For the LRP measurement, an arrangement of three electrodes was used: a graphite counter electrode, the SCE as a reference electrode and the steel rods as working electrodes; with one measurement per sample according to the established test days. Both electrodes were placed as close as possible to the working electrode, next to the concrete block and inside the 3% NaCl solution, as shown in Figure 4. The LPR technique was measured according to the standard (ASTM G59, 2014), with operating parameters of ± 20 mV with respect to the E_{corr}, at a scanning rate of 10 mV/min and it was plotted as a function of time. The measurement equipment used was a Potentiostat/Galvanostat/ZRA, Gamry Instruments, interface 1000, Gamry framework software. The polarization resistance (R_p) was determined as the slope of the PC around the E_{corr} (Andrade and Alonso, 1996; Díaz Blanco et. al., 2019). Table 5 shows the intervals of current density (I_{corr}) and corrosion rate (CR), as well as the condition of steel bars according to the advance degree of corrosion (Andrade and Martínez, 2010).
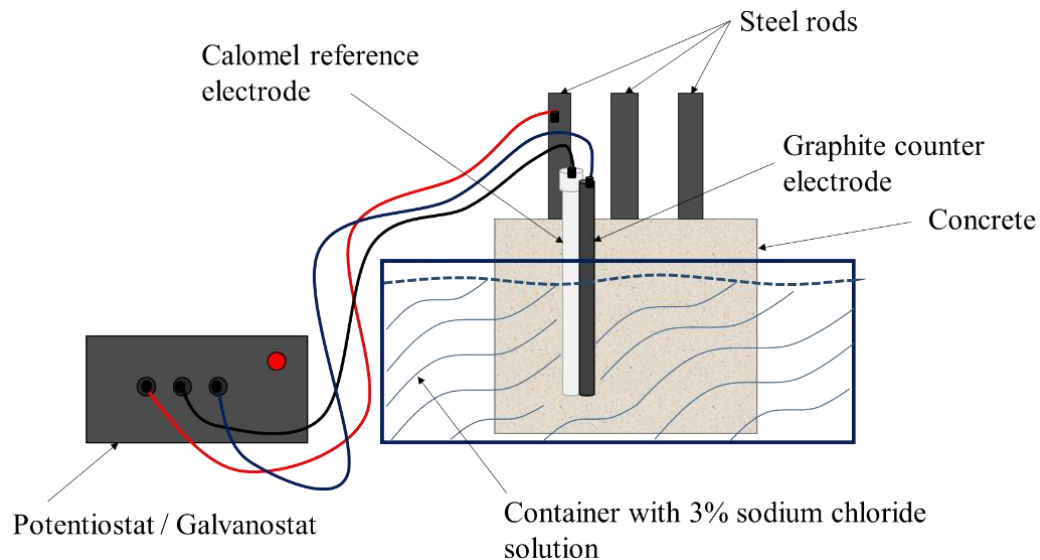
Figure 4. Representation of an electrochemical cell for the LPR measurement.

Table 5. I_{corr} and CR criteria in terms of service life.

Corrosion current I_{corr} ($\mu A/cm^2$)	CR (mm/y)	Rebar condition
I_{corr}< 0.1	<0.001	Negligible.
I_{corr} 0.1 - 0.5	0.001-0.005	Low to moderate corrosion.
I_{corr} 0.5 - 1.0	0.005-0.010	Moderate to high corrosion.
I_{corr}> 1.0	> 0.010	High corrosion.

2.5.4. Electrochemical noise (EN).

The acquisition and analysis of data obtained by the EN technique were carried out following the block diagram, represented in Figure 5.
1. Application of the EN technique for the acquisition of EN signals, from the established operating parameters.
2. Processing of electrochemical noise potential (EPN) and electrochemical noise current (ECN) signals using linear regression method.

3. Determination of electrochemical parameters such as: standard deviation of potential noise (σ_v), standard deviation of current noise (σ_i) and noise resistance (R_n); by means of the statistical method (SM).
4. Graphic representation and comparison of R_n data as a function of time between the different concrete samples.
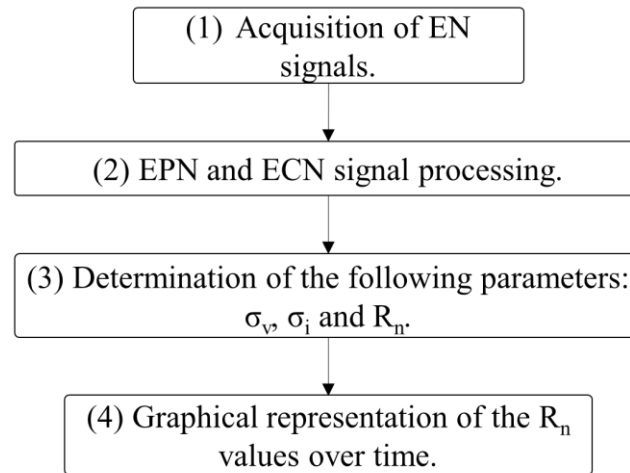
Figure 5. Block diagram for the analysis of EN data.

For the EN measurement, the standard method of analysis of three electrodes (steel rods embedded in concrete) nominally "identical" was used (Genesca et. al., 2002), making a measurement for each concrete sample according to the designated test days. The equipment used was an automatic ZRA potentiostat from ACM Instruments. A sampling frequency of 1 data/s was used, and the readings recorded were 1024 data. R_n is one of the most widely used parameters for the study of noise signals. By analogy with Ohm's law, R_n was determined, and defined as the relationship between σ_v and σ_i (Sanchez-Amaya et. al., 2005). For the processing of data, a trend removal of the time series of potential and current was carried out by the linear regression method (Mansfeld et. al., 2001).

2.6. Surface characterization. Scanning Electron Microscope (SEM).
The samples were coated with a thin layer of gold to give them conductive properties. Steel rods samples with coatings elaborate from chitosan dissolved in apple vinegar were studied. The uncoated working specimen was also analyzed. The measuring equipment is LEO 1450 VP.

3. RESULTS AND DISCUSSION.
3.1. Compressive strength.
Figure 6 shows the results of the compressive strength test for the specimens with different proposed aggregates, with the aim of observing if there were improvements in the mechanical properties of mortar (Aydin and Saribiyik, 2010).
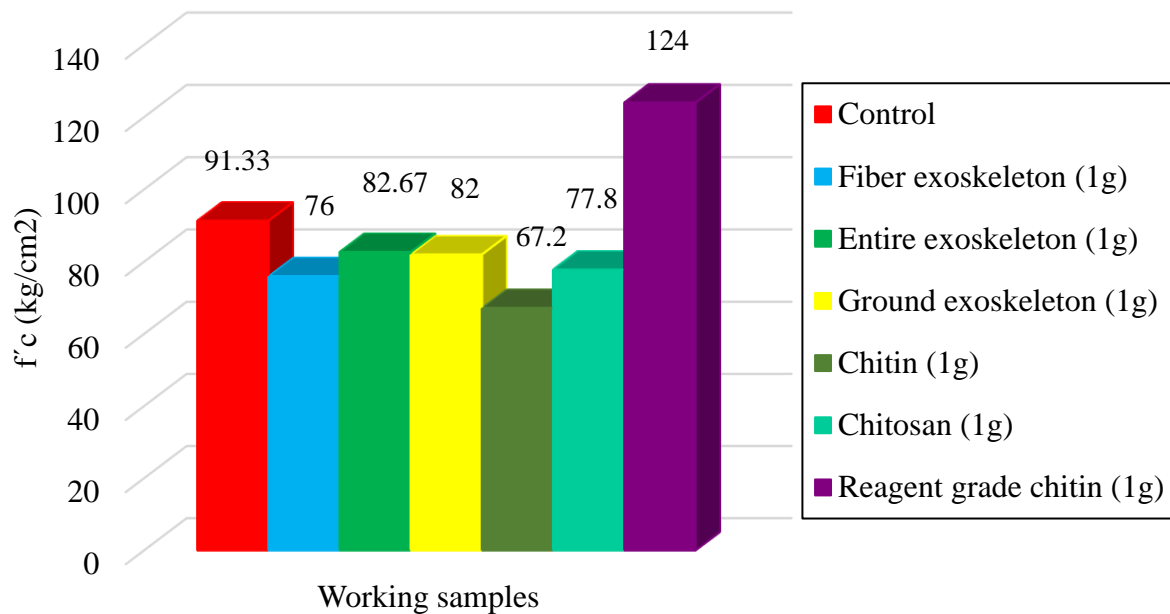
Figure 6. Compressive strength tests of the mortar specimens with different aggregates at 28 days of curing.

As can be seen, the compressive strength values with the use of the different aggregates (entire exoskeleton, fiber and ground) decrease between 9 and 17 % with respect to the control sample resistance. In the case of chitin and chitosan, the resistance values decrease by up to 26 %. Some authors report the retarding effect that chitosan has on the cement hydration, which acts as a viscosity modifying agent, possibly due to the interaction between the biopolymer and the cement compounds (Cano-Barrita and León-Martínez, 2016). In contrast, a resistance of 136 % was achieved for the sample containing reagent grade chitin, with particles retained at the 100 mesh (150 µm). According to Bezerra, chitin in cementitious mixtures can form polymeric networks that improve mechanical properties by incorporating the cement paste hydrates into their chains (Bezerra, 2016), consequently the resulting mortar cubes were possibly more compact. Certainly the shape and small size of the particles played a very important role (Page et. al., 1990), influencing the void content of the composite material, compaction and consequently in the compressive strength (Zhou et. al., 2019).

3.2. Electrochemical techniques.
3.2.1. Polarization curves.
Figure 7 shows the PC graphs for the encapsulated samples coated with different amounts of chitosan dissolved in acetic acid and apple vinegar, and immersed in a solution of calcium hydroxide with calcium chloride. Both graphs present a similar behavior, more noble E_{corr} values are observed for the samples coated with low amounts of chitosan. On the contrary, E_{corr} becomes more active for the control sample and the samples coated with the highest amount of dissolved chitosan, except for the sample with the 0.5 g coating in acetic acid that presents a more noble corrosion potential.
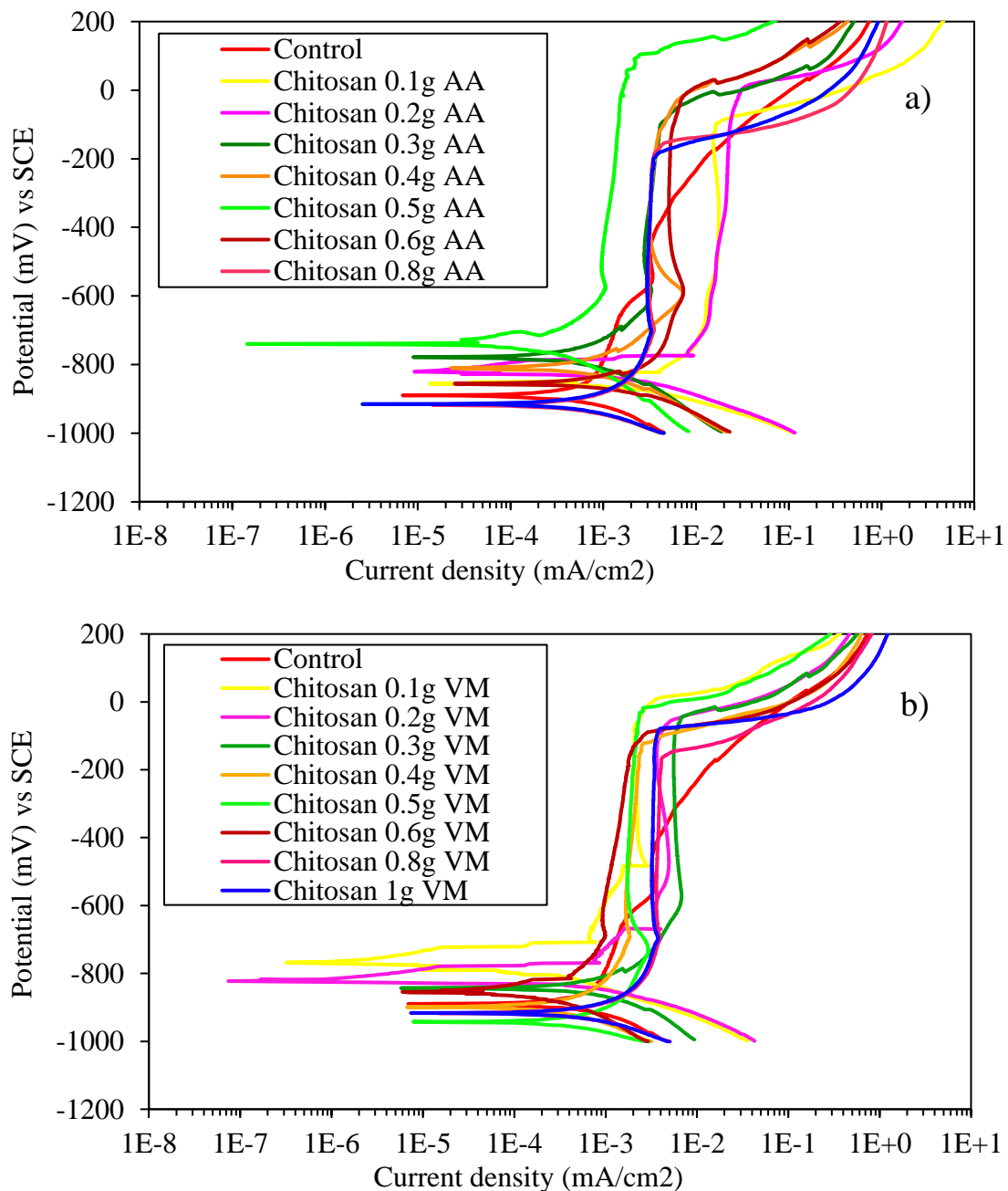
Figure 7. Polarization curves of samples coated with chitosan dissolved in a) acetic acid and b) apple vinegar, exposed to a solution of calcium hydroxide with calcium chloride.

All coated specimens have a region of passivity between -800 and -100 mV. The observed behavior suggests the metal oxidation with the subsequent formation of a more stable passive layer in the presence of the coating as a physical barrier. Chitosan as a polysaccharide is an organic polymer suitable as a coating due to its high adherence to metallic substrates (Carneiro et. al., 2015). This property is increased because chitosan and its derivatives have a notable ease of chemical functionalization (Ashassi-Sorkhabi and Kazempour, 2020). The passivation current densities are close to 1E-3 mA/cm^2, whereas the control sample presents higher passivation current density values. The start of the passivation region for all samples is very similar, but the control sample shows a tendency to increase the current density, which means that the passive layer is not as stable. The specimen with the coating of 0.5 g of chitosan has a greater passivation potential range (greater

stability of the passive layer) than the other specimens, with a pitting potential close to +200 mV for the sample with coating dissolved in acetic acid (AA) and -10 mV for the coating dissolved in apple vinegar (VM). Therefore, the amount of 0.5 g of chitosan dissolved in apple vinegar was considered the best coating, which acts as a physical barrier against the entry of aggressive agents such as chloride ions (Carneiro et. al., 2013).

In Figure 8a, the PC graph of 0.5 g of chitosan dissolved in apple vinegar with respect to the white vinegar solvent of sugarcane alcohol can be seen. It is appreciated that the sample with a coating dissolved in white vinegar did not present a passivation zone, but a zone of formation of corrosion products. This confirms the use of apple vinegar as a better chitosan solvent, with the consequent formation of the best coating.

Being chitosan an organic biopolymer, a degradation of the compound as a function of time would be expected. In this sense, a concentration of 0.1 g of chitosan dissolved in apple vinegar was prepared and stored in a closed container for 17 months. The effect of the storage time and subsequent application on the metal surface was observed through the PC technique, as represented in Figure 8b.
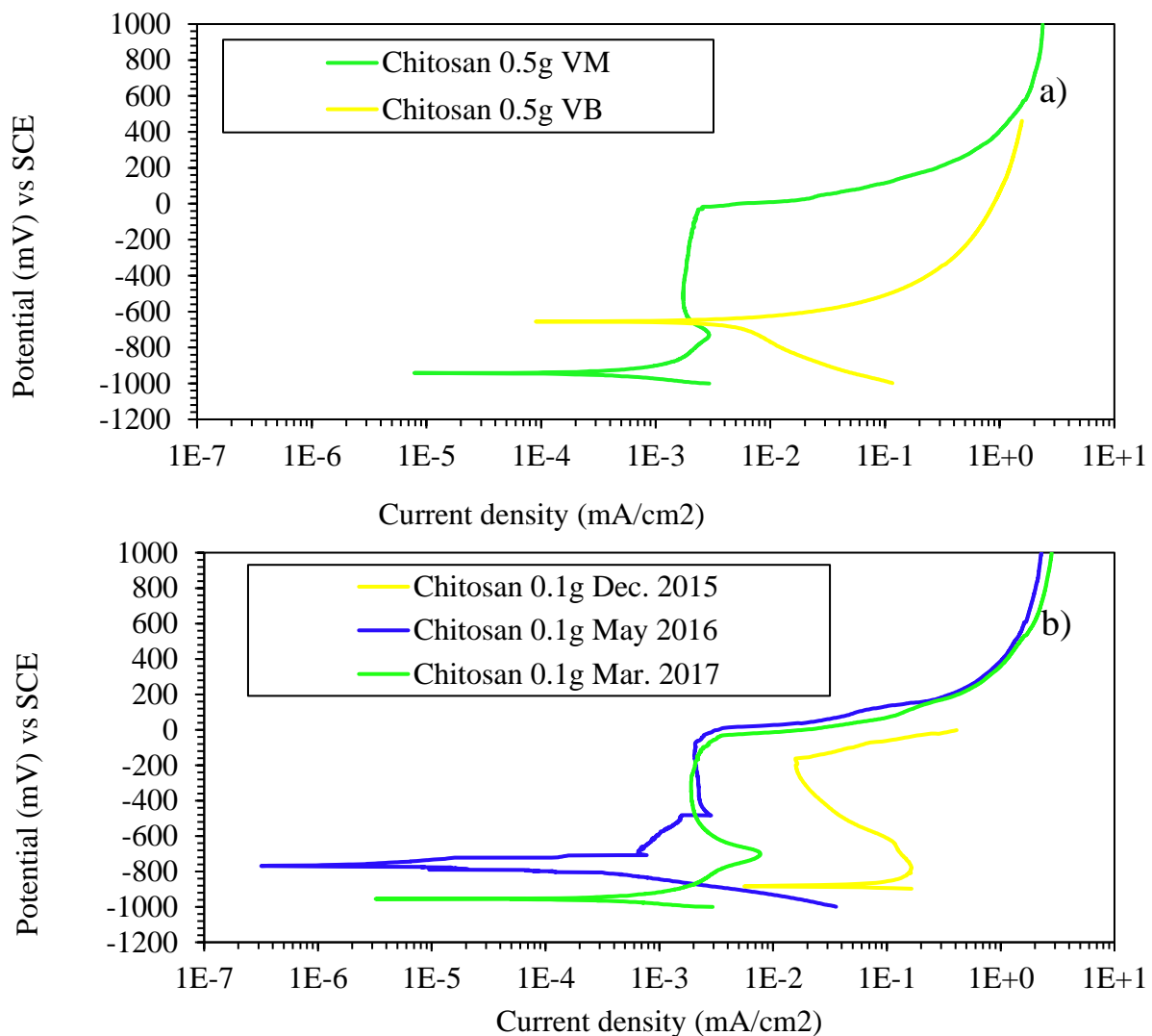
Figure 8. Polarization curves of samples with a) chitosan coating dissolved in white vinegar of cane alcohol and apple vinegar and b) chitosan coating stored and dissolved in apple vinegar; exposed to the simulated solution.

As can be seen, after 5 months of storage the chitosan coating improved its performance considerably. The passivation current decreased from the first application by more than three orders of magnitude. After 17 months of storage, the passivation potential range was wider between -1000 and 50 mV and the passivation current was two orders of magnitude lower with respect to the first application. The preservation for a long time, the favorable adhesion properties, the possible interactions of chemisorption and physisorption chitosan on the metal surface, and the availability of N and O heteroatoms of the coating are some of the characteristics that directly affect its anticorrosive behavior (Ashassi-Sorkhabi and Kazempour, 2020).
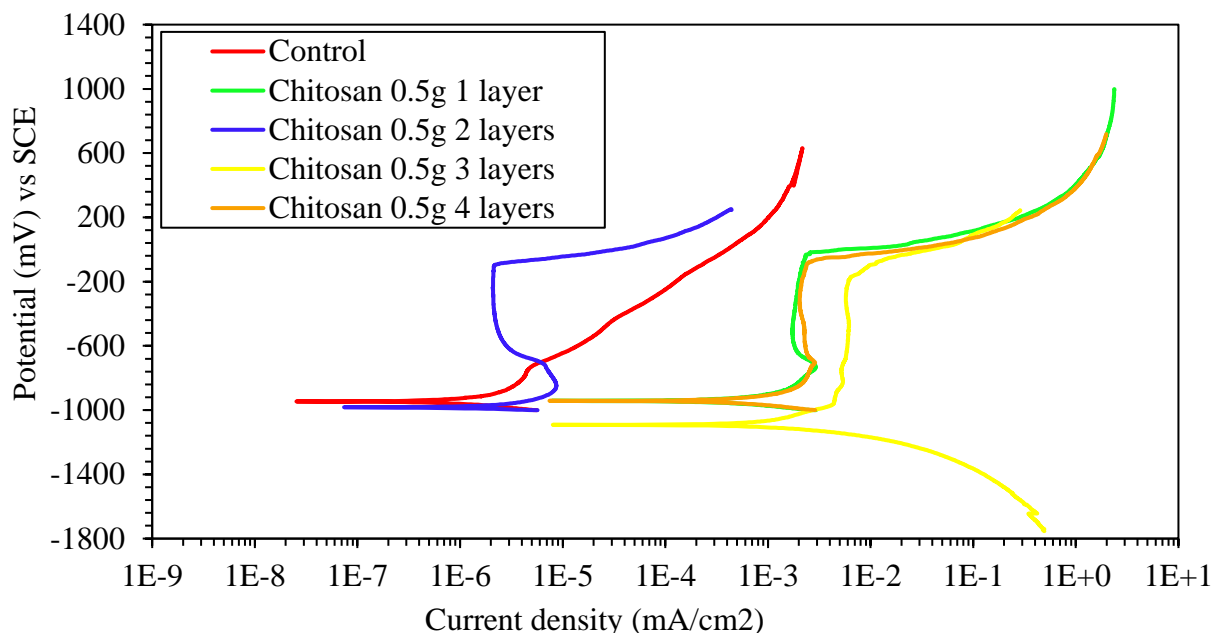
Figure 9. Polarization curves of samples with different layers (dip coating) of chitosan coating in apple vinegar, in solution of calcium hydroxide with calcium chloride.

Figure 9 shows the PC of the encapsulated samples, with and without coating of 0.5 g of chitosan dissolved in apple vinegar. One to four dips were made, forming a layer by each dipping.
In the graphs, E_{corr} values around -950 mV for all samples are shown. The sample with two layers and the control sample have a lower passivation current density of 1E-6 mA/cm^2, with values up to three orders of magnitude lower than the values reported for the coated specimens with one, three and four layers. This is possibly due to the fact that the specimens with the highest number of layers had poor adhesion at the metal edges (gap between the metal and the epoxy encapsulation). On the other hand, the sample with two coating layers presented a well-defined passivation zone, with a pitting potential close to -50 mV; whereas, in the anodic branch of the control sample, the behavior is different with a significant increase in current density associated with the formation of corrosion products on steel. Gebhardt et al. report a similar behavior of the anodic branch for the substrate, with and without a chitosan coating, demonstrating its favorable effect against corrosion (Gebhardt et. al., 2012). This suggests that the best coating is the two-layer one, the first one covers the metal and the second one seals the pores or defects present in the first layer.

3.2.2. Electrochemical parameters such as: E_{corr}, R_n, R_p and I_{corr}.
Figure 10 shows the results of the E_{corr} variation as a function of time for the SR embedded in the concrete coated with 0.5 g of chitosan, dissolved in apple vinegar (0.5 g VM) and in acetic acid (0.5 g AA).
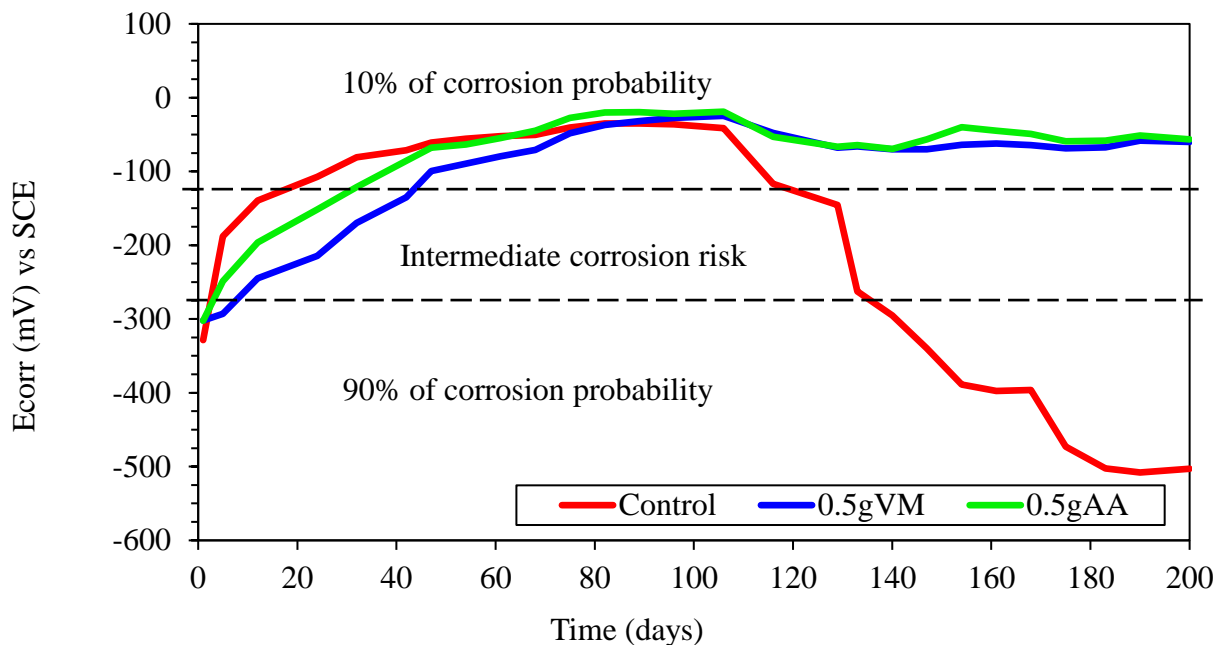
Figure 10. Variation of E_{corr} over time for coated and uncoated steel embedded in concrete and exposed to a 3% NaCl solution.

At the beginning of the test period (concrete curing) the control sample quickly reached very noble E_{corr} values, close to -100 mV at 28 days; steel under conditions of high alkalinity, presence of humidity and oxygen forms a passive layer of oxides that protects the metal when the aggressive ions are not present (Hansson, 1984). The coated specimens reached these E_{corr} values between to 40 and 50 days of testing, possibly due to the presence of the coating that delayed the formation of the oxides passive layer. In the long term, it can be observed that both samples with coating dissolved in apple vinegar or acetic acid present a corrosion probability of 10 %, having a constant behavior from 100 to 200 days. On the other hand, E_{corr} of the sample without coating begins to show a drastic fall after 100 days, reaching the range of corrosion probability of 90 % from 160 days till 200 days, according to the established criteria (Taji et. al., 2018).

Comparing both specimens with coating, the values of E_{corr} are very similar and improve with the immersion time. This behavior is associated with the chitosan coating; possibly the high adherence (Carneiro et. al., 2015), absence of film defects (Hernández et. al., 2009), as well as the permanence of the physico-chemical characteristics of the coating (Ashassi-Sorkhabi and Kazempour, 2020), limits that chloride ions reach the steel and cause the breakdown of the passive layer (Alonso et. al., 2000). The favorable effect of chitosan coatings by increasing resistance against localized corrosion has been reported (Gebhardt et. al., 2012).

In Figure 11a and 11b the R_p and R_n values are presented for the concrete samples with steel coated with chitosan, dissolved in apple vinegar and acetic acid.
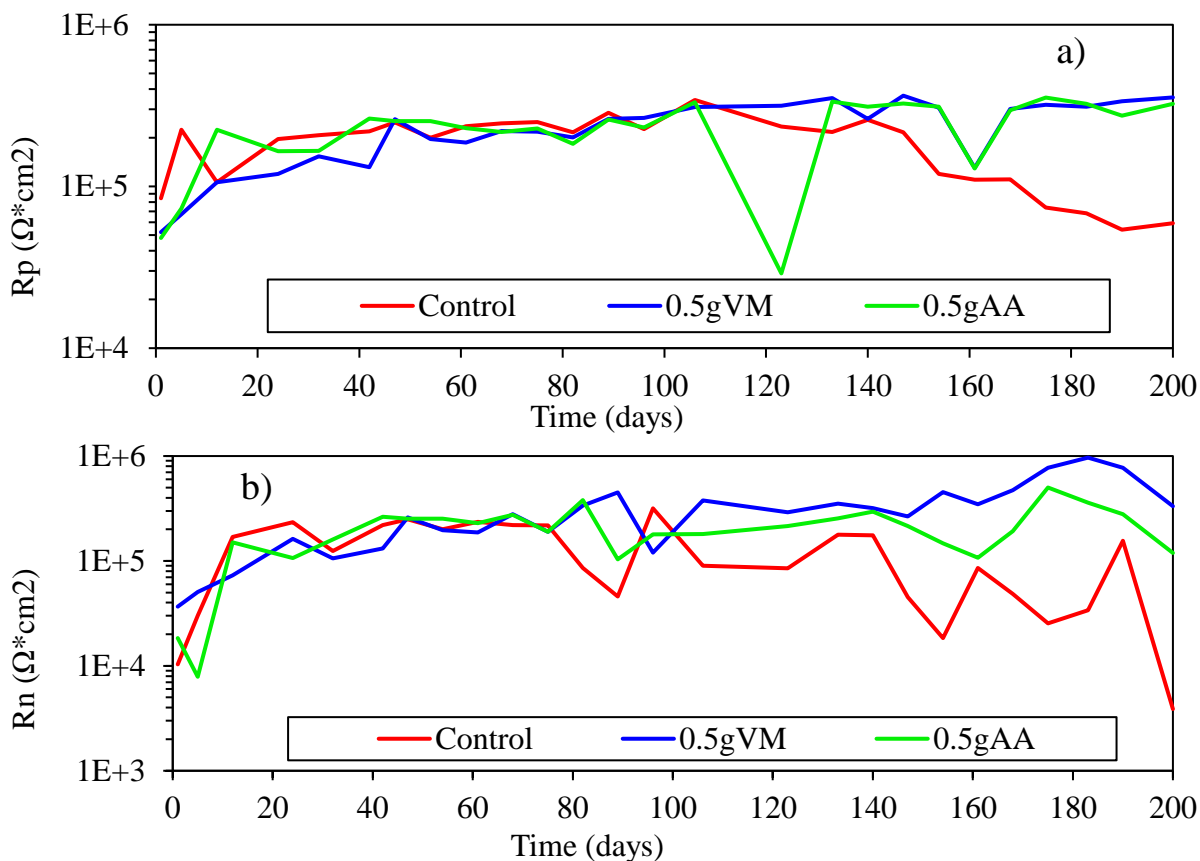
Figure 11. Variation of a) R_p and b) R_n for the reinforcing steel with and without coating embedded in the concrete, in 3% NaCl solution.

Both results show a similar trend with an increase in resistance values during the first months of testing. Between 80 and 110 days the control sample begins to decrease its R_p and R_n values, perhaps due to the breakdown of the passive layer suggesting attacks on its surface and increasing the corrosion rate.

From a linear regression between the R_p and R_n values, a mean value of correlation coefficient of 0.557 was obtained. Some authors propose by analogy with Ohm's law that the R_n and R_p can be considered equivalent for many systems (Aballe et. al., 2001; Girija et. al., 2007; Díaz Blanco et. al., 2019).

All samples show small variations in R_p values, but coated samples progressively increase their values up to 3E+5 $\Omega*cm^2$, after 200 days of testing. This behavior may be due to small defects in the coating, with possible rupture and repassivation of the passive layer. The difference between the R_p values of the control sample and the coated ones is approximately one order of magnitude at the end of the test (Hernández et. al., 2009). On the other hand, the R_n values, especially for the control sample, show large fluctuations after 110 days of testing, due to the sensitivity of this technique capable of detecting small changes in potential and current on the metal surface. Furthermore, the EN technique is sensitive to the localized corrosion type present in this system.

From R_p data, the corrosion rate was determined in terms of the I_{corr} using the Stern and Geary equation (Stern and Geary, 1957; Zhou et. al., 2018), as shown in Figure 12. Results at the beginning show, a high level of corrosion for the control sample, located in the moderate to high corrosion zone. The concrete samples that have coated rods are in the low to negligible corrosion zone according to the criteria established in the literature (Andrade and Martínez, 2010), which indicates that the coating with both solvents is effective as protection against chloride-induced corrosion.
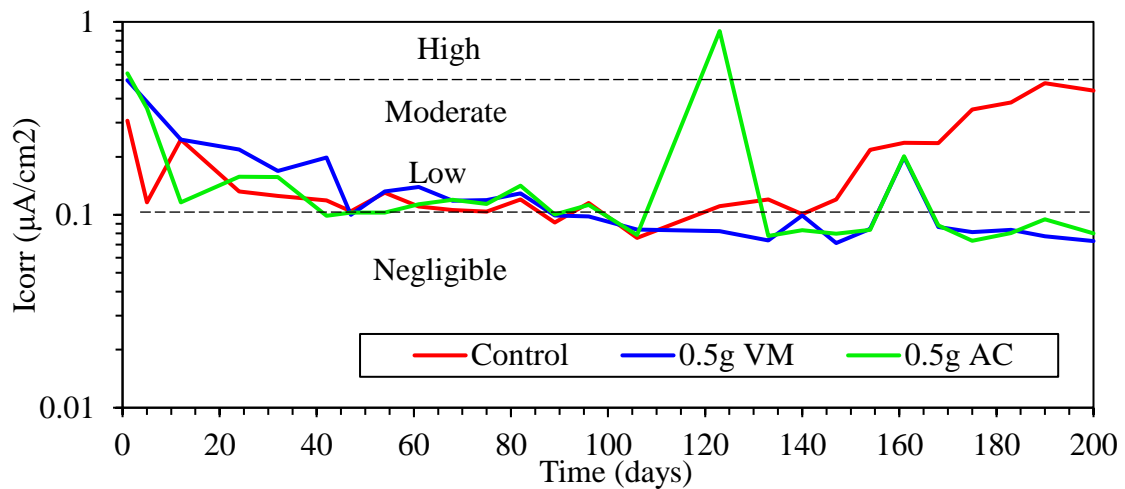
Figure 12. Graph of I_{corr} (corrosion rate) of concrete for RS with and without coating, in 3% NaCl solution.

3.3. Characterization.
3.3.1. SEM images.
Figure 13 shows the metal surface with the coating using 0.1 and 1g of chitosan with apple vinegar as solvent.
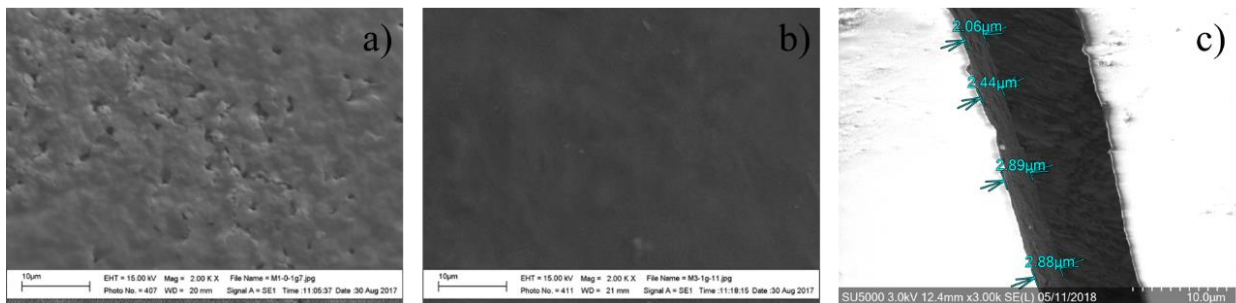
Figure 13. Comparative micrograph of coating film a) 0.1g of chitosan with VM and b) 1g of chitosan with VM c) thickness of coating film.
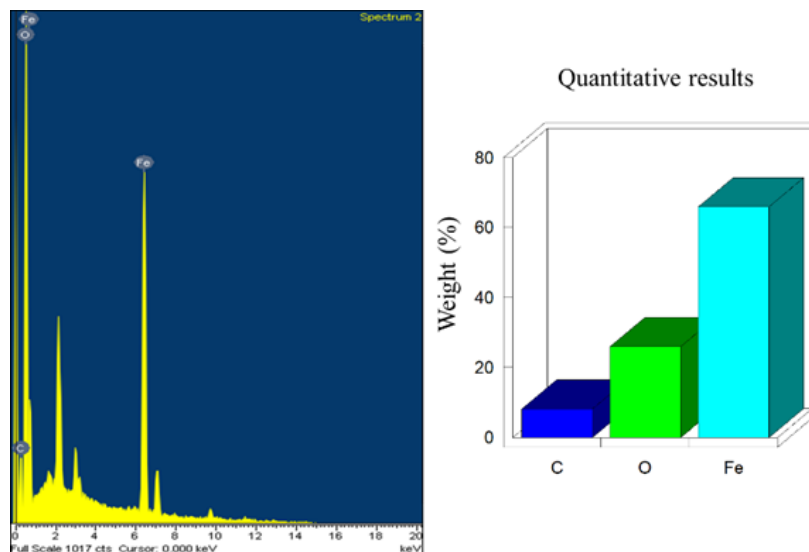
Figure 14. SEM elemental chemical analysis of the 0.5 g of chitosan coating with apple vinegar solvent.

In the first case (Figure 13a) the coating presents porosities while in the second case (Figure 13b) it is more homogeneous. In the micrograph (Figure 13c) and elemental chemical characterization (Figure 14) obtained by means of SEM, the thickness of the coating composed of 0.5g VM is observed, with a film thickness of 2.06 μm to 2.89 μm, this being a thin film. Elemental analysis presents only carbon from the coating, oxygen, and iron from the base metal.

3.3.2. *Visual observation of the reinforcing rods.*
In Figure 15 the real state of the rods extracted from the concrete blocks can be observed, after 200 days of exposure to the aggressive medium of 3% NaCl.
The lower part represents the zone that was embedded in the concrete and the rods from the control sample present some corrosion products of tenuous orange, associated with the action of the aggressive medium (red arrows) which speaks of the good protection that concrete has alone. In the rods with chitosan coating, no rust products are observed, evidencing the good electrochemical behavior of the organic coating. Finally, in the upper part of the steel bars there are corrosion products caused by the action of the atmosphere, being very similar in all (black arrows).
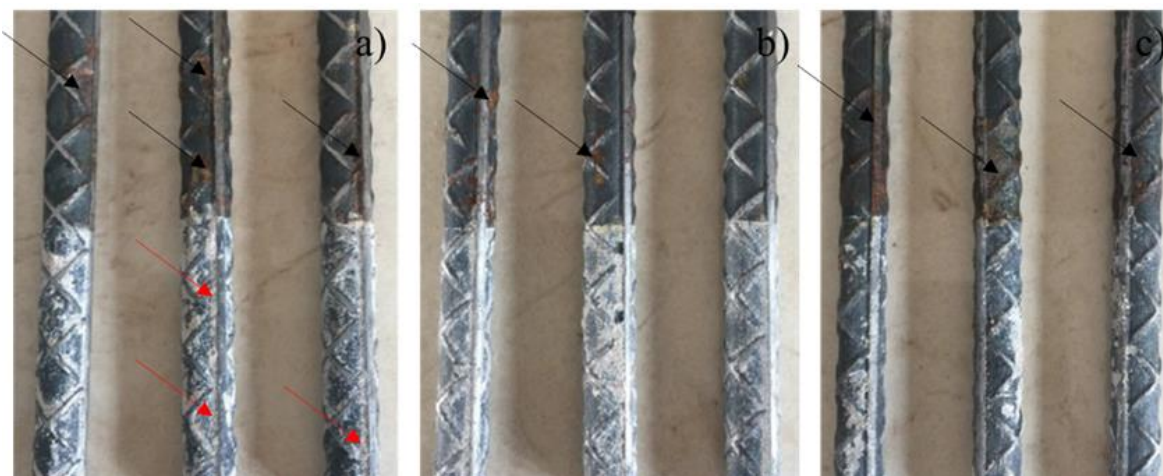
Figure 15. Physical state of the rods embedded in concrete partially submerged for 200 days in a 3% NaCl solution for a) control sample, b) steel coated with 0.5g VM and c) steel coated with 0.5g AA.

4. CONCLUSIONS

Chitosan-based coatings and acetic acid or apple vinegar solvents showed little difference between them. The best amount of chitosan used was 0.5 g, presenting the best results with a larger passivation zone, a more noble pitting potential and a lower current density.
The coating does not show degradation with storage time and further improves its performance. With two immersions the best protective layer is obtained, according to the electrochemical tests of PC. The compressive strength showed an improvement in the presence of reagent grade chitin aggregates in the mixture, over the control sample.
Based on the results of the electrochemical techniques on CR samples, I_{corr} values are obtained in a corrosion range from negligible to low according to existing criteria. The presence of chitin as the aggregate of concrete and the chitosan coating shows a good behavior in RCS during the exposure time and could contribute to the improvement of the structural properties and the environment.

5. ACKNOWLEDGMENTS

REFERENCES

Aballe, A., Bautista, A., Bertocci, U., Huet., F. (2001),'*Measurement of the Noise Resistance for Corrosion Applications*', CORROSION. 57(1):35-42. https://doi.org/10.5006/1.3290327

Alonso, C., Andrade, C., Castellote, M., Castro, P. (2000), '*Chloride threshold values to depassivate reinforcing bars embedded in a standardized OPC mortar*', Cement and Concrete Research. 30:1047-1055. https://doi.org/10.1016/S0008-8846(00)00265-9

Anandhavelu, S., Dhanasekaran, V., Sethuraman, V., Park, H. J. (2017), '*Chitin and Chitosan Based Hybrid Nanocomposites for Super Capacitor Applications*', Journal of Nanoscience and Nanotechnology. 17:1321-1328. https://doi.org/10.1166/jnn.2017.12721

Andrade, C., Alonso, C. (1996), '*Corrosion rate monitoring in the laboratory and on-site*', Construction and Building Materials. 10:315-328. https://doi.org/10.1016/0950-0618(95)00044-5

Andrade, C., Martínez, I. (2010), 'Techniques for measuring the corrosion rate (polarization resistance) and the corrosion potential of reinforced concrete structures' in: *Non-Destructive Evaluation of Reinforced Concrete Structures*. Elsevier W.P., cap. 14, pp. 284-316. https://doi.org/10.1533/9781845699604.2.284

Ashassi-Sorkhabi, H., Kazempour, A. (2020), '*Chitosan, its derivatives and composites with superior potentials for the corrosion protection of steel alloys: A comprehensive review*', Carbohydrate Polymers. 237:116110. https://doi.org/10.1016/j.carbpol.2020.116110

ASTM International (2003). *ASTM C33-03, Standard Specification for Concrete Aggregates, ASTM International.* https://doi.org/10.1520/C0033-03

ASTM International (2012). *ASTM C31/C31M-12, Standard Practice for Making and Curing Concrete Test Specimens in the Field.* https://doi.org/10.1520/C0031_C0031M-12

ASTM International (2014). *ASTM C192/C192M-14, Standard Practice for Making and Curing Concrete Test Specimens in the Laboratory.* https://doi.org/10.1520/C0192_C0192M-14

ASTM International (2014). *ASTM G59-97, Standard Test Method for Conducting Potentiodynamic Polarization Resistance Measurements.* https://doi.org/10.1520/G0059-97R14

ASTM International (2015). ASTM C876-15, *Standard Test Method for Corrosion Potentials of Uncoated Reinforcing Steel in Concrete.* https://doi.org/10.1520/C0876-15

ASTM International (2016). *ASTM C109/C109M-16a, Standard Test Method for Compressive Strength of Hydraulic Cement Mortars (Using 2-in. or [50-mm] Cube Specimens).* https://doi.org/10.1520/C0109_C0109M-16A

Aydin, F., Saribiyik, M. (2010), '*Correlation between Schmidt Hammer and destructive compressions testing for concretes in existing buildings*', Scientific Research and Essays. 5(13):1644-1648.

Bezerra, U. T. (2016), 'Biopolymers with superplasticizer properties for concrete' in: *Biopolymers and Biotech Admixtures for Eco-Efficient Construction Materials*. Elsevier W.P., cap. 10, pp. 195-220. https://doi.org/10.1016/B978-0-08-100214-8.00010-5

Cano-Barrita, P. F. J., León-Martínez, F. M. (2016), 'Biopolymers with viscosity-enhancing properties for concrete' in: *Biopolymers and Biotech Admixtures for Eco-Efficient Construction Materials*. Elsevier W.P., cap. 11, pp. 221-252. https://doi.org/10.1016/B978-0-08-100214-8.00011-7

Carneiro, J., Tedim, J., Fernandes, S. C. M., Freire, C. S. R., Gandini, A., Ferreira, M. G. S., Zheludkevich, M. L. (2013), '*Functionalized chitosan-based coatings for active corrosion protection*', Surface and Coatings Technology. 226:51-59. https://doi.org/10.1016/j.surfcoat.2013.03.035

Carneiro, J., Tedim, J., Ferreira, M. G. S. (2015), '*Chitosan as a smart coating for corrosion protection of aluminum alloy 2024: A review*', Progress in Organic Coatings. 89:348-356. https://doi.org/10.1016/j.porgcoat.2015.03.008

Castelló, M. E., Amalvy, J. I., Anbinder, P. S., Peruzzo, P. J. (2019), '*Obtención Y Caracterización De Quitosano Y Películas Quitosano- Glicerol*', 5º Jordanas ITE - Facultad de Ingeniería - UNPL. pp. 797-803.

Díaz-Blanco, Y. *et al.* (2019), '*Effect of Recycled PET (Polyethylene Terephthalate) on the Electrochemical Properties of Rebar in Concrete*', International Journal of Civil Engineering. 18:487-500. https://doi.org/0.1007/s40999-019-00478-3

Díaz Blanco, Y. *et al.* (2019), '*Natural additive (nopal mucilage) on the electrochemical properties of concrete reinforcing steel*', Revista ALCONPAT. 9(3):260-276. https://doi.org/10.21041/ra.v9i3.429

Dima, J. B., Zaritzky, N. E. (2019), '*Quitosano obtenido de desechos de la industria pesquera y su aplicación como adsorbente de metales pesados*', in: Perez, T. Los residuos que generamos. Su manejo sustentable, un gran desafío. Buenos Aires, ANCEFN, cap. 5, pp. 83-108.

Dodson, V. H. (1990), '*Water reducing chemical admixtures introduction*', in: Concrete Admixtures. Springer, cap. 3, pp. 39-71. https://doi.org/10.1007/978-1-4757-4843-7_3

Dodson, V., Hayden, T. (1989), '*Another Look at the Portland Cement/Chemical Admixture Incompatibility Problem*', Cement, Concrete and Aggregates. 11(1):52-56. https://doi.org/10.1520/CCA10102J

Feliu, S., González, J. A., Andrade, M. C., Feliu, V. (1989), '*Determining polarization resistance in reinforced concrete slabs*', Corrosion Science. 29(1):105-113. https://doi.org/10.1016/0010-938X(89)90083-8

Gacén, J., Gacén, I. (1996), '*Quitina y quitosano. Nuevos materiales textiles*', Boletin Intexter (U.P.C). 110:67-71.

Gebhardt, F., Seuss, S., Turhan M. C., Hornberger, H., Virtanen, S., Boccaccini, A. R. (2012), '*Characterization of electrophoretic chitosan coatings on stainless steel*', Materials Letters. 66:302-304. https://doi.org/10.1016/j.matlet.2011.08.088

Genesca, J., Meas, Y., Rodríguez, F. J., Mendoza, J., Durán, R., Uruchurtu, J., Malo, J. M., Martínez, E. A., Arganiz, C., Pérez, T., Martínez, A., Chacón, J. G., Goana, C., Almeraya, F. M., González, J. G. (2002), *Técnicas Electroquímicas para el Control y Estudio de la Corrosión.* UNAM, D. F., México, p. 244.

Gholamhosseinzadeh, M. R., Aghaie, H., Shahidi Zandi, M., Giahi, M. (2019), '*Rosuvastatin drug as a green and effective inhibitor for corrosion of mild steel in HCl and H_2SO_4 solutions*', Journal of Materials Research and Technology. 8(6):5314-5324. https://doi.org/10.1016/j.jmrt.2019.08.052

Girija, S., Kamachi Mudali, U., Khatak, H. S., Baldev Raj (2007), '*The application of electrochemical noise resistance to evaluate the corrosion resistance of AISI type 304 SS in nitric acid*', Corrosion Science. 49(11):4051-4068. https://doi.org/10.1016/j.corsci.2007.04.007

Hansson, C. M. (1984), '*Comments on electrochemical measurements of the rate of corrosion of steel in concrete*', Cement and Concrete Research. 14(4):574-584. https://doi.org/10.1016/0008-8846(84)90135-2

Hernández Cocoletzi, H., Águila Almanza, E., Flores Agustin, O., Viveros Nava, E. L., Ramos Cassellis, E. (2009), '*Obtención y caracterización de quitosano a partir de exoesqueletos de camarón*', Superficies y Vacío. 22(3): 57-60.

Hernández, M., Genescá J., Uruchurtu, J., Barba, A. (2009), '*Correlation between electrochemical impedance and noise measurements of waterborne coatings*', Corrosion Science. 51:499-510. https://doi.org/10.1016/j.corsci.2008.12.011

Hostalet Alba, F. (1994), '*Situación actual de las técnicas de ensayo no destructivo del hormigón*', Informes de la Construcción. 46(433):19-31. https://doi.org/10.3989/ic.1994.v46.i433.1114

Knorr, D. (1991) '*Recovery and Utilization of Chitin and Chitosan in Food Processing Waste Management*', Food Technology, 45:114-122.

Mansfeld, F., Sun, Z., Hsu, C. H. (2001), '*Electrochemical noise analysis (ENA) for active and passive systems in chloride media*', Electrochimica Acta. 46:3651–3664. https://doi.org/10.1016/S0013-4686(01)00643-0

Martínez-Barrera, G., Vigueras-Santiago, E., Hernández-López, S., Martínez-Barrera, G., Brostow, W., Menchaca-Campos, C. (2005), '*Mechanical improvement of concrete by irradiated polypropylene fibers*', Polymer Engineering & Science. 45(10):1426-1431. doi: https://doi.org/10.1002/pen.20418

O Reilly, V. (2007), '*Métodos para Dosificar Concretos de Elevado Desempeño*'. IMCYC, D.F., México, p. 207.

Pacheco, N. (2010), '*Extracción biotecnológica de quitina para la producción de quitosanos: caracterización y aplicación*', Food and Nutrition. Université Claude Bernard*;* Université autonome métropolitaine (Universidad Autónoma Metropolitana) (Iztapalapa), p. 124

Page, C. L., Treadaway, K. W. J., Bamforth, P. B. (1990), '*Corrosion of reinforcement in concrete*'. Elsevier Applied Science, London-New York. p. 612.

Pakdel, P. M., Peighambardoust, S. J. (2018), '*Review on recent progress in chitosan-based hydrogels for wastewater treatment application*', Carbohydrate Polymers. 201:264-279. https://doi.org/10.1016/j.carbpol.2018.08.070

Papavinasam, S. (2008), 'Electrochemical polarization techniques for corrosion monitoring', in: Yang, L. *Techniques for Corrosion Monitoring*. Elsevier W.P., cap. 3, pp. 49-85. https://doi.org/10.1533/9781845694050.1.49

Pech-Canul, M. A., Castro, P. (2002), '*Corrosion measurements of steel reinforcement in concrete exposed to a tropical marine atmosphere*', Cement and Concrete Research, 32(3): pp. 491-498. https://doi.org/10.1016/S0008-8846(01)00713-X.

Pérez-Quiroz, J. T., Terán, J., Herrera, M. J., Martínez, M., Genescá, J. (2008), '*Assessment of stainless steel reinforcement for concrete structures rehabilitation*', Journal of Constructional Steel Research. 64(11):1317-1324. https://doi.org/10.1016/j.jcsr.2008.07.024

Sanchez-Amaya, J. M., Cottis, R. A., Botana, F. J. (2005), '*Shot noise and statistical parameters for the estimation of corrosion mechanisms*', Corrosion Science. 47:3280-3299. https://doi.org/10.1016/j.corsci.2005.05.047

Shrinivas Rao, M., Aye Nyein, K., Si Trung, T., Stevens, W. F. (2007), '*Optimum parameters for production of chitin and chitosan from squilla (S. empusa)*', Journal of Applied Polymer Science. 103:3694-3700. https://doi.org/10.1002/app.24840

Sousa Andrade, V., de Barros Neto, B., Fukushima, K., de Campos-Takaki, G. M. (2003), '*Effect of medium components and time of cultivation on chitin production by Mucor circinelloides (Mucor javanicus IFO 4570) - A factorial study*', Revista Iberoamericana de Micologia. 20:149-153.

Stern, M., Geary, A. L. (1957), '*Electrochemical Polarization I. A Theoretical Analysis of the Shape of Polarization Curves*', Journal of The Electrochemical Society, 104(1):56-63. https://doi.org/10.1149/1.2428653

Taji, I., Ghorbani, S., de Brito, J., Tam, V. W. Y., Sharifi, S., Davoodi, A., Tavakkolizadeh, M. (2018), '*Application of statistical analysis to evaluate the corrosion resistance of steel rebars embedded in concrete with marble and granite waste dust*', Journal of Cleaner Production. 210:837-846. https://doi.org/10.1016/j.jclepro.2018.11.091

Taylor, H. F. W. (1990), '*Cement Chemestry*'. Thomas Telford, London, p. 437.

Zhou, B., Gu, X., Guo, H., Zhang, W., Huang, Q. (2018), '*Polarization behavior of activated reinforcing steel bars in concrete under chloride environments*', Construction and Building Materials. 164:877-887. https://doi.org/10.1016/j.conbuildmat.2018.01.187

Zhou, S., Zhang, S., Shen, J., Guo, W. (2019), '*Effect of cattle manure ash's particle size on compression strength of concrete*', Case Studies in Construction Materials. 10:e00215. https://doi.org/10.1016/j.cscm.2018.e00215

Use of chitosan as an organic coating to prevent / inhibit the corrosion of reinforced concrete
Rivera-Ortiz, I., Díaz-Blanco, Y., Menchaca-Campos, C., Uruchurtu-Chavarín, J.

Evaluation of chloride migration in ultra-high performance concrete (UHPC) with glass powder

L. V. Dias[1], S. M. Soares[2], J. A. Salvador Filho[2] (iD), F. G. S. Ferreira[1]* (iD)

*Contact author: fgiannotti@ufscar.br

ABSTRACT

The influence of glass powder incorporation to ordinary concrete regarding mechanical and durability properties has been studied. This work aims to evaluate the durability of ultra-high performance cementitious composites (UHPCC) with partial substitution of Portland cement by glass powder, through chloride migration test according to the NT Build 492 methodology. With this aim, specimens with 0%, 10%, 20%, 30% and 50% content of glass powder by weight of Portland cement were cast, cured in lime saturated water until the age of 28 days. The results indicate that minor contents of glass powder do not harm the concrete properties and higher contents maintain good mechanical and durability characteristics.

Keywords: cementitious composite; glass powder; chloride migration.

[1] Departamento de Engenharia Civil, Universidade Federal de São Carlos, São Carlos, Brasil.

[2] Instituto Federal de Educação, Ciência e Tecnologia de São Paulo, Caraguatatuba, Brasil.

Contribution of each author

In this work, the author L. V. Dias contributed with the activities of conceptualization, development, results and discussion, writing and preparation of the original text (30%); S. M. Soares contributed to the activities of conceptualization, development, results and discussion (30%); J. A. Salvador Filho contributed with conceptualization, supervision, discussion of results, writing and review (20%) and F. G. S. Ferreira contributed with conceptualization, supervision, discussion of results, writing and review (20%)..

Discussions and subsequent corrections to the publication

Any dispute, including the replies of the authors, will be published in the second issue of 2022 provided that the information is received before the closing of the first issue of 2022.

Avaliação da migração de cloretos em compósitos cimentícios de ultra alto desempenho com pó de vidro

RESUMO

O pó de vidro incorporado ao concreto convencional vem sendo estudado em relação à sua influência na resistência mecânica e durabilidade. Este trabalho visa avaliar a durabilidade de compósitos cimentícios de ultra alto desempenho (CCUAD) com substituição parcial do cimento por vidro finamente moído, por meio do ensaio de migração de cloretos utilizando o método da NT Build 492. Para tanto foram moldados corpos de prova com teores de pó de vidro de 0%, 10%, 20%, 30% e 50% em relação ao volume de cimento e a avaliação foi feita na idade de 28 dias. Os resultados indicam que, em teores baixos, o pó de vidro não prejudica as propriedades dos compósitos e em teores mais altos os compósitos mantêm boas características mecânicas e de durabilidade.
Palavras-chave: compósito cimentício; pó de vidro; migração de cloretos.

Evaluación de la migración de cloruro en compuestos cementosos de ultra alto rendimiento con polvo de vidrio

RESUMEN

Se ha estudiado la incorporación de polvo de vidrio en el hormigón convencional por su influencia en la resistencia mecánica y la durabilidad. Este trabajo tiene como objetivo validar la durabilidad de los compuestos cementosos de ultra alto desempeño (CCUAD) con reemplazo parcial de cemento por vidrio finamente molido, a través del ensayo de migración de cloruros, utilizando el método NT Build 492. Para ello, fueron moldeadas probetas conteniendo valores de 0%, 10%, 20%, 30 % y 50% de polvo de vidrio en relación al volumen de cemento, y la evaluación se realizó a los 28 días de edad. Los resultados indican que, con valores bajos, el polvo de vidrio no perjudica las propiedades de los compuestos y, a niveles superiores, los compuestos mantienen características mecánicas y durabilidad adecuadas.
Palabras clave: compuesto cementoso; polvo de vidrio; migración de cloruro.

Evaluation of chloride migration in ultra-high-performance concrete (UHPC) with glass powder
Dias, L. V., Soares, S. M., Salvador Filho, J. A., Ferreira, F. G. S.

1. INTRODUCTION

The term ultra-high-performance concrete was first used by de Larrard and Sedran (1994). It is usually related to a high compressive strength composite (reaching 4 times the strength of ordinary concrete), according to Bahedh and Jafar (2018). Morover, its development applies particle packaging models that leads to a high durability material (Alkaysi *et al.,* 2015).

Silica fume is usually employed in the production of ultra-high performance cementitius composite, in addition to a high Portland cement consumption (about 800 – 1000 kg/m³) (Bahedh and Jafar, 2018; Ganesh and Murthy, 2018), and smaller aggregates when compared to ordinary concrete. However, due to the high environmental impact generated in Portland cement production, since about 0.8 tons of CO_2 are released to produce one ton of Portland cement (Mehta and Ashish, 2020), ultra-high performance cementitious matrices meet current trends in carbon footprint reduction, with the use of high levels of supplementary cementitious materials in partial replacement of Portland cement. Supplementary cementitious materials have been widely used to as partial replacement of Portland cement in concrete either as filler or pozzolanic material.

Adaway and Wang (2015) used residual glass as a partial substitute for the fine aggregate in structural concrete and found that concrete containing up to 30% of fine glass aggregate exhibits greater compressive strength than ordinary concrete.

Du and Tan (2017) studied the incorporation of high volume of glass powder as a partial substitute of Portland cement in cementitious composites and obtained better mechanical behaviors and higher performance in terms of durability.

Studies conducted by Afshinnia and Rangaraju (2015) showed satisfactory results in mitigating the alkali-silica reaction when glass powder was used as a pozzolanic material in partial replacement to cement.

High and ultra-high-performance concretes should solve the durability problem on chloride attack in ordinary structural concrete due to their dense microstructure (Sohail et al., 2021).

The European Union generated about 25.8 Mt of glass waste in 2007 (Abdollahnejad *et al.,* 2017). Brazil consumed 5.5 kg/inhabitants. of which 80% were not recycled in 2008, according to data from the Institute for Applied Economic Research (IPEA, 2012). Thus, glass residue is an abundant material whose use can help to reduce the environmental impact, both as supplementary cementitious material in concrete production, as well as in Portland cement manufacture as a pozzolanic material. Glass powder can be used as partial replacement of Portland cement aiming to reduce carbon emissions from the Civil Construction industry considering its high silica (SiO_2) content, its amorphous structure and pozzolanic characteristics, (Mehta and Ashish, 2020).

Thus, the main objective of this work is to evaluate the durability of ultra-high-performance cementitious composites (UHPCC) with partial substitutions of Portland cement by glass powder, at the contents of 10%, 20%, 30% and 50%, focusing on chloride penetration, through chloride migration assay.

2. MATERIALS AND METODOS

2.1 Materials

Portland cement type CPV-ARI, silica fume and glass powder were used as binders. Glass powder with particles size smaller than 75 μm was used. Glasses classified as soda-lime were processed from post-consumption amber bottles to minimize uncontrolled variations due to pigments. After collecting, the glass bottles were washed in water with detergent to remove labels, caps, glue, and impurities. It was air dried and crushed in a concrete mixer loaded with chrome-steel spheres. After grinding, the crushed glass was grounded in a ball mill, with balls of the same material. The glass resulting from grinding in ball mill was dried in an oven at 110°C ± 5°C for 24 hours. After dried,

Evaluation of chloride migration in ultra-high perfomance concrete (UHPC) with glass powder
Dias, L. V., Soares, S. M., Salvador Filho, J. A., Ferreira, F. G. S.

63

the glass was sifted in a mechanical sieve shaker in batches of 200g for 15 minutes. Figure 1 presents the glass powder processing.

Figure 1. Recycled glass powder processing.
Source: Adapted from Freitas (2019).

Ground materials were packed in paper and plastic bags, avoiding contact with moisture. In addition, a natural fine quartz aggregate with a maximum dimension of 1.2 mm was used. Superplasticizer admixtures based on polycarboxylate were also used to ensure low water/binder ratio and shrinkage reducing admixture to avoid matrix cracking. The physical characteristics of Portland cement, silica fume, glass powder and sand are presented in Tables 1, 2 and 3, respectively. The number of tests were fulfilled according to each specific Brazilian standard.

Table1. Portland Cement physical characteristics.

Parameter		Method	Results	Reference values NBR 16697 (ABNT, 2018)
Specific gravity		NBR 16605 (ABNT, 2017)	3.16 g/cm³	-
Initial setting time		NBR 16607 (ABNT, 2018)	135 min	≥ 60 min
Final setting time		NBR 16607 (ABNT, 2018)	210 min	≤ 600 min
Water for normal consistency		NBR 16606 (ABNT, 2018)	30.0%	-
% retained in the 75 μm sieve		NBR 16372 (ABNT, 2015)	0.1%	$\leq 6.0\%$
Blaine surface area		NBR 16372 (ABNT, 2015)	665.0 m²/kg	-
Compressive strength	1 day	NBR 7215 (ABNT, 2019)	27.5 MPa	≥ 14.0 MPa
	3 days		42.0 MPa	≥ 20.0 MPa
	7 days		48.7 MPa	≥ 34.0 MPa
	28 days		52.2 MPa	-

Table2. Silica fume and glass powder physical characteristics.

Parameter	Silica fume		Glass powder	
	Test result	Reference values NBR 13956-1	Test result	Reference values
Specific gravity	2.25 kg/dm³	-	2.55 kg/dm³	-
Moisture	Max. 3.0%	≤ 3.0%	-	-
% retained in the 45 μm sieve	Max. 10.0%	≤ 10.0%	-	-
Blaine surface area	247.0 m²/kg	-	393.0 m²/kg	-
Pozzolanic activity index	Min. 105.0%	≥ 105.0%	6.4 MPa±0.10 *	6.0 MPa**

*tested according NBR 5751 (ABNT, 2015) method.
** Reference values from NBR 12653 (ABNT, 2015).

Table3. Fine aggregate physical characteristics.

Parameter	Method	Result
Water absorption	NBR NM 30 (ABNT, 2000)	0.64%
Specific mass	NBR NM 52 (ABNT, 2009)	2.56 g/cm³
Weight Unit	NBR NM 45 (ABNT, 2006)	1475.78 kg/m³
Unit weight (compacted)	NBR NM 45 (ABNT, 2006)	1617.83 kg/m³
Organic impurities	NBR NM 49 (ABNT, 2006)	Clearer solution than standard
Fine material passing through 75 μm sieve, by washing	NBR NM 46 (ABNT, 2003)	1.66%

In Table 4 the chemical characteristics of Portland cement, silica fume, glass powder and fine aggregate are presented.

Table4. Materials chemical composition.

Component	Materials (values in mass %)			
	Portland cement	Silica fume	Glass powder	Fine aggregate
Loss on ignition (LOI)	4.05 (≤ 6.50) *	3.60 (≤ 6.00) **	0.58	0.58
Calcium oxide (CaO)	61.40	<0.20	9.10	0.071
Aluminum oxide (Al_2O_3)	4.31	<0.20	3.70	3.40
Silicon dioxide (SiO_2)	23.00	94.10	74.00	94.00
Sulfur trioxide (SO_3)	2.97 (≤ 4.5) *	-	-	-
Iron oxide (Fe_2O_3)	2.49	<0.50	0.42	0.67
Potassium oxide (K_2O)	0.96	1.28	0.56	1.20
Phosphoric oxide (P_2O_5)	0.52	-	-	-
Strontium oxide (SrO)	0.27	<0.20	0.039	-
Chlorine Ion (Cl^-)	0.12	-	-	-
Thorium dioxide (ThO_2)	<0.01	<0.01	<0.01	<0.01
Uraninite (U_3O_8)	<0.01	<0.01	<0.01	<0.01

Titanium dioxide (TiO_2)	-	<0.20	-	0.35
Chromium Oxide (Cr_2O_3)	-	-	-	0.049
Magnesium Oxide (MgO)	-	-	0.74	-
Rubidium oxide (Rb_2O)	-	-	0.016	-
Sodium oxide (Na_2O)	-	-	11.00	0.37

* Reference values from NBR 16697 (ABNT, 2018).
** Reference values from NBR 13956-1 (ABNT, 2012).

In Figure 2 the granulometric distribution of Portland cement, silica fume, glass powder and fine aggregate (quartz sand) from three samples each test are presented. In these results it is possible to observe D_{50} parameter of 0.8 µm for silica fume, 7 µm for Portland cement, 15 µm for glass powder and 270 µm for quartz sand.
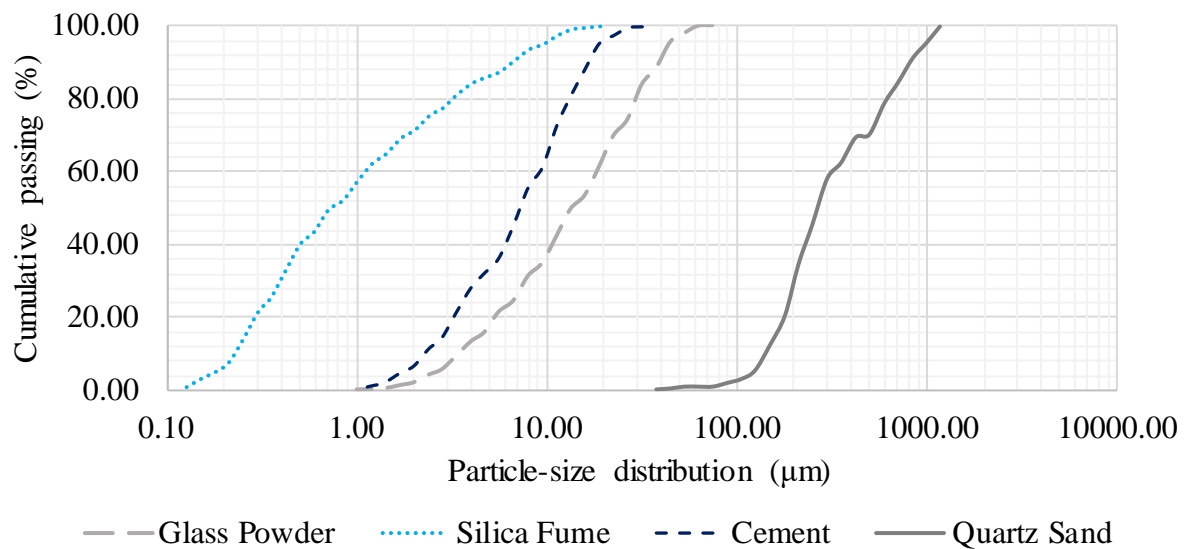
Figure 2. Particle-size distribution.

2.2 Methodology

For ultra-high performance cementitious composites production, a water/binder ratio of 0.18 was adopted for all mixtures, the silica fume content was 0,8% of the Portland cement weight of the reference mixture. Glass powder was added in contents of 0%, 10%, 20%, 30% and 50% in volumetric replacement of Portland cement, and the mixtures were named REF, VD10, VD20, VD30 and VD50, respectively. In addition, an amount of 2.25% of superplasticizer admixture was used to obtain a consistency index of 380±10mm (fluid consistency), and shrinkage reductor admixture in content of 1%, as recommended by the manufacturer. The binder-admixture compatibility was evaluated by the mini slump test, according to the Kantro test (1980).

The consistency of cementitious composites (Figure 3) was verified according to NBR 13276 (ABNT, 2016) and the mass density and incorporated air content of the composites in the fresh state were determined according to NBR 13278 (ABNT, 2005).

Figure 3. Slump flow test for consistency determination.

In Table 5 it is shown the unitary proportions, Portland cement consumption and consistency for each mixture. The nomenclature SP refers to the superplasticizer admixture and RR, to the shrinkage reducing admixture.

Table 5. Mixture ratios and consistency index for each composite.

Mixture	Portland cement	Silica fume	Glass powder	Fine aggregate	Water	SP	RR	Consistency (mm)
REF	1	0.08	0.00	1.07	0.194	0.020	0.010	380.0
VD10	1	0.09	0.09	1.19	0.216	0.027	0.012	377.0
VD20	1	0.10	0.20	1.34	0.243	0.030	0.014	375.5
VD30	1	0.11	0.35	1.53	0.278	0.035	0.015	381.5
VD50	1	0.16	0.81	2.15	0.389	0.049	0.022	384.5

The materials consumption of each cementitious composites mixture evaluated are presented in Table 6.

Table 6. Cementitious composites material consumption in kg/m³.

Mixture	Portland cement	Silica fume	Glass powder	Fine aggregate	Water*	SP	RR
REF	1000.00	80.00	0.00	1074.00	181.28	24.3	10.80
VD10	900.00	80.00	81.00	1074.00	181.28	24.3	10.80
VD20	800.00	80.00	161.00	1074.00	181.28	24.3	10.80
VD30	700.00	80.00	242.00	1074.00	181.28	24.3	10.80
VD50	500.00	80.00	403.00	1074.00	181.28	24.3	10.80

*Water consumption adjusted considering the solids content present in superplasticizer.

For the hardened state properties assay, 5x10 cm cylindrical specimens were manually dense molded and cured in lime saturated water. The axial compressive strength test for UHPCC was performed according to NBR 5739 (ABNT, 2018) at the age of 28 days on four specimens per mixture. The test to obtain the static modulus of elasticity of UHPCC was performed according to NBR 8522 (ABNT, 2017) at the age of 28 days on three specimens per mixture.

For durability assay, water absorption by capillarity of CCUAD at the age of 28 days was performed, following the recommendations of NBR 9779 (ABNT, 2012) in three 5x10 cm cylinder specimens per mixture, and chloride migration coefficient in the non-stationary state (according to NT Build 492) on two 10x20 cm cylinder specimens for each mixture.
The chloride diffusion test device is shown in Figure 4.

Figure 4. Chloride diffusion test apparatus.

The specimens were cut into four equal parts of 10 x 5 cm, using the two inner samples for the test. After being cut, the samples underwent the preconditioning process in a vacuum container with both faces exposed to an internal pressure between 1 and 5 KPa. Subsequently, the container was filled with a $Ca(OH)_2$ solution until the samples were fully immersed. The vacuum was kept in the container to ensure the saturation of the cementitious composite pores with the solution. Two solutions were then prepared, the reaction solution of water with sodium chloride (NaCl) at 10%, and the anode solution of water with sodium hydroxide (NaOH) at 0.3 M. After being removed from the vacuum, the samples were placed in tubes, and the interfaces sealed with silicone to ensure that only the faces were in contact with the solutions. A container was filled with NaCl solution and the NaOH solution was placed in the tubes above the samples. The tubes with the samples were then placed in the container containing the NaCl solution. The positive pole of the energy source was connected to the anode and the negative to the frame, and the current was passed through the system to accelerate the Cl⁻ ions migration through the samples. The test time and voltage are defined based on the initial current passing through the system, according to the recommendations of NT Build 492. The samples were then removed from the apparatus, splitted by diametral compression, and a 0.1M silver nitrate ($AgNO_3$) solution was sprayed to highlight the chloride penetration depth in the samples. This depth was then measured with a caliper and the chloride migration coefficient was determined in the non-stationary state by Equation 1, where D_{nssm} represents the migration coefficient in the non-stationary state (10^{-12} m²/s), U the applied voltage (V), T the average of the initial and final temperature of the anode (°C), L the sample height (mm), x_d the penetrations depth average (mm), and t the test duration (hours).

$$D_{nssm} = \frac{0.0239(273 + T)L}{(U - 2)t}\left(x_d - 0.0238\sqrt{\frac{(273 + T)Lx_d}{U - 2}}\right) \qquad (1)$$

The results were analyzed in terms of analysis of variance (ANOVA), and in cases where F > F$_{critical}$, the Tukey test was applied.

3. RESULTS AND DISCUSSION

The results of mass density, incorporated air content, compressive strength, static elasticity modulation and water absorption by capillarity of ultra high performance cementitious composites at the age of 28 days are shown in Table 7. In the Table 7 the letter *A* indicates that the value is statistically equal to the reference, while the letter *B* indicates statistical difference compared to the reference mixture.

Table 7. Mechanical and physical characteristics of the UHPCC studied.

Mixture	Unit weight (kg/m³)	Air content (%)	Compressive strength (MPa)	Modulus of elasticity (GPa)	Water absorption (g/cm²)
REF	2307.0	4.0	115.58±12.77/-	43.09±1.81/-	0.079±0.008/-
VD10	2338.0	2.0	119.40±2.76/A	45.51±3.35/A	0.077±0.007/A
VD20	2326.0	2.0	113.57±6.84/A	41.67±3.54/A	0.092±0.007/A
VD30	2322.0	1.0	110.66±6.13/A	42.94±2.73/A	0.091±0.003/A
VD50	2273.0	1.0	83.37±6.83/B	41.51±0.80/A	0.088±0.02/A

An increase of around 1% in mass density was observed for the VD10, VD20 and VD30 samples when compared to the REF samples, while the composite density with 50% replacement of Portland cement by glass powder decreased by 1.47%. The incorporated air content results presented a reduction with the increase of glass powder content. Regarding compressive strength, static modulus of elasticity and water absorption, there is a variation between the values, however no sample presents a statistically significant difference when compared to the reference sample, except for VD50 compressive strength which decreased by 23.5% in comparison to REF.
Li *et al.* (2019) and Lee *et al.* (2018) added glass powder to the Portland cement paste in contents from 0% to 25% with a/c ratio 0.41, and observed the compressive strength decrease with increasing of glass powder amount. The decrease in the compressive strength of the Portland cement paste with glass powder can be explained by the dilution effect. The dilution effect of glass powder reduces the Portland cement content and increases the effective water/cement ratio, to reduce the formation of hydration products and, finally, reduces the compressive strength of the Portland cement paste (Du et al., 2020). This is also observed in other studies. According to Du and Tan (2017), the pozzolanic reaction of glass powder is relatively slower and therefore the resistance in the early ages of concrete is reduced when compared to Portland cement hydration. However, with a longer curing age, the benefits of the glass powder's pozzolanic reaction begin to appear.
Sohail *et al.* (2018) have charted several studies relating compressive strength results and the respective water/binder ratio. The results of the 28-day compressive strength tests of reference cementitious composites and Portland cement replacement by glass powder found in the present study were included into the same chart (Figure 5).
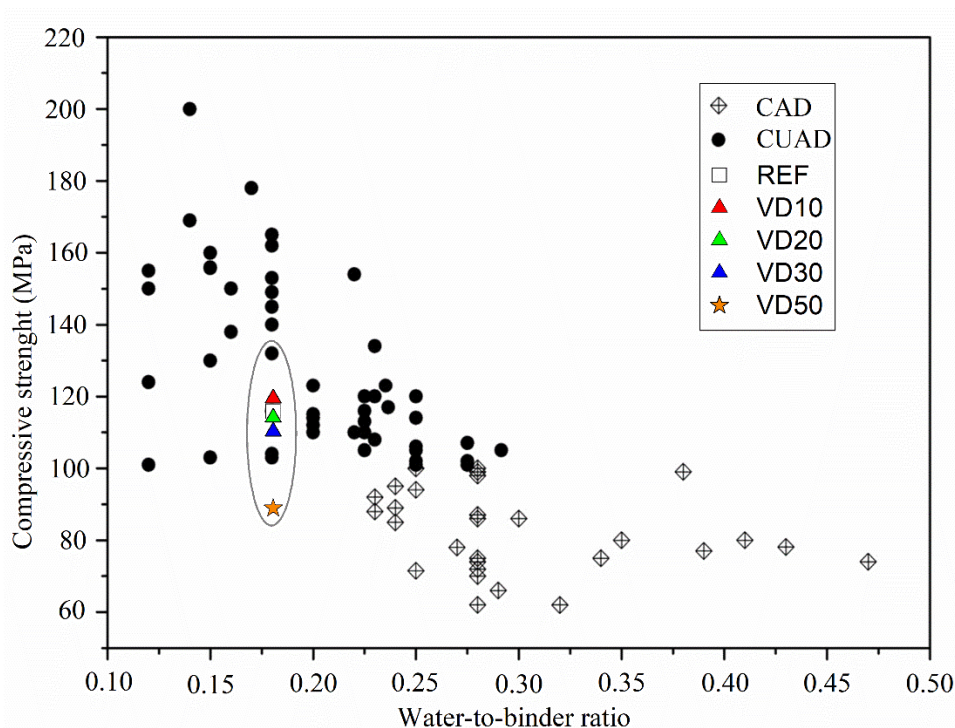
Figure 5. Effect of water-to-binder ratio on compressive strength of HPC and UHPC
Fonte: Adapted from Sohail et al. (2018).

By reducing the water/binder ratio the compressive strength increases; however, for CCUAD mixtures in the same water/binder ratio, different compressive strengths were achieved due to other factors, such as the amount and type of Portland cement or silica fume.

The results of the chloride penetration depth and the chloride diffusion coefficients in the non-stationary state are presented in Table 8.

Table 8. Chloride penetration depth and chloride diffusion coefficient on 28-day age samples.

Mixture	Chloride penetration depth (mm)		Chloride diffusion coefficient (10^{-12} m^2/s)	
	Value	Variation	Value	Variation
REF	1.17	1.26	0.196	0.019
VD10	1.14	0.93	0.191	0.026
VD20	1.55	0.88	0.141	0.018
VD30	1.46	0.91	0.261	0.059
VD50	1.63	0.67	0.340	0.021

The results of chloride diffusion coefficient at 10 -12m²/s, as well as the average depth of chloride penetration are shown in Figure 6. It is emphasized that the sample results pointed with the letter *A* are statistically equal to the reference samples, while those pointed with the letter *B* are statistically different when compared to the reference results.
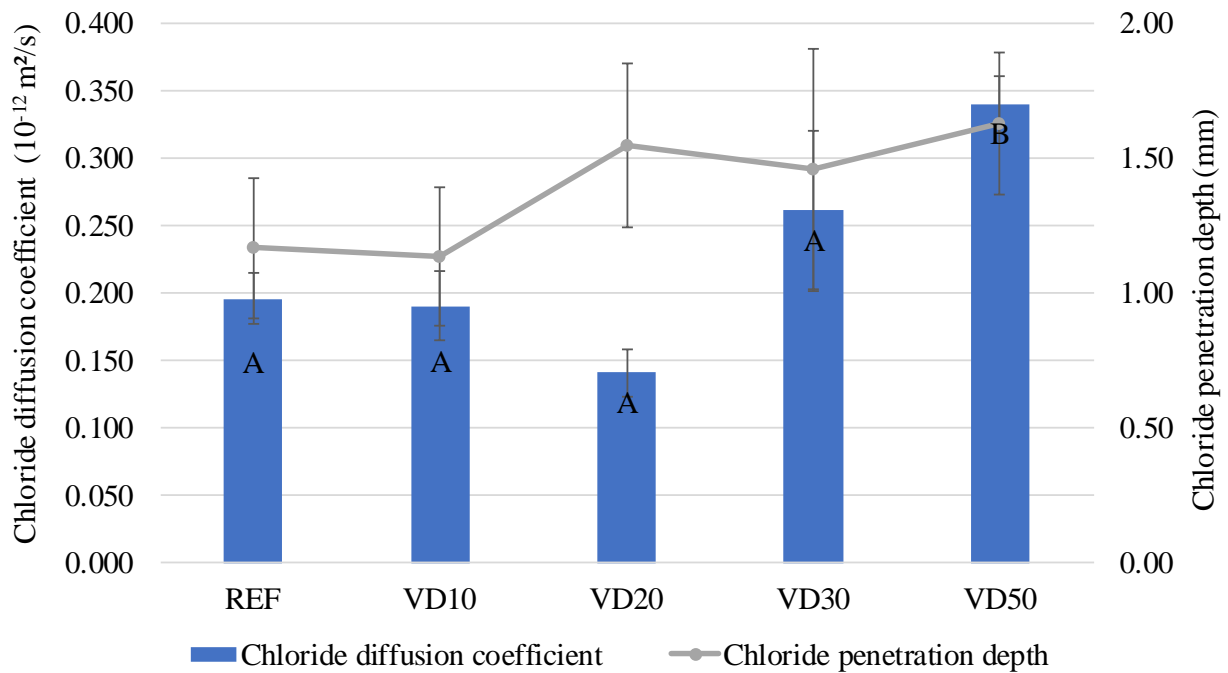
Figure 6. Chloride diffusion coefficient and penetration depth.

It is observed that there was an increase in the migration coefficient of cementitious composites with the increase of glass powder content (except for the vd20 mixture). This fact can be explained due the glass powder particles (D_{50}=15µm) are larger than Portland cement particles (D_{50}=7µm), leading to a different particle packaging (filer effect of glass powder), in addition to the pozzolanic reactions of glass powder being slower than the Portland cement hydration reactions, that can develop up to older ages as observed by Du and Tan (2015). Thus, samples with higher glass content trend to present a lower C-S-H content at intermediate ages when compared to those with lower content or without glass powder. Tam *et al.* (2012) found that a higher C-S-H content leads to a lower volume of pores and their disconnection, so samples with lower C-S-H content tend to have a higher chloride penetration depth.

Also, the fact that water absorption content tends to increase as the percentage of glass powder increases, as shown in Table 7, is another indication of porosity growth with the increase in glass powder content.

The depth of chloride penetration at 28 days results follows the chloride diffusion coefficient for all mixtures, except for the mixture with 20% of glass powder replacement.

For the chloride diffusion coefficient, the statistical analysis shows that the replacement of Portland cement by 50% of glass powder induced a significant effect when compared to all mixtures evaluated.

However, it is worth mentioning that all obtained results for chloride penetration depth and chloride migration were lower than those observed in other studies with ultra-high performance materials. Chen *et al.* (2018) and Mosavinejad *et al.* (2020) evaluated the diffusion coefficient of chlorides in UHPCC obtaining chloride penetration depths around 5 mm and diffusion coefficients of $2*10^{-12}$m²/s. In addition, when comparing the values obtained in this work with those in Table 9, it is verified that all mixtures are classified with extreme high resistance to chloride penetration.

Tabela 9. Resistance to chloride penetration of various types of concrete based on the 28-day chloride diffusivity.

Chloride diffusion coefficient (10^{-12} m²/s)	Chloride penetration depth (mm)
>15	Low
10.0-15.0	Moderate
5.0-10.0	High
2.5-5.0	Very High
<2.5	Extremely High

Source: Adapted from Teng *et al.* (2018).

Castellote, Andrade and Alonso (2001) and Santos (2006) analyzed the chloride diffusion tests in ordinary concretes with and without silica fume incorporation, varying the water/cement ratio, and justified the reduction of diffusion coefficients due to a reduction in the water/binder ratio followed by a reduction in total porosity due to the decrease in this relationship. In the present work, the water/binder ratio was constant, which provided a significant increase in the water/cement ratio of the VD50, which may have caused its porosity increase.

According to Li *et al.* (2020), the chloride ions diffusion coefficients of UHPCC varied from 0.02 x 10^{-12} m²/s to 0.41 x 10^{-12} m²/s depending on the water/cement ratio, curing procedure, fiber volume and age of the tests. Due to the large number of parameters involved in performed tests available in the literature, it is difficult to compare quantitatively the chloride ions diffusion in CCUAD.

4. CONCLUSIONS

In accordance with the results obtained, it is concluded that:
1. Whereas all mixtures studied achieved high compressive strength and high modulus of elasticity, low water absorption and high resistance to penetration and diffusion of chlorides, all are ultra-high performance cementitious composites, with or without the incorporation of glass powder.
2. Partial replacement of large Portland cement contents by glass powder (50%) may cause changes on the properties of the cementitious composites at the age of 28 days.
3. The coefficients obtained are still much lower than those in the literature, indicating high mechanical resistance and extremely high resistance to chloride penetration. Thus, glass powder is a viable substitute for Portland cement in terms of chloride penetration durability.
4. Considering the significant reduction of Portland cement amount in cementitious composite with the replacement of 50% of cement by glass powder, and depending on the characteristics presented by the material, its use is recommended when compared to the other composites studied. This is the most economical alternative and provides lower environmental impacts.

72

Evaluation of chloride migration in ultra-high-performance concrete (UHPC) with glass powder
Dias, L. V., Soares, S. M., Salvador Filho, J. A., Ferreira, F. G. S.

5. ACKNOWLEDGMENT

6. REFERENCES

Abdollahnejad, Z., Kheradmand, M., Pacheco-Torgal, F. (2017), *Short-Term Compressive Strength of Fly Ash and Waste Glass Alkali-Activated Cement-Based Binder Mortars with Two Biopolymers.* Journal of Materials in Civil Engineering. 29(7). https://doi.org/10.1061/(ASCE)MT.1943-5533.0001920

Adaway, M., Wang, Y. (2015), *Recycled glass as a partial replacement for fine aggregate in structural concrete – Effects on compressive strength.* Electronic Journal of Structural Engineering. 14(1):116-122.

Afshinnia, K., Rangaraju, P. R. (2015), *Influence of fineness of ground recycled glass on mitigation of alkali-silica reaction in mortars*. Construction and Building Materials. 81: 257-267. https://doi.org/10.1016/j.conbuildmat.2015.02.041

Alkaysi, M., El-Tawil, S., Liu, Z., Hansen, W. (2016), *Effects of silica powder and cement type on durability of ultra high performance concrete (UHPC).* Cement and Concrete Composites. 66: 47-56. https://doi.org/10.1016/j.cemconcomp.2015.11.005

Associação Brasileira de Normas Técnicas. (2000). *NM 30: Agregado miúdo – Determinação da absorção de água*. Rio de Janeiro.

Associação Brasileira de Normas Técnicas. (2006). *NM 45: Agregados - Determinação da massa unitária e do volume de vazios*. Rio de Janeiro.

Associação Brasileira de Normas Técnicas. (2003). *NM 46: Agregados - Determinação do material fino que passa através da peneira 75 μm, por lavagem*. Rio de Janeiro.

Associação Brasileira de Normas Técnicas. (2001). *NM 49: Agregado miúdo - Determinação de impurezas orgânicas*. Rio de Janeiro.

Associação Brasileira de Normas Técnicas. (2009). *NM 52: Agregado miúdo - Determinação da massa específica e da massa específica aparente*. Rio de Janeiro.

Associação Brasileira de Normas Técnicas. (2003). *NBR 248: Agregados - Determinação da composição granulométrica*. Rio de Janeiro.

Associação Brasileira de Normas Técnicas. (2018). *NBR 5739: Concreto – Ensaio de compressão de corpos de prova cilíndricos*. Rio de Janeiro.

Associação Brasileira de Normas Técnicas. (2015). *NBR 5751 Materiais pozolânicos – Determinação da atividade pozolânica com cal aos sete dias*. Rio de Janeiro.

Associação Brasileira de Normas Técnicas. (2019). *NBR 7215: Cimento Portland - Determinação da resistência à compressão de corpos de prova cilíndricos*. Rio de Janeiro.

Associação Brasileira de Normas Técnicas. (2013). *NBR 7681-2: Calda de cimento para injeção. Parte 2: Determinação do índice de fluidez e da vida útil – Método de ensaio*. Rio de Janeiro.

Associação Brasileira de Normas Técnicas. (2017). *NBR 8522: Concreto – Determinação dos módulos estáticos de elasticidade e de deformação a compressão*. Rio de Janeiro.

Associação Brasileira de Normas Técnicas. (2012). *NBR 9779: Argamassa e concretos endurecidos - Determinação da absorção de água por capilaridade*. Rio de Janeiro.

Associação Brasileira de Normas Técnicas. (2013). *NBR 11579: Cimento Portland - Determinação do índice de finura por meio da peneira 75 μm (nº200)*. Rio de Janeiro.

Associação Brasileira de Normas Técnicas. (2015). *NBR 12653: Materiais pozolânicos — Requisitos*. Rio de Janeiro.

Evaluation of chloride migration in ultra-high perfomance concrete (UHPC) with glass powder
Dias, L. V., Soares, S. M., Salvador Filho, J. A., Ferreira, F. G. S.

73

Associação Brasileira de Normas Técnicas. (2016). *NBR 13276: Argamassa para assentamento e revestimento de paredes e tetos – Determinação do índice de consistência*. Rio de Janeiro.

Associação Brasileira de Normas Técnicas. (2005). *NBR 13278: Argamassa para assentamento e revestimento de paredes e tetos - Determinação da densidade de massa e do teor de ar incorporado*. Rio de Janeiro.

Associação Brasileira de Normas Técnicas. (2012). *NBR 13956-1: Sílica ativa para uso com cimento Portland em concreto, argamassa e pasta. Parte 1: Requisitos*. Rio de Janeiro.

Associação Brasileira de Normas Técnicas. (2010). *NBR 15895: Materiais pozolânicos – Determinação do teor de hidróxido de cálcio fixado – Método Chapelle modificado*. Rio de Janeiro.

Associação Brasileira de Normas Técnicas. (2015). *NBR 16372: Cimento Portland e outros materiais em pó - Determinação da finura pelo método de permeabilidade ao ar (método de Blaine)*. Rio de Janeiro.

Associação Brasileira de Normas Técnicas. (2017). *NBR 16605: Cimento Portland e outros materiais em pó - Determinação da massa específica*. Rio de Janeiro.

Associação Brasileira de Normas Técnicas. (2018). *NBR 16606: Cimento Portland - Determinação da pasta de consistência normal*. Rio de Janeiro.

Associação Brasileira de Normas Técnicas. (2018). *NBR 16607: Cimento Portland - Determinação dos tempos de pega*. Rio de Janeiro.

Associação Brasileira de Normas Técnicas. (2018). *NBR 16697: Cimento Portland - Requisitos*. Rio de Janeiro.

Bahedh, M. A., Jaafar, M. S. (2018), *Ultra High-Performance Concrete Utilizing Fly Ash as Cement Replacement under Autoclaving Technique*. Case Studies in Construction Materials. 9. https://doi.org/10.1016/j.cscm.2018.e00202

Castellote, M., Andrade, C., Alonso, C. (2001), *Measurement of the steady and non-steady-state chloride diffusion coefficients in a migration test by means of monitoring the conductivity in the anolyte chamber. Comparison with natural diffusion tests*. Cement and Concrete Research**.** 31(10): 1411-1420 https://doi.org/10.1016/S0008-8846(01)00562-2

Chen, Y., Yu, R., Wang, X., Chen, J., Shui, Z. (2018), *Evaluation and optimization of Ultra-High Performance Concrete (UHPC) subjected to harsh ocean environment: Towards an application of Layered Double Hydroxides (LDHs)*. Construction and Building Materials. 177: 51-62. https://doi.org/10.1016/j.conbuildmat.2018.03.210

de Larrard, F., Sedran, T. (1994), *Optimization of ultra-high perfomance concrete by the use of a packing model*. Cement and Concrete Research. 24(6):997-1009. https://doi.org/10.1016/0008-8846(94)90022-1

Du, H., Tan, K. H. (2014). *Effect of particle size on alkali-silica reaction in recycled glass mortars*. Construction and Building Materials. 66: 275-285. https://doi.org/10.1016/j.conbuildmat.2014.05.092

Du, H., Tan, K. H. (2017), *Properties of high volume glass powder concrete*. Cement and Concrete Composites.75: 22-29.

Du, Y., Yang, W., Ge, Y., Wang, S., Liu, O. (2020), *Thermal conductivity of cement paste containing waste glass powder, metakaolin and limestone filler as supplementary cementitious material*. Journal of Cleaner Production. 287. https://doi.org/10.1016/j.jclepro.2020.125018

Freitas, T. O. (2019), *"Efeito do pó de vidro na mitigação da reação álcali-sílica de compósitos cimentícios de alto desempenho"*, Dissertação de Mestrado, Universidade Federal de São Carlos, p.148.

Instituto de pesquisa econômica aplicada (IPEA) (2012), *Diagnóstico dos Resíduos Sólidos Urbanos*. Disponível em: https://www.ipea.gov.br/portal/images/stories/PDFs/relatoriopesquisa/121009_relatorio_residuos_solidos_urbanos.pdf. Acesso em: 27 de março de 2020.

Kantro, D. (1980), *Influence of Water-Reducing Admixtures on Properties of Cement Paste—A Miniature Slump Test*. Cement, Concrete and Aggregates. 2(0):95-102. https://doi.org/10.1520/CCA10190J

Lee, H., Hanif, A., Usman, M., Sim., J., Oh, H. (2018), *Performance evaluation of concrete incorporating glass powder and glass sludge wastes as supplementary cementing material*. Journal of Cleaner Production. 170: 683-693. https://doi.org/10.1016/j.jclepro.2017.09.133

Li, J., Wu, Z., Shi, C., Yuan, Q., Zhang, Z. (2020), *Durability of ultra-high performance concrete: a review*. Construction and Building Materials. 255. https://doi.org/10.1016/j.conbuildmat.2020.119296

Li, P. P., Yu, Q.L., Brouwers, H.J.H., Chen, W. (2019), *Conceptual design and performance evaluation of two-stage ultra-low binder ultra-high performance concrete*. Cement and Concrete Research.125. https://doi.org/10.1016/j.cemconres.2019.

Mehta, A., Ashish, D. K. (2020), *Silica fume and waste glass in cement concrete production: A review*. Journal of Building Engineering. https://doi.org/10.1016/j.jobe.2019.100888

Mosavinejad, S. H. G., Langaroudi, M. A. M., Barandoust, J., Ghanizadeh, A. (2020), *Electrical and microstructural analysis of UHPC containing short PVA fibers*. Construction and Building Materials. 235. https://doi.org/10.1016/j.conbuildmat.2019.117448

Nordtest Method (1999). *NT BUILD 492*: *Concrete, mortar and cement-based repair materials: chloride migration coefficient from non-steady-state migration experiments*

Santos, L. (2006), *"Avaliação da resistividade elétrica do concreto como parâmetro para a previsão da iniciação da corrosão induzida por cloretos em estruturas de concreto"*. Dissertação de Mestrado, Universidade de Brasília, p.178

Sohail, M. G., Kahraman, R., Nuaimi, N.A., Gencturk, B., Alnahhal, W. (2021), *Durability characteristics of high and ultra-high performance concretes*. Journal of Building Engineering. 33. https://doi.org/10.1016/j.jobe.2020.101669

Sohail, M. G., Wang, B., Jain, A., Kahraman, R. (2018), *Advancements in concrete mix designs: high-performance and ultrahigh-performance concretes from 1970 to 2016*. Journal of Materials in Civil Engineering.30(3). http://dx.doi.org/10.1061/(ASCE)MT.1943-5533.0002144

Tam, C. M., Tam, V. W. Y., Ng, K. M. (2012), *Assessing drying shrinkage and water permeability of reactive powder concrete produced in Hong Kong*. Construction and Building Materials. 26:79-89. https://doi.org/10.1016/j.conbuildmat.2011.05.006

Teng, S, Afroughsabet, V., Ostertag, C. P. (2018). *Flexural behavior and durability properties of high-performance hybrid-fiber-reinforced concrete*. Construction and Building Materials. 182:504-515. https://doi.org/10.1016/j.conmat.2018.06.158

Yang, R., Yu, R., Shui, Z., Gao, X., Xiao, X., Zhang, Z., Wang, Y., He, Y. (2019), *Low carbon design of an Ultra-High Performance Concrete (UHPC) incorporating phosphorous slag*. Journal of Cleaner Production. 240. https://doi.org/10.1016/j.jclepro.2019.118157

Procedure to detect the penetration of chlorides into carbonated concrete with silver nitrate

C. Vieira Pontes[1,2], G. Costa Reus[1]*, A. Calvo[1,2], M. H. F. Medeiros[1,2,3]
*Contact author: giovanacostareus@gmail.com
DOI: https://doi.org/10.21041/ra.v11i2.480

ABSTRACT

The main objective of this work is to propose a standard procedure that enables the use of the colorimetric method to measure the depth of chloride penetration during inspections of concrete structures exposed to both chlorides and carbonation. To avoid the occurrence of false positive results, solutions of calcium hydroxide ($Ca(OH)_2$) and sodium hydroxide ($NaOH$) were tested as a pretreatment. The tests were carried out on carbonated only samples, and on carbonate and chloride contaminated samples. The results show that the $NaOH$ solution eliminates the carbonation interference. Therefore, a suitable method was found to introduce depth readings of chloride contamination in concrete field inspections.

Keywords: durability of concrete; chloride attack; silver nitrate; carbonation; environmental aggressiveness.

[1] Programa de Pós-graduação em Engenharia de Construção Civil (PPGECC)
[2] Universidade Federal do Paraná (UFPR), Brasil
[3] Centro de Estudos em Engenharia Civil (CESEC)

Contribution of each author

In this work, the main author is Réus G. C., contributed with the bibliographic review, with the planning of the experimental program, execution of the planned tests, consequent data collection, analysis of the results and subsequent writing of the work in question. Regarding the author Pontes, C. V., she contributed to the execution of the laboratory tests and data collection. Author Medeiros, M. H.F. contributed the original idea together with the main author, was involved in the writing of the work and in the analysis and discussion of the results obtained in the experimental stage. Finally, the author Calvo, A. participated in the revision and correction of the manuscript, made images that appear in the text and translated the work into Spanish. Thus, the contribution in percentage of each of the authors was: 40%, 25%, 25% and 10%, in the order mentioned above.

Discussions and subsequent corrections to the publication

Any dispute, including the replies of the authors, will be published in the second issue of 2022 provided that the information is received before the closing of the first issue of 2022.

Procedimento para detectar a penetração de cloretos com nitrato de prata em concreto carbonatado

RESUMO

Este trabalho tem por objetivo principal propor um procedimento padrão para a utilização do método colorimétrico para medir a profundidade de penetração de cloretos nas inspeções de estruturas de concreto em que existe a exposição aos cloretos e à carbonatação simultaneamente. Para evitar a ocorrência de resultados "falsos positivos" foram testadas as soluções de hidróxido de cálcio (Ca(OH)$_2$) e hidróxido de sódio (NaOH) como tratamento prévio. Os testes foram conduzidos em amostras apenas carbonatadas e em amostras contaminadas por cloretos e carbonatadas. Os resultados mostram que a solução de NaOH elimina a interferência da carbonatação. Desse modo, chegou-se a indicação de um método adequado para introdução de leituras de profundidade de contaminação por cloretos nas inspeções do concreto em campo.
Palavras-chave: durabilidade do concreto; ataque por cloretos; nitrato de prata; carbonatação; agressividade ambiental.

Procedimiento para detectar la penetración de cloruros con nitrato de plata en hormigón carbonatado

RESUMEN

Este trabajo tiene como objetivo principal proponer un procedimiento estándar que viabilice el uso del método colorimétrico para medir la profundidad de penetración de cloruros durante las inspecciones de estructuras de hormigón expuestas tanto a cloruros como a carbonatación. Para evitar la aparición de resultados "falsos positivos", se probaron soluciones de hidróxido de calcio (Ca(OH)$_2$) e hidróxido de sodio (NaOH) como pretratamiento. Las pruebas se llevaron a cabo en muestras solamente carbonatadas, y en muestras contaminadas por cloruros y carbonatadas. Los resultados muestran que la solución de NaOH elimina la interferencia de la carbonatación. Por lo tanto, se llegó a un método adecuado para introducir lecturas de profundidad de contaminación por cloruro en inspecciones de estructuras de hormigón en campo.
Palabras clave: durabilidad del hormigón; ataque por cloruros; nitrato de plata; carbonatación; agresividad ambiental.

1. INTRODUCTION

Corrosion of steel is one of the most common degradation mechanisms in reinforced concrete structures, the main causes of which are carbonation and attack by chloride ions (Corral et al., 2013). Both phenomena are responsible for dissolving the thin layer of iron oxide, a passive layer which covers and protects steel bars against corrosion in environments with a pH above 11 (Helene, 1993; Montemor et al., 2003; Moreira, 2006; France, 2011).

The entry of chloride ions into the concrete occurs at different speeds in the same building, depending on the different microclimates that occur throughout it, as mentioned by Medeiros et al. (2013), Medeiros Junior et al. (2015a) and Medeiros Junior et al. (2015b). As reported by different authors (Helene, 1993; Montemor et al., 2003; Medeiros et al., 2009a; France, 2011; Real et al., 2015), the presence of chloride ions in reinforced concrete is due to the diffusion of these ionic elements from the external environment to the interior of the structure, or the use of contaminated raw materials for the production of concrete.

The attack by chlorides in steel generates an expansive reaction; that is, the chloride ions react with the iron ions in the reinforcement and form products (iron oxides and hydroxides) that have larger volumes than the original iron ions. This phenomenon generates internal stresses that can cause cracks in the structure if they exceed the concrete's tensile strength (Cascudo, 1997; Montemor et al., 2003). In addition, chloride ions corrode the reinforcement locally (in the form of pits), reducing the cross section of the bearing element and affecting its structural function (França, 2011).

Within this context, the penetration of chlorides into concrete structures is a possible cause of reinforcement corrosion, and it is important to know the depth of penetration of this aggressive ion for inspection and diagnosis work of reinforced concrete.

2. RELEVANCE OF THE THEME

To inspect or monitor concrete structures to detect the presence, depth and/or evolution of chloride ion penetration, the colorimetric method of spraying silver nitrate solution ($AgNO_3$) is used (Baroghel-Bouny et al., 2007; Real et al., 2015). The spraying of the silver nitrate solution chemical indicator is a visual colorimetric method of inspection and was originally standardized by UNI 7928 in 1978. It is a qualitative technique of practical application in samples of concrete structures, in addition to being low cost if compared to concrete dust extraction and chloride profile determination in titration or potentiometry procedures (França, 2011; He et al., 2012).

According to Baroghel-Bouny et al. (2007), Medeiros et al. (2009b) and Kim et al. (2013), the technique consists of spraying silver nitrate solution on the recently fractured cross section of concrete cores to form two distinct regions in terms of color: one with brown precipitate corresponding to the region without chlorides, and the other without color change in the region affected by chlorides. Figure 1 shows the colorimetric method of spraying $AgNO_3$ solution as applied to a concrete specimen.
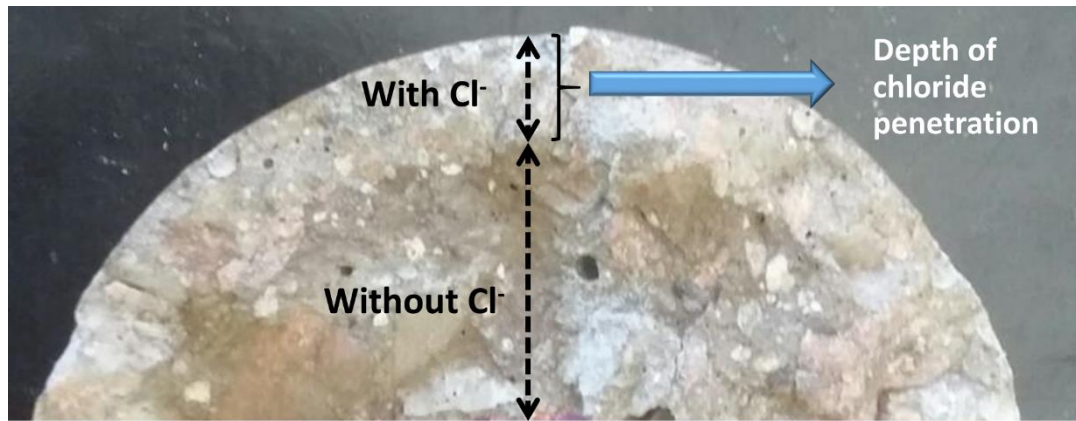
Figure 1. Chloride penetration depth measurement by visual colorimetric method by spraying an aqueous solution of 0.1 M $AgNO_3$.

The photochemical reactions after spraying the silver nitrate solution correspond to the combination of silver ions and free chloride ions forming silver chloride (AgCl), which has a whitish color, according to Equation (1). In regions with no free chlorides, there is a photochemical reaction between silver ions and hydroxyl ions forming AgOH, and later Ag_2O, which gives the concrete a brown color (Yuan et al., 2008; France, 2011; He et al., 2012; Kim et al., 2013; Real et al., 2015).

$$AgNO_3 + Cl^- \rightarrow AgCl + NO_3^- \qquad (1)$$

The colorimetric method of spraying silver nitrate is widely used in experimental works in which the tested concrete is found in saturation conditions and free from the carbonation process. Many works published in recent years in high-impact magazines (such as: Ferreira et al., 2016; Weiss et al., 2017; Wei et al., 2018; He et al., 2018; Slomka-Slupik et al., 2018; Fernández-Ruiz et al., 2018; Lau et al., 2018; Azarijafari et al., 2018) confirm its frequent use in current research.

However, some studies (França, 2011; Real et al., 2015) point out that the silver ions (Ag+) in the silver nitrate solution react with the carbonation product CO_3, forming Ag_2CO_3, which also gives a whitish color to the concrete. Thus, carbonation interferes with the colorimetric method of spraying silver nitrate solution on cementitious materials, generating a possible false positive result, as reported by Medeiros et al. (2018).

Therefore, when inspecting carbonated structures with the colorimetric method of silver nitrate solution, there is an indication of the presence of chloride ions in regions that do not necessarily have chlorides, but rather have carbonates with a pH less than 10. For this reason, the false positive result can invalidate the application of the colorimetric method of silver nitrate solution to cement structures exposed to the environment, since carbonation is a degradation mechanism inherent to constructions exposed to the environment.

In addition, due to the occurrence of large Brazilian demographic densities in coastal areas associated with industrialization processes, it appears that the phenomena of attack by chloride ions and carbonation occur simultaneously in numerous reinforced concrete structures (Real et al., 2015; Medeiros et al., 2013).

Within this context, there is a limitation to the use of silver nitrate solution spraying to detect the front of chloride penetration in real constructions exposed to environments with chlorides and the carbonation process, both simultaneously interacting with the concrete in service conditions. The objective of this research is, therefore, to develop a standard procedure to detect the penetration depth of chlorides in carbonated concrete.

3. MATERIALS AND METHODS

3.1 Materials

The cylindrical concrete specimens used in both phases of the research were dosed with C PV-ARI type cement, with dimensions of 100 mm in diameter and 200 mm in height. For each case of the study, three repetitions were performed, that is, three specimens under the same conditions for each measurement. The results were then averaged.

Table 1 shows the chemical composition of the cement and quartz filler used to provide the materials in the concrete dosage. In addition, the physical characteristics of the cement and quartz filler are shown in Table 2.

Table 1. Chemical analysis, by X-ray fluorescence, of CP V-ARI cement and quartz filler.

Binder	Chemical analysis (%)							
	CaO	SiO_2	Al_2O_3	Fe_2O_3	MgO	SO_3	K_2O	TiO_2
CP V - ARI	73.21	10.45	3.59	3.71	3.66	3.05	1.36	0.00
Quartz filler	0.00	95.65	2.43	0.00	0.00	1.77	0.00	0.04

Table 2. Physical characteristics of CP V-ARI cement and quartz filler.

Binder	Specific Mass (g/cm³)	BET specific area (m²/kg)
C PV-ARI	3.09	1.070
Quartz filler	2.60	1.227

Natural quartz sand from Balsa Nova, Brasil was used as fine aggregate, which has a specific mass of 2.63 g/cm³, a unit mass of 1.54 g/cm³ and a fineness module of 2.34. The coarse aggregate was basalt, having a maximum dimension of 19 mm and specific gravity of 2.64 g/cm³.

The mixing ratio of the concrete used was 1: 0.10 : 2.25 : 3.00 (cement : quartz filler : fine aggregate : coarse aggregate) with a water/cement ratio of 0.50. The slump was kept constant in the range of 10 ± 2 cm. This concrete presented compressive strength of 43 MPa and its water sorptivity was 0.0059 g/cm².hours^{0,5}.

Before beginning the accelerated carbonation, a seasoning process was adopted, which consisted of the NORIE method as presented in Pauletti (2004). The process consists of arranging the specimens in an air-conditioned room with controlled humidity and temperature. When the weight variation of the specimen is less than 0.10 g in 24 hours, the sample is suitable for the accelerated carbonation test.

The samples were subjected to accelerated carbonation for 12 weeks in a carbonation chamber with a CO_2 content of $5 \pm 0.5\%$. The relative humidity inside the equipment was set at $60 \pm 1\%$ and the temperature at 40 ± 0.3ºC. The carbonation coefficient of the substrate concrete was 1.96 mm/week$^{0.5}$. These data agree with those published by Medeiros, Raisdorfer and Hoppe Filho (2017).

3.2 Methods

Carbonated concrete – Chloride-free:

Initially, the validity of sodium hydroxide and calcium hydroxide solutions was analyzed in the pH increase of the concrete surface and subsequent elimination of the false positive result caused by carbonation in the $AgNO_3$ solution spraying method.

For this, carbonated and chloride-free specimens were used. Each specimen was sectioned

longitudinally in four slices of the same height for spraying NaOH and Ca(OH)$_2$ solutions. Saturated aqueous sodium hydroxide solution (150.00 g/L) was sprayed onto two slices of the specimen, and saturated aqueous calcium hydroxide solution (1.85 g/L) was sprayed on the other two sections, aiming to test the effectiveness of the solutions. To quickly dry the slices, they were put in a dry chamber with $55 \pm 5\%$ relative humidity and temperature at $23 \pm 2°C$ for about an hour. After this procedure, a solution of phenolphthalein was applied to one half of the cross section of each quarter of sectioned sample, in the proportion of 5 g of phenolphthalein to 276.15 g of ethyl alcohol to 150 g of distilled water. Silver nitrate solution was sprayed twice in succession on the other half at a concentration of 0.10 mol/L. The application of silver nitrate was repeated to increase the color contrast between the areas with and without chlorides, as was done in the work of Baroghel-Bouny et al. (2007).

Then, visual evaluation was carried out on the samples. If the fraction with a chemical phenolphthalein indicator acquired a crimson red color throughout, the alkaline solution would have been effective in increasing the pH of the carbonation front and avoiding the false positive. At the same time, the half with AgNO$_3$ solution should change color to brown throughout; that is, it should not indicate the false positive result for the presence of chloride ions because the specimens were carbonated without chlorides. Figure 2 shows the schematic of the idealized experiment.
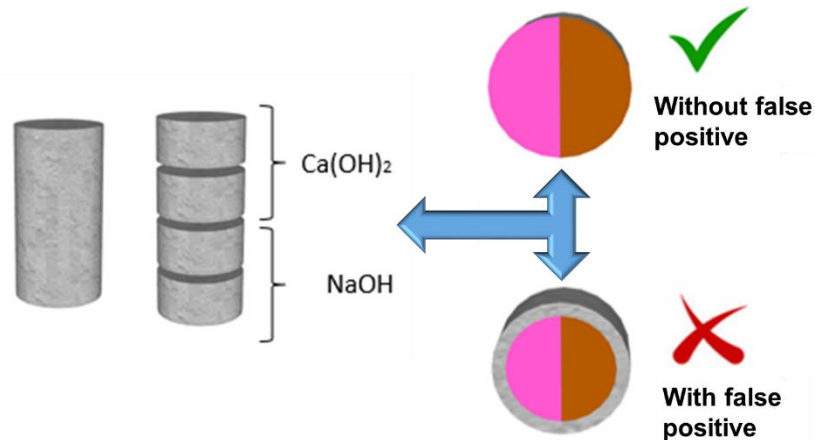
Figure 2. Schematic of the experiment to eliminate the false positive result caused by carbonation.

Carbonated concrete - With chlorides:

Then, the experiment was carried out to measure, with an aqueous solution of silver nitrate, the depth of penetration of chlorides in specimens affected by carbonation and attack by chlorides, simultaneously. The alkaline solution inhibiting the effects of carbonation on the concrete surface was previously applied. For this, three specimens were used for each accelerated chloride penetration time (24h, 48h and 72h), totaling 9 specimens.

To induce the entry of chlorides in the samples quickly, a system based on the migration of chlorides was elaborated. The migration of ions is caused by the difference in electrical potential between the mediums. The positive ions move towards the negative pole and the negative ions move towards the positive pole. According to Medeiros (2008), this movement occurs both through migration and through diffusion. However, migration is more considerable in these test conditions. For testing this experiment, all specimens were saturated and then immersed in an aqueous solution with 3% NaCl, since migration occurs in a saturated medium. Then, a steel bar and a wire mesh were connected to a 30 V electrical source, inducing the positive pole in the hole inside the sample. In this way, the Cl⁻ anions, disassociated in the sodium chloride solution, were electrostatically

attracted into the specimens. Figure 3 shows a schematic of the apparatus assembled to induce chloride penetration in concrete specimens.

After the chloride immersion/migration period, the concrete elements were dried in an oven at 40°C for 24 hours, cooled for another day and then broken up to be sprayed by the alkaline solutions. The alkaline solution was applied to raise the pH of the carbonation front on the newly fractured surface and prevent the occurrence of the false positive result. After spraying this solution, the test specimens remained in a dry chamber (55±5% and 23±2°C temperature) for 01 hour to eliminate excess moisture on the concrete surface.

Subsequently, phenolphthalein solution was applied to confirm that the solution had alkalized the surface, and silver nitrate solution was applied to try to measure the depth of chloride penetration. With the distinction of the whitish and brown regions in the half with silver nitrate, it was possible to measure the penetration depth of chlorides from the surface of the element. Measurements were taken with a caliper at five different points from half the cross section, as shown in Figure 4.

Figure 3. Schematic of the chloride migration test: (a) schematic of the electrical connection; (b) photo of the assembled experiment.
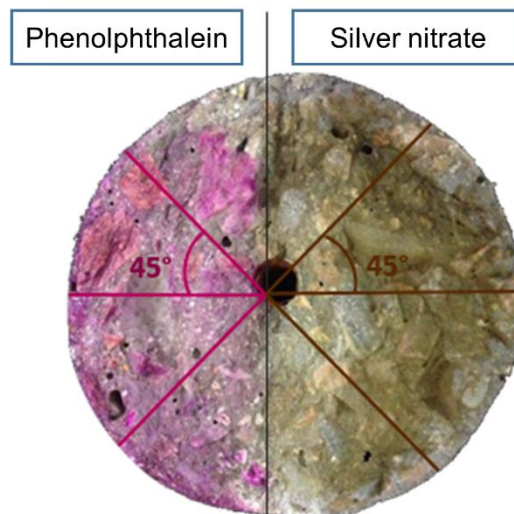
Figure 4. Schematic of the locations for measuring the depth of carbonation and the penetration of chloride ions.

To confirm the depth of chloride penetration with the colorimetric test, the chloride profile was determined by using the RILEM TC 178-TMC sample collection procedure published by

Vennesland, Climent, Andrade (2013). Thus, after the chloride migration process, the specimens were dried in an oven at 40°C for 24 hours and cooled by air for another 24 hours. After that, one third of the Ø10 x 20 cm cylindrical specimens was used to collect concrete dust from a drill. The sample collection was performed every 10 mm in depth, up to 40 mm in depth. For each depth of dust collection, the determination of the content of acid-soluble chlorides (total chlorides) was carried out by titration with silver nitrate after an attack with nitric acid, as detailed in ASTM C1152 (2020).

4. RESULTS AND DISCUSSIONS

4.1 Carbonated concrete - Chloride-free:

Figure 5 shows the result of the attempt to neutralize the effect of carbonation in the test with silver nitrate using the spray of an aqueous solution saturated with calcium hydroxide and another saturated with sodium hydroxide. All samples were carbonated and free from chloride contamination.

It is observed that the spraying of a saturated solution of calcium hydroxide did not raise the pH of the carbonated concrete layer to the point of reaching the turning point of the phenolphthalein chemical indicator solution. This probably occurred because of the low concentration of hydroxyl in the saturated solution as calcium hydroxide. This is due to the low solubility of $Ca(OH)_2$, as reported by Defendants (2017).

On the other hand, the sodium hydroxide solution increased the basicity of the concrete, which was verified in the visual analysis after spraying the chemical pH indicator and the $AgNO_3$ solution. This result was like that found by Pontes et al. (2020). The NaOH solution was also effective in re-alkalizing concrete samples in the work of Réus (2017) and Réus and Medeiros (2020).

Thus, it can be said that the spraying of solution saturated with sodium hydroxide was effective in eliminating the occurrence of false positive results when an aqueous solution of silver nitrate is sprayed on carbonated concrete that is not contamination by chlorides.
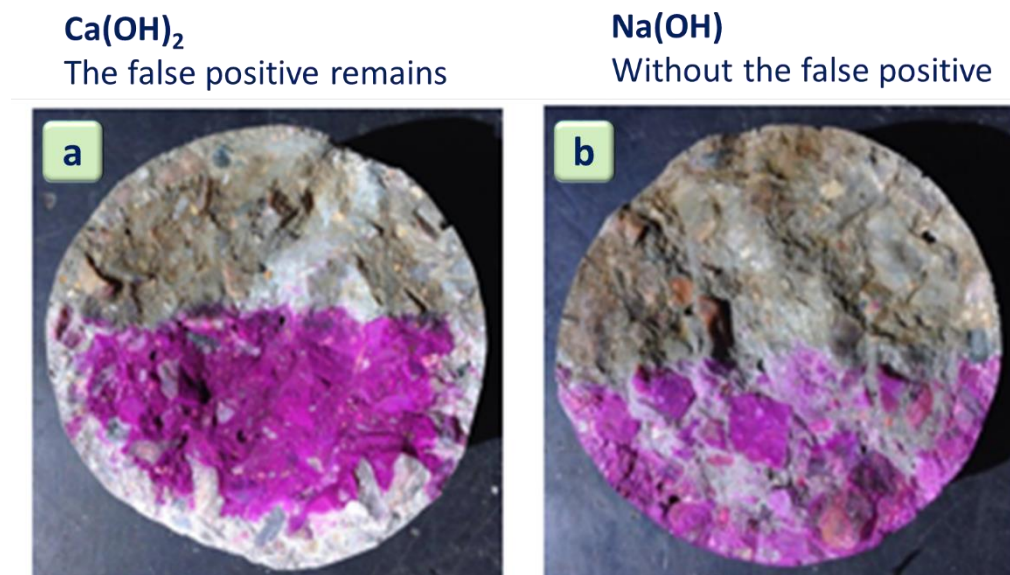
Figure 5. Carbonated specimens with (a) previous spraying of $Ca(OH)_2$ solution (b) previous spraying of NaOH solution.

4.2 Carbonated concrete - With chlorides:

After the immersion of the concrete samples in the sodium chloride solution during the chloride migration test, the penetration depth of chloride ions was measured at the end of the 24-hour, 48-hour and 72-hour test cycles (Figure 6-a). This measurement was performed with the previous application of the sodium hydroxide solution, effective in alkalinizing the carbonated concrete as shown in Figure 5. This procedure was performed to prevent the occurrence of the false positive result that the silver nitrate solution presents in carbonated samples.

The entry of chlorides occurred gradually over the test time and the final depth of chloride penetration in the concrete was 26.8 mm.

Figure 6-b shows the total chloride profile determined in the concrete of this experiment, after 72 hours of migration with 30 V ddp. The data show the coherence of the chloride penetration depth result by the colorimetric method, in which the color change occurred from the chloride content of 0.08% in relation to the cement mass. This comparison was carried out to obtain proof of the coherence of the proposed method for determining the penetration depth of chlorides.
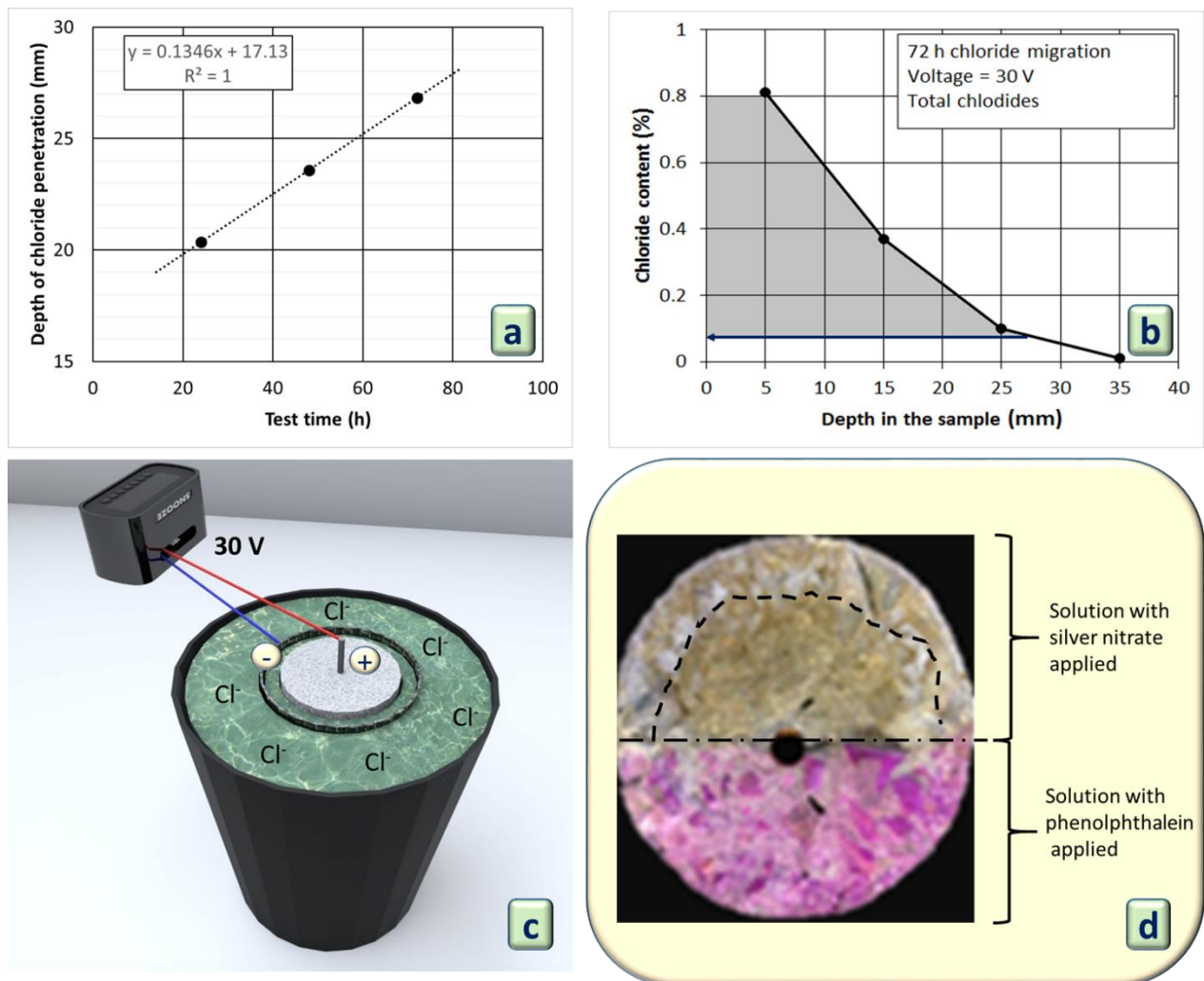
Figure 6. Results in the specimens of carbonated concrete and concrete contaminated with chlorides: (a) Depth of penetration of chlorides with the colorimetric method; (b) Chloride profile to verify the effectiveness of the colorimetric method; (c) Illustration of the acceleration of the entry of chlorides by migration; (d) Carbonated specimens with chloride penetration - pretreatment with NaOH solution and subsequent application of AgNO₃ solution.

Figure 6-c illustrates the chloride ion migration experiment and Figure 6-d shows a photo of a specimen after applying the colorimetric method. This photo shows a freshly fractured specimen whose surface was previously treated with a NaOH solution spray, after which the AgNO₃ solution was applied. Once again, it was observed that the sodium hydroxide solution eliminated the false positive effect generated by the carbonation of the concrete in the silver nitrate spraying method. This is evident, as the region of the samples sprayed with phenolphthalein did not identify the carbonated area. Only the section with AgNO₃ solution generated a color change in the regions with the presence of free chlorides, since in this phase the samples were carbonated and contaminated by chlorides.

5. CONCLUSIONS

This work presents a possible path for the use of the colorimetric method of spraying silver nitrate solution under service conditions in which reinforced concrete is exposed to chloride attack and to the concurrent carbonation process. The work indicates what can be done before the application of the silver nitrate solution to avoid a false positive, which has prevented the use of this colorimetric method in inspection work on real constructions.

In this context, it is concluded that the step-by-step procedure is effective to enable the use of the colorimetric method with silver nitrate to obtain the depth of penetration of chlorides in concrete in situations where it is exposed to the penetration of chlorides and to the carbonation process.

The steps are:

Step 1 - Part of the concrete piece must be sectioned and a saturated aqueous solution of sodium hydroxide (150 g/L) is applied on the newly fractured surface by spraying. Wait about an hour for the surface to dry;

Step 2 - Spray a solution of silver nitrate twice in succession (5 minutes interval between each time) at a concentration of 0.10 mol/L. Wait about an hour for the surface to dry and the reactions to occur, generating the color contrast. As illustrated in Figure 7, the brown color corresponds to the region without chlorides, and the other without color change corresponds to the region affected by chlorides;

Step 3 - Measure the depth of chloride penetration using a ruler or caliper. Work with average, minimum and maximum values of chloride penetration depth to interpret the results.
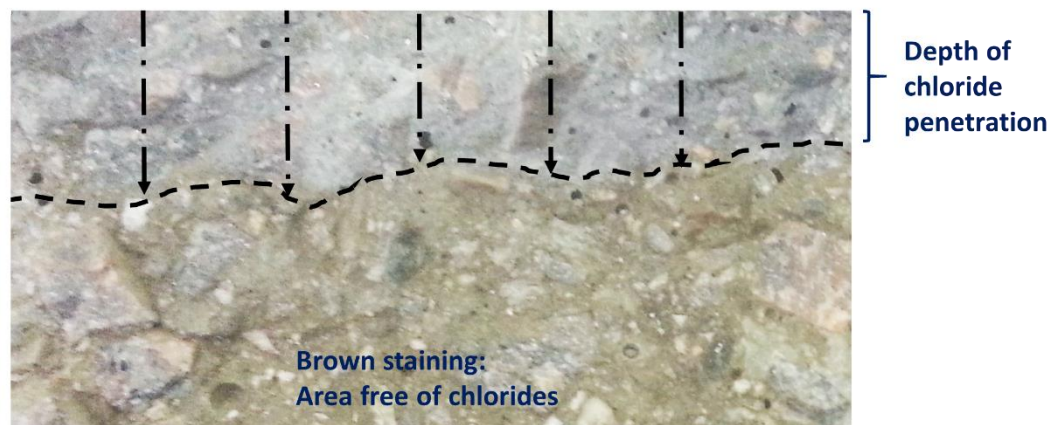
Figure 7. Illustration of the contrast obtained with the application of the colorimetric method to determine the depth of penetration of chlorides, using a spray of a solution of NaOH and one of AgNO₃.

6. ACKNOWLEDGEMENTS

7. REFERENCES

ASTM International. (2020). *ASTM C1152/C1152M-20 Standard Test Method for Acid-Soluble Chloride in Mortar and Concrete.* https://doi.org/10.1520/C1152_C1152M-20

Azarijafari, H., Azarijafari H., Tajadini, A., Rahimi, M., Berenjian, J. (2018), *Reducing variations in the test results of self-consolidating lightweight concrete by incorporating pozzolanic materials*. Construction and Building Materials. 166: 889-897. https://doi.org/10.1016/j.conbuildmat.2018.01.121

Baroghel-Bouny, V., Belin, P., Maultzsch, M., Henry, D. (2007), *AgNO₃ spray tests: advantages, weaknesses, and various applications to quantify chloride ingress into concrete. Part 1: Non-steady-state diffusion tests and exposure to natural conditions*. Materials and Structures. 40: 759-781. https://doi.org/10.1617/s11527-007-9233-1

Cascudo, O. (1997), *"Controle da Corrosão de Armaduras em concreto: inspeções e técnicas eletroquímicas"*. PINI, 1.ed., São Paulo, Brasil.

Corral, R., Arredondo, S., Almaral, J., & Gómez, J. (2013). *Chloride corrosion of embedded reinforced steel on concrete elaborated from recycled coarse aggregates and supplementary cement materials*. Revista Ingeniería de Construcción, 28(1): 21-35. http://dx.doi.org/10.4067/S0718-50732013000100002

Fernández-Ruiz, M. A., Gil-Martín, L. M., Carbonell-Márquez, J. F., Hernández-Montes, E. (2018), *Epoxy resin and ground tyre rubber replacement for cement in concrete: Compressive behaviour and durability properties*. Construction and Building Materials. 173: 49-57. https://doi.org/10.1016/j.conbuildmat.2018.04.004

Ferreira, R. M., Castro-Gomes, J. P., Costa, P., & Malheiro, R. (2016). *Effect of metakaolin on the chloride ingress properties of concrete*. KSCE Journal of Civil Engineering, 20(4), 1375-1384. https://doi.org/10.1007/s12205-015-0131-8

França, C. B. (2011), *"Avaliação de cloretos livres em concretos e argamassas de cimento Portland pelo método de aspersão de solução de nitrato de prata"*. Dissertação de Mestrado, Programa de Pós-graduação em Engenharia Civil, Universidade Católica de Pernambuco, Recife, 85 p.

He, F., Shi, C., Yuan, Q., Chen, C., Zheng, K. (2012), *AgNO₃-based colorimetric methods for measurement of chloride penetration in concrete*. Construction and Building Materials. 26: 1-8. https://doi.org/10.1016/j.conbuildmat.2011.06.003

He, F., Shi, C., Yuan, Q., An, X., Tong, B. (2018), *Corrosion of cement pastes made of CEM I and CEM III/A caused by a saturated water solution of ammonium chloride after 4 and 25 days of aggressive immersion*. Construction and Building Materials. 170: 279–289. https://doi.org/10.1016/j.conbuildmat.2018.03.073

Helene, P. (1993), *"Contribuição ao estudo da corrosão em armaduras de concreto armado"*. Tese de Livre Docência, Escola Politécnica, Universidade de São Paulo, São Paulo, 231 p.

Kim, M-Y., Yang, E-I., Yi, S-T. (2013), *Application of the colorimetric method to chloride diffusion evaluation in concrete structures*. Construction and Building Materials. 41: 239-245. https://doi.org/10.1016/j.conbuildmat.2012.11.084

Lau, P. C., Teo, D. C. L., Mannan, M. A. (2018). *Mechanical, durability and microstructure properties of lightweight concrete using aggregate made from lime-treated sewage sludge and palm oil fuel ash*. Construction and Building Materials. 176: 24-34. https://doi.org/10.1016/j.conbuildmat.2018.04.179

Medeiros, M. H. F. (2008), *"Contribuição ao estudo da durabilidade de concretos com proteção superficial frente à ação de íons cloretos"*. Tese de Doutorado, Universidade de São Paulo, São Paulo.

Medeiros, M. H. F., Hoppe Filho, J., Helene, P. (2009a), *Influence of the slice position on chloride migration tests for concrete in marine conditions*. Marine Structures. 22: 128-141. https://doi.org/10.1016/j.marstruc.2008.09.003

Medeiros, M. H. F., Helene, P. (2009b), *Surface treatment of reinforced concrete in marine environment: Influence on chloride diffusion coefficient and capillary water absorption. Construction and building materials*. 23(3): 1476-1484. https://doi.org/10.1016/j.conbuildmat.2008.06.01

Medeiros, M. H. F., Gobbi, A., Réus, G. C., Helene, P. (2013), *Reinforced concrete in marine environment: Effect of wetting and drying cycles, height and positioning in relation to the sea shore*. Construction and Building Materials. 44: 452-457. https://doi.org/10.1016/j.conbuildmat.2013.02.078

Medeiros Junior, R. A., Lima, M. G., Brito, P. C., Medeiros, M. H. F. (2015a), *Chloride penetration into concrete in an offshore platform-analysis of exposure conditions*. Ocean Engineering. 103: 78-87. https://doi.org/10.1016/j.oceaneng.2015.04.079

Medeiros-Junior, R. A., Lima, M. G., Yazigi, R., Medeiros, M. H. F. (2015b), *Carbonation depth in 57 years old concrete structures*. Steel and Composite Structures. 19(4): 953-966. https://doi.org/10.12989/scs.2015.19.4.953

Medeiros, M. H. F. D., Raisdorfer, J. W., & Hoppe Filho, J. (2017). Influência da sílica ativa e do metacaulim na velocidade de carbonatação do concreto: relação com resistência, absorção e relação a/c. Ambiente Construído, 17(4), 125-139. https://doi.org/10.1590/s1678-86212017000400189

Medeiros, M. H. F., Réus, G. C., Pontes, C. V. (2018), "Nitrato de prata como método colorimétrico para detecção da penetração de cloretos: análise crítica". in: 3° Simpósio Paranaense de Patologia das Construções, 2018, Curitiba., v. único. pp. 35-46. https://doi.org/10.4322/2526-7248.017

Montemor, M. F., Simões, A. M. P., Ferreira, M. G. S. (2003), *Chloride-induced corrosion on reinforcing steel: from the fundamentals to the monitoring techniques*. Cement and Concrete Composites. 25: 491-502. https://doi.org/10.1016/S0958-9465(02)00089-6

Moreira, C. (2006), *"Realcalinização de estruturas de concreto carbonatado com utilização de gel saturado de solução alcalina"*. Dissertação de Mestrado, Escola de Engenharia Civil, Universidade Federal de Goiás, Goiânia, 122 p.

Pauletti, C. (2004), *"Análise comparativa de procedimentos para ensaios acelerados de carbonatação"*. Dissertação de Mestrado, Universidade Federal do Rio Grande do Sul, Porto Alegre, 176 p.

Pontes, C. V., Réus, G. C., Araújo, E. C., Medeiros, M. H. F. (2020), *Silver nitrate colorimetric method to detect chloride penetration in carbonated concrete: how to prevent false positives*. Journal of Building Engineering. https://doi.org/10.1016/j.jobe.2020.101860

Real, L. V., Oliveira, D. R. B., Soares, T., Medeiros, M. H. F. (2015), *Método colorimétrico por aspersão de nitrato de prata para avaliação da penetração de cloretos em concreto: estado da arte*. Revista Alconpat. 5(2): 149-159. https://doi.org/10.21041/ra.v5i2.84

Réus, G. C. (2017), *"Realcalinização química como meio de recuperação de estruturas de concreto armado carbonatadas"*. Dissertação de Mestrado, Pós-graduação em Engenharia de Construção Civil, Universidade Federal do Paraná, Curitiba, 104 p.

Réus, G. C., Medeiros, M. H. F. (2020), *Chemical realkalization for carbonated concrete treatment: Alkaline solutions and application methods*. Construction and Building Materials, 262, 120880. https://doi.org/10.1016/j.conbuildmat.2020.120880

RILEM. TC 178-TMC - Testing and modelling chloride penetration in concrete. Madrid: Elsevier; 2013. p. 3.

Vennesland, Ø., Climent, M. Á., Andrade, C. (2013). *Recommendation of RILEM TC 178-TMC: Testing and modelling chloride penetration in concrete*. Materials and Structures. 46: 337-344. https://doi.org/10.1617/s11527-012-9968-1

Slonka-Slupik, B., Podwórny, J., Staszuk, M. (2018), *Corrosion of cement pastes made of CEM I and CEM III/A caused by a saturated water solution of ammonium chloride after 4 and 25 days of aggressive immersion*. Construction and Building Materials. 170: 279-289. https://doi.org/10.1016/j.conbuildmat.2018.03.073

Yuan, Q., Shi, C., He, F., Schutter, G. D., Audenaert, K., Zheng, K. (2008), *Effect of hydroxyl ions on chloride penetration depth measurement using the colorimetric method*. Cement and Concrete Research. 38: 1177-1180. https://doi.org/10.1016/j.cemconres.2008.04.003

Wei, Y., Guo, W., Liang, S. (2018), *Chloride Ingress in Internally Cured Concrete under Complex Solution. Journal of Materials in Civil Engineering*. 30(4) p. 04018037. https://doi.org/10.1061/(ASCE)MT.1943-5533.0002215

Weiss, J., Couch, J., Pease, B., Laugesen, P., Geiker, M. (2017), *Influence of Mechanically Induced Cracking on Chloride Ingress in Concrete*. Journal of Materials in Civil Engineering 29(9): 04017128. https://doi.org/10.1061/(ASCE)MT.1943-5533.0001922

Damage assessment proposal for two bridges located on Highway No. 14 in the State of Sonora México by using stiffness invariant as global comparison parameter

G. Ramos-Torres[1]*, H. Navarro-Gómez[2], E. Perez-Isidro[2],
J. Gautherau-Lopez[1], I. Palma-Quiroz[2]
*Contact author: calculista@prodigy.net.mx
DOI: https://doi.org/10.21041/ra.v11i2.454

ABSTRACT

The elastic rigidity invariant method is used to obtain the mechanical response of the superstructure of simply supported bridges; it is based on the bridge's response to the impact of known masses applied on mid span to obtain the maximum displacement that defines the point stiffness. This value is compared with the values of the theoretical curve formed with the stiffness invariants, constructed from the design characteristics of the bridge. The method was implemented in two bridges located on federal highway No. 14 of the State of Sonora Mex., with results according to the damage manifested. The evaluation is the result of a global parameter, obtained in environmental conditions in the absence of wind and at a constant temperature, suitable for the diagnosis of the present structural state, having limitations on bridges with screw cross sections.

Keywords: bridges; superstructure; impact; mechanical response; stiffness.

_____

[1] Departamento de Ingeniería Civil y Minas, Universidad de Sonora, Hermosillo, México.
[2] Instituto de Ciencias Básicas e Ingeniería, Universidad Autónoma del Estado de Hidalgo, México

Contribution of each author

In this work author Ramos-Torres, G. contributed 30%, author Navarro-Gómez, H. contributed 25%, author Perez-Isidro, E. contributed 15%, author Gautherau-Lopez, J. contributed 15%, and author Palma-Quiroz. I. contributed 15%.

Discussions and subsequent corrections to the publication

Any dispute, including the replies of the authors, will be published in the second issue of 2022 provided that the information is received before the closing of the first issue of 2022.

Propuesta de evaluación de daño para dos puentes ubicados en la carretera No. 14 en el estado de Sonora México usando invariante de rigidez como parámetro global de comparación

RESUMEN

El método de la invariante elástica de rigidez permite obtener la respuesta mecánica de la superestructura de puentes; se basa en la respuesta al impacto de masas conocidas aplicadas al centro del claro para obtener el máximo desplazamiento que define la rigidez puntual, éste se compara con los valores de la curva formada con los invariantes de rigidez, construida a partir de las características de diseño del puente. El método se implementó en dos puentes localizados en la carretera federal No. 14 del Estado de Sonora Mex., con resultados acordes a los daños manifestados. La evaluación es cualitativa a partir de un parámetro global, obtenido en condiciones ambientales en ausencia de viento y a temperatura constante, adecuado para el diagnóstico del estado estructural presente, teniendo limitantes en puentes esviajados.

Palabras clave: puentes; superestructura; impacto; respuesta mecánica; rigidez.

Proposta de avaliação de danos para duas pontes localizadas na rodovia No. 14 no estado de Sonora, México, usando a variável de rigidez como parâmetro de comparação global

RESUMO

O método da variável de rigidez elástica permite obter a resposta mecânica da superestrutura da ponte; baseia-se na resposta ao impacto de massas conhecidas aplicadas ao centro do vão (luz) para obter o deslocamento máximo que define a rigidez do ponto, este é comparado com os valores da curva formada com as variáveis de rigidez, construídos a partir do características do projeto estrutural da ponte. O método foi implantado em duas pontes localizadas na rodovia federal nº 14 do Estado de Sonora Mex., com resultados compatíveis com os danos manifestados. A avaliação é qualitativa a partir de um parâmetro global, obtido em condições ambientais na ausência de vento e a temperatura constante, adequado para o diagnóstico do estado estrutural presente, havendo limitações em pontes esconsas.

Palavras-chave: pontes; superestrutura; impacto; resposta mecânica; rigidez.

Damage assessment proposal for two bridges located on Highway No. 14 in the State of Sonora México by using stiffness invariant as global comparison parameter.

Ramos-Torres, G., Navarro-Gòmez, H., Perez-Isidro, E., Gautherau-Lopez, J., Palma-Quiroz. I.

1. INTRODUCTION.

Worldwide, the design and construction of bridges is governed by regional standards and involves a series of studies prior to their design and construction that are supported by permanent research aimed at reducing the risk of collapse or premature failure; These standards include operational maintenance protocols, however, failures and even collapses frequently occur. A sample of 384 collapsed bridges worldwide in the period from 1944 to 2004 revealed that 28% collapsed due to natural causes, 21% due to design errors, 18% due to impact, 10% due to overloading, 10% due to human error, 10% from unknown causes, 2% from corrosion and 1% from vandalism (Imhof, 2004). The greatest difficulty in the inspection of bridge structures is obtaining a damage index for making maintenance, repair, or replacement decisions.

A summary of some methods to obtain mechanical response in bridges is presented below: For non-linear ranges, the dynamic plastic hinge method was proposed; It is used to obtain the modal load-deformation curve from a one-degree-of-freedom model. The structure is subjected to the acceleration of a given earthquake until the maximum response is obtained in which the plasticization of a previously proposed ball joint is reached, the system becoming a mechanism; This simplified method allows visualizing the ductility demand of the structure (E. Maldonado, et al. 1998). By means of numerical methods, an amplification factor can be obtained that considers the dynamic effects applicable to the mechanical design elements of continuous bridges, considering flexible beams and mobile loads damped by the suspension of the analyzed type trucks. motion equation of the bridge is assumed in forced vibration by the equation of motion of the test truck that has a point of application of load per axle, the beam is idealized as a series of masses concentrated in discrete intervals uniformly distributed in its total length and the effects of truck loading are computed on the front axle; This procedure makes it possible to obtain an impact factor for the mobile load, also known as the dynamic amplification factor, which results from the displacement curves generated for both static and dynamic loads.

The procedure allows to include a friction factor due to the participation of the suspension of the analyzed truck (N. Munirudrappa et al. 1999). The method frequency response functions consist of obtaining a structural characteristic matrix, which is a function of mass, damping and its stiffness. It is obtained by inverting the frequency vector functions cofactors matrix of the motion equation´s Fourier transforms and is known as frequencies response functions matrix. This matrix has only the structure properties and is independent of the excitation, so any change generated in it is due to changes in the constitution of the structure. To obtain the frequency response functions matrix of the displacement vectors and their excitation forces must be known in terms of their Fourier transforms. This is a complex method compared to the modal analysis method, since it requires a much greater number of sensors and a large numerical processing that couples the local and global effects.

The sensitivity analysis method consists of obtaining a sensitivity factor that is equivalent to the quotient between the rate of change in frequency and the rate of change in stiffness. This method helps to select the parameters with the greatest impact on the response and to rule out possible errors in the experimental instrumentation, in such a way that it allows to choose the most significant or highest impact values and to visualize the structural elements with the greatest contribution to dynamic effects. Based on this information, it is possible to determine with good precision the points where the sensors should be placed for experimental studies. A group of experimental methods that make use of numerical simulation methods, where numerical methods such as Runge-Kutta, Euler, etc. can be used to solve the differential equations of motion from the Jacobian of the quotient between the rate of change of the forces and the rate of change of the displacements whose real solutions must be negative to guarantee the stability of the method and its integration in time. In short, the finite element method is the most used to solve the motion

Damage assessment proposal for two bridges located on Highway No. 14 in the
State of Sonora México by using stiffness invariant as global comparison parameter
Ramos-Torres, G., Navarro-Gómez, H., Perez-Isidro, E., Gautherau-Lopez, J., Palma-Quiróz. I.
91

equations, as it uses discretization and interpolation using functions that are compatible with stresses and strains, considering internal equilibrium, equilibrium at the boundary and the compatibility of deformations of the discrete elements that are solved by direct integration and assembled in linear systems of equations provided that the differential equations are ordinary (Carrión FJ et al. 1999). A model to study the effects of temperature compared to the effects of damage in the change of the natural frequency of a span bridges, using finite element models for box girders and prestressed ASHHTO type girders; The article indicates that the changes in the frequency of the superstructure of a bridge of a clearing due to thermal effects (temporary softening), are similar to the effects of damage accumulated over a long period of time (Balmes Etienne et al. , 2005).

A study was carried out by instrumenting two slab bridges and prestressed girders, both of two independent spans; data was collected by means of acceleration sensors; numerical methods were used to find the spectra of speeds and displacements. Likewise, with an adequate frequency filtering, it was possible to separate the static and dynamic effects of the obtained spectrum; The results evaluation indicates that the impact factors obtained by means of the quotient between the load dynamic effect and the load static effect, under certain mass and speed conditions of the test vehicle, exceed those established in the design codes. (Valdez J. et al. 2008). A comparative analysis to obtain the dynamic response of a reinforced concrete bridge located in Italy using a finite element model with Shell-type elements and the excitation of a typical truck at different speeds.

The theoretical analysis was carried out assuming the non-existence of cracking to ignore the contribution of reinforcing steel in estimating stiffness. The results obtained in the analysis indicated that with a single truck it was not possible to obtain the basic dynamic parameters, so a continuous convoy of trucks was used, offering results more in line with reality; the contrast was performed with the data obtained from the application in the excitation site using an electric vibrator placed in the quarter of the bridge span and placing a series of 17 acceleration sensors to obtain the response in real time. The results obtained in the analysis presented errors ranging from 1% to 46% compared with the frequencies obtained on site, the torsion frequency being the one with the lowest error and that of the fourth bending mode the one with the highest error (Veles H. et al. 2011). A methodology to determine the concrete bridges superstructure fatigue deterioration of the reinforced, using Monte Carlo techniques; The method estimates probabilistically according to the statistical data the number of load cycles and their impact on the stress level, using the most popular damage models that allow an estimate of the crack size to be given. This method is speculative and can be applied with relative ease if the operating statistics of the bridge under analysis are known, however, as it is presented, it does not include factors such as extraordinary loads, or earthquakes and corrosion effects, among others, (Crespo E. et al. 2013).

The results of the application of the environmental vibrations method (spectral ratio) applied to the instrumentation of a post-tensioned bridge that allowed them to evaluate the superstructure's present state, the instrumentation results were compared with the results of the structural model made using commercial software. (Viviescas Al. et al. 2017).

2. METHODOLOGY.

Of the bridge infrastructure on federal highways in Mexico, 57% are built of reinforced concrete, followed by 28% built of prestressed concrete, 7% built in steel and concrete, 6% in structural steel, 1% in masonry and 1% in 3dsalb system (IMT-2014). According to the statistics of the Mexican Institute of Transportation, the largest number of bridges is built using reinforced concrete, so the present work studies two reinforced concrete bridges; one based on solid slabs and the other built on beams and slabs with diaphragms of reinforced concrete.

The present work consists of the application of a methodology that uses global parameters; includes the real present point stiffness of the structure, which is obtained from field measurements on the real structure; the value obtained is compared with the stiffness value obtained from the design parameters of the bridge that result from the stiffness invariant function; the quotient between these values corresponds to the residual capacity of the structure, allowing a damage index to be obtained.

2.1. General concepts.

The structural mechanical behavior under service loads depends on the level of efforts achieved and the number of repetitions or load cycles; Factors such as deterioration, corrosion, fatigue and / or an increase in the level of service loads, can generate permanent damage that modify the conditions of its mechanical response. Design considerations for the structural performance is based on elastic linear mechanical behavior and the structure is considered healthy if this behavior is preserved. When the accumulated damage modifies this behavior, non-linear behavior begins where the proportion between the displacements and the applied forces is no longer constant; It is under this basic principle that the proposed method offers information on the present structure state. Figure 1 presents the structural system's mechanical behavior under monotonic load with gradual load increase; First, a straight line can be seen beginning at the origin and reaching the coordinates (δ_E, P_E); (δ_E) corresponds to the displacement up to the linear elastic limit and (P_E) to the load in the same limit; the curved part indicates that the structural system has a non-linear behavior.

The proposed method considers that if three increasing point loads are applied, a load-displacement graph is obtained that describes a mechanical behavior like the real one; From the applied load increments, joining the coordinates of the three points, two lines are obtained that have the same slope if working in a linear range or secant to the real stress-strain curve of the structure if the work is in a non-linear range. If the load increments are small, the upper and lower areas of the real curve are remarkably like the upper and lower areas of the graphs of the lines obtained, reducing the error of the method. The areas described provide a way to measure the damage.

Damage assessment proposal for two bridges located on Highway No. 14 in the
State of Sonora México by using stiffness invariant as global comparison parameter 93
Ramos-Torres, G., Navarro-Gómez, H., Perez-Isidro, E., Gautherau-Lopez, J., Palma-Quiróz. I.
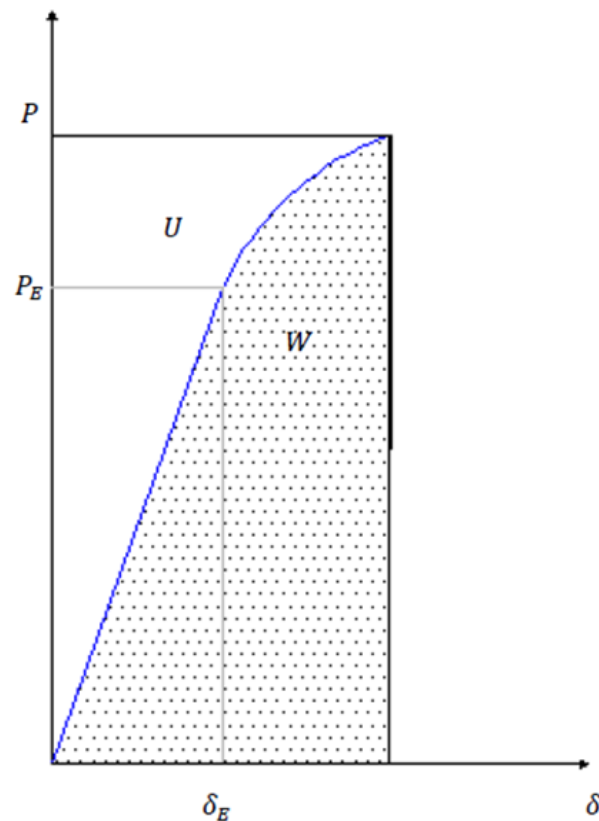
Figure 1. Load displacement relationship

2.2. Damage assessment.

Figure 1 is divided into two regions, a lower one whose area corresponds to the work W that was produced during the loading process and an upper one whose area corresponds to the deformation energy U stored by the structure, which allows it to recover its original shape if the load is removed fully or partially. When the structural mechanical behavior is linear elastic, the work and the deformation energy have the same magnitude, which implies that the structure can recover its original configuration if the loads are removed; if the behavior is non-linear, the values of the work done and the stored deformation energy are different, which implies that, when the load is removed, the structure will partially recover its configuration. Disregarding the energy generated in the form of heat, if the structure has non-linear behavior, the stored deformation energy is less than the work done by the system; This consideration is applicable in reinforced concrete structures.

There are some semi-empirical expressions to evaluate the damage in reinforced concrete structures obtained from experimental tests; One of the expressions that allows obtaining a damage index considering the slope of the elastic part of the discharge curve, is defined by the following expression:

$$d = 1 - \frac{z}{z_0} \qquad (1)$$

Where d is a damage index, Z is the slope of the discharge branch elastic part and Z_0 is the slope value of the initial elastic branch (Perdomo M. E. et al, 2006). For elastic behavior, the expression (1) has a null value and for inelastic behavior near the failure point the value is close to unity. With this expression, an energy restitution curve for the test elements can be obtained and the damage index generated prior to failure is achieved, the difficulty of its use entails carrying out experimental tests for each type of structural element.

According to the proposal of the present work, the real deformation is obtained from the acceleration-time spectrum double integration that results from the impact applied to the real structure with known masses and their free fall heights, only considering the maximum amplitude of the displacement; from these values a kinetic energy vs. displacement graph can be constructed; the upper area of the graph is identified with area A_{sup}, analogous to the deformation energy density U and the lower region is identified with area A_{inf},, analogous to the density of work done W. The quotient of these two quantities Δk, is a measure of damage based on the energetic change due to the decrease in the rigidity of the system because of damage and is applicable to the major test load.

$$\Delta k = \frac{A_{sup}}{A_{inf}} \qquad (2)$$

2.3. Invariant elastic stiffness.
It is formed with the stiffness values below the limit of proportionality along the length of a structural element. In (3) K, corresponds to the theoretical design stiffness value, F corresponds to the applied force and δ is the resulting displacement.

$$K = \frac{F}{\delta} \qquad (3)$$

If the virtual work principle is applied and considering only the contribution of the bending moment, the expression for the stiffness at a point corresponds to (4).

$$K = F \left[\int_0^l \frac{M^*M}{EI} \, dx \right]^{-1} \qquad (4)$$

If the value of the force F is kept constant throughout each point of the structure, under the limit of proportionality the stiffness curve is obtained and has the character of invariant at each point. According to figure 2, if F is applied in the coordinate $X = a$, it is necessary to determine the displacement δ and the stiffness K (a).

$$\delta = \left(\frac{(a^3 b^2 + a^2 b^3)}{3EIL^2} \right) F \qquad (5)$$

Damage assessment proposal for two bridges located on Highway No. 14 in the
State of Sonora México by using stiffness invariant as global comparison parameter
Ramos-Torres, G., Navarro-Gómez, H., Perez-Isidro, E., Gautherau-Lopez, J., Palma-Quiróz. I.

95
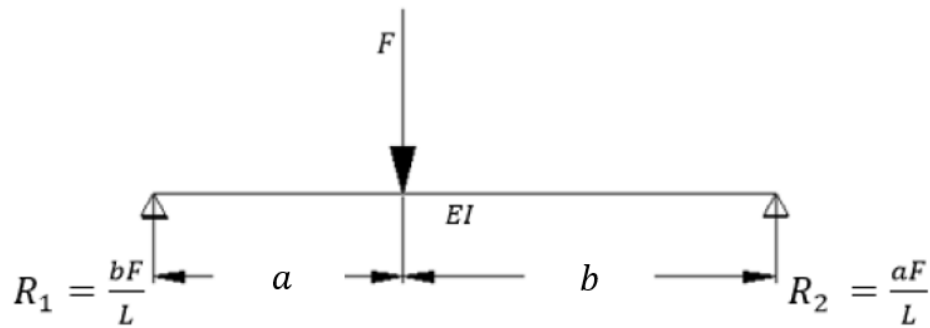
Figure 2. Load displacement relationship

Once the displacement is known, the stiffness is obtained in the coordinate $x = a$; considering $b = L\text{-}a$, where (6) is the stiffness invariant applied for beams and (7) the invariant for solid slabs.

$$K(x) = \frac{3EIL^2}{X^3(L-X)^2 + X^2(L-X)^3} \tag{6}$$

$$K(x) = \frac{3EIL^2}{(X^3(L-X)^2 + X^2(L-X)^3)(1-v^2)} \tag{7}$$

2.4. Measurement of actual point stiffness.
The actual point stiffness is obtained with the maximum displacement that occurs when subjecting the superstructure to impact loads applied to the center of the span; Small masses are used for excitation, which minimally modify the dynamic parameters of the structure. To calculate the impact force F_R, the fundamental expressions of clasic mechanics are used, which are described below:

$$v = \sqrt{2gh} = impact\ velocity \tag{8}$$

$g = acceleration\ of\ gravity$
$h = fall\ height$

Since the impact is made in a deformable medium, the magnitude of the force depends on the reaction stiffness; (9) corresponds to the kinetic energy now of impact.

$$E_c = \frac{mv^2}{2} = m\ g\ h = Kinetic\ energy. \tag{9}$$

$m = mass.$

From the kinetic energy-displacement graph, as previously mentioned, the upper area of the curve A_{sup}, is analogous to the deformation energy (U) and the lower area A_{inf}, is analogous to the work done (W), so Δk corresponds to a residual stiffness factor, which with a unit value indicates structural health and any value less than one indicates permanent damage to the structural system. The residual stiffness factor Δk (2) is applicable to reinforced concrete structures. It corresponds to the increase in the cracking of the cross section, due to the creep of the reinforcing steel as damage accumulates which is reflected in the decrease of the compression area since the cracking as the steel receives greater deformation, grows in the tension zone. Therefore, the moment of inertia of the cross section is reduced, expressed by I_D for its consideration within method (10). To know the value of the present real stiffness, it is required to obtain the effective force when the kinetic energy is zero at the instant of maximum displacement. The value of the real force for each group of impacts is obtained from the use of (11) considering the impact load applied to the center of the span.

$$I_D = \Delta k I_{crt} \tag{10}$$

$$\overline{F_R} = \frac{48 E I_D}{L^3} \frac{1}{n} \sum_{i=1}^{n} \delta_i \tag{11}$$

With (12), the actual present stiffness K_R is obtained; $\overline{F_R}$ corresponds to the average effective impact force and $\bar{\delta}$ to the average of the displacements measured in the field for each mass.

$$K_R = \frac{\overline{F_R}}{\bar{\delta}} \tag{12}$$

$$d_e = 1 - \frac{K_R}{K} \tag{13}$$

In(13), d_e is considered a damage index and is a measure of the degradation or decrease in stiffness. in healthy structures the value is null; for collapse it is close to unity and depends on the characteristics of each structure. In the proposed method, the system preload corresponds to the permanent load of the structure, which can be of the order of up to 85% of its total capacity. This allows the use of small load increments to obtain deformations in advanced areas of the hysteresis stress strain curve envelope. Figure 3 shows the methodology flow diagram used for the studies case. First of all, it is necessary to have the project structural plans. For field measurements, a mass system is used that during the impact is coupled to the movement of the structure to avoid rebound. Preferably, the amount of mass for each group of tests should have proportional values, in order to facilitate the corresponding calculations. It is very important that when choosing the test masses, the structure response acceleration is at least 20% below the maximum acceleration limit of the sensor and that the acceleration values for each different mass have sufficient discrimination for numerical processing. The rest of the activities are presented in the same figure.

Damage assessment proposal for two bridges located on Highway No. 14 in the
State of Sonora México by using stiffness invariant as global comparison parameter
97
Ramos-Torres, G., Navarro-Gómez, H., Perez-Isidro, E., Gautherau-Lopez, J., Palma-Quiróz. I.
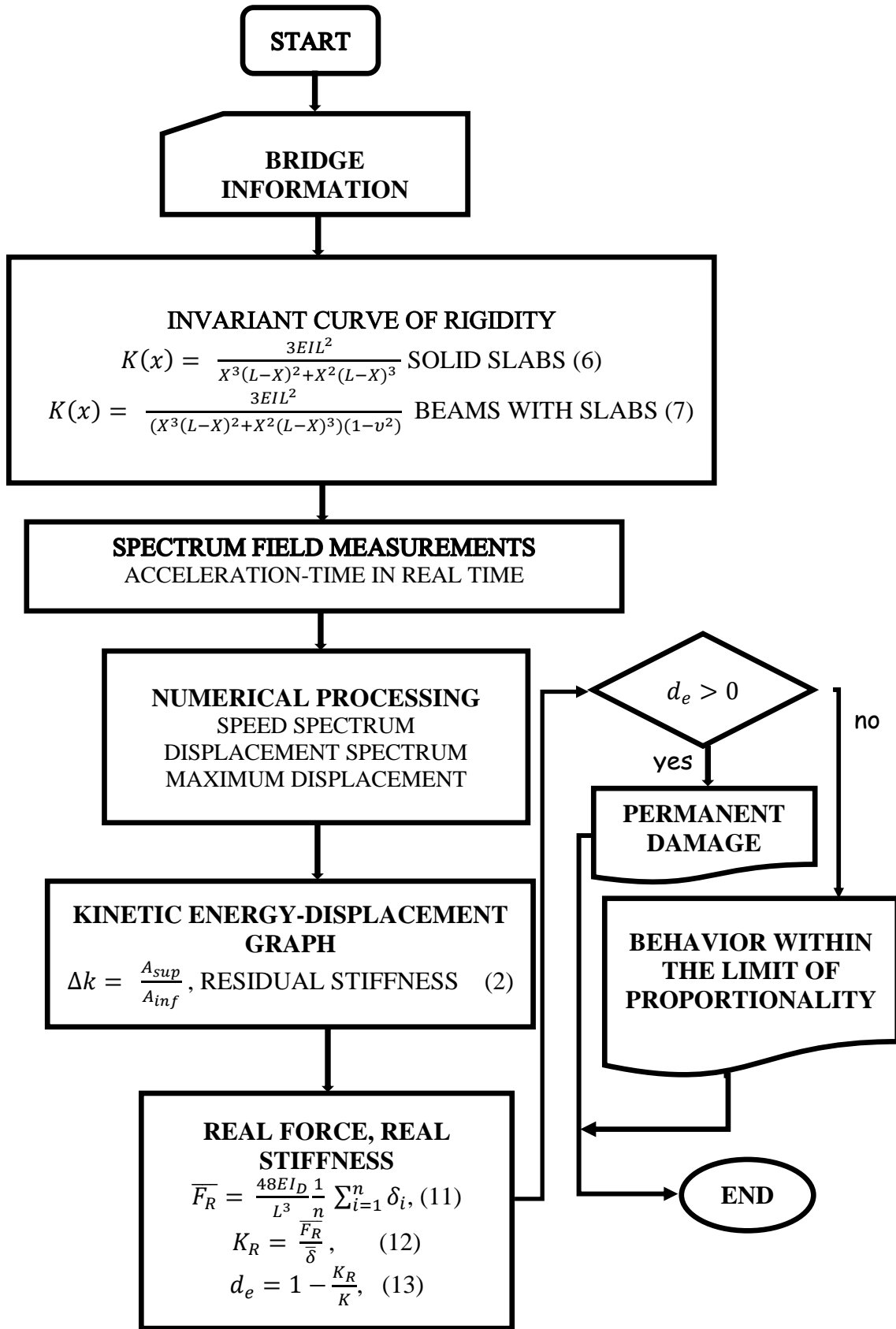
Figura 3. Flow diagram, Stiffness invariant method.

3. STUDY CASES.

The instrumented bridges are located on federal highway 14, Hermosillo-Moctezuma, in the state of Sonora, México; one of the bridges bears the name of "El Testarazo" figure 4, which is located at km 23 + 900. The bridge has a superstructure made of three reinforced concrete slabs, simply supported on abutments made up of reinforced concrete walls. The other instrumented bridge is called "El Gavilán" figure 5; The super structure is formed by a system of reinforced concrete beams, slabs, and diaphragms, with a section skewed at 48 ° from its transverse direction, located at Km 60 + 100 of the same roads.

3.1. Information on the case studies.
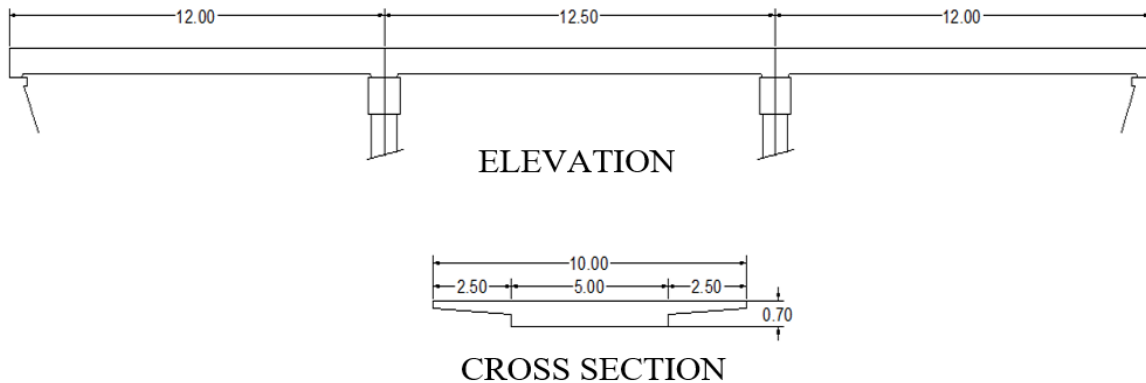
Figure 4. "El Testarazo" bridge superstructure Geometry (Dimension m).
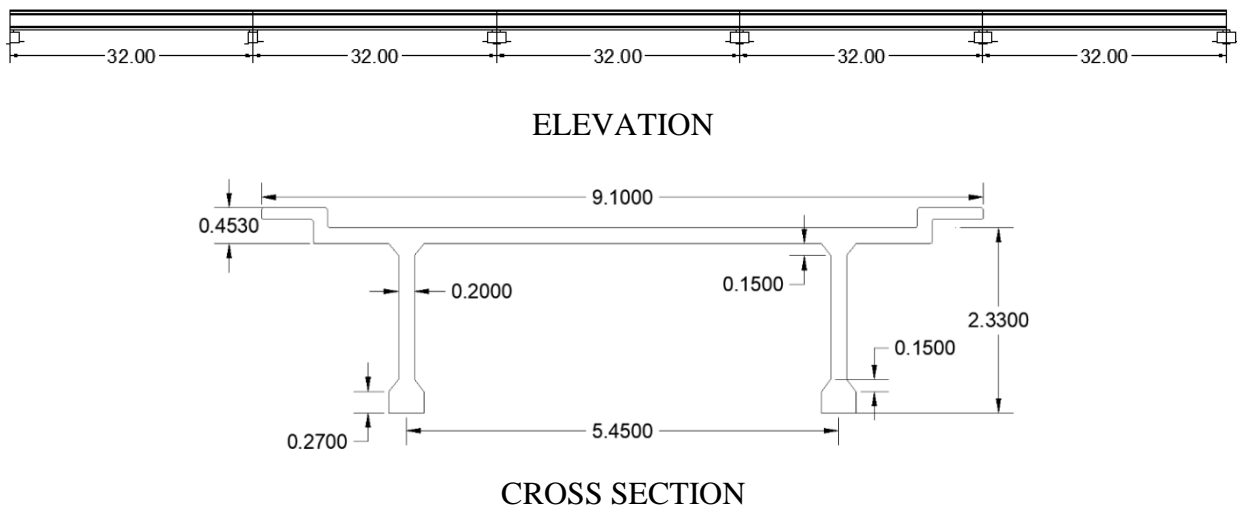
Figure 5. "El Gavilán" bridge superstructure geometry (Dimension m).

The cross sections geometric properties were obtained under the transformed section criterion, and the project data were obtained from the Type Project of Reinforced Concrete Elements, Part I, published by the now extinct SAHOP.

Table 1. Geometric properties transformed section of bridges (m).

Bridge	b_w	h_f	b_f	n	$A_s(m^2)$	d	k_d	$I_{crt}(m^4)$	$A(m^2)$
Testarazo	5.2	0.30	10.0	8.796	0.035	0.645	0.1858	0.1108	2.95
El Gavilán	1.08	0.18	7.5	8.796	0.0386	2.182	0.481	1.199	2.89

Damage assessment proposal for two bridges located on Highway No. 14 in the
State of Sonora México by using stiffness invariant as global comparison parameter   99
Ramos-Torres, G., Navarro-Gómez, H., Perez-Isidro, E., Gautherau-Lopez, J., Palma-Quiróz. I.

For the bridge "El Testarazo" $EI = 2,595\ MN - m^2$ (for solid slab stiffness); for the El Gavilan bridge $EI = 28,082\ MN - m^2$ (for beam stiffness). With these values the stiffness curve was obtained. In both cases, only bending effects are considered. The concrete elasticity modulus value used was $E = 23.414\ Mpa$, based on the expression $E = 15100\sqrt{f_c'}\ (\frac{Kg}{cm2})$.

3.2. Stiffness invariant curve.
Figures 6 and 7 show the cofactors graphs corresponding to the stiffness invariants, obtained from (4) for the "El Gavilán" bridge and from (5) for El Testarazo bridge. The K_E project stiffness values at the superstructure mid span are presented in table 2; said values result from the product of the cofactors illustrated in Figures 6 and 7 with the respective $EI´s$ values.

Table 2. Stiffness values under the limit of proportionality.

Bridge	"El Testarazo"	"El Gavilán"
K_E(MN/m)	66.432	41.237
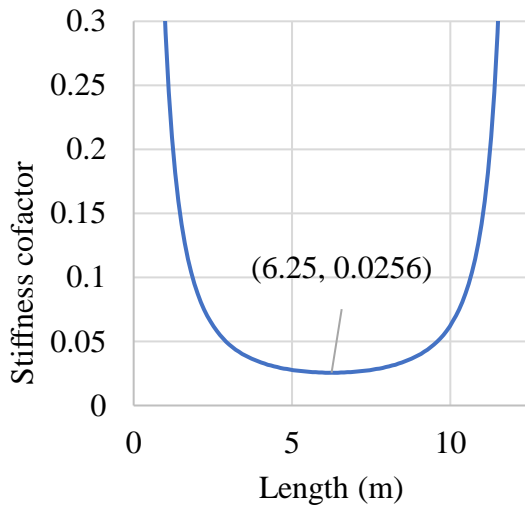
Figure 6. "El Testarazo" bridge stiffness cofactor.
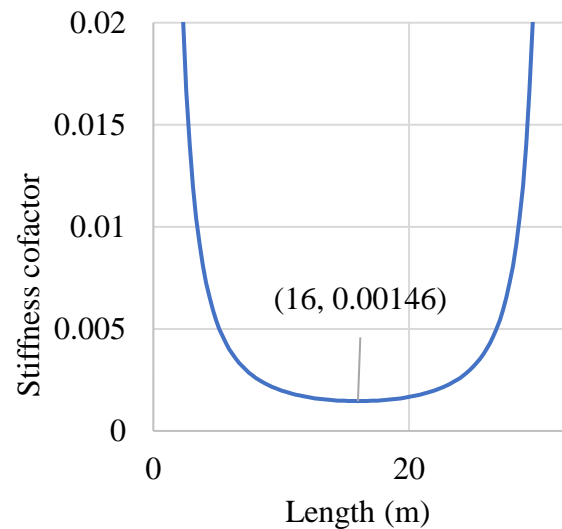
Figure 7. "El Gavilán" Bridge Stiffness Cofactor.

3.3. Procedure to obtain the structure real stiffness.
The field measurements were made using a structure for lifting and unloading the excitation masses. The equipment consists of a quadruped skeleton that allows the masses to be raised by means of a 2250 N capacity winch; the container holding mechanism is made up of an electromagnet with a capacity of 6 KN that enables the excitation mass to be clamped by means of a safety hook with a torsional freedom degree (fig. 8).

Figure 8. General appearance of the field test equipment.

Sand containers were used, with plastic behavior during the impact, to avoid rebound; Three sacks of 25, 50 and 75kg capacity were manufactured, which were filled up to the test mass; the impact was achieved by raising the sacks to an average height of 1.50m, subsequently, the electromagnet electrical flow that held them was interrupted to release them and produce the impact on the bearing bridge surface; The remaining equipment consists of a low frequency acceleration sensor (0.2 Hz), with a sensitivity of 500 mV / g, placed in bridge´s mid span that allowed obtaining the response in real time. In addition, a 4-channel capture card for data reception from 0 to 25 khz was used. The card allowed the capture of analog signals produced by the sensor during measurements. The capture card was placed on a chassis with capacity for eight 11-30 V cards of 15 W, to operate from -40º to 70º C communicated to the USB port of the software carrier computer to process the analog signal where the spectra were obtained from the acceleration-time response of the structure. The analog signals captured were processed using the Labview Signal Express version 3.0 Software, license 501701A-00, which allowed the capture of the time-acceleration spectrum in a numerical matrix in ASCII code TXT format, in raw state for numerical processing. The acceleration-time spectra obtained are presented in Figures 9, 10 and the displacements were obtained by twice integrating the spectra with the Constant Average Acceleration and Linear Acceleration Methods.

Damage assessment proposal for two bridges located on Highway No. 14 in the State of Sonora México by using stiffness invariant as global comparison parameter
Ramos-Torres, G., Navarro-Gómez, H., Perez-Isidro, E., Gautherau-Lopez, J., Palma-Quiróz. I.

101

3.4. Field measurements results.

Figures 9 and 10 show the acceleration-time spectra captured during field measurements.
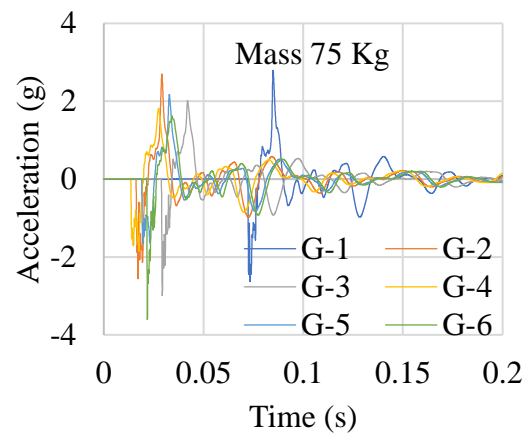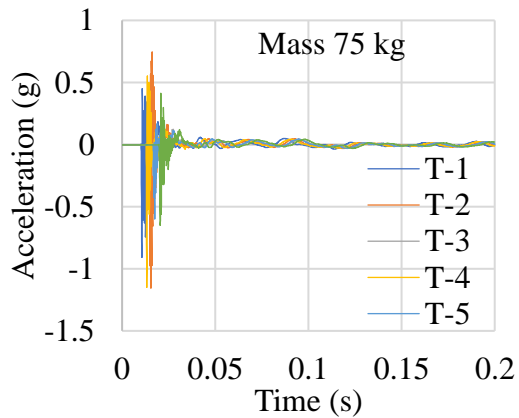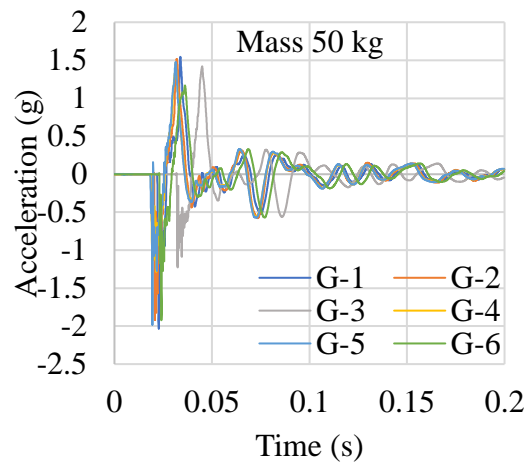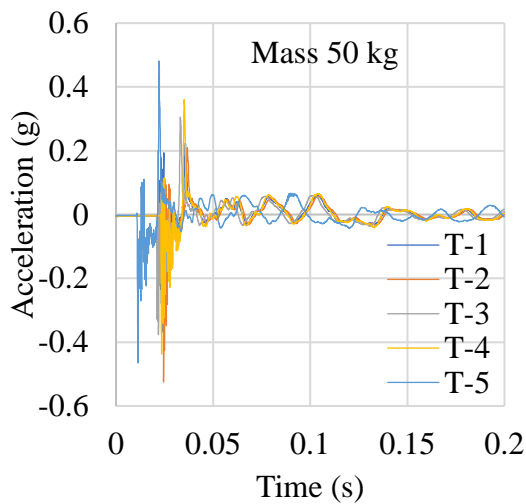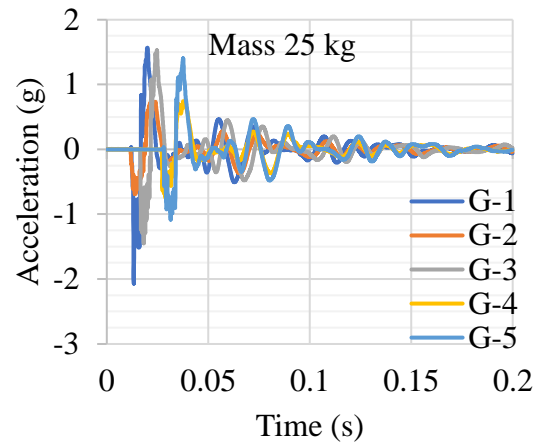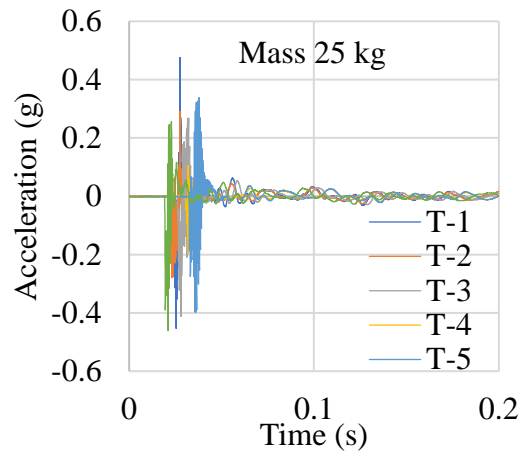
Figure 9. Acceleration-real time spectrum, "El Testarazo" bridge.

Figure 10. Acceleration-real time spectrum, "El Gavilán" bridge.

The acceleration-time spectra of Figures 9 and 10 were subjected to a numerical treatment, which consisted, first, in the correction of the spectral baseline, and later, in the double integration with the methods already described to obtain the maximum displacements produced by the impact of the masses. Tables 3 and 4 show the results that include the test mass, the height of free fall and the displacements obtained from the numerical processing.

Damage assessment proposal for two bridges located on Highway No. 14 in the State of Sonora México by using stiffness invariant as global comparison parameter.
Ramos-Torres, G., Navarro-Gòmez, H., Perez-Isidro, E., Gautherau-Lopez, J., Palma-Quiroz. I.

Table 3. Field and numerical post-process results El Testarazo bridge.

MASS (Kg)	HEIGHT (m)	DISPLACEMENT (m)
25	1.525	-2.92927E-05
25	1.5	-2.89101E-05
25	1.484	-2.84981E-05
25	1.46	-2.8037E-05
25	1.48	-2.83313E-05
25	1.55	-2.98126E-05
50	1.38	-5.11297E-05
50	1.53	-5.69176E-05
50	1.55	-5.76141E-05
50	1.47	-5.473E-05
50	1.548	-5.7467E-05
50	1.56	-5.77907E-05
75	1.51	-8.83783E-05
75	1.49	-8.69951E-05
75	1.5	-8.74758E-05
75	1.51	-8.85254E-05
75	1.49	-8.7103E-05

Table 4. Field and numerical post-process results El Gavilán bridge.

MASS (Kg)	HEIGHT (m)	DISPLACEMENT (m)
25	1.54	-0.000167776
25	1.52	-0.000141068
25	1.55	-0.00017
25	1.5	-0.00013734
25	1.53	-0.000163631
50	1.5	-0.000260161
50	1.53	-0.000268009
50	1.52	-0.000266636
50	1.5	-0.00026644
50	1.54	-0.000273797
50	1.5	-0.000258101
75	1.67	-0.000491775
75	1.5	-0.000440763
75	1.52	-0.000448023
75	1.4	-0.000412609
75	1.39	-0.000408783
75	1.41	-0.000414767

3.5. Statistical analysis of field data.

To know the validity of the data obtained in the measurements made on a natural scale of the study cases, we proceeded to the analysis of variance or ANOVA; The main purpose is to know with the bifactorial analysis if the displacements obtained are dependent on the mass and height in free fall used in the tests and to rule out the possibility that other factors have influenced the results. The null hypothesis H_0 assumes that the results obtained are independent of the test factors; the alternative hypothesis H_1 assumes that the results are dependent on at least one of the factors, both, for a 95% confidence value.

3.5.1. Analysis of variance for the data in Table 3.

Table 5. Bifactorial analysis of variances "El Testarazo".

	Degrees of freedom	Sum of squares	Average of squares	F	Critical value of F	f
Regression	2	1.04213E-08	5.2107E-09	2866.0866	4.2148E-20	0.05146909
Waste	15	2.72706E-11	1.818E-12			
Total	17	1.04486E-08				

Since the distribution function $f < F$, the null hypothesis H_0 is discarded and the alternative hypothesis is accepted; Therefore, it is stated that the displacement results obtained are dependent on at least one of the factors masses and / or height of free fall with a confidence value of 95%.

Damage assessment proposal for two bridges located on Highway No. 14 in the
State of Sonora México by using stiffness invariant as global comparison parameter
Ramos-Torres, G., Navarro-Gómez, H., Perez-Isidro, E., Gautherau-Lopez, J., Palma-Quiróz. I.

103

Table 6. Analysis of variances (mass-displacement) of "El Testarazo".

Origin of variations	Sum of squares	Degrees of freedom	Average of squares	F	Probability	Critical value for F	f
Between groups	20018.428	1	20018.4283	93.677634	5.0095E-11	4.1490974	0.0039
Within groups	6838.2352	32	213.694853				
Total	26856.663	33					

As in the bifactorial case, from the values in Table 6, the null hypothesis is discarded, and the alternative hypothesis is accepted since $f < F$; it can be stated that the displacements obtained are dependent on the applied mass with a 95% confidence value.

Table 7. Analysis of variances (height-displacement) of "El Testarazo".

Origin of variations	Sum of squares	Degrees of freedom	Average of squares	F	Probability	Critical value for F	f
Between groups	19.17911772	1	19.1791	20252.1	2.061E-46	4.149097	0.00399
Within groups	0.03030448	32	0.00095				
Total	19.2094222	33					

As can be seen in table 7, $f < F$ which allows ruling out the null hypothesis, so the displacements obtained are dependent on the fall heights of the masses with a 95% confidence value.

3.5.2. Analysis of variances for the data in table 4.

Table 8. Bifactorial analysis of variances "El Gavilán".

	Degrees of freedom	Sum of squares	Average of squares	F	Critical value of F	f
Regression	2	2.22636E-07	1.1E-07	322.93	1.93519E-12	0.051481683
Waste	14	4.82596E-09	3.4E-10			
Total	16	2.27462E-07				

Table 8 presents the results of the analysis of variance; since $f < F$, the null hypothesis H_0 is discarded and the alternative hypothesis is accepted; Therefore, it is stated that the displacement results obtained are dependent on at least one of the factors masses and/or height of free fall with a confidence value of 95%.

Table 9. Analysis of variances (mass-displacement) "El Gavilán".

Origin of variations	Sum of squares	Degrees of freedom	Average of squares	F	Probability	Critical value for F	f
Between groups	22518.64	1	22518.6391	105.37	1E-11	4.14909744	0.00399430
Within groups	6838.235	32	213.694852				
Total	29356.87	33					

 From the analysis in Table 9, the null hypothesis is discarded, and the alternative hypothesis is accepted since $f < F$; it can be stated that the displacements obtained are dependent on the applied mass with a 95% confidence value.

Table 10. Analysis of variances (height-displacement) of "El Gavilán".

Origin of variations	Sum of squares	Degrees of freedom	Average of squares	F	Probability	Critical value for F	f
Between groups	19.31294	1	19.312944	9230.5	6E-41	4.1490974	0.0039943
Within groups	0.066953	32	0.0020922				
Total	19.3799	33					

As illustrated in Figure 10, $f < F$; the null hypothesis is discarded, so the displacements obtained are dependent on the fall heights of the masses with a confidence value of 95%.
Regarding the analysis of variance of the data obtained in the field measurements of both bridges; It can be affirmed that the results of the measured displacements depend on the masses used in the impact and their free fall heights with a confidence level of 95%, likewise, it is also affirmed that they are the factors of greatest influence with a probability greater than 99%.

3.6. Damage factor estimation.
From the the signals' numerical processing show in Figures 8 and 9, the velocity and displacement spectra were obtained; Knowing the masses´s free fall heights, we proceeded to the construction of the kinetic energy vs. displacement graphs, using (9) to estimate the kinetic energy. Figures 11 and 12 show kinetic energy vs average displacements graphs for the study cases.

Damage assessment proposal for two bridges located on Highway No. 14 in the
State of Sonora México by using stiffness invariant as global comparison parameter
Ramos-Torres, G., Navarro-Gómez, H., Perez-Isidro, E., Gautherau-Lopez, J., Palma-Quiróz. I.

105
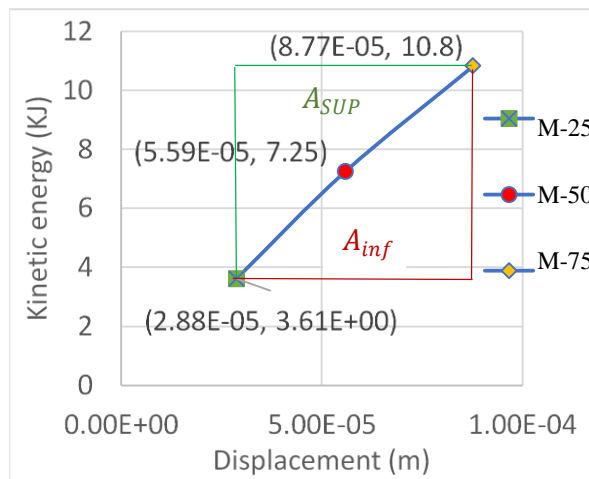
Figure 11. Kinetic Energy-Displacement graph, "El Testarazo" bridge
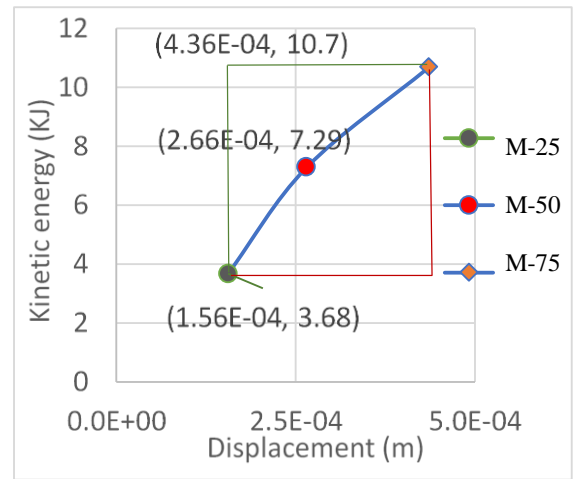
Figure 12. Kinetic Energy-Displacement graph, "El Gavilán" Bridge

The values obtained for the reduction inertia moment by damage according to (10) and (11), are presented in table11; the areas correspond to the upper and lower surfaces of the 3 points' enveloping.

Table 11. Modification values for geometric properties (*I*).

Puente	"El Testarazo"	"El Gavilán"
$\dfrac{A_{sup}}{A_{inf}}$	$\dfrac{21.1165}{23.0434}$	$\dfrac{89.50145}{114.803}$
ΔK	0.916	0.78

4. RESULTS AND DISCUSSION.

To find the effective forces that defined the values of the real present stiffness obtained because of the masses' impact, (11) was applied; Table 12 shows the results of the forces and the average displacements obtained that were used to obtain the average values of the actual superstructures point stiffness of the study cases.

Table 12. Values of effective forces and average displacements.

BRIDGE	L (m)	E (Mpa)	I_{crt} (m^4)	I_D (m^4)	$\sum_{i=1}^{n} \delta_i$ (m)	$\overline{F_R}$ (N)
El Testarazo	12.50	23414	0.1108	0.1015	0.0000876954	5121.88
El Gavilán	32.00	23414	1.199	0.9352	0.00043612	13988.70

Once the average values of the displacements and the real forces are obtained, (12) can be applied to obtain the real stiffness value for the elements under study. The contrast was performed with the values obtained from the *EI* product by the stiffness invariant cofactors illustrated in Figures 6 and 7, respectively, for each bridge; the results are presented in table 13.

Table 13. Values of real stiffness, design elastic stiffness and damage percentage.

PUENTE	Masa (kg)	$\overline{\delta}/100$ (m)	$\overline{F_r}$ (N)	$\overline{K_R}$ (MN/m)	K_E (MN/m)	d_e (%)
El Testarazo	75	0.00876955	5121.88	58.405	66.432	12.08
El Gavilán	75	0.043612	13988.70	32.075	41.136	22.03

When assessing the mechanical status of the studies cases, it is important to clarify that the damage index for healthy structures must have a null value; According to table 14, which summarizes the results obtained, the following is stated: For the bridge "El Testarazo" built with solid slabs, the damage index value is 12.08%, which indicates that the structure has 87.9% of its original capacity; It can be interpreted that, during the service life, the superstructure has lost rigidity by 12.08% compared to its original state, accumulating irreversible damage, as manifested in its pathology by excessive deflection and alternating transverse cracking at the center of the clearing. The evidence presented in fig. (10), where the three points obtained for the different masses form two lines with different slopes with decreasing behavior, showing that the state of the structure exceeded the limit of proportionality.

In the case of the "El Gavilán" bridge built with reinforced concrete beams, slabs, and diaphragms with a deviation of 48 °, the resulting damage index is 22.03%, which indicates that it has a capacity of 77.97% with respect to its design capacity, which matches cracking and excessive sag in the structure. It is important to clarify that the stiffness to vertical displacement depends on the contribution to bending and torsion (Deng Kai, 1998); Under this consideration, the calculated damage index expressed in table 13 includes the reduction in flexural and torsional stiffness, but it is not possible to distinguish which percentage corresponds to each degree of freedom.

5. CONCLUSIONS.

The use of the stiffness invariant allowed the obtention of damage index values for the study cases according to their physical conditions. The procedure is relatively simple, especially when you have the information used in its construction. The ease in the analysis to obtain the contrast data, likewise, the ease with which the real stiffness values are obtained in present time, are the main advantages of the method. The disadvantages correspond to the measurement stage in the field since it requires environmental conditions of constant temperature and the absence of wind. Another disadvantage is that for skewed bridges, a more refined analysis is required to obtain the stiffness invariant, since the reduction percentages corresponding to both flexural and torsional stiffness are not appreciated with the proposed procedure.

The method is governed by energetic principles; it can be used in reinforced and prestressed concrete structures with an acceptable approximation, since the amount of deformation energy includes the area of the region that forms the secants with the real force-displacement curve and corresponds to method error; This error is a small portion of the work done that is added to the deformation energy, so the test masses should be chosen with the smallest possible increments in order to minimize the error or, failing that, estimate the error logistically adjusting the three points and obtaining the area of the arcs to be subtracted from the deformation energy and added to the work done. The development of the adjustment by mistake is outside the scope of the present work. Another condition in the use of the method is that the structure's own weight must be an important part of the service load, so it is recommended for use in slabs and beams bridges.

Damage assessment proposal for two bridges located on Highway No. 14 in the
State of Sonora México by using stiffness invariant as global comparison parameter
Ramos-Torres, G., Navarro-Gómez, H., Perez-Isidro, E., Gautherau-Lopez, J., Palma-Quiróz. I.
107

6. REFERENCES.

Balmes, E., Corus, M., Siegert, D. (1998). *Modeling thermal effects on bridge dynamic responses,* Ecole Centrale Paris/MSSMat, SDTools, LCPC, balmes@sdtools.com.

Carrión Viramontes, F. J., Lozano Guzmán, A., Fabela Gallegos, M., Vázquez Vega, D., Romero Navarrete, J. A. (1999). *"Evaluación de puentes mediante el análisis de vibraciones",* Instituto Mexicano del Transporte, Publicación Técnica No. 132, ISSN: 0188-7297. URL: http://www.imt.mx/archivos/Publicaciones/PublicacionTecnica/pt132.pdf

Crespo Sánchez, S. E., Carrión Viramontes, F., Quintana Rodríguez, J. A., Hernández Guzmán, A., López López, J. A. (2013), *"Análisis del deterioro estructural por fatiga y prognosis de un puente típico de concreto utilizando simulación MonteCarlo"*, Instituto Mexicano del Transporte, Publicación Técnica No. 379, ISSN: 0188-7297, URL: https://imt.mx/archivos/Publicaciones/PublicacionTecnica/pt379.pdf

Deng, K. (1998), *"Dynamic response of certain types of highway bridges to moving vehicles"*, Phd. Thesis, The Doctor of Philosophy program in Civil and Environmental Engineering is a joint program with the University of Ottawa administered by The Ottawa-Carleton Lnstitute for Civil Engineering. URL: https://www.collectionscanada.gc.ca/obj/s4/f2/dsk2/ftp02/NQ37062.pdf

Singer, F. L. (1975), *"Engineering Mechanics: Statics and Dynamics",* Third Edition, Harper & Row, New York, I.S.B.N. 968-6034 16-1.

Imhof, D. (2004). *Risk assessment of existing bridge structures.* (Doctoral thesis) University of Cambridge. https://doi.org/10.17863/CAM.19092

Valdés, J., De la Colina, J. (2008). *Análisis de la Amplificación Dinámica de la Carga Viva en Puentes con Base en Pruebas Experimentales.* Revista Tecnológica - ESPOL, 21(1), 149 – 156. Recuperado a partir de http://www.rte.espol.edu.ec/index.php/tecnologica/article/view/150

Luthe, R. (1971), *"Análisis Estructural"*, Representaciones y Servicios de Servicios de Ingeniería, S. A. México.

Maldonado, E., Canas, J., Casas, J., Pujades, L. (1998), *Respuesta de puentes frente a acciones sísmicas,* Monograph Series in Earthquake Engineering, editor A. H. Barbat. MIS27, ISBN: 84-89925-23-2, URL: https://www.scipedia.com/public/Maldonado_et_al_2019a

Munirudrappa, N., Dhrujavara Iyengar, H. N. (1999), *"Dynamic Analysis of Continuous Span Highway bridge"*, ISET Journal of Earthquake Technology, No. 392, 36 (1), 73 – 84. URL: http://home.iitk.ac.in/~vinaykg/Iset392.pdf

Park, R., Paulay, T. (1988), *"Estructuras de Concreto Reforzado"*, Editorial Limusa, S. A. de C. V. México, D. F., Cuarta reimpresión, I.S.B.N. 968-18-0100-8.

Perdomo, M. E., Castro, L., Picón, R., Marante, M. E., Flórez-López, J. (2006). *Modelo de daño para elementos de concreto armado sometidos a corte y flexión.* Revista de la Facultad de Ingeniería Universidad Central de Venezuela, 21(4), 23-36. ISSN 0798-4065.

Secretaría de Asentamientos Humanos y Obras Públicas (1980), "*Puentes para Carreteras. Proyectos Tipo de Elementos de Concreto Reforzado. Parte I.*", Cuarta colección. Diciembre de 1980, México, Editado por SAHOP.

Timoshenko, S., Woinowsky-Krieger, S. (1989), "*Theory of plates and Shells"*, Second edition, McGRAW-HILL BOOK COMPANY, New York, ISBN 0-07-064779-8.

Vélez Gómez, W. H., Riveros Jerez, C. A. (2011), *"Caracterización dinámica en condiciones de excitación natural de puentes de concreto reforzado"*, Vector, 6, 36 – 44.

Damage assessment proposal for two bridges located on Highway No. 14 in the State of Sonora México by using stiffness invariant as global comparison parameter.
Ramos-Torres, G., Navarro-Gòmez, H., Perez-Isidro, E., Gautherau-Lopez, J., Palma-Quiroz. I.

Safety verification of fatigue of a reinforced concrete bridge according to ABNT NBR 6118 2014

M. D. Rossato[1]*, G. S. Munhoz[2] (iD), R. B. P. dos Santos[1], L. M. O. Scoz[1]

*Contact author: mateusrossato.engcivil@gmail.com

DOI: https://doi.org/10.21041/ra.v11i2.515

ABSTRACT

In this case study, the fatigue security of a bridge designed in 1987 was examined considering the current Brazilian standard. A structural model was developed to determine and verify fatigue security in the most critical section considering the Brazilian Load Model and the literature's vehicle spectrum. According to the stress variation method, it concludes that the concrete submitted to compression meets the minimum criteria, but the steel section is not enough to resist shearing and flexural stresses. Pursuant to the Palmgren-Miner rule, the fatigue service life of the reinforcement's bars under flexural stress is 14,91 years. A more detailed structural analysis of the bridge and the vehicle spectrum is necessary to confirm these results.

Keywords: fatigue; bridge; Palmgren-Miner rule; service life.

[1] Departamento de Engenharia Civil, Escola do Mar, Ciência e Tecnologia, Universidade do Vale do Itajaí - UNIVALI, Itajaí, Brasil.

[2] Departamento de Construção Civil, Universidade Federal do Paraná - UFPR, Curitiba, Brasil.

Verificação de Segurança à fadiga de um ponte em concreto armado conforme ABNT NBR 6118, 2014

RESUMO

Nesse estudo de caso, a segurança à fadiga de uma ponte projetada em 1987 foi verificada segundo a norma vigente brasileira. Elaborou-se um modelo estrutural para determinar e verificar a seção mais crítica considerando o trem-tipo e o espectro de veículos da literatura. Segundo o método de limitação de variação de tensões, conclui-se que o concreto sujeito à compressão atende aos critérios, mas a área de aço não é suficiente para combater os esforços cortante e de flexão. Pela regra de Palmgren Miner, a vida útil à fadiga nas armaduras sujeitas à flexão é de 14,91 anos. Uma análise mais detalhada da estrutura e do espectro de veículos é necessária para reiterar tais resultados.
Palavras-chave: fadiga; ponte; regra de Palmgren-Miner; vida útil.

Verificación de seguridad de la fatiga de un puente de hormigón armado según ABNT NBR 6118 2014

RESUMEN

En este estudio se verificó la seguridad a la fatiga de un puente proyectado en 1987 según la normativa brasileña vigente. Se construyó un modelo estructural para determinar y verificar la sección más crítica considerando el modelo estándar brasileño y el espectro de vehículos en la literatura. Según el método de variación de esfuerzos, se concluye que el hormigón sometido a compresión cumple con los criterios, pero la sección de acero no es suficiente para resistir los esfuerzos cortantes y de flexión. Por la regla de Palmgren-Miner, la vida útil a la fatiga de las armaduras sometidas a flexión es de 13,91 años. Es necesario un análisis más detallado de la estructura y del espectro de carga para confirmar estos resultados.
Palabras clave: fatiga; puente; regla de Palmgren-Miner; vida útil.

1. INTRODUCTION

In Brazil, the transportation of assets and people is mostly carried in a huge network of roads, with approximately 1.7 million kilometers extent. The movement of loads in this mode of transport corresponds to 61% of the national transport matrix (CNT, 2018). In this context, (Baroni, 2010) argues that "Special Engineering Structures" (SES) – such as bridges and viaducts - are pivotal elements of the transportation system. Therefore, ensuring its functionality, safety and durability is significant.

In the last decades, the lack of maintenance and repairing policies for SES in Brazil has contributed to accelerate the deterioration process of these structures. Several Brazilian bridges were built between the 50s and 70s and, therefore, were designed by standards that did not foresee the current loadings, nor the current traffic intensity (Silva et.al., 2018).

The main damages that compromise the performance of SES are related to corrosion, physical impact, and erosion of foundations. Nevertheless, (Fathalla et.al., 2018) point out that the bridges and viaducts service life is also directly associated with cyclical stress variations due to vehicle traffic. (Hobbacher et.al., 2016) point out that after a certain number of loading-unloading cycles, cracks are formed and propagated, and this can lead to the collapse of the structure due to fatigue. (Gao et.al., 2020) studied the fatigue service life (FSL) of bridges with steel-concrete composite structures and observed that, in this case, the strength of the concrete had a small impact in FSL's determination. This was reiterated by (Santos, 2013), who proved that fatigue collapse can happen with stresses lower than the elastic limit of the steel-concrete composition.

The Brazilian standard (ABNT NBR 6118, 2014) is used to evaluate damage to concrete structures due to cyclical actions. This standard determines the criteria that must be adopted to check the ultimate fatigue limit state (unlimited life method) and the limit service state. In this case, the verification of fatigue through stress limitation is preferably recommended, adopting loadings presented in (ABNT NBR 7188, 2013).

The proposed loading by the Brazilian standard (ABNT NBR 7188, 2013), which approaches mobile loads for bridges and replaced (ABNT NBR 7188, 1984), does not present configurations about the real traffic flow, but a hypothetical Brazilian Load Model. In addition, it is provided an evenly distributed load per unit area, aiming to represent light vehicles or crowds' transit. Exceptionally, if the load spectrum is available, the Palmgren-Miner rule can be used. This allows to determine the fatigue service life. According to this method, it is assumed that the damage due to fatigue accumulates linearly with the number of cycles and these damages are, according to (Fan and Sun, 2019), the deterioration process that reduces the cross-sectional resistant area.

This study was developed to verify the fatigue security of a bridge designed in 1987 according to (ABNT NBR 6118, 2014). Two methods were used, the limitation of stress variation and fatigue service life. The most critical section of the structure was studied - the girder beam in the middle of the central span.

2. CONTEXTUALIZATION

2.1. The fatigue mechanism in the deterioration of bridges

According to (Yadav and Thapa, 2020), fatigue is a mechanism of structural failure that occurs in a material subjected to repetitive stress variations, that is, which oscillate intermittently during a certain time interval. The set of loading and unloading actions is called cycle. Several cycles culminate with the appearance of new micro cracks or with the propagation of pre-existing ones, which can cause the structure collapse (Cervo, 2004). The greater the magnitude of intermittent loads, the smaller the number of cycles required to fail the structure (BT / PCC, 2000).

Safety verification of fatigue of a reinforced concrete bridge
according to ABNT NBR 6118,2014.   111
Rossato, M. D., Munhoz, G. S., P. dos Santos, R. B., Scoz, L. M.

Bridges and viaducts are structures subjected to fatigue due to the accumulation of damage from non-uniform cycles of stress variation caused by the traffic flow of vehicles with different characteristics. The analysis of this phenomenon in SES structures, especially in situations of intermittent traffic, is essential to guarantee structural security (Santos and Pfeil, 2014).

(Callister and William, 2008) affirm that fatigue rupture is brittle. There is little (or none) plastic deformation. In general, the collapse occurs with the propagation of cracks, and when the fracture surface is perpendicular to the direction of the stress application. However, in the concrete realm, (Euro-International du Béton Committee, 1988) argues that there is not an exclusive collapse due to fatigue. In this case, the rupture of the concrete structure occurs due to the progressive deterioration of cracks caused by cyclic loading.

Considering reinforced concrete structures, (Meneghetti, 2007) proved that fatigue in reinforcement's bars is not usually a relevant factor. However, due to the increase of structures subjected to cyclic loads designed based on rupture state (ultimate limit state), it is important that the effects associated with fatigue are analyzed.

2.2. Durability and fatigue service life

The standard (ACI 318, 2019) emphasizes that the structures' durability concerns to the ability to resist degradation processes, preserving its integrity when submitted to the environment where it was designed. In this context, the Brazilian standard (ABNT NBR 15575, 2013) defines project's service life (PSL), as the time interval in which the structure maintains its durability and performance requirements, meeting the objectives that were proposed.

According to (Branco and Paulo, 2012), a structure achieves its PSL when pathological manifestations (aesthetic or structural) which impair its performance are detected. However, there are maintenance operations that allow restoring the service life of damaged structures.

Unlike the term PSL, which addresses the service life of the structure, FSL is more restricted and is specifically associated with the time interval required for cyclical stresses to promote and propagate cracking in the structural element. (Baroni, 2010) argues that the FSL does not necessarily culminate with the structure collapse, but with cracks in critical dimensions that can be the indirect object of failure. Thus, along the PSL of bridges and viaducts, vehicle transit should not promote excessive stress variations that weakens the structure regarding fatigue.

3. METHODOLOGY

3.1. Characterization of the bridge over the Chapecó River

The bridge over the Chapecó River was designed in 1987, with the objective of connecting the cities of Xaxim and São Domingos, both in the state of Santa Catarina - Brazil. The bridge studied has a total extension of 170 m (longitudinally), distributed in 3 central spans of 33,60 m, 2 spans of 28,00 m (one for each side) and 2 spans of 6,60 m, one in each extremity.

The bridge deck has a total width of 9,00 m, of which 7,20 m is for the rolling tracks, and two lanes with 0,90 m (one at each edge) are intended for pedestrians and cyclists. The deck slab is supported by two girders (30x170 cm), six beams of section 30 x 170 cm (one at each support), and ten beams of section 30 x 170 cm (two in each span - except for the end spans). The cross section of the central span of the bridge is illustrated in Figure 1A. To construct the beams and girders a concrete with a characteristic compressive strength of 20 MPa and CA-50 steel as reinforcement was used.

Safety verification of fatigue of bridges in reinforced concrete according to ABNT NBR 6118,2014.

112

Rossato, M. D., Munhoz, G. S., P. dos Santos, R. B., Scoz, L. M.
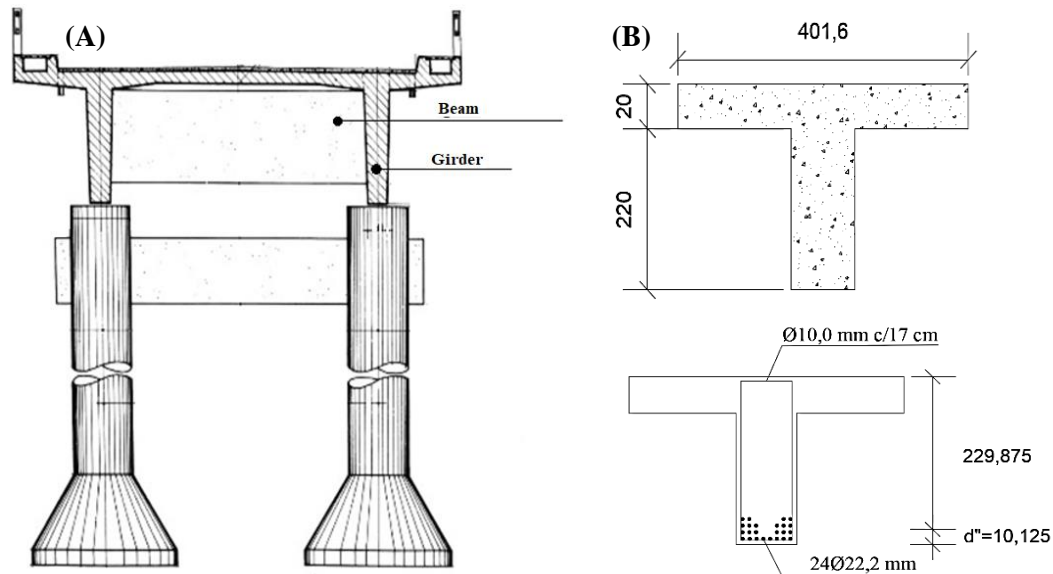
Figure 1. (A) Bridge's cross section over the Chapecó River; (B) Cross section, in centimeters, of the investigated section of the girder (Adapted from the Departamento de Estradas e Rodagem Santa Catarina, 1987).

A preliminary structural analysis about the bridge revealed that the most critical fatigue-based condition occurs in the middle of the central spans of the bridge. Therefore, it was decided to determine the FSL of the girder present in this section (Figure 1B).

3.2. Determination of active stresses

The structural model was built considering the permanent and mobile loads, and the respective weighting coefficients of vertical loads (*WCV*), according to (ABNT NBR 7188, 2013). The determination of the influence and envelope lines was made using the software Ftool (2018), which performs structural analysis in a 2D-level.

As recommended by the Brazilian standard (ABNT NBR 6118, 2014) to verify the fatigue, the stresses applied on concrete and steel were determined in the elastic region and the calculation of the compound flexural stresses in the second deformation stage - disregarding the concrete tensile strength. Regarding the bending moments, the combination of actions for the service limit state (SLS) to fatigue was adopted, recommended by the aforementioned standard.

To determine the resistant moment and the other stresses on the structure, the balance of forces equations and those from (Pfeil, 1989) were used, respectively. As for the calculation of the stresses on the longitudinal reinforcement's bars and concrete, the equations (1) - (2), from (Süssekind, 1980), and Equation (3) from (ABNT NBR 6118, 2014) were adopted to the transverse reinforcement's bars ($\alpha = 90°$).

$$\sigma s = n * \frac{M * (d - x)}{I_{II}} \tag{1}$$

$$\sigma c = \frac{M * x}{I_{II}} \tag{2}$$

$$\sigma v = \left(\frac{Vd - Vc}{0,9 * Asw * d}\right) * Sw \tag{3}$$

Safety verification of fatigue of a reinforced concrete bridge
according to ABNT NBR 6118,2014.   113
Rossato, M. D., Munhoz, G. S., P. dos Santos, R. B., Scoz, L. M.

Where "σs" represents the stress in the reinforcement's bars submitted to tensile (kN/cm²); n is the division between the elasticity module of steel and concrete; M is the moment of inertia (kN.cm); d is the distance from the compressed portion to the gravity center of the reinforcement's bars submitted to tensile (cm); x is the neutral line (cm); I_{II} represents the equivalent inertia in the second deformation stage (cm⁴); "σc" is the compressive stress in concrete (kN/cm²); "σv" is the stress in the transverse reinforcement's bars (α = 90º) (kN/cm²); Vd is the effort shearing of a project over the stirrups (kN); Vc is the effort shearing absorbed by complementary mechanisms (concrete); and, Asw is the transversal steel area necessary over 1 m (cm²/m).

A structural analysis revealed that the center of the largest span of the structure had the biggest stress variation to the reinforcement's bars subjected to bending and shearing, and for concrete subjected to simple compression. Thus, the fatigue verification - according to (ABNT NBR 6118, 2014) criteria - was made about this section (critical condition). As for the stress variation, this is the difference between the maximum and the minimum stresses calculated, if these values have opposite signs, the difference will be between 0 (zero) and the highest value in module. In case of bridges, this variation in tension will be the relation between the active stresses due to permanent loads and those caused by mobile loads plus permanent loads.

In addition, the structural model was created considering the loads specified in (ABNT NBR 7188, 1984 and NB-2, 1961), to prove that the bridge was designed according to the standards of that time (1987). This also made possible to validate the method of calculating the reinforcement's bars using the strength balance equations and the representative model of the bridge.

3.3. Fatigue security verification

The fatigue security verification of the bridge was made according to the guidelines of (ABNT NBR 6118, 2014) by two methodologies: stress limitation and fatigue's service life. The first methodology should be considered the verification by the ultimate limit state (ULS) to fatigue (unlimited life method) and service limit state should be considered. In this work, the analysis will be carried only in the ULS.

3.3.1 Stress limitation

The verification of safety due to fatigue by the stress limitation method was made according to the current regulations to evaluate the security of the structure considering damages caused by cyclical actions. This verification followed all the recommendations of (ABNT NBR 6118, 2014), and was made considering the frequent combination of actions, according to (ABNT NBR 8681, 2004). The calculation of mobile loads was made according to the train-model of (ABNT NBR 7188, 2013), positioned at the most unfavorable point of the structure.

As recommended (ABNT NBR 6118, 2014), the verification was made on the concrete submitted to compression and on reinforcement's bars subjected to bending and shearing. The structural analysis did not identify tension efforts at the studied point, therefore, the security verification of the concrete subjected to tension was neglected.

3.3.2 Fatigue service life

The FSL verification of the bridge was made to the reinforcement's bars subjected to bending, in the middle of the largest span. This was based on the guidelines from (ABNT NBR 6118, 2014), which presents the S-N curve for the bars of reinforced concrete structures. According to (Bolotin, 1998), fatigue curves were introduced in 1860 by the German August Wöhlner. The curve relates the magnitude of the stress cycles and the number of cycles required to bring the material to rupture. According to (ABNT NBR 6118, 2014), to use a real spectrum of loads (or from the literature), it must consider the Palmgren-Miner rule, which relates N (number of cycles to collapse the structure due to fatigue, for a certain stress variation) with the number of cycles experienced (n). Thus, the

calculation of FSL is given by Equation (4). According to (ACI 215R-74, 1997; Nussbaumer et. Al., 2011), fatigue damage must be accumulated linearly, assuming the end of service life when this sum is equal to 1.

$$VU = \frac{1}{D} \tag{4}$$

Where VU represents the service life; and D, the accumulated damage.
For the frequency of vehicle flow, the model presented by (Rossigali, 2013) was adopted. And, regarding the number of steel's N cycles (damage), it was calculated according to Equations (5) - (6), proposed by (Bolotin, 1998) and derived from the S-N curves such as the one in (ABNT NBR 6118, 2014).

$$D = \frac{n_1}{N_1} + \frac{n_2}{N_2} + \frac{n_3}{N_3} + ... = \sum_{i=1}^{m} \frac{n_i}{N_i} = \int \frac{dn}{N} \leq 1 \tag{5}$$

$$N = N_b * \left(\frac{S_b}{S}\right)^m \tag{6}$$

Where D represents the accumulated damage; n_i is the number of cycles applied to the i-th stress level; N_i is the fatigue life of the i-th stress level that corresponds to the number of cycles until the failure of this level; N is the number of cycles associated with fatigue failure; Nb is a dimensionless constant from the S-N curves that arises from (ABNT NBR 6118, 2014); Sb is a constant with a unit of tension; S is the stress in the material; and, m is the exponent of the fatigue curve.
All load's values for each vehicle were increased by the *WCV* from (ABNT NBR 7188, 2013). Therefore, the loading for each type of traffic spectrum (according to the literature) was considered individually, closely to the structure's weight, determining the maximum and minimum bending moments in the middle of the largest span.
According to (ABNT NBR 6118, 2014), it was adopted the index of the elasticity modulus of steel (Es) and concrete (Ec) as 10; and the damage caused by vehicles with loads below 30 kN was ignored. As for the neutral line (X_{II}) and the inertia (I_{II}) of the section in the second deformation stage, and the distance from the compressed section of the beam to the reinforcement's bars gravity center submitted to tensile stresses (d), these will be the same as those used in the fatigue verification by limiting the stress variation.
Given that the FSL determination was performed for the girder reinforcement's bars submitted to flexural stresses, Equation 1 was used to determine the tension due its own weight and to vehicle loads.
As for the characterization of the vehicle spectrum, this was based on the literature, to determine the active loading on the structure and the FSL. Considering the impossibility of measuring the current vehicle traffic, the database described by (Rossigali, 2013; Santos, 2013) was used. According to the authors, the heavy commercial vehicle traffic can be represented by 27 classes with different dimensions (longitudinal and transversal), different distances between axles, and different loads per axle. An example of the characteristics from one of the 27 classes studied (2CC) is presented in Table 1. The characterization of heavy vehicles that travel on the Brazilian road system, described by (Rossigali, 2013; Santos, 2013), was made at different intervals (1999 - 2011) and with different aids from different highway administrators.

Safety verification of fatigue of a reinforced concrete bridge
according to ABNT NBR 6118,2014.
Rossato, M. D., Munhoz, G. S., P. dos Santos, R. B., Scoz, L. M.
115

Table 1. Relative frequency of vehicle class 2CC, by weight range.

Silhouette	Vehicle dimensions and axles	Weight range	Total weight (kN)	Absolute frequency (%)	Volume (vehicle / day)	Relative frequency (%)
	2 single axles: 1 wheel axle 1.20 m from the front; 1 axle with double wheels at 3.84 m from the first axle; Rear overhang = 1.75 m; Total width = 2.20 m; Transverse distance between adjacent tires = 0.25 m; Axle gauge (distance between wheel centers) = 1.70 m.	1	18,93	0,260	15,60	2,35
		2	37,28	1,995	119,70	18,03
		3	55,62	5,490	329,40	49,61
		4	73,96	2,609	156,54	23,58
		5	92,31	0,634	38,04	5,73
		6	110,65	0,037	2,22	0,33
		7	128,99	0,022	1,32	0,20
		8	147,34	0,019	1,14	0,17
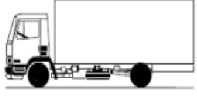
The vehicle type (according to the class) and the number of vehicles (in each class) directly influence the intensity of the bending moments, stress cycle and, consequently, the damage due to fatigue. The volume of vehicles in each class was determined by multiplying the average daily volume of vehicles by the absolute frequency (in each weight range, for each class).

According to (Rossigali, 2013), highways with only one lane per direction (such as the bridge studied here) have an average daily volume of 6 thousand vehicles per day. The absolute frequency represents the number of observations in each range regarding the total number of observations. The relative frequency is the relation between the volume of vehicles from the same class. The total number of vehicles in each class is shown in Table 2.

Table 2. Vehicle volume for each of the 27 classes (considering all ranges).

Class	Volume (vehicles)	Class	Volume (vehicles)	Class	Volume (vehicles)	Class	Volume (vehicles)
2CC	663,96	3C3	15,30	2I3	22,26	3T4	278,40
2C	745,32	3D4	9,60	3S1	10,14	3T6	51,18
3C	1026,96	2S1	268,92	3S2	44,52	3M6	10,02
4C	8,70	2S2	718,08	3S3	368,82	2CB	477,12
2C2	89,88	2S3	681,24	3I1	12,72	3CB	122,16
2C3	16,62	2I1	8,82	3I2	7,86	3BB	122,16
3C2	17,10	2I2	106,98	3I3	95,16	-	-
Total							**6000**

The position of the vehicles also influences the stress diagram. In this work, the position of the vehicles (according to the literature spectrum), was adopted in the center of the lane as recommended by (National Department of Infrastructure and Transport, 2005) and (Toledo, 2011). For the envelope of efforts, the loads due to traffic were increased by *WCV*, proposed by (ABNT NBR 7188, 2013).

116

Safety verification of fatigue of bridges in reinforced concrete according to ABNT NBR 6118,2014.

Rossato, M. D., Munhoz, G. S., P. dos Santos, R. B., Scoz, L. M.

4. RESULTS AND DISCUSSION

4.1. Girder mechanical properties

The resistant section (width) of the girder flange, neutral line and inertia were determined in the second deformation stage. With these results, the structure resistant moment was calculated so that structural reinforcement's bars could be made. (in case it was smaller than the bending moments due to the loads from (ABNT NBR 7188, 2013)).

This way, given that the flange width of the girder is 401,60 cm, the neutral line of the section in the ultimate limit state (x) is 10,35 cm, the neutral line of the section in Deformation Stage II (x_2) is 32, 45 cm, the moment of inertia (M_k) is 6.512,37 kN.m and the resistant moment (I_2) is equal to 4.05×10^7 cm4.

Considering that the bridge was designed according to (ABNT NBR 7188, 1984) (current standard at the time when the project was designed), the structure was analyzed considering the permanent loads (Brazilian Load Model equal to 300 kN), and the impact coefficient (φ) of 1,23, specified in (ABNT NBR NB-2, 1961), as indicated by (Pfeil, 1979). The result is shown in Figure 2.
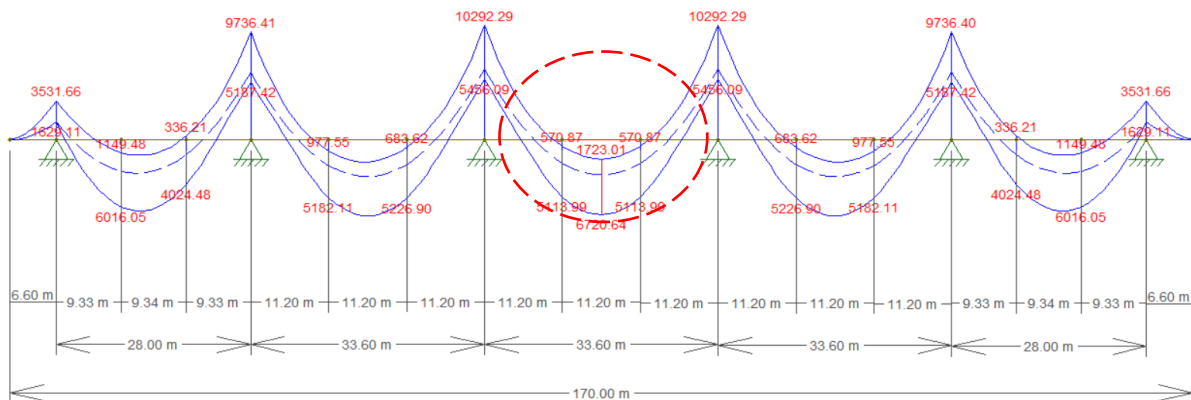

Figure 2. Envelopment of efforts due to the 300 Brazilian Load Model and $\varphi = 1.23$.

The bending moment in the middle of the central span is 6.720,64 kN.m, therefore, close to that calculated using the balance equations of forces, with a difference of 208.27 kN.m, or approximately 3.2%. In this way, it is attested that the bridge was designed according to the standards of that time (1987). The methodology to calculate the strength of the reinforcement's bars was validated by the balance of forces equations and the representative model of the bridge structure.

4.2. Fatigue verification

The fatigue efforts were determined according to the loadings of (ABNT NBR 7188, 2013). After determining the permanent loads, the Brazilian Load Model (TB-450 kN) and the crowd load were increased by the *WCV* (*WCV* = 1.60), obtaining maximum and minimum shear forces (467,43 kN and -467,38 kN, respectively) and maximum bending moments (8.904,07 kN.m) and minimum (1.083,10 kN.m), as shown in Figures 3 and 4, in the middle of the largest span of the bridge.

Safety verification of fatigue of a reinforced concrete bridge
according to ABNT NBR 6118,2014.   117
Rossato, M. D., Munhoz, G. S., P. dos Santos, R. B., Scoz, L. M.
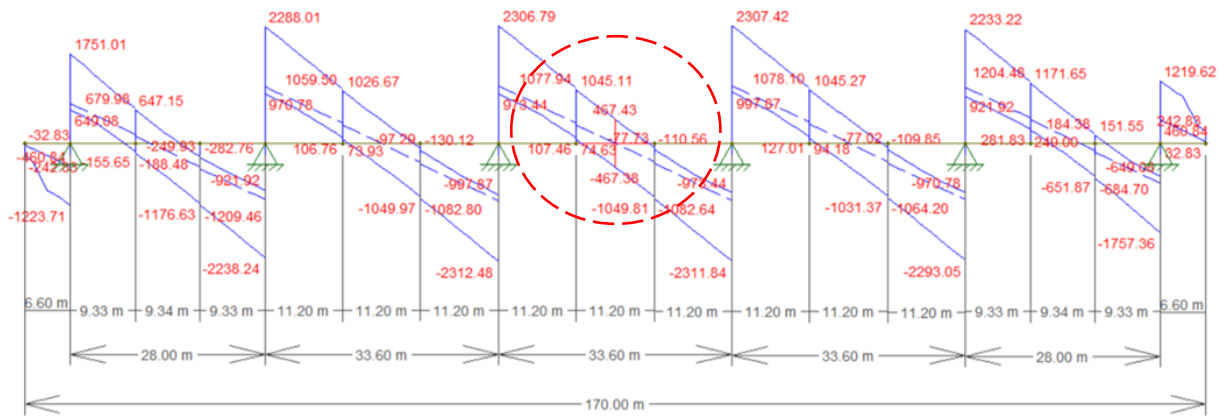
Figure 3. Shearing envelope with TB-450 increased by *WCV* (ABNT NBR 7188, 2013).
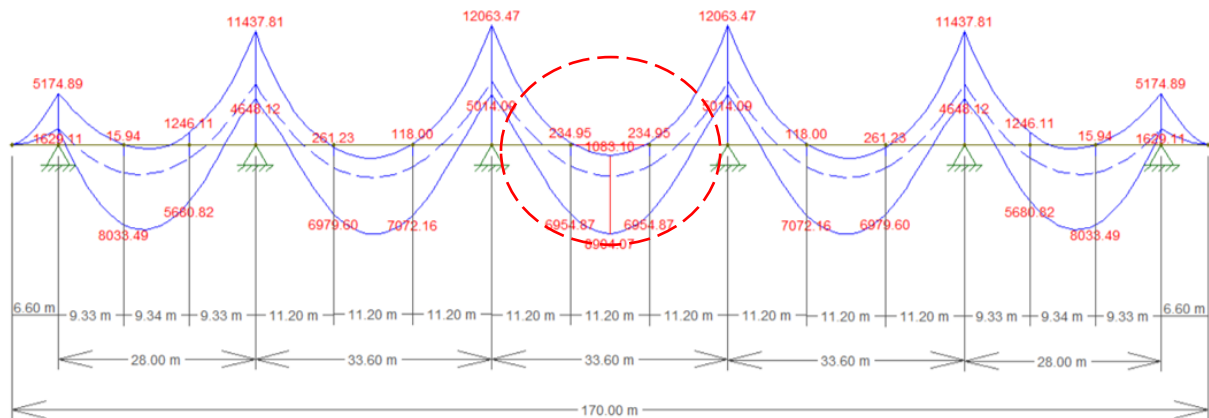

Figure 4. Bending moment envelope with TB-450 increased by *WCV* (ABNT NBR 7188, 2013).

Therefore, it was performed the fatigue verification about the bridge over the Chapecó River, considering the recommendations of (ABNT NBR 6118, 2014) for reinforcement's bars subject to bending, compressed concrete and for shear reinforcement's bars (stirrups).

4.2.1 Flexural reinforcement
The verified section of the girder has 24 steel bars with a diameter equal to 22,2 mm (Steel area = 92,90 cm²). For this diameter, (ABNT NBR 6118, 2014) recommends that the stress in the reinforcement's bars must be limited to $\Delta f_{sd,fad}$ = 180 MPa. Thus, considering the mechanical properties of the studied girder section, it was performed a fatigue analysis for reinforcement's bars submitted to flexural moments in the middle of the largest span of the bridge over the Chapecó River, considering the loads of 450 kN (Brazilian model) and the weighting coefficients of the vertical loads from (ABNT NBR 7188, 2013).
To determine the maximum and minimum stresses on the bars, Equation 1 was adopted. In the section investigated, the stress variation (σs_{max} - σs_{min}) was 190,39 MPa, in other words, bigger than the limit (180 MPa) for 22,2 mm bars. Therefore, this section is not safe against fatigue.

4.2.2 Concrete in compression
The fatigue verification for the concrete in the middle of the bridge span was performed only with compressive loadings because this represents a real situation. According to (ABNT NBR 6118, 2014) this tension must be limited to 45% of the concrete project resistance. In addition, the tensions must be obtained in a distance no longer than 30 cm from the compressed section. Thus,

Safety verification of fatigue of bridges in reinforced concrete
according to ABNT NBR 6118,2014.

118

Rossato, M. D., Munhoz, G. S., P. dos Santos, R. B., Scoz, L. M.

given that the neutral line at the second deformation stage was equal to 32,45 cm, tension variation was corrected by triangle similarity.

To determine the stress variation caused by the maximum and minimum moments in the middle of the largest span of the structure, Equation 2 was used. The compressive stress variation at this point was equal to 3,56 MPa, lower than the standardized limit (6,43 MPa). In this way, the compressed concrete section is safe against fatigue.

It is important to note that, according to (Al-Khaiat and Fattuhi, 2001; Elaty, 2014), concrete has gained resistance over the years. This resistance gain depends on variables such as water/cement ratio, exposure conditions (temperature, humidity) and curing regime. Despite a higher strength, the concrete contributes to reducing the damage associated with fatigue. This consideration could not be included in the present study due to administrative limitations. Thus, this verification assumed the worst-case scenario, that is, keeping the concrete resistance constant.

4.2.3 Shear reinforcement's bars
The girder section under investigation has steel stirrups $\phi 10.0$ mm (steel area = 4,62 cm² / m), spaced at 17 cm. For this diameter, (ABNT NBR 6118, 2014) recommends that the tension be limited to $\Delta f_{sd,fad}$ = 85 MPa. As addressed by (Pfeil, 1979), the shear stress variation in the middle of the longest span of the bridge was 467,43 kN to -467,38 kN. However, the tensions must be considered ranging from 0 (zero) to the maximum value, in this case 467,43 kN.

To determine the stress variation in shear reinforcement's bars, Equation 3 was adopted, according to (ABNT NBR 6118, 2014). Regarding efforts, they were corrected for the combination according to the service limit state (SLS) to fatigue.

The stress variation in reinforcement's bars for shear efforts (stirrups) was 122,26 MPa. This value is higher than the limit (85 MPa) for $\phi 10.0$ mm bars, according to (ABNT NBR 6118, 2014). Therefore, the section under shear is not safe against fatigue.

### 4.3. Accumulated damage and fatigue service life
The calculation of the damage must consider the tensions due to the real vehicle spectrum and the S-N curve (Wöeller Curve), from (ABNT NBR 6118, 2014), as described by Equation 6. The tension limit value was calculated based on reinforcement's bars type T1, which according to (ABNT NBR 6118, 2014) has an S-N curve with angular coefficients of k_1 = 5 and k_2 = 9. The limit number of cycles to fatigue adopted was N = 1×10^6 cycles. This number represents the point of change in the slope of the S-N curve. Therefore, the tension limit value was 194,41 MPa.

For values of stress variation lower than 194,41 MPa, it will be considered the curve stretch with a slope equal to 9. For variations above the limit value of $N = 1 \times 10^6$, a slope equal to 5 will be adopted. Considering Equation 5 with N_b equal to 1×10^6 cycles, S_b equal to 194,41 MPa, exponent of the fatigue curve (m) varying between 5 and 9 and the tension in the material (S) due to each weight range for each vehicle class, the number of cycles N to fatigue was determined.

Then, adopting the traffic volume equal to 6.000 vehicles / day (2,19 million/year), it was calculated the damage in the structure and the accumulation of damage per year (D_{ano}), according to the Palmgren rule Miner (Equation 5), that is, the summation of the division between the number of vehicles in each class and weight range that transited for one year and the number of fatigue cycles due to their loading.

The service life of the structure is reached when the summation of the damages is equal to 1. Therefore, the difference between the unitary value and the total damage in the reinforcement's bars submitted to fatigue for a year, determines the service life, in years. Table 3 shows the damage accumulation for each vehicle class in the spectrum of (Rossigali, 2013), and the FSL, considering the weighting coefficients of the vertical loads from (ABNT NBR 7188, 2013).

Safety verification of fatigue of a reinforced concrete bridge according to ABNT NBR 6118,2014.

119

Rossato, M. D., Munhoz, G. S., P. dos Santos, R. B., Scoz, L. M.

Table 3. Accumulation of damage and fatigue service life of the bridge over the Chapecó River.

Class	Silhouette	Description	Total Damage	Class	Silhouette	Description	Total Damage
2CC		Truck	1,53E-08	2I3		Semi-trailer truck	3,18E-04
2C		Truck	2,97E-07	3S1		Semi-trailer truck	3,17E-07
3C		Truck	6,27E-05	3S2		Semi-trailer truck	4,10E-05
4C		Truck	3,52E-06	3S3-C		Semi-trailer truck	5,44E-03
2C2		Truck + Trailer	2,19E-06	3S3-L		Semi-trailer truck	9,29E-03
2C3		Truck + Trailer	4,32E-05	3I1		Semi-trailer truck	3,71E-04
3C2		Truck + Trailer	3,92E-05	3I2		Semi-trailer truck	1,69E-05
3C3		Truck + Trailer	8,38E-05	3I3		Semi-trailer truck	5,01E-03
3D4		Truck + Trailer	7,47E-04	3T4		B-Double Cattle Trailer	2,21E-02
2S1		Truck + Trailer	1,37E-06	3T6		Road Train	7,88E-03
2S2		Truck + Trailer	3,17E-05	3M6		B-Double Cattle Trailer	3,04E-03
2S3-C		Truck + Trailer	6,63E-03	2CB		Bus	1,35E-06
2S3-L		Truck + Trailer	5,75E-03	3CB		Bus	9,88E-06
2I1		Truck + Trailer	1,55E-04	3BB		Bus	9,88E-06
2I2		Semi-trailer truck	2,15E-05	∑ total			6,71E-02
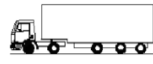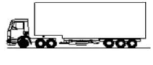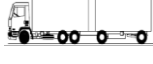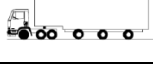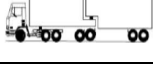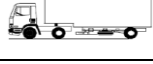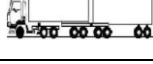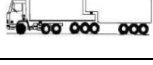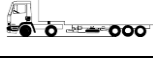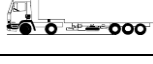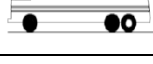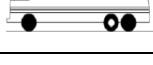
Therefore, the service life of the bridge over the Chapecó River, considering the vehicle traffic of Rossigali (2013) increased by the impact coefficients of (ABNT NBR 7188, 2013), is equal to 14,91 years, with an accumulated total damage of 6,71E-02.

Safety verification of fatigue of bridges in reinforced concrete according to ABNT NBR 6118,2014.

120

Rossato, M. D., Munhoz, G. S., P. dos Santos, R. B., Scoz, L. M.

5. CONCLUSIONS

This study was developed to verify if a bridge designed in 1987, according to the current standards at that time (ABNT NBR NB-2, 1961; ABNT 7188, 1984) is still safe against fatigue considering the current standards (ABNT NBR 7188, 2013; ABNT NBR 6118, 2014). The most critical situation of the structure was studied - the girder in the middle of the central span. It was possible to draw the following conclusions:

- In the fatigue verification for longitudinal reinforcement's bars subjected to simple bending, considering the loads from (ABNT NBR 7188, 2013), the acting stress was above the limit specified by the standard, (190,39 > 180 MPa). In relation to the transverse reinforcement's bars, the stress was approximately 44% higher than the limit specified in the standard, also did not meet the safety criteria for fatigue either.
- In the verification of concrete under compression, considering the loads of (ABNT NBR 7188, 2013), the section investigated proved to be safe, with an acting stress of 3,56 MPa, below the limit of 6,43 MPa. Thus, it can be concluded that if fatigue occurred in the structure, it would initially occur in the stirrups, and not in the concrete.
- The FSL, due to the real vehicle traffic spectrum of (Rossigali, 2013) and increasing coefficients of dynamic loads from (ABNT NBR 7188, 2013), was 14,91 years. This was because the current loads considered here performed in tensions much higher than the fatigue limit for the flexural reinforcement's bars.
- After the fatigue verification using the stress limitation method and the damage accumulation, it was concluded that the flexural reinforcement's bars and the stirrups of the bridge over the Chapecó River did not meet the fatigue verification. In fact, only the concrete compression met the requirements considering (ABNT NBR 7188, 2013). For a real vehicle spectrum, the reinforcement's bars submitted to flexural stresses did not meet the safety criteria of the Palmgren-Miner rule (damage accumulation).

It is important to note that although the analyses were made on a real case, the loads characteristics (vehicles, traffic) does not necessarily represent the real traffic conditions to which the bridge is subjected. Thus, measuring vehicle characteristics and traffic *in situ* could result in different ages of FSL.

In addition, it is recommended that a thorough study of the structure is performed for an overall assessment of fatigue, as long as some of the other elements are also subjected to relevant stress variations. Therewith, a global analysis is required for a better understanding of fatigue behavior.

6. REFERENCES

Al-Khaiat H., Fattuhi, N. (2001), *Long-term strength development of concrete in arid conditions.* Cement and Concrete Composites. 23(4-5)363-373. https://doi.org/10.1016/S0958-9465(01)00004-X

American Concrete Institute, ACI (1997), *"ACI 215R-2: Considerations for Design of Concrete Structures Subjected to Fatigue Loading"*. Michigan, Estados Unidos.

American Concrete Institute, ACI (2019). *"ACI 318: Building Code Requirements for Structural Concrete"*. Michigan, Estados Unidos.

Associação Brasileira de Normas Técnicas (1961). *NB-2: Cálculo e Execução de Pontes de Concreto Armado*. Rio de Janeiro.

Associação Brasileira de Normas Técnicas (1984). *NBR 7188: Carga móvel em ponte rodoviária e passarela de pedestre*. Rio de Janeiro.

Safety verification of fatigue of a reinforced concrete bridge
according to ABNT NBR 6118,2014.

121

Rossato, M. D., Munhoz, G. S., P. dos Santos, R. B., Scoz, L. M.

Associação Brasileira de Normas Técnicas (2013). *NBR 7188: Carga móvel em ponte rodoviária e passarela de pedestre*. Rio de Janeiro.

Associação Brasileira de Normas Técnicas (2013). *NBR 15575: Desempenho de edificações habitacionais*. Rio de Janeiro.

Associação Brasileira de Normas Técnicas (2014). *NBR 6118: Projeto de estruturas de concreto – Procedimento*. Rio de Janeiro.

Baroni, H. J. M. (2010), "*Simulação da vida útil de fadiga do concreto em vigas de tabuleiro de pontes em função do fluxo de veículos pesados*", Tese de Doutorado em Engenharia, Universidade Federal do Rio Grande do Sul, Porto Alegre.

Bolotin, V. V. (1998), Introduction. In: Bolotin V. V. "*Mechanics of Fatigue*", Boca Raton, CRC Press LLC, cap. 1, pp. 01-17.

Branco, F., Paulo, P. (2012), *O projecto de pontes para vidas superiores a 100 anos.* Revista ALCONPAT. 2(1):1-9. http://dx.doi.org/10.21041/ra.v2i1.20

Callister J., William D. (2008), "*Ciência e engenharia de materiais: Uma introdução*". LTC, Rio de Janeiro, Brasil, p. 620. Tradução: Soares, S. M. S.

Cervo, T. C. (2004), "*Estudo da resistência à fadiga de concretos de cimento Portland para pavimentação*", Tese de Doutorado em Engenharia, Universidade de São Paulo, São Paulo.

Confederação Nacional de Transporte, CNT (2018), "*Pesquisa CNT de rodovias 2018: Relatório gerencial*". Brasília, Brasil.

Comité Euro-International du Betón, CEB (1988), "*Fatigue of Concrete Structures. Bulletin d'Information Nº. 188*". Dubrovnik, Croácia.

Departamento de Estradas de Rodagem de Santa Catarina, DER (1987), "*Projeto da Ponte sobre o Rio Chapecó na rodovia SC 451, entre os municípios de Xaxim e São Domingos*". Florianópolis, Brasil.

Departamento Nacional de Infraestrutura e Transporte, DNIT (2005), "*Manual de Conservação Rodoviária*". Rio de Janeiro, Brasil.

Elaty, M. A. A. A. (2014), *Compressive strength prediction of Portland cement concrete with age using a new model.* HBRC Journal. 10(2)145-155. https://doi.org/10.1016/j.hbrcj.2013.09.005

Fan, Z., Sun, Y. (2019), *Detecting and evaluation of fatigue damage in concrete with industrial computed tomography technology.* Construction and Building Materials. 223:794-805. https://doi.org/10.1016/j.conbuildmat.2019.07.016

Fathalla, E., Tanaka, Y., Maekawa, K. (2018), *Remaining fatigue life assessment of in-service road bridge decks based upon artificial neural networks.* Engineering Structures. 171:602-616. https://doi.org/10.1016/j.engstruct.2018.05.122

Boletim Técnico da Escola Politécnica da USP, BT/PCC (2000), *"Concreto com Fibras de Aço - Boletim Técnico PCC/260"*. São Paulo, Brasil.

Ftool (2018), "*A Graphical-Interactive Program for Teaching Structural Behavior*". Available in: <https://www.ftool.com.br/Ftool/>. Access in 15 Mar. 2018.

Gao, Q., Dong, Z., Cui, K., Liu, C., Liu, Y. (2020), *Fatigue performance of profiled steel sheeting–concrete bridge decks subjected to vehicular loads.* Engineering Structures. 213:110558. https://doi.org/10.1016/j.engstruct.2020.110558

Hobbacher, A. F., Hicks, S. J., Karpenko, M., Franz, T., UY, B. (2016), *Transfer of Australasian bridge design to fatigue verification system of Eurocode 3.* Journal of Constructional Steel Research. 122:532-542. https://doi.org/10.1016/j.jcsr.2016.03.023

Meneghetti, L. C. (2007), "*Análise do comportamento à fadiga de vigas de concreto armado reforçadas com PRF de vidro, carbono e aramida*", Tese de Doutorado em Engenharia, Universidade Federal do Rio Grande do Sul, Porto Alegre.

Safety verification of fatigue of bridges in reinforced concrete
according to ABNT NBR 6118,2014.

122

Rossato, M. D., Munhoz, G. S., P. dos Santos, R. B., Scoz, L. M.

Nussbaumer, A., Borges, L., Davaine, L. (2011), "*Fatigue design of steel and composite structures*". Wiley, Hoboken, Estados Unidos, p. 167.

Pfeil, W. (1979), "*Pontes em concreto armado: Elementos de projeto, solicitações, dimensionamento*". LTC, Rio de Janeiro, Brasil, p. 433.

Pfeil, W. (1989), "*Concreto armado*". LTC, Rio de Janeiro, Brasil, p. 812.

Rossigali, C. E. (2013), "*Atualização do modelo de cargas móveis para pontes rodoviárias de pequenos vãos no Brasil*", Tese de Doutorado em Engenharia Civil, Universidade Federal do Rio de Janeiro, Rio de Janeiro.

Santos, L. A., Pfeil, M. S. (2014), *Desenvolvimento de modelo de cargas móveis para verificação de fadiga em pontes rodoviárias.* Engenharia Estudo e Pesquisa ABPE 14(1):40-47.

Santos, L. F. (2013), "*Desenvolvimento de um modelo de cargas móveis para verificação de fadiga em pontes rodoviárias*", Trabalho de Conclusão de Curso em Engenharia Civil, Universidade Federal do Rio de Janeiro, Rio de Janeiro.

Silva, C. J. G., Monteiro, E. C. B., Vitório, J. P. A. (2018), *Condições estruturais e funcionais de pontes e viadutos das rodovias federais de Pernambuco.* Revista ALCONPAT. 8(1)79–93. http://dx.doi.org/10.21041/ra.v8i1.199

Süssekind, J. C. (1980), "*Curso de Concreto: Concreto Armado - Volume I*". Globo, Porto Alegre, Brasil, p. 376.

Toledo, R. L. S. (2011), "*Avaliação de vida útil à fadiga em ponte mista aço-concreto considerando o espectro de veículos reais*", Trabalho de Conclusão de Curso em Engenharia, Universidade Federal do Rio de Janeiro, Rio de Janeiro.

Yadav, I. N., Thapa, K. B. (2020), *Fatigue damage model of concrete materials.* Theoretical and Applied Fracture Mechanics. 108:102578. https://doi.org/10.1016/j.tafmec.2020.102578

Safety verification of fatigue of a reinforced concrete bridge according to ABNT NBR 6118,2014.

123

Rossato, M. D., Munhoz, G. S., P. dos Santos, R. B., Scoz, L. M.

Recovery procedures for foundation elements with alkali/aggregate reaction problems. Documental research

C. S. Silva[1*] , E. C. B. Monteiro [1,2] , M. S. C. Santos[3] , T. W. C. O. Andrade[4] ,
W. A. Soares[6] , D. C. M. Neves[6]
*Contact author: cristiane_santana@msn.com
DOI: https://doi.org/10.21041/ra.v11i2.490

ABSTRACT

The alkali-aggregate reaction (AAR) is a problem that has affected numerous foundations. This study, through an investigation of fifty foundations, seeks to create a profile of the recovery processes through consultations with inspection companies that have carried out recoveries in the city of Recife and neighboring areas. The methodology consisted on the application of a survey with seventeen questions. The results obtained made possible to establish similarities in the foundations affected, the diagnoses, processes applied during recovery, advances in materials, conditioning factors for the use of the reinforcement, and costs, and also identified the foundations where an inspection window was left for future checks. The results conclude with an evaluation of the treatments for foundations affected by AAR.

Keywords: foundations; alkali-aggregate reaction; diagnosis; procedures; recovery.

_____

[1] Department of Civil Engineering, Catholic University of Pernambuco, Recife-PE, Brazil.
[2] Department of Civil Engineering, University of Pernambuco, Recife-PE, Brazil.
[3] Department of Civil Engineering, Federal University of Santa Catarina, Santa Catarina, Brazil.
[4] Department of Civil Engineering, Federal University of Pernambuco, Recife-PE, Brazil.
[5] Department of Civil Engineering, Pernambuco University, Recife-PE, Brazil.

Contribution of each author

In this work the authors E.C.B. and T.W.C.O. contributed to the original idea, supervision and guidelines of this article. The participants M. S.C., W. A. and D.C.M., with the research of the content of the research, development, in contact with companies for data collection, in the formatting of the conclusions of the work and in the translations in English and Spanish.

Discussions and subsequent corrections to the publication

Any dispute, including the replies of the authors, will be published in the second issue of 2022 provided that the information is received before the closing of the first issue of 2022.

Procedimentos de recuperações em elementos de fundações por problemas de reação álcali agregado. Investigação documental

RESUMO

A Reação Álcali Agregado (RAA) atingiu muitas fundações e observou-se a importância de realizar uma verificação nos procedimentos de recuperações, compreendendo uma investigação em cinquenta fundações, objetivando traçar um perfil dos processos de recuperações através de consulta no acervo de empresas fiscalizadoras ou executoras de recuperações na cidade de Recife e cidades vizinhas. A metodologia consistiu na aplicação de um questionário com dezessete perguntas. Esses resultados possibilitaram estabelecer as semelhanças das fundações afetadas, o diagnóstico, processos aplicados na recuperação, os avanços dos materiais, fatores condicionantes para utilização da armadura, os custos, e possibilitaram a identificar as fundações que deixaram uma janela de inspeção para posteriores verificações. Concluindo-se com os resultados uma avaliação dos tratamentos nas fundações acometidas pela reação RAA.
Palavras-chave: fundações; reação álcali agregado, diagnóstico, procedimentos, recuperações.

Procedimientos de recuperación en fundaciones por problemas de reacción álcali/agregado. Investigación documental

RESUMEN

La reacción álcali/agregado (AAR) ha afectado muchas cimentaciones lo cual señala la importancia de realizar una verificación de los procedimientos de recuperación, la cual se realizó en cincuenta cimentaciones. El objetivo fue construir un perfil de los procesos de recuperación a través de una consulta con empresas de inspección o ejecutores de recuperaciones en la ciudad de Recife y ciudades vecinas. Para ello se aplicó en forma metodológica un cuestionario con diecisiete preguntas. Estos resultados permitieron establecer las similitudes de las cimentaciones afectadas, el diagnóstico, los procesos aplicados en la recuperación, los avances en materiales, los condicionantes para el uso de la armadura, los costos, y permitieron identificar las cimentaciones que dejaron una ventana de inspección para controles adicionales. El resultado fue una evaluación de los tratamientos en las bases afectadas por la reacción química AAR.
Palabras clave: fundaciones; reacción alcalina agregada; diagnóstico; procedimientos; recuperaciones.

1. INTRODUCTION

In the early 1940s, the scientific community was faced with a "disease" affecting large concrete structures. It was a slow and progressive reaction that developed through a chemical process between alkaline hydroxides, found in the existing solutions in the pores of the concrete paste, and reactive minerals found in certain types of aggregates, in the presence of water. The alkali-aggregate reaction, better known as AAR, is a deleterious long-duration chemical reaction, which can result in the formation of an expansive gel, forming cracks and chips in concrete, leading to a loss of durability, among other properties.

In Brazil, the pioneering scholars who studied this reaction were Heraldo de Souza Gitahy and Murilo Dondici Ruiz. In 1963, through the Institute for Technological Studies in São Paulo (IPT), they reported on the AAR reaction, its behavior, the materials involved, as well as mitigating actions, aimed at the Urupungá Power Plants.

Despite all of the scientific discoveries and the firm intention to improve and consolidate studies on concrete, problems related to structural aging, linked to a lack of maintenance and the incipient knowledge regarding some pathologies, such as the alkali-aggregate reaction (AAR), responsible for high recovery costs, many uncertainties about the results and durability of these interventions remain.

The existence of the alkali-aggregate reaction in building projects was verified in the Recife Metropolitan Region (RMR) in Pernambuco for the first time, because of the interest generated in inspecting the foundations of several residential buildings, following the collapse of the Areia Branca building in 2004. It should be clarified that the causes of the collapse of the Areia Branca were properly investigated and nothing was found to indicate AAR as the cause of the incident. However, foundation inspections of several other buildings in that region made possible to verify the existence of many cases of cracked concrete in pile caps and footings. The accurate analysis of these occurrences by experts, based on concrete samples extracted from the foundation elements, showed that the cracking was indeed caused by the alkali-aggregate reaction, with laboratories of the Brazilian Portland Cement Association (ABCP) having studied more than 60 cases (Battagin, 2016).

According to Otoch (2016), the occurrence of expansion caused by AAR was, until recently, mainly an issue with large constructions, such as dams or parts of hydroelectric plants. More recently, at the end of 2014 and throughout 2015, several cases of AAR were found in the Recife/PE area, mainly in foundation blocks and footings of buildings constructed within the last 3 to 20 years. Shortly thereafter, the first cases of AAR in foundation blocks in Fortaleza/CE were also discovered, as previously mentioned. (Otoch, 2016).

According to Battagin (2016), through IBRACON's dissemination work and the standardization of the number of tests performed at the ABCP laboratories, in the absence of statistics from other laboratories, it was found that the number of tests sent to ABCP has increased considerably throughout the country, in many construction-related areas. Aggregate samples have been sent by a diverse group, including aggregate suppliers (quarries), concrete service companies, construction companies, designers, universities, and even other laboratories, showing that the entire construction supply chain has gradually become aware of the importance of preventing pathological manifestations related to AAR. The profile of clients requesting tests and their geographic origin was determined, based on 1621 fine and coarse aggregate samples received by the ABCP laboratories, which had sufficient information, as shown in Figure 1. Most requests come from São Paulo (532 samples) and Pernambuco (228 samples), with requests being recorded from all Brazilian states except for Acre. (Battagin, 2016).

Considering this scenario found in Recife and neighboring cities in Pernambuco, a region with a high rate of occurrence of AAR, verified by the large increase in tests seeking to elucidate the

conditions of the aggregate, this paper presents the result of a documentary investigation performed at the main structural recovery companies of the RMR. The objective of the study was to trace a historical profile of the buildings' constructive characteristics, how the diagnosis was made, the procedures used in the intervention, the materials applied during the recovery, the use of jacketing with reinforcement, and the costs, as well as how the foundations that would be monitored after the recovery through an inspection window were identified. The interview provided data on fifty foundations affected by AAR, but this number is likely higher, providing ample possibilities for larger future studies.
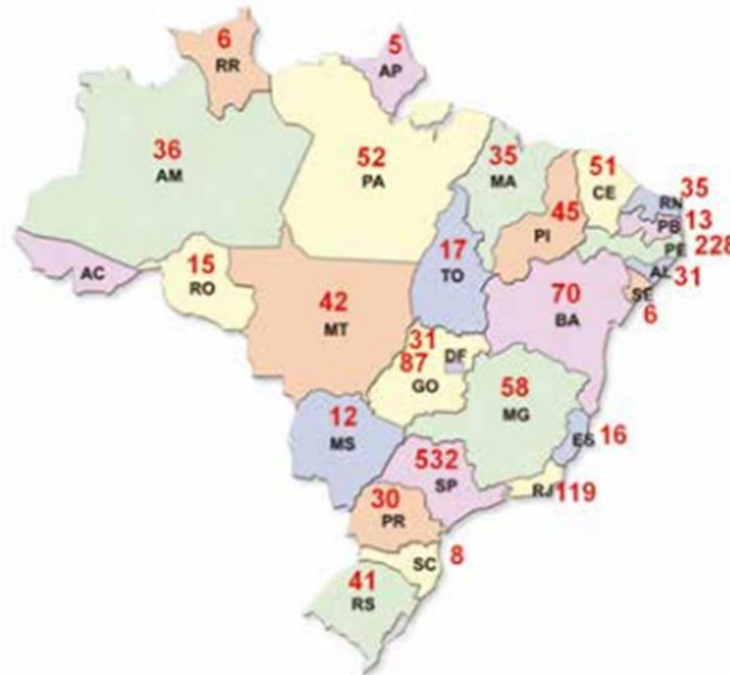

Figure 1. Distribution of samples by state (Battagin, 2016).

1.1 Description of the reaction and its types
The alkali-aggregate reaction is a chemical reaction that occurs in the internal structure of concrete and involves the alkaline hydroxides that appear because of cement hydration, and reactive minerals present in the aggregate. As a result of the reaction, products are generated that can expand in the presence of moisture, generating cracks, displacement, and the possible compromise of concrete structures. There are two types of alkali-aggregate reaction, classified according to the aggregate's reactive mineralogical composition, each with specific expansion mechanisms. The reactions are known as the alkali-silica reaction (ASR), the alkali-silicate reaction (ASSR), and the alkali-carbonate reaction (ACR).

1.1.1 Alkali-Silica Reaction (ASR)
According to Hasparyk (2005), the alkali-silica reaction is the most well-known type of AAR reported in the technical environment, as it is the one that usually occurs most rapidly, due to the reactive silica minerals involved. Among the most common minerals are opal or amorphous silica, chalcedony, cristobalite, tridymite, natural and artificial glass, microcrystalline/ cryptocrystalline quartz, and deformed quartz.

1.1.2 Alkali-Silicate Reaction (ASSR)

A specific type of alkali-silica reaction, called the alkali-silicate reaction, takes place between alkalis and reactive silicates present in sedimentary, metamorphic, and igneous rocks. It presents the same mechanism as the alkali-silica reaction but occurs more slowly. (Andrade, Silva, 2006).

1.1.3 Alkali Carbonate Reaction (ACR)

This reaction occurs more rarely and without gel formation. It is characterized by the expansion of carbonate rocks, because of the reaction with alkalis, mainly from the cement paste and dolomitic limestone, generating crystallized compounds such as brucite, alkaline carbonates, calcium carbonate, and magnesium silicate. This expansion, called dedolomitization, is the cause of cracks that appear in concrete because of the weakening of the paste-aggregate bond. In this reaction, alkalis are formed again, allowing the dedolomitization to continue until the dolomite has reacted completely or until the alkali concentration is sufficiently reduced. (Andrade, Silva, 2006).

1.2 Behavior of affected structures

The symptoms of a structure with AAR present themselves through the appearance of a gel exudation on the concrete surface, edges around aggregates, pores filled with white or glassy material, cracking, and discoloration of the concrete. Cracks having a map configuration occur more frequently in road pavements, airport runways, walls, and faces of structural elements, which have low restriction to expansion in the three directions. According to Hasparyk (2005), the main deleterious effects caused by AAR in a structure are the following: cracking on the concrete surface and between concrete layers; debonding of the concrete surface; loss of watertightness; displacement (loss of adhesion) of mortar near the surface of aggregates; movement (opening or relative displacement) of contraction joints; opening of construction joints, with horizontal cracks; movement/misalignment of free surfaces (such as raising of a dam's crest and spillway sills or deflections in dam structures) and locking or displacement of equipment and moving parts (gates, turbines, shafts, and pistons, among others).

2. METHODOLOGY

2.1 Initial considerations

The study designed for this paper was a documentary investigation, developed in the cities of Recife and Jaboatão dos Guararapes, cities where the largest number of foundations affected by the alkali-aggregate reaction were found. In Brazil all reported cases of the reaction to date are exclusively of the alkali-silica type (ASR), as will be shown below. This study compiles and analyzes the building characteristics, diagnoses, procedures, costs, results obtained from consulting company files, as well as interviews with engineers working in the field of rehabilitation, for fifty cases where foundations have been affected by this reaction.

It is worth pointing out that, while there were no problems or restrictions on the part of the companies involved in providing the information, only a small number of records regarding recovered foundations were found. This is likely because condominiums make their budgets with companies that have proven experience, and these, when issuing their reports with the materials necessary to remedy the damage caused by the deleterious reaction, are dismissed. As time goes by, it is verified that these recoveries were executed by those with "doubtful" skills, which may compromise the efficacy of the services rendered. When this occurs, these foundations are no longer properly analyzed, and consequently the results of these recoveries may end in failure, due to poorly executed processes.

Although the technical community has been aware of this reaction for more than 85 years, as well as its forms of prevention, the deterioration of concrete resulting from the reaction is still

considered relevant, especially because of its serious repercussions to foundations and the great inconvenience caused to infrastructure and building projects.

Based on this context and considering that Recife is among the cities having the highest number of AAR cases recorded in the Brazilian literature, an investigation was conducted to collect data on the topic, starting in December 2018 and concluding in July 2019. The methodology used was divided into four stages, as shown in Figure 2. This methodology was based on interviews at the largest possible number of companies that carried recoveries on foundations affected by the alkali-aggregate reaction, through the application of a 17-question survey, shown in Table 1.
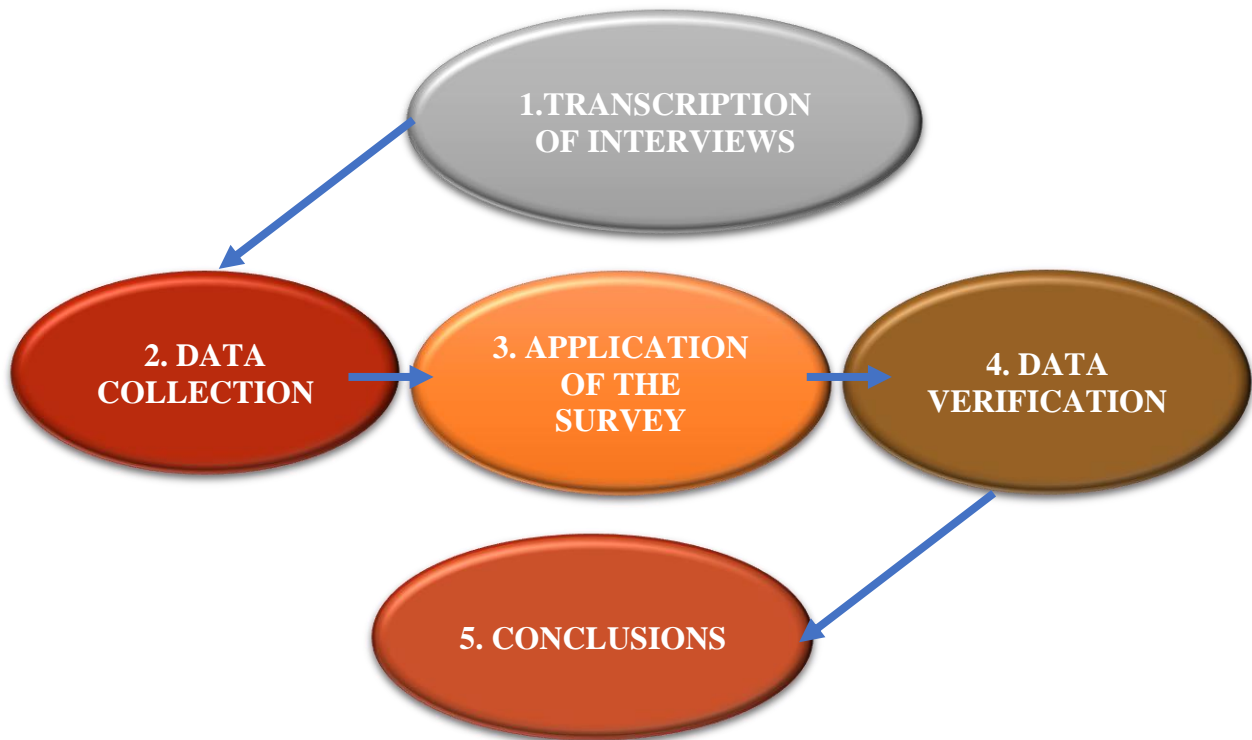
Figure 2. Methodology applied at the interviewed companies.

2.2 Transcription of Interviews

The first step was to conduct interviews at the companies in the construction chain, informing them about the purpose of the study and the need for updated data regarding any foundations that were recovered.

Table 1. Survey applied during the interviews.

	Building:		
1.0	**Building Characteristics:**		
1.1	What is the building function?		
	Residential		Commercial
1.2	How many floors?		
1.3	What is the height of the water table?		
1.4	What is the building age?		
1.5	How was the problem discovered?. What were the symptoms?		
1.6	How far from the sea is the building?		
1.7	What is the type of the foundation?		
2.0	**How was the diagnosis made?**		
2.1	Location of cracks' incidence in the building:		
2.2	How was the pathology diagnosed?		
2.3	What test were performed to determine the pathology?		
3.0	**How were the recovery procedures made?**		
3.1	What steps have been taken?		
3.2	How was the filling of the cracks done?. What equipment was used in the recovery?		
3.3	Was the reinforcement project prepared by the structural engineer?		
3.4	Was it done any encapsulation?		
	Yes		No
3.5	Was waterproofing done?		
4.0	**Who was responsible for the costs of recovery?**		
4.1	Who was responsible for the payment?		
4.2	Was an inspection window left after recovery?		
5.0	**Comments:**		

2.3 Data Collection

For this study, information was gathered on fifty buildings, both commercial and residential, for which their foundations had undergone a recovery procedure.

In the city of Recife, the recoveries had been performed on buildings located in the districts of Graças, Casa Forte, Espinheiro, Derby, Boa Vista, Madalena, Boa Viagem, and Setúbal, with an emphasis on the district of Boa Viagem.

In the city of Jaboatão dos Guararapes, the recoveries were performed in a building located in Piedade.

The companies that participated in this universe of information were very receptive and provided all the necessary elements, with the understanding that the identities of the buildings listed and of the companies themselves would remain confidential. Thus, each company was referred to by a random letter, not associated with its name. Table 2 provides a general survey of the companies consulted, showing their activities and the total number of foundations detected.

The first company interviewed was A Engineering.

Founded in 1995, Company A operates in the field of civil construction, specializing in recovery and strengthening structures made of reinforced and prestressed concrete. With a collection of more than 600 concluded projects during 24 years in the market, its portfolio includes excellence in building structures in marine environments, treating apparent concrete, recovering and reinforcing water mains, and structural reinforcement, among others.

In this company, thirty buildings were cataloged in the period from December 2018 to May 2019 in which AAR was identified.

The second company was X Engineering.

Founded in 1981, its construction portfolio contains a wide range of modern buildings, including port structures, real estate developments, special works of art, recovery and structural reinforcement in buildings and works of art, and conservation and restoration of buildings of historical heritage.

Three buildings from this company were catalogued with identified AAR, including a restoration project on a commercial building. However, the other recoveries executed by the company in question are outside the scope of this work, which, despite dealing with the recovery of foundations with ASR, are neither residential nor commercial buildings.

The third company was Y Engineering.

It was founded in April 2000, with the objective of providing specialized technical services to the civil construction sector, including restoration and reinforcement of reinforced concrete structural elements, which is its principal activity. The specialized services of restoration and structural reinforcement make delicate to disclose by name the projects that make up its technical portfolio, which consists of approximately 350 executed projects. In this company, seven buildings that went through the restoration process were catalogued.

The fourth company was Z Engineering.

With more than 12 years of experience, this company provides technical civil engineering services in the areas of building restoration and maintenance. Three buildings where AAR was identified were catalogued from this company.

The fifth company was T Engineering.

Founded in January 2003 in the city of Recife, it is now active nationally with a portfolio that includes more than 500 customers. It offers services in the areas of expert technical assistance, consultancy, project management and inspection, expert reports, monitoring, and technical follow-up, among others. Seven buildings from this company with AAR were catalogued.

Table 2. Companies participating in the interviews.

Company	Operation	Experience	Time Experience	Number of cases
A	Structural reinforcement	Marine structures, concrete treatments, recovery, and reinforcement	24 years	30
X	Structural reinforcement	Port structures, special works of art, recovery, and reinforcement and restorations	38 years	03
Y	Structural reinforcement	Recovery and reinforcement of foundations	19 years	07
Z	Structural reinforcement	Recovery and reinforcement of foundations and maintenance of buildings	12 years	03
T	Monitoring of reinforcement	Expert technical assistance, consultancies, report, and technical monitoring	16 years	07
TOTAL				50

2.4 Application of the questionnaire

The third step was the application of a questionnaire containing fifteen questions about commercial and residential buildings where the ASR pathology was proven and recovered. During application of the questionnaire, shown in Table 2, information was sought about the pathological manifestation, a history of the project's characteristics, how the diagnosis was determined, the recovery process, and its costs.

2.5 Data verification

After collecting the data, the fourth step began, that of analyzing all the material acquired during the study, searching for photos, reports, and test results to add to the researched material.

A spreadsheet was created based on the answers supplied to the questionnaires, with data on each construction project, including characteristics such as age, recovery type, materials used, test type, year of recovery, etc. This can be seen in Table 3. These data were added up and the percentages for each item analyzed were obtained. The graphs (Figures) were created from these results with their respective identifications.

Table 3. Spreadsheet with compositions.

SPREADSHEET WITH COMPOSITIONS																
COMPANY X	REFERENCES	CHARACTERISTICS					DIAGNOSIS			REINFORCEMENT			COSTS		PECT	
		USE	NO. FLOORS	WATER TABLE	AGE	SYMPTOMS	FOUNDATION	LOCATION	PATHOLOGY	TESTS	PHASES	STRUCT. ENG.	AP. SULAT	CONDOMNIUM	CONST. COMPANY	Y N

2.6 Discussion

Finally, all the collected materials were verified to analyze the characteristics of each project, the procedure applied in determining its pathological manifestation, the diagnosis, the recovery process, and the cost.

It was found that interventions in the foundations occurred because of the need to investigate and verify their condition. It is believed that these investigations occurred due to two main factors. The

first was the collapse of the Areia Branca building, which put many condominium owners in a state of alert to check their structures, and the second was the obligation imposed by Law Nº 13341. This law made periodic inspections mandatory, making it possible to identify a greater number of foundation recoveries and other pathologies previously neglected due to poor or infrequent maintenance habits.

3. RESULTS AND DISCUSSION

3.1 Data analysis
For the data analysis, the questionnaire was divided into four parts. The first part dealt with characteristics of the building, the second part with the diagnosis, the third part described how the restoration was performed, and the final part was on the restoration costs.

3.2 Building Characteristics
The first data collected were the building characteristics, consisting of seven questions, from which it was possible to get a relevant idea of any preponderant factors for the appearance of AAR. The questions followed this order: building use, number of floors, height of the water table, age of the building, how the problem was discovered and what symptoms were found, the distance from the sea to the building, and the foundation type.

3.2.1 Building Use
Of the 50 buildings verified, only 4% were commercial buildings, with the remaining 96% being residential buildings. Most of the buildings currently verified and recorded in this study are effectively residential buildings, as shown in Figure 3.

3.2.2 Number of Floors
The study analyzed buildings that varied in their number of floors. The floor count included common floors such as basements, the ground floor, open floors, typical floors, and any penthouse floor.
Figure 4 shows the percentage of buildings based on their floor count, divided into categories having 15 floors or fewer, 16 to 25 floors, and more than 25 floors (with the tallest building having 41 floors) for a total of 50 catalogued buildings.
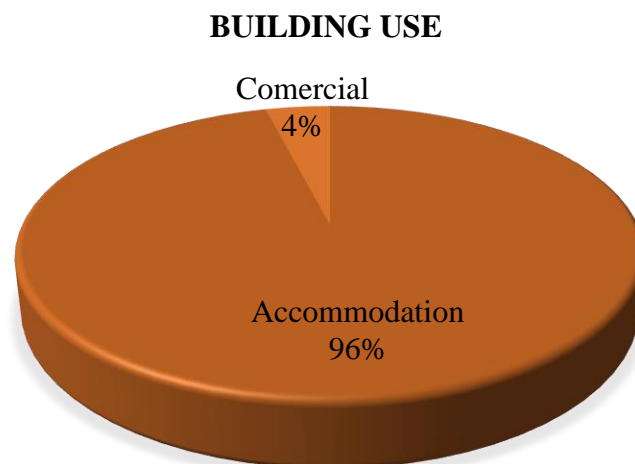
BUILDING USE

Figure 3. Building Function
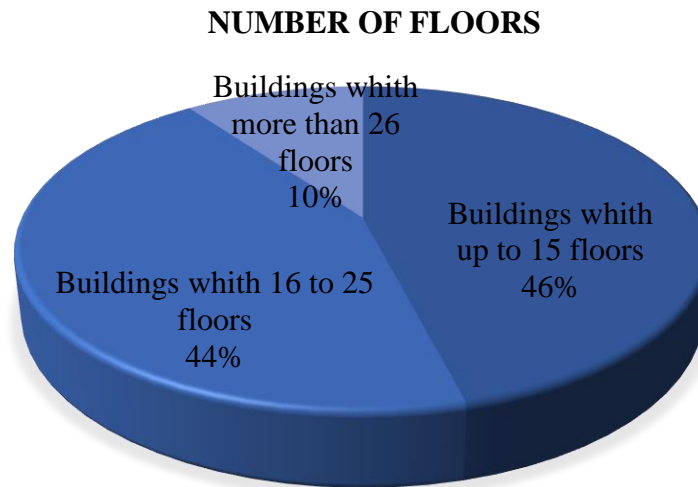
NUMBER OF FLOORS

Figure 4. Number of Floors

3.2.3 Height of the Water Table

The occurrence of ASR is directly linked to three factors: alkali materials normally found in the cement, reactive aggregate, and the presence of water. In this study, attempts were made to determine whether any water was found during the recovery process that would favor the occurrence of the reaction.

When the foundation was excavated, any occurrence of water was identified, either from the water table or from any other source. In foundations where the water table could be identified, the elements were either partially below it or with water just reaching their lowest point. The AAR phenomenon develops not only in concrete elements that are below the water level, but also those where only the lowest part of the block was in contact with water.

At some companies, this information was made available during the interviews, while in other cases it was possible to identify from the collection of photos. In still other situations, the itemization of the budget showed costs for lowering the water table, i.e., the recovery work could only be performed after lowering the water table. In these cases, the original water level was unknown, and was therefore considered to be at the bottom of the block. In a few cases, there was no information at all regarding the presence of water, so the water table was not found.

Based on these assumptions, the level of the water table was grouped into four categories, defined by its level in relation to the elevation of the foundation element: Level 1, Level 2, Level 3, and NE, described below:

      Level 1: water table at the bottom level of the block.
      Level 2: water table in the middle of the block.
      Level 3: water table at the top of the block.
      NF: water table not found.

After all the analyses at the company level, Table 4 was created to summarize the water table results and address their relationship with the 50 foundations in a general way. Forty percent of the foundations had water at the bottom level of the block (level 1); 18% had water in the middle of the block (level 2); while no foundations were identified with water at the top of the block (level 3). Water table information was not found for 42% of the foundations surveyed.

Table 4. Water table levels found.

Summary of water table levels				
Companies	LEVEL 1 – Water at the bottom level of the clock	LEVEL 2 – Water in the middle of the block	LEVEL 1 – Water at the top of the block	NF – Level not found
Z Engineering	50%	25%	0	25%
X Engineering	67%	33%	0	0
A Engineering	17%	20%	0	63%
Y Engineering	100%	0	0	0
T Engineering	61%	17%	0	17%
Total	40%	18%	0	42%

3.2.4 Building Age

The study also attempted to identify the ages of each building, starting from year 1, when construction was finished, until the time it was catalogued by the company responsible for its recovery. However, this information was not made available for all the cases studied. The buildings were of different ages at the time of their recovery from ASR.

The youngest buildings found were thirteen years old at the time of recovery, with footing foundations. Other buildings had pile and footing foundations with ages of 16, 19, 20, 30, and up to 45 years. In Figure 5, the information was categorized into ranges of up to 20 years, from 21 to 30 years, from 31 to 40 years, and finally 41 years and up.
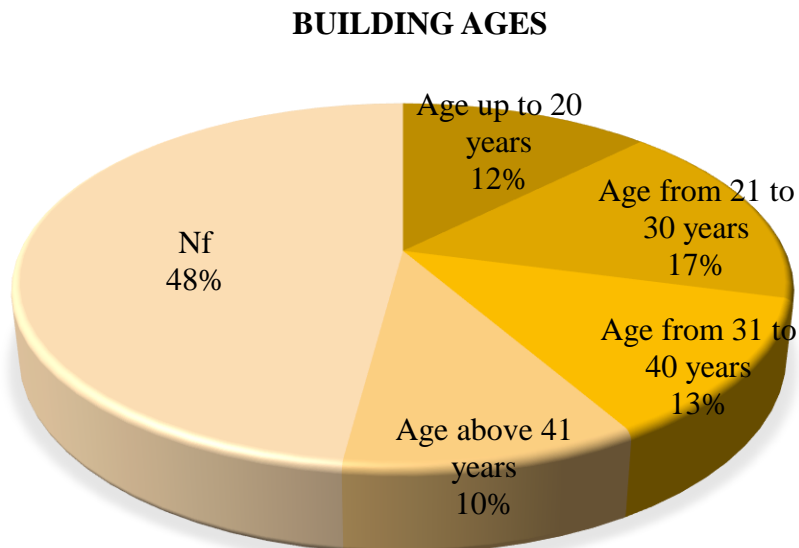
BUILDING AGES

Figure 5. Building age ranges.

These AAR-affected foundations were discovered because of the situations previously mentioned, the collapse of the Areia Branca building and, consequently, Law 13.032, which required condominiums to perform inspections. From then on, the discoveries were determinant, with

verification of the reaction through tests, such as the Petrographic test, to identify the degree of aggressiveness of the reaction in the foundation elements, a parameter that would indicate the necessity of any urgent intervention.

The years in which the recoveries took place also varied, but the occurred mainly in 2005, 2008, 2009, 2011, 2012, and extend until today.

3.2.5 Discovery of the pathology and the symptoms found.

There are usually difficulties associated with interpreting the occurrence of cracks or structural damage, has been recurrent lately. These problems may be caused by various factors such as failures during the design phase of the project, use of incorrect materials, poor construction procedures, or lack of proper maintenance.

Symptoms are the characteristic external manifestations of pathological problems, from which the nature, origin, and mechanisms of the phenomena involved can be deduced, as well as their probable consequences. These symptoms, also called lesions, damage, defects, or pathological manifestations, can be described and classified from detailed and experienced visual observations, guiding an initial diagnosis of the problem (Helene, 1992).

In this study, the symptoms found are easily confused with the discovery of the pathology, because in 80% of the cases identified, the causes cited were cracks. These usually propagate across the floor, and in some cases were found on the pillars of the basement, ground floor, or open floor, and are identified by their effect on the floor immediately above the blocks or footings.

3.2.6 Distance of the building from the sea

The proximity to marine areas was analyzed because, according to NBR 6118: (2014), these areas are considered to have a degree of aggressiveness of III, considered strong.

It was found that most of the recovered foundations, 54%, are in the southern zone, in the Boa Viagem neighborhood near the sea. The remaining foundations are in the northern zone, in more distant areas. Normally, in the south zone, the water table is high, which could have provided a favorable environment for the reaction to begin in the foundations.

3.2.7 Foundation Type

Cracks were one of the most common symptoms found in foundations. There are numerous difficulties in interpreting the pathologies caused by the alkali-silica reaction (ASR), however it is correct to state that a structure affected by this reaction will show the presence of the exuded gel that results from the reaction. In the early stages, or under conditions where only small amounts were formed, ASR cannot be visualized with the naked eye, requiring specialists and tests performed on samples taken from the affected material, to detect it.

According to Silva (2013), renowned engineers active in the construction market indicated that some changes have been done to foundation designs to mitigate the deleterious effects of the reaction. There was a change in the reinforcement detailing of the foundation elements, especially in the pile caps, which, because of their high concrete volumes, have thicker reinforcement on the sides and top (through meshes forming a cage), to avoid or minimize possible cracking due to concrete expansion.

In the case of this study, where the buildings in question were older than 15 years, the projects had not undergone any changes as a response to the reaction. Figure 6 shows that, of the fifty buildings mentioned, only two had footings as a foundation element (4%), while the other 96% had block foundations.

TYPES OF FOUNDATIONS
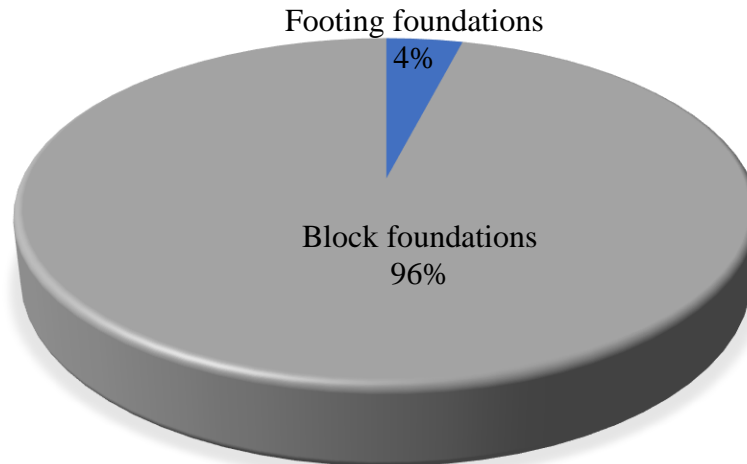
Figure 6. Foundation Types.

3.3 Diagnosis

The diagnosis of concrete structures affected by the alkali-aggregate reaction is carried out in steps: information collection, visual inspection, concrete component material sample and extracted core tests, sonic auscultation, and follow-up of its evolution through mathematical modeling (Priszkulnik, 2005).

The diagnosis of the affected foundations was performed using visual information and the results of the tests performed on the concrete cores, concluding the existence of the alkali-silica reaction. Detailed situations were reported about the state of the foundations affected by the reaction, such as the formation of cracks. The core extraction was an important tool that allowed for the identification of internal cracks, loss of mortar adherence at the interface with the aggregates, reaction edges around the aggregates that have reacted with alkali, gel within the voids, and the carbonation depth.

3.3.1 Location of cracks in the building

The locations where cracks were found were very similar among the buildings. The cracks were found mostly through routine inspections or because of their effects on the floors. The foundation elements were cracked on the top and on the sides. A preliminary mapping of the structural elements was carried out, where the positioning of the cracks, their direction, their thickness, and where they were most concentrated was verified.

Only after joining all the information from the visual inspections, the tests, and the building's design and construction documentation, was it possible to analyze and diagnose the problem. It is important to emphasize the need for laboratory tests to confirm the presence of the alkali-silica reaction.

The companies involved the recovery work also reported that visual inspections, as well as project verifications, are done, but only 48% of the companies used laboratory tests. The other 52% only took into consideration visual information, as shown in Figure 7. In some circumstances, due to financial issues, the tests are dispensed with. In other cases, after checking *in loco* the state of the foundation, the deleterious reaction was so advanced, as shown in Figure 8, that recovery became critical, causing condominium owners to accept the diagnosis solely based on the companies' experience.

DIAGNOSIS OF PATOLOGY
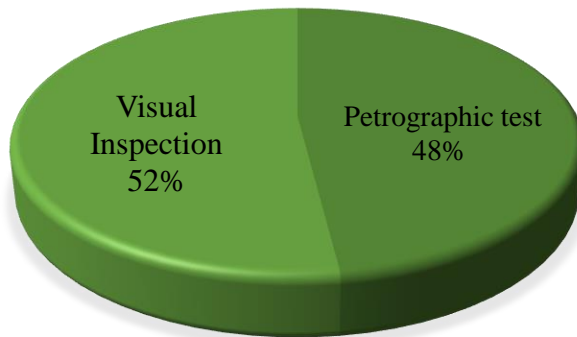
Figure 7. Diagnosis of the pathology.

Figure 8. Cracks on a block with AAR.

There are currently several standardized methods on the market to characterize the potential expansive reactivity of mineral aggregates in Portland cement concrete. Petrographic analysis is used to diagnosis the presence of reactive material and also to find any occurrences of manifestations associated with the reaction, such as a reaction edge around the aggregate, microcracks caused by expansion, or presence of gel within the pores, among others.

The test used to determine the pathologies in this research was the NBR 15577-3: (2013) Petrographic test. Unfortunately, as presented above, due to costs, the tests were not performed. In the cases investigated, the cores extracted from the foundation elements were sent to the Brazilian Association of Technical Standards (ABCP) or to the Institute for Technological Research (IPT), both in São Paulo. Most of the petrographic tests (80%) were performed by ABCP and the rest by IPT.

3.4 Recovery Procedures

With recovery processes for concrete structures, the quality of the result depends primarily on an accurate diagnosis and an appropriate choice of recovery method, which includes the selection of materials and equipment necessary to carry out the service.

This was evidenced when examining the requests for foundation recovery projects where the expansive reaction had reached a high level of deterioration. In addition to these issues, information on the properties of the concrete exposed to the reaction was sought, a condition imposed by the companies to verify the condition of the previous concretes to be able to guarantee good results from the intervention and recovery services.

With this data available, the recovery process and the steps to be followed can be determined, , the safety procedures applied, and the materials chosen that be used in the fight against ASR.

3.4.1 Steps followed in the recovery process.

The steps followed in the foundation recovery intervention process resemble a prescription for treating a disease. This process was followed and carried out by all five companies interviewed in this study for most of the recoveries, with only the materials used being changed for monolithization.

The formulation of these recovery treatments was adjusted regarding size, direction, and depth of the cracks. When it comes to the ASR recovery process, the aim is to guarantee that the structural pieces can return to working, monolithically, by closing of cracks through the injection of an adherent and resistant material. The steps that make up the recovery and their order of execution are described below:

Demolition and excavation of the materials; washing of the concrete surfaces; chipping of the surfaces; drilling of the concrete; filling and placement of the ports; injection into the cracks; and mounting of the reinforcement and structural concrete.

3.4.2 Crack filling and materials used.
Injection is the last step in the recovery process and its purpose is to perfectly fill the space formed between the edges of a crack, recomposing the foundation, and promoting its monolithism. The procedures executed during crack filling had some slight variations from one company to another, depending on the state in which the structural element was found, and the criteria developed for the injection.

In the various treatments studied it was necessary to use materials that had a high mechanical resistance to compression, traction, and shear, and epoxy resin was one of the materials recommended for the treatment of cracks and fissures affected by ASR. Because it is a rigid material after curing, it is important to restrict its use to passive fissures and cracks, i.e., those that present no movement, as was the case with the foundations cited in this study.

The second material used for the injections was microcement. Relatively new for this procedure, it is a material created from cement itself having a grain fineness of less than 8 micrometers, or 8 thousandths of a millimeter, with 95% of the particles having the same size. It is a rigid material after curing and can be used for passive crack filling in wet or dry areas. Some companies have opted for this material because it provides structure along with alkaline protection for the reinforcement, resistance to compression, traction, and shear, and fills voids, bringing back the structure's monolithism and resistance.

In the research it was found a greater use of epoxy resins in 82% of the foundations, followed by microcement in 6% of the foundations, and in 10% the material used was not identified, as shown in figure 9.

This study found that epoxy resins were used in 82% of the foundations, with microcement used in only 6% of the foundations. For the remaining 10%, the material used was not identified, as shown in figure 9.

In the injection process, plastic and metallic ports were used, as shown in Figures 10 and 11. The metallic ports are part of the new advances in the injection process, to which an injection can be applied under higher pressure, and consequently the penetration of the material to areas of greater depths can occur in a shorter span of time. However, from the data collected in this study, filling was done to close external cracks and ensure the injection, and the most used materials were plastic ports, which are simpler and easier to find on the market.

MATERIALS USED IN THE INJETION
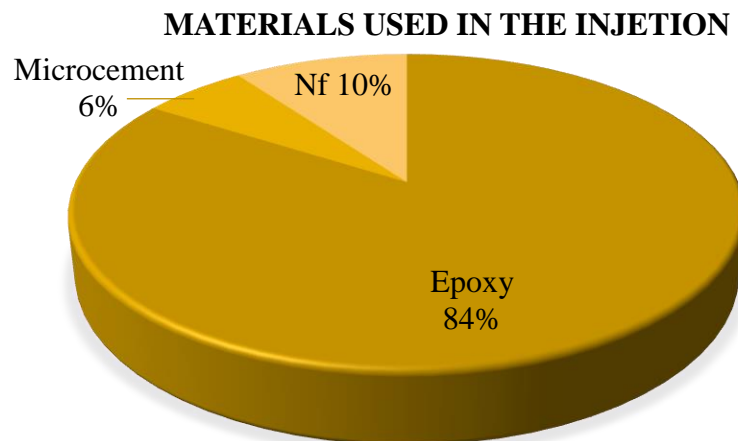
Figure 9. Materials used for injection.
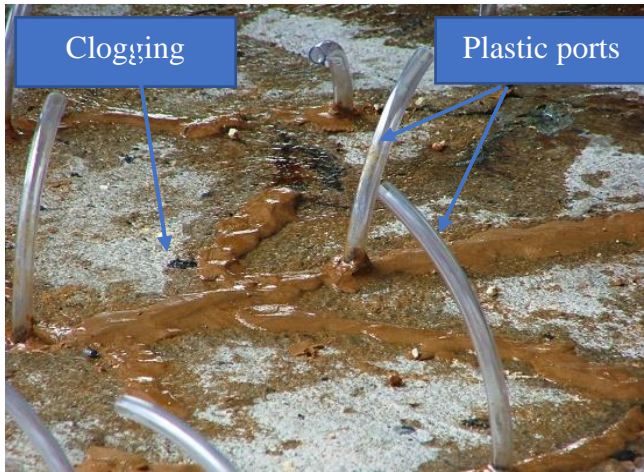
Figure 10. Plastic ports.

Figure 11. Metallic ports.

3.4.3 Jacketing and calculation of reinforcement

According to Silva (2007), to encapsulate the blocks affected by the expansive phenomenon of ASR, it is important to first have an understanding about the behavior of the structure to be recovered. With the appearance of the alkali-silica reaction in the foundation blocks of buildings in the Recife Metropolitan Region, understanding the behavior of these structures has become a challenge for technicians and structural engineers. It is important to establish an accurate diagnosis and adopt techniques that effectively resolve the problem, that is, those that give the building back its stability and reliability.

Regarding the affected foundations, areas with little reinforcement were susceptible to expansion caused by the reaction. Laboratory tests have shown that, in concrete, the expansion is restricted to areas where no strong compressions occur. In other words, foundations such as footings, which at the time had little or reinforcement, and that only on the lower and upper areas, were susceptible to expansion. Calculation of the reinforcement was determined in some cases through the intervention of engineers. The evaluation for use in the recovery project was determined as a function of the expansion found. In foundations with advanced deleterious reaction, verification by an engineer was requested. Reinforcement jacketing was used in 81% of the foundation elements with 19% not being identified, as shown in Figure 12.

ENCAPSULATION
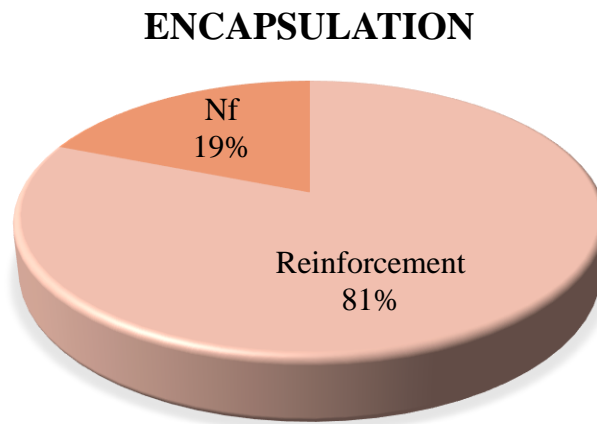
Figura 12. Use of reinforcement.

3.4.4 Waterproofing

During construction of the foundations, either footings or blocks, the health and durability of the foundation was ensured through waterproofing. This is an important step due to these elements being in permanent contact with soil moisture, which, when not treated, will conduct water into the block through capillarity.

To avoid possible pathological problems caused by moisture, it is imperative to use a waterproofing system that is compatible with the geometry of the pieces and the characteristics of the structure, such as the level of the water table. It was verified in this study that all the recovered foundations used waterproofing on the tops and sides of the elements, as shown in Figure 13.

Figure 13. Waterproofed block.

3.5 Recovery costs

The resources spent on the recovery depended on the type of intervention requested and the values presented. The cost of the recovery was directly proportional to the solution adopted for execution, considering methodology, material specifications, labor used, as well as complementary work, such as shoring and scaffolding, sump pumps, and others.

The study verified that the costs, which are quite onerous, are the condominium's responsibility and were varied and divided into two groups, according to the ability of each condominium to pay. The first group performed a complete recovery in 100% of the foundations, while the second group performed recovery in parts and over long periods.

3.6 Inspection window

As a result, it was found that, of the 50 foundations surveyed, only two left the inspection windows. The windows are small openings left in the foundation elements that make it possible to monitor the recoveries from the floors above, as shown in Figure 14. Internally, small pieces of glass are placed, shown in Figure 15, where cracks had previously been identified, so that they can be periodically monitored after their recovery. If any new movement of the foundation block occurs, the tendency will be for this glass to break, indicating a possible continuing of the ASR, or of some other pathological manifestation.

Figure 14. Inspection window.

Figure 15. Interior of inspection window.

4. FINAL CONSIDERATIONS

This study aimed to create a profile of the processes used in the recovery of foundations affected by the alkali-silica reaction, by analyzing case studies of 50 recovered foundations. The results are presented in four parts: characteristics, diagnosis, recovery, and costs. The analyses of the initial results provided the following statements about the construction characteristics:

- With regard to building use, 96% are residential and 4% are commercial.
- Structures with 15, 25, 30, and up to 41 floors were found.
- Regarding conditioning factors that influence the reaction, it was established that several foundations had their elements partially submerged below the water table. It was found that 40% of the foundations were at level 1, i.e., the water table was in permanent contact with the lower part of the block; for 18% of the foundations, water reached the middle of the block, level 2; while no blocks were found at level 3. In 42% of the foundations the water table was not identified.
- The ages of the buildings ranged from 10, 15, 16, 20, 22, 25, 30, 40, 41, up to 45 years old.
- Discovery of the pathologies occurred through routine checks that found the appearance of cracks on the parking lot floors in 80% of the cases studied.
- Regarding distance from the sea, 54% of the buildings were located in the south zone of the city (near the sea), while 46% were in the north zone.
- Only 4% of the foundations were of the footing type, with the other 96% made of blocks.

Regarding diagnosis, the following information was found:
- The location of the cracks was identified as being on the sides and tops of the blocks and footings.
- Only 42% of diagnoses made use of laboratory tests. Through studies that included the participation of engineers and concrete specialists, and considering the evident cracks, the age of the building, and the environment where the foundation was located, an ASR recovery ASR methodology was developed based on test results from core extractions that supported a procedure to combat expansion. However, in 58% of the cases, the opinions of business owners were sought, some of whom had considerable experience working with recovery processes and others who had experience with other aspects of construction, who, without the presence of engineers nor laboratory test results, determined that the intervention should be treated as alkali-silica reaction, and followed a recovery procedure used in other cases.

🔸 The Petrographic test was used to diagnose the reaction in 42% of the foundations, while the remaining 58% were diagnosed through visual tests only.

The following information was observed about the recoveries:
🔸 The recoveries were similar in most of the fifty verified foundations and followed this procedure: demolition and excavation of the structural elements, washing of the surface of the elements, chipping and drilling of the concrete, filling of holes, injection, assembly of the reinforcement, concreting, and waterproofing.
🔸 The materials used to fill the cracks were epoxy in 84% of the foundations, microcement in 6% of the foundation, and were not identified for 10% of the foundations. Filling was done with the aid of a pneumatic injection pump.
🔸 Jacketing was used in 81% of the foundations and was not identified for the other 19%. The choice of this process was based on the degree of deterioration of the foundation. In most degraded foundations, recoveries were performed through the intervention of an engineer's design.

The following information was compiled regarding costs and the use of a recovery window:
🔸 The costs were paid in full by the condominiums, except for two recoveries. One split the costs fifty-fifty between the condominium and the construction company, while the other was the recovery of only four footings and was paid for by the builder. The cost of the recovery varied according to the dimensions of the elements, the degree of degradation of the foundation, and also the procedure chosen for restoration.
🔸 The final objective was to verify whether an inspection window was left to facilitate future maintenance. In only 4% of the foundations was an inspection window placed.

5. CONCLUSIONS

The results of this study help to form a true panorama of the procedures used in recoveries from 2004 to the present day. The treatments applied had great similarities with only a few minor changes. In an interview with some of those responsible at the companies, it was found that, since the recovery carried out on the Paulo Guerra bridge in 2000, the materials and recovery procedures used have had few advances. For example, injection using plastic and metal ports, even although the system using plastic ports is still the most requested. Another verified change occurred in the materials used for injection, with the use of microcement. Epoxy remains, however, the most used material.

After the recovery of the foundations, an effective and systematic follow-up is necessary, because the alkali-silica reaction can reappear due to potential faults in the results of the interventions. This highlights the importance of installing inspection window that helps enable the follow-up checks, especially regarding the recovered foundations that were not monitored by qualified personnel nor used laboratory tests, important items for a coherent and proper determination of the procedures to follow. As a result, a complete diagnosis is lacking, which could lead to the use of improper recovery procedures that fail to correct the pathology. The attempts to keep costs as low as possible is often detrimental to best practices and the guarantee of good results. Of the fifty foundations surveyed, only two left inspection windows, meaning that a mere 4% of the surveyed projects made it possible to conduct a proper follow-up.

Information regarding the reaction chemistry, the aggregate microstructure, mitigating measures, and preventions, were verified in the researched materials, however it is necessary to look more closely at recovered foundations that did not respond efficiently to these procedures, nor retained their durability. The effectiveness of future results in combating AAR in older foundations should

also be a reason for systematic follow-ups to guarantee their structural health.

5. ACKNOWLEDGMENTS

6. REFERENCES

Andrade, T., Silva, J. J. R., Almeida R., Figueirôa, J. P., Kihara, Y., Pecchio, M. (2006), "*Diagnóstico de Reação Álcali-Agregado em Blocos de Fundação de um Edifício Público situado na Cidade do Recife/PE.*" In: II Simpósio Sobre Raa em Estruturas de Concreto. IBRACON.

Andrade, T. (2006) "*Histórico de Casos de RAA Ocorridos Recentemente em Fundações de Edifícios na Região Metropolitana do Recife.*", In: II Simpósio Sobre Raa em Estruturas de Concreto. IBRACON.

Associação de Normas Técnicas (2013). *NBR 15577: Guia para avaliação da reatividade potencial e medidas preventivas para uso de agregados em concreto*. Rio de Janeiro.

Associação de Normas Técnicas (2013*). NBR 15577-1: Guia para Avaliação da Reatividade Potencial e Medidas Preventivas para Uso de Agregado em Concreto.* Rio de Janeiro, 2008. 11p.

Associação de Normas Técnicas (2013*). NBR 15577-2: Coleta, Preparação e Periodicidade de Ensaios de Amostras de Agregados para Concreto.* Rio de Janeiro, 2008. 2p.

Associação de Normas Técnicas (2013) *NBR 15577-3: Análise Petrográfica para Verificação de Potencialidade Reativa de Agregados em Presença de Álcalis do Concreto*. Rio de Janeiro, 2008. 8p.

Associação de Normas Técnicas (2013). *NBR 15577-4: Determinação da Expansão em Barras de Argamassa pelo Método Acelerado.* Rio de Janeiro, 2008. 12p.

Associação de Normas Técnicas (2013). *NBR 15577-5: Determinação da Mitigação da Expansão em Barras de Argamassa pelo Método Acelerado.* Rio de Janeiro, 2008. 5p.

Associação de Normas Técnicas (2013). *NBR 15577-6: Determinação da Expansão em Prismas de Concreto.* Rio de Janeiro, 2008. 16p.

Associação de Normas Técnicas (2014). *NBR 6118: Estruturas de concreto armado – Procedimento.* Rio de Janeiro, 2014. 238 p.

Battagin, A., Silveira, A.L., Munhoz, F., Battagin, I. (2016), "*A Evolução da Cultura da Prevenção da Reação Álcali-Agregado no Mercado Nacional.*" Associação Brasileira de Cimento Portland. In: Concreto e construções. Ano 44. Ed. IBRACON.

Hasparyk, N. P. (1999), "*Investigação dos Mecanismos da reação Álcali-Agregado – Efeito da Cinza de Casca de Arroz e da Sílica Ativa*." Dissertação de Mestrado em Engenharia, Universidade Federal de Goiás, Goiânia.

Hasparyk, N. (2005), "*Investigação do Concreto Afetados pela Reação Álcali Agregado e Caracterização Avançada do Gel Exsudado.*" Tese de Doutorado em Engenharia, Universidade Federal do Rio Grande do Sul, Porto Alegre.

Helene, P. (1992), *Manual para Reparo, Reforço e Proteção de Estruturas de Concreto.* 2ª Ed. São Paulo, PINI.

Priszkulnik, S. (2005), *Inspeção e Diagnóstico de Estruturas de Concreto Afetadas pelas reações Cimento-Agregado.* In: ISAIA, G.C. Concreto: Ensino, pesquisa e realizações. São Paulo: Ed.

Ibracon. Vol 2.

Silva, C. S. (2013), "*Reação Álcali-Agregado: Diagnóstico, Tratamento e Cuidados na Execução de Elementos em Concreto Armado nas Fundações da RMR.*" Monografia em Engenharia, Universidade de Pernambuco, Recife.

Silva, G. A. (2007), "*Recuperação de Blocos de Coroamento afetados pela reação Álcali-Agregado.*" Dissertação de Mestrado em Engenharia, Universidade Católica de Pernambuco, Recife, 2007.

Munhoz, F. A. C. (2007), "*Efeito de Adições Ativas na Mitigação das reações Álcali-Sílica e Álcali-Silicato.*" Dissertação de Mestrado em Engenharia, Universidade de São Paulo, São Paulo.

Otoch, S. (2016), Reação álcali-agregado: o que é e como evitar?. "*A Evolução da Cultura da Prevenção da Reação Álcali-Agregado no Mercado Nacional.*" Associação Brasileira de Cimento Portland. In: Concreto e construções. Ano 44. Ed. IBRACON.

Revista Alconpat: 10 years of history (2011 - 2021)

P. Castro-Borges[1]* , E. Sabido-Maldonado[2], J. M. Mendoza-Rangel[3] , P. Helene[4] ,
P. Garcés-Terradillos[5] , A. A. Torres-Acosta[6] , M. Fernández-Cánovas[7] , R. Husni[8],
O. Troconis-Rincón[9] , F. Branco[10] , J. I. Escalante-García[11] , F. Alonso-Farrera[12] ,
M. A. Olavarrieta-Parisot[13]

*Contact author: pcastro@cinvestav.mx

DOI: https://doi.org/10.21041/ra.v11i2.534

ABSTRACT

The objective of this paper is to present to the community the achievements attained and the challenges, met, current and coming, during the first ten years of existence of the Alconpat Journal. A narration is made of: how the idea of having a scientific/technical journal in Alconpat International arose; when, how and where the discussions and the project took place; the implementation, the first issue, the punctuality; the requirements and challenges to meet for the first indexations (Scielo México, Scielo WoS, Redalyc, Latindex, Google); the Conacyt projects that made it possible to gradually meet the requirements for eventual applications at higher indexes (Scopus and WoS), repositories, directories (DOAJ) and super servers; electronic markings, publication in three languages (Spanish, Portuguese and English), administrative times for timely publication, etc. The efforts of all those who have collaborated in these initial 10 years are also acknowledged.

Keywords: Alconpat Journal; Scielo; WoS; Redalyc, Latindex, Google Scholar.

[1] Cinvestav del IPN, Unidad Mérida, Yucatán, México; **Founding Editor in Chief,** Alconpat Journal, **México**.

[2] Alconpat-Internacional, **Assistant Editor,** Alconpat Journal, **México**.

[3] Facultad de Ingeniería Civil, UANL; **Founding Managing Editor,** Alconpat Journal, **México.**

[4] Universidad de Sao Paulo; **Founding Associate Editor and Language Editor**, Alconpat Journal, **Brasil.**

[5] Universidad de Alicante; **Associate Editor,** Alconpat Journal, **España**.

[6] Tecnológico de Monterrey, Campus Querétaro; **Associate Editor,** Alconpat Journal, **México**.

[7] Universidad Politécnica de Madrid; **Founding Associate Editor,** Alconpat Journal, **España**.

[8] Universidad de Buenos Aires; **Founding Associate Editor,** Alconpat Journal, **Argentina**.

[9] Universidad de Zulia; **Founding Associate Editor,** Alconpat Journal, **Venezuela.**

[10] Instituto Superior Técnico; **Founding Associate Editor,** Alconpat Journal, **Portugal.**

[11] Cinvestav del IPN, Unidad Saltillo, Coahuila, México; **Founding Associate Editor,** Alconpat Journal, **México.**

[12] Universidad Autónoma de Chiapas, México; **Co-Editor in Chief** (2020-2021), Alconpat Journal, **México**

[13] Universidad Centroccidental Lisandro Alvarado; **Language Editor,** Alconpat Journal, **Venezuela**

Contribution of each author

In this work P. Castro-Borges conceptualized the work, led the discussion, and wrote the article; E. Sabido-Maldonado performed the formatting, collected the information, prepared the figures and tables, and contributed to the discussion of how to present the information; the other co-authors participated in the discussion and review of the work.

Revista Alconpat: 10 años de historia (2011 – 2021)

RESUMEN

El objetivo de este artículo es presentar a la comunidad los logros y retos, enfrentados, actuales y por venir, de la Revista Alconpat en sus primeros diez años de existencia. Se realiza una narración de: cómo surgió la idea de tener una revista científico/técnica en Alconpat Internacional; cuando, como y donde se llevaron a cabo las discusiones y el proyecto; la implementación, el primer número, la puntualidad; los requisitos y retos a cumplir para las primeras indizaciones (Scielo México, Scielo WoS, Redalyc, Latindex, Google); los proyectos Conacyt que permitieron cumplir poco a poco los requisitos para eventuales aplicaciones a índices superiores (Scopus y WoS), repositorios, directorios (DOAJ) y super servidores; marcaciones electrónicas, publicación en tres idiomas (español, portugués e inglés), los tiempos administrativos para publicación puntual, etc. Al final se hace un extenso agradecimiento a todos los que han intervenido en estos 10 años iniciales.

Palabras clave: Revista Alconpat; Scielo; WoS; Redalyc, Latindex, Google Académico.

Revista Alconpat: 10 anos de história (2011 - 2021)

RESUMO

O objetivo deste trabalho é apresentar à comunidade as conquistas e desafios da Revista Alconpat em seus primeiros dez anos de existência. Narra-se: como surgiu a ideia de termos uma revista científica / técnica na Alconpat Internacional; quando, como e onde as discussões e o projeto ocorreram; a implementação, a primeira questão, a pontualidade; os requisitos e desafios a cumprir para as primeiras indexações (Scielo México, Scielo WoS, Redalyc, Latindex, Google); os projetos do CONACyT que possibilitaram atender gradativamente os requisitos para eventuais aplicações em índices superiores (Scopus e WoS), repositórios, diretórios (DOAJ) e super servidores; marcações eletrônicas, publicação em três idiomas (espanhol, português e inglês), tempos administrativos para publicação oportuna, etc. Ao final, um extenso agradecimento a todos aqueles que participaram desses primeiros 10 anos.

Palavras-chave: Revista Alconpat; Scielo; WoS; Redalyc, Latindex, Google Scholar.

1. INTRODUCTION

The idea of creating the ALCONPAT Journal came up within the framework of the 2003 CONPAT Congress, when the actual need to have a formal dissemination mechanism in said association was raised for the first time; a serious, academic, and original journal that would focus on its efforts on those subjects cultivated for almost 30 years in the Association. The evolution of the idea and the project took several years to consolidate, but everything was reinforced as the collection of quality works presented at CONPAT events increased. It was during the 2009 CONPAT Congress that the formal project for the creation of the Journal was formally presented to the Superior Council, the highest administrative body of the Association, obtaining its approval to officially start its activities in the following year. During 2010, intensive work was carried out on the design and implementation of the website to attend the mechanisms for sending, receiving, evaluating, and publishing articles; finally, on December 31, 2010, the first issue was electronically published, corresponding to the year 2011, making itself known as "ALCONPAT Journal" (or RA for its acronym).

In 2013, the legal information registry was generated, that includes the right of exclusive international use of the name "Revista ALCONPAT" and its corresponding ISSN number: 2007-6835.

In 2015, during the publication of the Volume 5, RA participated in the Call to belong to the index of Scientific and Technological Journals of Conacyt (National Council of Science and Technology - Mexico), achieving such distinction in the same year. This fact is a watershed that drove the RA towards higher standards, such as membership in prestigious indices, migration to the OJS (Open Journal System) platform and DOI (Digital Object Identifier) number, among others. Currently the journal has risen to the highest level of "Internationally Competent Journal" in Conacyt.

In 2016, thanks to the indexing of CONACyT, it was possible to incorporate the journal into the Scielo Mexico index, as well as into the SciELO Citation Index, a database that is part of the Web of Science. In 2017 RA started in Google Scholar where important data can be consulted.

In 2018 the RA applied for a long process towards its inclusion in Scopus, and a year later the feedback received suggested small changes, which were implemented and will be evaluated again in May 2021. In 2018 the RA was incorporated into other Indexes such as Redalyc, and in the OJS 2 platform a statistics section was incorporated to enable monitoring which articles are downloaded the most, which country visits us the most, which is the most consulted number, etc., as well as the implementation of publishing XML Jats. Similarly, the RA was included in 2018 in the Latindex Catalog and directory.

In 2020 the RA moved to the most recent and stable version of the OJS evaluation system (Version 3.2.1.4), a new portal design, with new built-in plugins such as XML Viewer, Catch module, article sharing module, etc.; the editorial and ethical policies were updated, accordance with the COPE (Committee on Publication Ethics) in order to increase visibility and accessibility. The option was chosen to change the Creative Commons license to a more open one with fewer restrictions (CC BY, https://creativecommons.org/licenses/by/4.0/), which is a requirement to belong to the DOAJ (Directory of Open Access Journals). Another important index requirement is the digital preservation system, that we currently have, an anti-plagiarism software license (iThenticate with Crossref Similarity Check), and also a Google Analytics tool, which provides individual statistics per item and other enhancements that will allow the entry, during 2021-2022, to DOAJ and probably to Scopus and JCR. It is noteworthy that the RA currently had an Impact Factor (IF) in Scielo Analytics (Table 1) of 0.03 in 2016, which later increased to 0.16 in 2019; we are confident that it will improve and be endorsed when it is incorporated into other indices.

Table 1. Impact factor of the Alconpat Journal since 2016 (Scielo México)

Base year 2016	Dating in 2016			Articles published in			Impact factor	Appointments made in 2016 for articles of 2016	Articles published in 2016	Immediacy index
	Every year	2015	2014	2015+2014	2015	2014	2015+2014				
	Every year	2015	2014	2015+2014	2015	2014	2015+2014				
	7	0	1	1	18	18	36	0.028	0	22	0

Base year 2017	Dating in 2017			Articles published in			Impact factor	Appointments made in 2017 for articles of 2017	Articles published in 2017	Immediacy index
	Every year	2016	2015	2016+2015	2016	2015	2016+2015				
	7	0	1	1	22	18	40	0.025	2	22	0.091

Base year 2018	Dating in 2018			Articles published in			Impact factor	Appointments made in 2018 for articles of 2018	Articles published in 2018	Immediacy index
	Every year	2017	2016	2017+2016	2017	2016	2017+2016				
	13	2	1	3	22	22	44	0.068	0	16	0.0000

Base year 2019	Dating in 2019			Articles published in			Impact factor	Appointments made in 2019 for articles of 2019	Articles published in 2019	Immediacy index
	Every year	2018	2017	2018+2017	2018	2017	2018+2017				
	14	2	4	6	16	22	38	0.160	0	7	0

As a result of the increased visibility of the RA, there has also been an increase in queries and downloads, as shown in Figure 1. The variety of countries that consult the RA is particularly striking, as can be seen in Figure 2, and in quantitative form in Table 2. The RA has been reviewed and/or downloaded in more than 130 countries; the trend in distribution of these downloads reflects, in some way, the geographical distribution of authors, access to information sources, the degree of scientific development, etc.
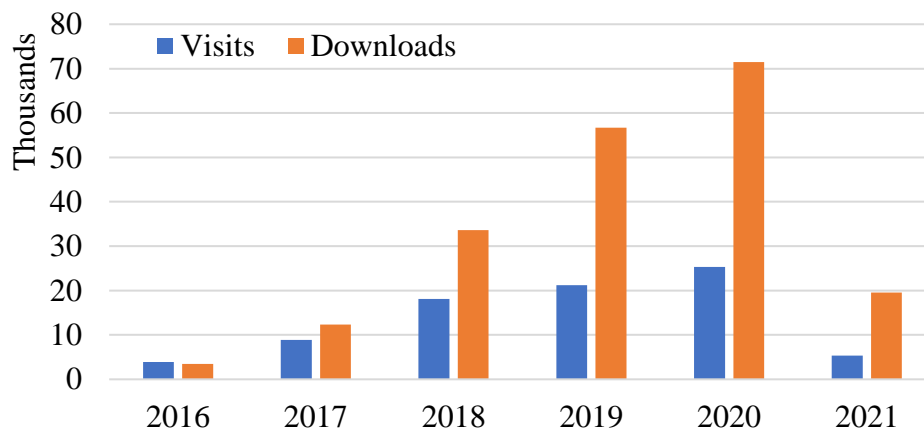

Figure 1. Downloads and visits to the page, number of queries to summarize the articles from 2016 to 2021. (source: OJS of the Revista Alconpat)

Revista Alconpat: 10 years of history (2011-2021)
149
Castro-Borges, P., Sabido-Maldonado, E., Mendoza-Rangel, J. M., et al.
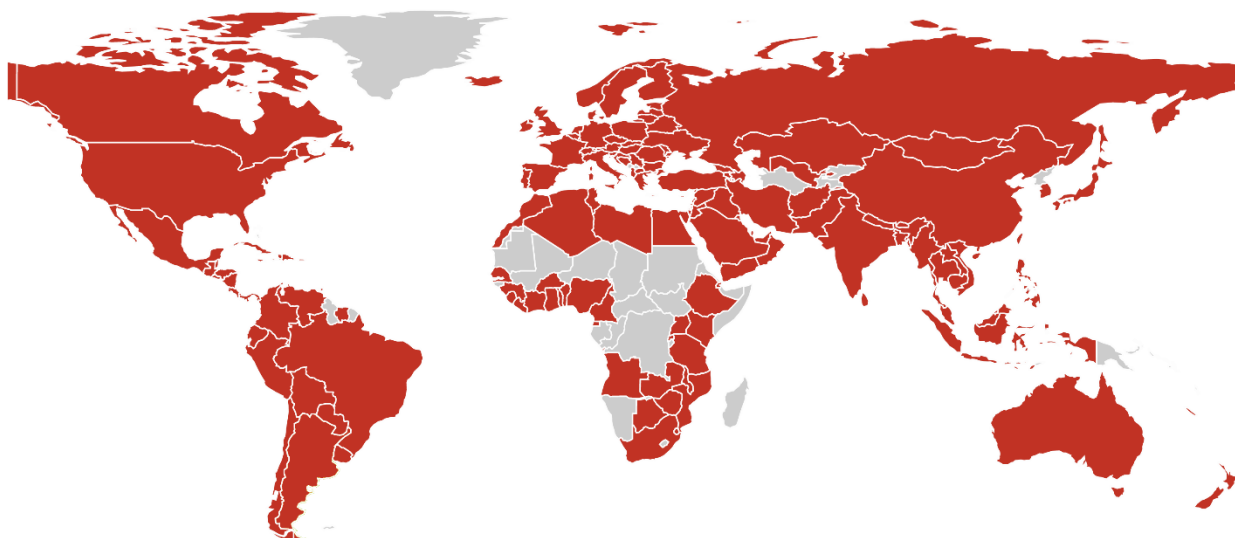
Figure 2. Countries with the highest number of visits, in red. (OJS from Revista Alconpat)

Table 2. Countries with number of visits in 2020.

Country	No. of visits	Country	No. of visits	Country	No. of visits	Country	No. of visits
Brazil	9303	Indonesia	89	Nepal	19	Belize	4
Mexico	3672	Uruguay	74	United Republic of Tanzania	17	Senegal	4
United States of America	3320	Greece	73	Republic of Serbia	17	Togo	4
Peru	2152	Iraq	70	Denmark	16	Zimbabwe	4
India	1685	Australia	65	Lithuania	15	Yemen	4
Colombia	1421	South Africa	64	Mongolia	15	Belarus	4
Russia	1138	Honduras	62	Morocco	14	Jamaica	3
Spain	886	Dominican Republic	60	Bulgaria	13	Haiti	3
Bolivia	783	Poland	60	Austria	13	Iceland	3
Argentina	565	Malaysia	60	New Zealand	13	Benin	3
China	565	Egypt	59	Slovenia	12	Guinea	2
Germany	456	Thailand	58	Syria	11	Sierra Leone	2
Ecuador	436	Ethiopia	56	Albania	11	Liberia	2
Czech Republic	408	United Arab Emirates	54	Puerto Rico	10	Ivory Coast	2
France	402	Nigeria	49	Lebanon	10	Botswana	2
Portugal	395	Costa Rica	48	Kazakhstan	10	Djibouti	2
South Korea	350	Vietnam	45	Rwanda	9	Macedonia	2
Chile	342	Mozambique	42	Kuwait	9	Georgia	2
Ukraine	325	Israel	40	Qatar	8	Laos	2
United Kingdom	298	Belgium	38	Latvia	8	Surinam	1
Panama	231	Kenya	37	Estonia	8	Burkina Faso	1

Castro-Borges, P., Sabido-Maldonado, E., Mendoza-Rangel, J. M., et al.

Venezuela	170	The Savior	36	Afghanistan	8	Equatorial Guinea	1
Ireland	170	Angola	32	Cameroon	7	Swaziland	1
Canada	168	Norway	28	Uganda	7	Malawi	1
Italy	160	Ghana	28	Tunisia	7	Armenia	1
Philippines	130	Norway	28	Croatia	7	Azerbaijan	1
Sweden	125	Bangladesh	28	Zambia	6	Uzbekistan	1
Japan	123	Saudi Arabia	27	Cyprus	6	Bhutan	1
Netherlands	118	Switzerland	27	Cambodia	6	Myanmar	1
Cuba	116	Nicaragua	26	Trinidad and Tobago	5	New Caledonia	1
Turkey	115	Algeria	26	Libya	5	Fidji	1
Paraguay	110	Jordan	26	Bosnia and Herzegov	5		
Guatemala	108	Finland	26				
Pakistan	100	Taiwan	26				
		Oman	23				

The RA has the highest internationalization index considered by Redalyc, Figure 3, which is made up of 5 groups and 5 subgroups. The highest level of internationalization is defined by G1 and the lowest G5. This index is derived from three variables with different weights:
1. Proportion (%) of foreign authors (value 0.25);
2. Number of foreign countries (value 0.35);
3. Proportion of articles with at least one foreign author (value 0.45).
The level of internationalization of a journal allows observing the level of foreign participation.
Group G11 indicates the highest level of internationalization and G55 the least internationality or greater endogeneity. Redalyc considered the creation of the subgroups important because G21 indicates that it is very close to G1, while G25 indicates that it is much closer to G3 and with the probability of descending from the group. Maintaining the G1 is a challenge for any journal, and especially those that aspire belonging to important scientific indexes.
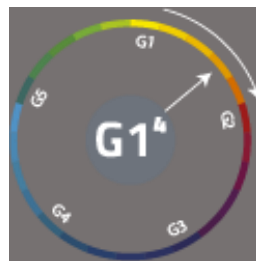

Figure 3. Internationalization index of the Revista Alconpat
(Data and figure courtesy of Redalyc).

One of the challenges of the RA has been to maintain a standard in terms of timeliness and publication times. From the beginning, an optimal average trend was established towards 17 weeks (4 months) from submission to publication, which according to Redalyc has remained very close to 17.39 as shown in Figure 4.

Revista Alconpat: 10 years of history (2011-2021)   151

Castro-Borges, P., Sabido-Maldonado, E., Mendoza-Rangel, J. M., et al.
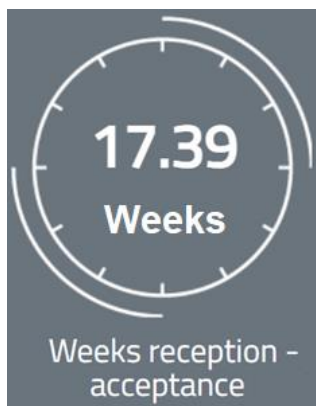
Figure 4. Average weeks of reception - acceptance of the Revista Alconpat: 17.39 weeks (Data courtesy of Redalyc).

Like other journals that are evaluated in various indexes, the Alconpat Journal must maintain a citable production, The trends in these 10 years have been those of an increase in citable production as denoted by research and review articles published since then. The distribution by type of article during these 10 years can be seen in Figure 5.
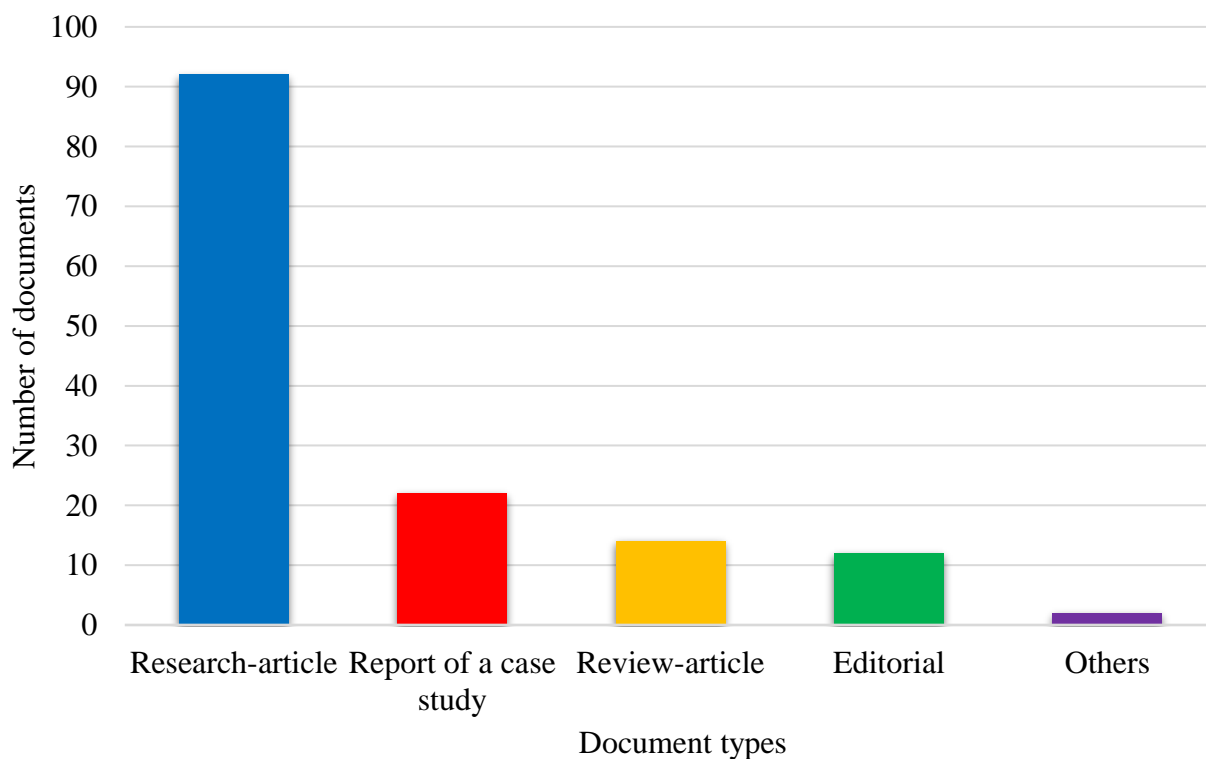

Figure 5. Distribution of documents by type of article (Data courtesy of Scielo Analytics)

Undoubtedly, the internationalization of the RA is still mostly from Latin America, as seen in Figure 6, although papers from the rest of the world are becoming more common. A strong influence from Brazil and Mexico have marked the course of the RA in these 10 years.

152

Revista Alconpat: 10 years of history (2011-2021)
Castro-Borges, P., Sabido-Maldonado, E., Mendoza-Rangel, J. M., et al.
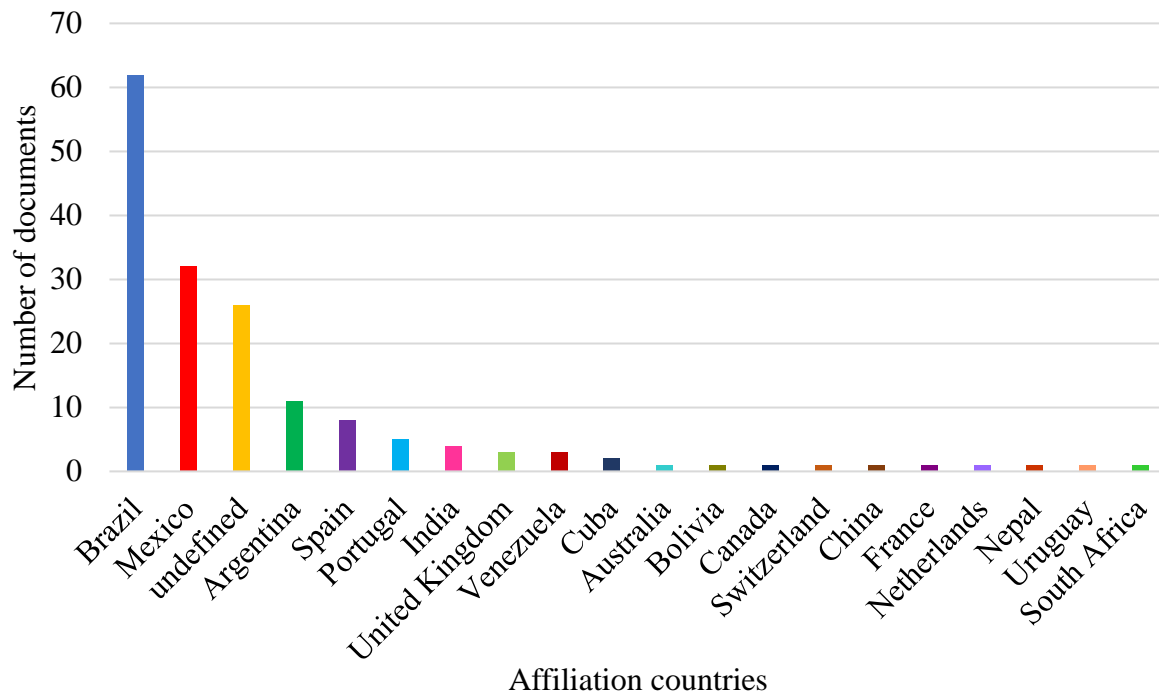
Figure 6. Distribution of documents by country of publication (data from Scielo Analytics)

The number of authors per article is an issue that increasingly involves evaluation in the Science and Technology Councils of our countries. Figure 7 shows this trend in the RA, showing a predominance of 3-4 authors, which is quite attractive for evaluation systems such as Mexico or Brazil. It is also worth noting the significant presence of articles with a single author, which denotes independence and leadership of the authors that choose the RA, which coincide with the trajectory of those authors regarding their citation.
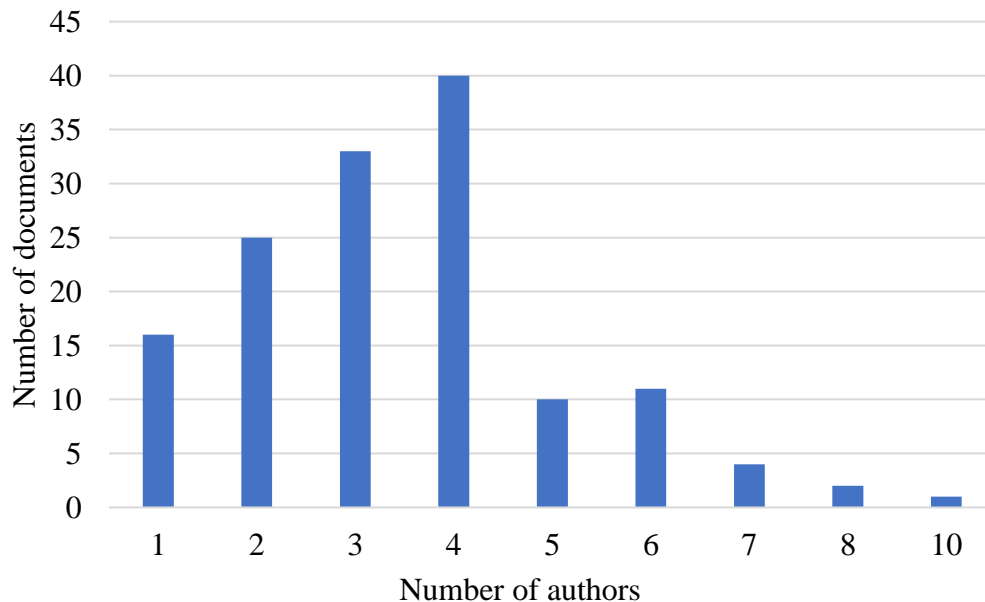

Figure 7. Distribution of documents by number of authors per article (data from Scielo Analytics).

Another important aspect in the quality of a Journal is the number of references in the papers, which for the RA the average is of around 20, see Figure 8, which is an acceptable number after taking

into account that the citable production relative to basic or applied research articles and to reviews is around 2/3 of the total production, Figure 5.

To sum up, the RA has a general positive trend (upward, lasting, and constant step) in its modest statistics so far, which could be summarized in a gradual and constant increase of its impact factor, Table 1. By the time of this publication, we already have had feedback from DOAJ, so it is likely that, according to the plans, we will be applying with very good possibilities to Scopus and JCR.
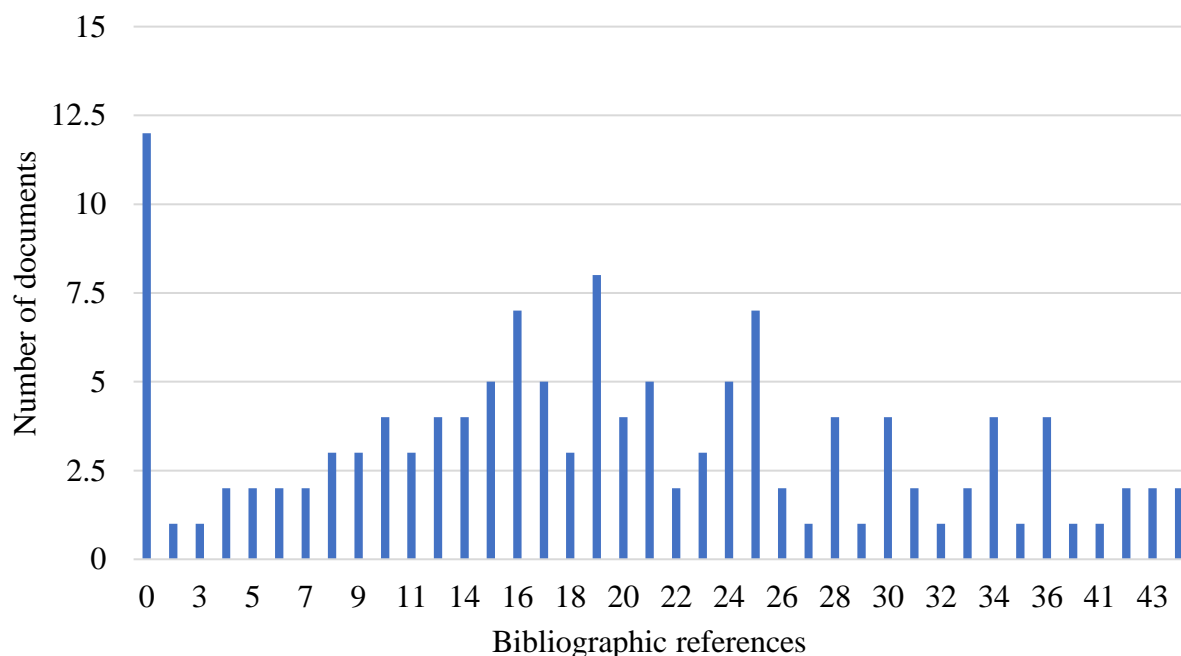

Figure 8. Distribution of documents by number of bibliographic references per article (Scielo Analytics)

The future of RA looks bright and fruitful. 10 years away, a wide recognition must be made of the original editorial staff and those who have joined this initiative, which has led us to where we are now. Undoubtedly, the greatest recognition belongs to our article authors, who have trusted our journal and invested time, money, and effort to publish their research work with us, despite the fact that many of them have had better options at their moment. Finally, our readers, whom without them we are nobody, deserve our appreciation for reading, downloading, and citing us; their preference will certainly provide the RA, in a short period of time, opportunities to continue improving through better tools for consultation and indexing. On behalf of the Editorial Board, many, many, many thanks to all of you. During 2021, and at the close of this edition, these 10 years were honored with an academic celebration on May 19; the schedule of said act is included here as a tribute for the posterity in the annex.

A special thanks are due to the National Council of Science and Technology (Conacyt) of Mexico, through which we have had the support of the projects (2013 call, declared as a competent national magazine (September 2, 2013), 2014 -2015 call, project no.140028 (October 30, 2014), call 2016, declared as an international competent journal (September 5, 2016), Call 2017, project 290978 (March 21, 2017) and the last call 2018-2019, project 297368 (July 16, 2018) to finance Alconpat Journal in various stages that have allowed it to reach standards with which it has been possible to be applying and obtaining important indexes.

154

Revista Alconpat: 10 years of history (2011-2021)
Castro-Borges, P., Sabido-Maldonado, E., Mendoza-Rangel, J. M., et al.

ANNEX

Academic Celebration Program for the 10th Anniversary of Revista Alconpat
May 19, 2021, Online, 09:00-13:00 (GMT-5)

09:00-09:10	Welcome remarks to the event by Carmen Andrade (President of Alconpat)
09:10-09:40	Presentation on the history and statistics of the Journal, as well as the immediate and future plans (Pedro Castro Borges).
09:40-10:20	Conversation between Associate Editors. Anecdotes, experiences, history, and open topics. Chairmen: Raúl Husni and Manolo Fernández Cánovas. Participants: Oladis Troconis de Rincón, Andrés A. Torres Acosta, Jorge Branco, Paulo Helene, Pedro Garcés Terradillos.
10:20-10:40	Presentation and Recognition of the Editorial Board that has served in these 10 years, both in office and those who are no longer on the committee (Patricia Martínez, Sergio Espejo, Margita Kliewer, Mauricio López and Luis Fernandez, among others), chaired by José Manuel Mendoza Rangel.
10:40-11:00	Presentation of New Associate Editors of the Journal (Ravindra Gettu from India and Filippo Uberttini from Italy) and Co-Editor in Chief, 2021-2022 (Edna Possan from Brazil). Chaired by Pedro Castro Borges.
11:00-12:45	Short presentations of the most representative "Reviews and collection" (by subject, citations, downloads and time) of Alconpat Journal representing North and South America, Africa, Asia and Europe. Chaired by a member of the Editorial Committee for each work (see list below). Each Presentation is 12 minutes and 3 minutes for initial presentation and questions.
12:45-12:55	Words by Paulo Helene, Associate Editor in Representation of the Editorial Board.
12:55-13:00	Closing with e-toast of honor, Pedro Castro Borges.

Selected Reviews

2015

Integrated management systems building technique: inspection and repair of non-structural elements. **PORTUGAL** (42 REF). **Chairman Pedro Garcés Terradillos**.
G. T. Ferraz (IST, Lisboa; Portugal)
J. De Brito (Instituto Superior Técnico, Universidade Técnica de Lisboa)
V. P. De Freitas (Faculdade de Engenharia, Universidade do Porto)
J. D. Silvestre (IST, Lisboa; Portugal)
DOI: https://doi.org/10.21041/ra.v5i2.83

2017

Infrared thermography as a non-destructive test for the inspection of reinforced concrete bridges: A review of the state of the art. **BRASIL** (75 REF). **Chairman Raúl Husni**.
Joaquin Humberto Aquino Rocha **(Universidade de Pernambuco, Brasil)**
Yêda Vieira Póvoas Tavares (Universidade de Pernambuco)
DOI: https://doi.org/10.21041/ra.v7i3.223

Revista Alconpat: 10 years of history (2011-2021)

155

Castro-Borges, P., Sabido-Maldonado, E., Mendoza-Rangel, J. M., et al.

2018

Service life design and modelling of concrete structures – background, developments, and implementation. **SOUTHAFRICA** (57 REF). **Chairman Andrés Torres Acosta**.
Mark Gavin Alexander **(University of Cape Town)**
DOI: https://doi.org/10.21041/ra.v8i3.325

2019

Adhesion, strengthening and durability issues in the retrofitting of Reinforced Concrete (RC) beams using Carbon Fiber Reinforced Polymer (CFRP) – A Review. **MEXICO** (67 REF). **Chaired by Edna Possan.**
Pedro J. Poot Cauich (Escuela de Ingeniería Civil, Universidad Marista de Mérida, Periférico Norte tablaje catastral 13941, Carretera Mérida - Progreso. C.P. 97300, Mérida, Yucatán)
Rodolfo Martínez-Molina (Escuela de Ingeniería Civil, Universidad Marista de Mérida, Periférico Norte tablaje catastral 13941, Carretera Mérida - Progreso. C.P. 97300, Mérida, Yucatán)
José Luis Gamboa Marrufo (Escuela de Ingeniería Civil, Universidad Marista de Mérida, Periférico Norte tablaje catastral 13941, Carretera Mérida - Progreso. C.P. 97300, Mérida, Yucatán)
Pedro Jesus Herrera Franco (Unidad de Materiales, Centro de Investigación Científica de Yucatán, A.C., Calle 43 # 130, Col. Chuburná, C.P. 97205, Mérida, Yucatán)
DOI: https://doi.org/10.21041/ra.v9i2.401

2020

Use of supplementary cementitious materials (SCMs) in reinforced concrete systems – Benefits and limitations. **INDIA** (39 REF). **Chaired by J. Iván Escalante-Garcia**
R. G. Pillai (Department of Civil Engineering, Indian Institute of Technology Madras, Chennai, India)
R. Gettu (Department of Civil Engineering, Indian Institute of Technology Madras, Chennai, India)
M. Santhanam (Department of Civil Engineering, Indian Institute of Technology Madras, Chennai, India)
DOI: https://doi.org/10.21041/ra.v10i2.477

Fire impacts on concrete structures. A brief review. **BRASIL** (35 REF). **Chaired by Fernando Branco**
Paulo Helene (Professor Titular da Escola Politécnica da USP, PhD Engenharia, São Paulo)
Carlos Britez (Pesquisador de Pós-Doutorado na Escola Politécnica da USP, Britez Consultoria, São Paulo)
M. Carvalho (Universidade Presbiteriana Mackenzie, São Paulo)
DOI: https://doi.org/10.21041/ra.v10i1.421

Review collection about Resistivity from Carmen Andrade, Chaired by Oladis Troconis

2011
La resistividad eléctrica como parámetro de control del hormigón y de su durabilidad. **ESPAÑA** (14 REF)
C. Andrade (Centro de Investigación en Seguridad y Durabilidad de Estructuras y Materiales, CISDEM (CSIC-UPM), IETcc-CSIC, España)
R. D'Andrea (Instituto Español del Cemento y sus Aplicaciones IECA- España)
DOI: https://doi.org/10.21041/ra.v1i2.8

2018
Design and evaluation of service life through concrete electrical resistivity. **ESPAÑA** (24 REF)
C. Andrade (International Center for Numerical Methods in Engineering. CIMNE. UPC)
DOI: https://doi.org/10.21041/ra.v8i3.349

2020
Rebar corrosion modelling and deterioration limit state. **ESPAÑA** (22 REF)
C. Andrade (Centro Internacional de Métodos Numéricos en Ingeniería, Madrid, España)
DOI: https://doi.org/10.21041/ra.v10i2.478